



Prepared for the U.S. Department of Energy
under Contract DE-AC05-76RL01830

Characterization and Leach Testing for REDOX Sludge and S-Saltcake Actual Waste Sample Composites

SK Fiskum
EC Buck
RC Daniel
KE Draper
MK Edwards
TL Hubler
LK Jagoda
ED Jenson

AE Kozelisky
GJ Lumetta
PJ MacFarlan
K McNamara
RA Peterson
SI Sinkov
LA Snow
RG Swoboda

July 2008

DISCLAIMER

This report was prepared as an account of work sponsored by an agency of the United States Government. Neither the United States Government nor any agency thereof, nor Battelle Memorial Institute, nor any of their employees, makes **any warranty, express or implied, or assumes any legal liability or responsibility for the accuracy, completeness, or usefulness of any information, apparatus, product, or process disclosed, or represents that its use would not infringe privately owned rights.** Reference herein to any specific commercial product, process, or service by trade name, trademark, manufacturer, or otherwise does not necessarily constitute or imply its endorsement, recommendation, or favoring by the United States Government or any agency thereof, or Battelle Memorial Institute. The views and opinions of authors expressed herein do not necessarily state or reflect those of the United States Government or any agency thereof.

PACIFIC NORTHWEST NATIONAL LABORATORY

operated by

BATTELLE

for the

UNITED STATES DEPARTMENT OF ENERGY

under Contract DE-AC05-76RL01830

Printed in the United States of America

Available to DOE and DOE contractors from the
Office of Scientific and Technical Information,

P.O. Box 62, Oak Ridge, TN 37831-0062;

ph: (865) 576-8401

fax: (865) 576 5728

email: reports@adonis.osti.gov

Available to the public from the National Technical Information Service,
U.S. Department of Commerce, 5285 Port Royal Rd., Springfield, VA 22161

ph: (800) 553-6847

fax: (703) 605-6900

email: orders@nits.fedworld.gov

online ordering: <http://www.ntis.gov/ordering.htm>

Characterization and Leach Testing for REDOX Sludge and S-Saltcake Actual Waste Sample Composites

SK Fiskum	AE Kozelisky
EC Buck	GJ Lumetta
RC Daniel	PJ MacFarlan
KE Draper	BK McNamara
MK Edwards	RA Peterson
TL Hubler	SI Sinkov
LK Jagoda	LA Snow
ED Jenson	RG Swoboda

June 2008

Test Specification: 24590-PTF-TSP-RT-06-003, Rev. 1
Work Authorization: 019
Test Plan: TP-RPP-WTP-467, Rev. 1
Test Exceptions: None
R&T Focus Area: Pretreatment
Service Requisition Number: 24590-QL-SRA-W000-00107, Rev 0

Prepared for the U.S. Department of Energy
under Contract DE-AC05-76RL01830

Pacific Northwest National Laboratory
Richland, Washington 99352

COMPLETENESS OF TESTING

This report describes the results of work and testing specified by Test Specification 24590-PTF-TSP-RT-06-003, Rev. 1 and Test Plan TP-RPP-WTP-467, Rev. 0, 2/2/07 and Rev. 1 7/31/07. The work and any associated testing followed the quality assurance requirements outlined in the Test Specification/Plan. The descriptions provided in this test report are an accurate account of both the conduct of the work and the data collected. Test plan results are reported. Also reported are any unusual or anomalous occurrences that are different from expected results. The test results and this report have been reviewed and verified.

Approved:



Gordon H. Beeman, Manager
WTP R&T Support Project

7-11-08
Date

Contents

Abbreviation/Acronym List.....	iii
References.....	v
Testing Summary.....	ix
Objectives.....	ix
Test Exceptions.....	xi
Results and Performance Against Success Criteria.....	xi
Quality Requirements.....	xiii
R&T Test Conditions.....	xiv
Simulant Use.....	xv
Discrepancies and Follow-on Tests.....	xv
1.0 Introduction.....	1.1
1.1 Tank Waste Pretreatment Operations at the WTP.....	1.1
1.2 Issues Identified by the External Flowsheet Review Team.....	1.1
1.3 Waste Groupings.....	1.3
1.4 Simulant Development.....	1.5
1.5 Testing of Groups 5 and 6.....	1.6
2.0 Test Sample Selection.....	2.1
2.1 Group 5—REDOX Sample Selection.....	2.1
2.2 S-Saltcake Sample Selection.....	2.5
3.0 Compositing, Homogenization, and Subdivision.....	3.1
3.1 REDOX Sludge Group 5.....	3.1
3.2 S-Saltcake Group 6.....	3.10
4.0 Characterization Methods.....	4.1
4.1 Physical Properties.....	4.1
4.2 Rheology.....	4.3
4.2.1 Shear-Strength Testing.....	4.3
4.2.2 Flow-Curve Testing.....	4.4
4.2.3 Rheology Instrumentation.....	4.6
4.2.4 Rheology Materials and Methods.....	4.6
4.3 Sample Preparation for Chemical Characterization.....	4.7
4.4 Chemical and Radioisotope Characterization.....	4.8

4.4.1	Free Hydroxide	4.8
4.4.2	Anions	4.8
4.4.3	TIC/TOC	4.8
4.4.4	Acid Digestion	4.8
4.4.5	KOH Fusion	4.9
4.4.6	NaOH/Na ₂ O ₂ Fusion	4.9
4.4.7	HF-Assisted Acid Digestion	4.9
4.4.8	Metals Analysis by ICP-OES	4.9
4.4.9	U (KPA)	4.9
4.4.10	Gamma Energy Analysis	4.9
4.4.11	Gross Alpha and Gross Beta	4.10
4.4.12	Pu Isotopes: ²³⁸ Pu and ²³⁹⁺²⁴⁰ Pu	4.10
4.4.13	Strontium-90	4.10
4.4.14	Chromate	4.10
4.5	Particle-Size Attributes	4.11
4.5.1	Particle-Size Distribution	4.11
4.5.2	Surface Area (BET)	4.12
4.6	Crystal Form and Habit	4.13
4.6.1	X-Ray Diffraction	4.13
4.6.2	Scanning Electron Microscopy	4.13
4.6.3	Transmission Electron Microscopy	4.14
4.6.4	Electron Energy-Loss Spectroscopy	4.14
4.7	Quality Assurance and Quality Control	4.15
4.7.1	Application of WTPSP Quality Assurance Requirements	4.15
4.7.2	Conduct of Experimental and Analytical Work	4.15
4.7.3	Internal Data Verification and Validation	4.16
5.0	Initial Characterization Results for REDOX Sludge Group 5	5.1
5.1	Physical Properties of the Composite Slurry	5.1
5.2	Rheology of the Composite Slurry	5.2
5.2.1	Shear Strength	5.2
5.2.2	Flow Curve	5.3
5.2.3	Chemical and Radiochemical Composition	5.6
5.3	Particle Size	5.11
5.4	Surface Area	5.14
5.5	Crystal Form and Habit	5.14
6.0	Initial Characterization Results for S-Saltcake Group 6	6.1
6.1	Physical Properties of the Solids Slurry	6.1
6.2	Rheology of the Composite Slurry	6.2
6.2.1	Shear Strength	6.2
6.2.2	Flow Curve	6.3
6.3	Pretreatment for Chemical Characterization	6.8

6.4	Chemical and Radiochemical Composition.....	6.9
6.5	Particle Size	6.13
6.6	Surface Area	6.16
6.7	Crystal Habit.....	6.16
7.0	Batch Contact Parametric Testing Methodology	7.1
7.1	Group 5 REDOX Sludge	7.1
7.1.1	Initial Washing of the Group 5 Solids	7.1
7.1.2	Division of the Washed Group 5 Solids.....	7.1
7.1.3	Caustic Leaching of the Washed Group 5 Solids	7.2
7.1.4	Washing of Caustic-Leached Group 5 Solids for Analysis	7.4
7.2	Group 6 S-Saltcake.....	7.5
7.2.1	Initial Washing of the Group 6 Solids	7.5
7.2.2	Caustic Leaching and Washing of the Group 6 Solids	7.5
7.2.3	Division of Caustic-Leached Group 6 Solids	7.6
7.2.4	Oxidative Leaching of the Caustic-Leached Group 6 Solids.....	7.7
8.0	Group 5 REDOX Sludge Parametric Caustic Leaching Test Results.....	8.1
8.1	Expected Boehmite Solubility	8.1
8.2	Time, Temperature, and Hydroxide Effects on Aluminum Dissolution.....	8.2
8.3	Analysis of Group 5 REDOX Sludge Boehmite Dissolution Kinetics.....	8.8
8.4	Effect of Sodium on Aluminum Dissolution	8.16
8.5	Chromium Leaching Behavior and Speciation.....	8.16
8.6	Anions, Phosphorus, Silicon, and Iron Leach Behavior	8.18
8.7	Assessment of Final Leach Conditions.....	8.18
8.8	Comparison of Initial and Caustic Leached and Washed Solids Properties.....	8.20
8.8.1	Leached Solids Wash Solution	8.20
8.8.2	Chemical and Radiochemical Composition.....	8.20
8.8.3	Particle-Size Distribution.....	8.23
8.8.4	Crystal Form and Habit.....	8.29
9.0	Group 6 S-Saltcake Water-Insoluble Solids Parametric Oxidative-Leaching Test Results.....	9.1
9.1	Group 6 Caustic-Leached Slurry	9.1
9.2	Parametric Oxidative Leaching Results.....	9.1
9.2.1	Chromium Behavior During Oxidative Leaching.....	9.1
9.2.2	Plutonium Behavior During Oxidative Leaching	9.4
9.2.3	Group 6 Oxidative Leaching Equilibrium Conditions.....	9.8
9.2.4	Composition of Group 6 Caustic and Oxidatively Leached Solids	9.8
10.0	Summary.....	10.1

Appendix A: Group 5 Parametric-Leach-Temperature Variation.....	A.1
Appendix B: Group 5 Parametric Analytical Results from Parametric Leaching	B.1
Appendix C: Group 6 Parametric Leach Data	C.1
Appendix D: Thermogravimetric Analysis for Chromium Phase Characterization	D.1

Figures

<u>No.</u>	<u>Figure Caption</u>	<u>Page</u>
2.1.	Sample Selection Decision Process (a) REDOX Sludge (Group 5), and (b) S-Saltcake (Group 6)	2.2
3.1.	Photographs of Group 5 REDOX Sludge S-101 As-Received Samples	3.5
3.2.	Photographs of Group 5 REDOX Sludge S-101, S-107, and S-110 As-Received Samples.....	3.6
3.3.	Photographs of Group 5 REDOX Sludge S-110 and SX-103 As-Received Samples	3.7
3.4.	Tank Source Distribution of Group 5 REDOX Sludge Composite	3.7
3.5.	RPL Homogenizer	3.8
3.6.	Sample TI477-G5-AR-J6.....	3.9
3.7.	Photographs of Group 6 S-Saltcake Samples	3.13
3.8.	Photographs of Group 6 S-Saltcake Samples	3.14
3.9.	Photographs of Group 6 S-Saltcake Samples	3.15
3.10.	Nominal Mass Distribution of S-Saltcake Tank Wastes in the Group 6 Composite	3.16
3.11.	Group 6 S-Saltcake Waste Debris Collected on the Sieve (cm scale).....	3.17
4.1.	Composite Group Analysis Scheme	4.2
5.1.	Shear Strength Versus Shear Rate for Group 5 REDOX Sludge Initial Characterization Sample G5-RH-2 at 25°C, 40°C, and 60°C (18.5 wt% UDS), Measured Using the MV1 Smooth Cup and Rotor.....	5.3
5.2.	Flow Curve Fits for Group 5 REDOX Sludge Sample G5-RH-2 at 40°C (18.5 wt% UDS).....	5.5
5.3.	Chemical Character-ization Sample of Group 5 REDOX Sludge Centrifuged Solids	5.7
5.4.	Wash Sequence of Group 5 REDOX Sludge Supporting Initial Characterization	5.7
5.5.	Selected Analyte Phase Distribution for Group 5 REDOX Sludge	5.11
5.6.	Group 5 REDOX Sludge Primary Sample PSDs (volume/weight basis) Before, During, and After Sonication.....	5.13
5.7.	Group 5 REDOX Sludge Duplicate Sample PSDs (volume/weight basis) Before, During, and After Sonication.....	5.13
5.8.	XRD Pattern of Washed Group 5 REDOX Sludge with Rutile (TiO ₂) Internal Standard	5.15
5.9.	XRD Pattern of Washed Group 5 REDOX Sludge, Background-Subtracted with Stick-Peak Identification.....	5.15
5.10.	Washed Group 5 REDOX Sludge Phase Composition (Entrained Supernatant Removed), Best Estimate.....	5.17

<u>No.</u>	<u>Figure Caption</u>	<u>Page</u>
5.11.	SEM-EDS Image of Washed Group 5 REDOX Sludge with Al, Na, U, Cr, Fe, Mn, and Si Maps	5.17
5.12.	SEM Images of Washed Group 5 REDOX Sludge, Various Magnifications and Views.....	5.19
5.13.	TEM Images of Washed Group 5 REDOX Sludge	5.20
5.14.	STEM Images of Washed Group 5 REDOX Sludge	5.21
6.1.	Group 6 S-Saltcake Solids Composite.....	6.1
6.2.	Group 6 S-Saltcake Solids Settling Test.....	6.1
6.3.	Shear-Strength Measurement for Group 6 S-Saltcake Initial-Characterization Slurry TI490-G6-AR-RH Settled Solids 66 Hours After Mixing (14.7 wt% UDS).....	6.3
6.4.	Flow Curve (shear stress versus shear rate) for Group 6 S-Saltcake Initial Characterization Slurry Sample TI490-G6-AR-RH at 25°C, 40°C, and 60°C (14.7 wt% UDS) as Measured Using the MV1 Cup and Rotor.Note: the second repeat measurement for 25°C is shown here, as it is the closest to the 40° and 60°C measurements in time.	6.4
6.5.	Two Repeat Measurements of the Flow Curve (shear stress versus shear rate) for Group 6 S-Saltcake Initial Characterization Slurry Sample TI490-G6-AR-RH at 25°C (14.7 wt% UDS) as Measured Using the MV1 Cup and Rotor	6.6
6.6.	Flow Curve (shear stress versus shear rate) for Group 6 S-Saltcake Initial Characterization Supernate Sample TI488-G6-AR-J2 at 25° C, 40° C, and 60°C as Measured Using the MV1 Cup and Rotor.....	6.8
6.7.	Wash Sequence for Group 6 S-Saltcake Solids Supporting Initial Characterization.....	6.9
6.8.	Selected Analyte Phase Distribution or Group 6 S-Saltcake	6.13
6.9.	Group 6 S-Saltcake Solids Primary Sample Particle Size Distributions (volume/weight basis) Before, During, and After Sonication.....	6.15
6.10.	Group 6 S-Saltcake Solids Duplicate Sample Particle-Size Distributions (volume/weight basis) Before, During, and After Sonication.....	6.15
6.11.	Group 6 S-Saltcake Washed Solids XRD Pattern, No Internal Standard	6.16
6.12.	Group 6 S-Saltcake Washed Solids XRD Pattern, Background-Subtracted with Alumina Internal Standard and Stick-Peak Identification	6.17
6.13.	Group 6 S-Saltcake Washed-Solids-Phase Identification (Entrained Supernatant and Sodium Oxalate Fractions Removed)	6.19
6.14.	SEM Images of Group 6 S-Saltcake Washed Solids, Magnified 8,000× and 10,000×.....	6.19
6.15.	SEM Micrographs of Group 6 S-Saltcake Washed Solids with EDS and Area Map	6.20
6.16.	EDS Area Maps, Selected Elements in Group 6 S-Saltcake Washed Solids.....	6.21
6.17.	EDS Map of Group 6 S-Saltcake Washed Solids	6.22
6.18.	EDS Analysis of an Al-Cr Phase in Group 6 S-Saltcake Washed Solids with STEM Image of an Agglomerate	6.23

<u>No.</u>	<u>Figure Caption</u>	<u>Page</u>
6.19.	TEM Images of Washed Group 6 S-Saltcake Solids (a-f) Showing High Surface Area Material that Dominated G6-S-WL (g-h) Boehmite Particles	6.24
6.20.	EDS and STEM Analysis Showing a Uranium-Rich Phase in the Group 6 S-Saltcake Washed Solids.....	6.24
7.1.	Batch Contact Shaker Supporting Parametric Testing.....	7.3
7.2.	Washing, Subdivision, and Analysis Scheme for the Group 5 REDOX Sludge Caustic-Leached Solids	7.4
7.3.	Washing, Subdivision, and Analysis Scheme for the Group 6 S-Saltcake Caustic-Leached Solids.....	7.6
7.4.	Washing, Subdivision, and Analysis Scheme for the Group 6 S-Saltcake Oxidatively Leached Solids	7.8
7.1.	Batch Contact Shaker Supporting Parametric Testing.....	7.3
7.2.	Washing, Subdivision, and Analysis Scheme for the Group 5 REDOX Sludge Caustic-Leached Solids	7.4
7.3.	Washing, Subdivision, and Analysis Scheme for the Group 6 S-Saltcake Caustic-Leached Solids.....	7.6
7.4.	Washing, Subdivision, and Analysis Scheme for the Group 6 S-Saltcake Oxidatively Leached Solids	7.8
8.1.	Theoretical Boehmite Solubility as a Function of Temperature in 1, 3, and 5 M NaOH Solutions Based on the Literature Model (Panias et al. 2001).....	8.2
8.2.	Aluminum Concentration Versus Time at 80°C Leach Temperature in 1, 3, and 5 M NaOH Solutions for Group 5, REDOX Sludge.....	8.3
8.3.	Aluminum Concentration Versus Time at 90°C Leach Temperature in 1, 3, and 5 M NaOH Solutions for Group 5, REDOX Sludge.....	8.4
8.4.	Aluminum Concentration Versus Time at 100°C Leach Temperature in 1, 3, and 5 M NaOH Solutions for Group 5, REDOX Sludge.....	8.4
8.5.	Aluminum Concentration and Percent Dissolved in 1 M NaOH for Group 5, REDOX Sludge	8.5
8.6.	Aluminum Concentration and Percent Dissolved in 3 M NaOH for Group 5, REDOX Sludge	8.6
8.7.	Aluminum Concentration and Percent Dissolved in 5 M NaOH for Group 5, REDOX Sludge	8.6
8.8.	Aluminum Concentration in Leach Solution as a Function of Process Temperature (a) 8-hr Contact Time and (b) 24-hr Contact Time for Group 5, REDOX Sludge.....	8.7
8.9.	Plot of Al Concentration Versus Time for Leaching of Group 5 Solids at 80°C with a) 1 M NaOH, b) 3 M NaOH, and c) 5 M NaOH (Group 5, REDOX Sludge Test Material)	8.9
8.10.	Plot of Al Concentration Versus Time for Leaching of Group 5 Solids at 90°C with a) 1 M NaOH, b) 3 M NaOH, and c) 5 M NaOH (Group 5 REDOX Sludge Test Material)	8.10

<u>No.</u>	<u>Figure Caption</u>	<u>Page</u>
8.11.	Plot of Al Concentration Versus Time for Leaching of Group 5 Solids at 100°C with a) 1 M NaOH, b) 3 M NaOH, and c) 5 M NaOH (Group 5 REDOX Sludge Test Material)	8.11
8.12.	Plot of the Initial Al Dissolution Rate Versus the NaOH Concentration During the Leaching of Group 5 Solids at a) 80°C, b) 90°C, and c) 100°C (Group 5 REDOX Sludge Test Material).....	8.13
8.13.	Traditional Arrhenius Plot of the Boehmite Dissolution Rate Constant Versus 1/T (Group 5 REDOX Sludge Test Material)	8.14
8.14.	Modified Arrhenius Plot of the Boehmite Dissolution Rate Versus 1/T, Based on Equation 8.5 (Group 5 REDOX Sludge Test Material)	8.15
8.15.	Dependence of the Boehmite Dissolution Apparent Activation Energy on the NaOH Concentration (Group 5 REDOX Sludge Test Material).....	8.15
8.16.	Matrix Effect of Na Concentration on Al (Boehmite) Dissolution (Group 5 REDOX Sludge).....	8.16
8.17.	Cr Dissolution as a Function of Time and Hydroxide Concentration for Group 5 REDOX Sludge.....	8.17
8.18.	Final Al Concentration Versus Temperature, 1, 3, and 5 M Free Hydroxide.....	8.19
8.19.	Group 5 REDOX Sludge Reduction in Solid Mass with Caustic Leaching	8.23
8.20.	Leached Group 5 REDOX Sludge PSD (G5-W-F) as a Function of Pump Speed Before Dispersion Sonication	8.25
8.21.	Leached Group 5 REDOX Sludge PSD (G5-W-F) as a Function of Applied Sonication	8.26
8.22.	Leached Group 5 REDOX Sludge PSD (G5-W-F Measurement 1/2) as a Function of Pump Speed After Dispersion Sonication	8.27
8.23.	Leached Group 5 REDOX Sludge PSD (G5-W-F Measurement 2/2) as a Function of Applied Sonication	8.28
8.24.	Effect of Caustic Leaching on the Measured PSD for Group 5, REDOX Sludge	8.29
8.25.	XRD Pattern of Caustic Leached Group 5 REDOX Sludge with Rutile (TiO ₂) Internal Standard (a) Raw Data and (b) Background-Subtracted with Stick-Peak Identification ..	8.30
8.26.	Group 5 REDOX Sludge Initial Characterization XRD Pattern.....	8.32
8.27.	SEM-EDS Image of Group 5 REDOX Sludge Leached and Washed Solids with U, Al, Na, Fe, Mn, Cr, and Si Maps	8.33
8.28.	SEM Images of Group 5 REDOX Sludge Caustic Leached and Washed (a) 10 kV, 4k×; (b) 10 kV, 5k×; (c) 10 kV, 4 k×.....	8.33
8.29.	Transmission Electron Microscopy Images of Boehmite Particles in Group 5 REDOX Sludge Solids Before Caustic Leach	8.34
8.30.	Cumulative Distribution Plot of Group 5 REDOX Sludge Boehmite Particle Sizes Before Caustic Leach and a Mathematical Fit to the Data	8.35

<u>No.</u>	<u>Figure Caption</u>	<u>Page</u>
8.31.	STEM Images of Particles in Group 5, REDOX Sludge Sample Before Caustic Leach (G5 IW) Showing Needle-Like Phases	8.35
8.32.	EDS Analysis of Elongated Particles in Group 5, REDOX Sludge Sample Before Caustic Leach (G5-IW).....	8.36
8.33.	High-Magnification Images of Group 5 REDOX Sludge Solids Post-Leaching (G5-W-B) Showing Elongated Uranium Phases and Spherical Particles	8.36
8.34.	STEM Images of Group 5, REDOX Sludge Solids Post-Leaching (G5-W-B1)	8.37
8.35.	EDS Analysis of Uranium and Mn-Ni Phases in Group 5, REDOX Sludge Post-Leaching Sample G5-W-B.....	8.37
8.36.	TEM images of Al and U Particles in Group 5, REDOX Sludge, Post-Leaching.....	8.38
8.37.	Energy-Filtered TEM Images of Group 5, REDOX Sludge Post-Leaching Sample G5-W-B1 and X-ray Analyses.....	8.38
9.1.	Chromium Concentration Versus Time at 25°C Leach Temperature and at Mn/Cr Mole Ratios of 0.75, 1, and 1.25 in (a) 0.25 M NaOH, (b) 1.25 M NaOH, (c) 3 M NaOH for Group 6 S-Saltcake (During Oxidative Leaching).....	9.5
9.2.	Chromium Concentration Versus Time at 50°C Leach Temperature at Mn/Cr Molar Ratios of 0.75, 1, and 1.25 in (a) 0.25 M NaOH and (b) 3 M NaOH for Group 6 S-Saltcake (During Oxidative Leaching)	9.6
9.3.	Chromium Conversion to the Aqueous Phase as a Function of Mn/Cr Mole Ratio and Time for Group 6 S-Saltcake (During Oxidative Leaching).....	9.7
9.4.	Total Chromium and Cr(VI) Concentrations Versus Time for Group 6 S-Saltcake (During Oxidative Leaching).....	9.7
9.5.	Effect of Free Hydroxide Concentration on Pu Mobilization during Oxidative Leaching for Group 6 S-Saltcake (During Oxidative Leaching)	9.8
9.6.	Relative Reduction in Component Mass with Caustic and Oxidative Leaching of Group 6 S-Saltcake Solids	9.13
9.7.	PSD for Group 6 S-Saltcake Solids Sample G6-IW-D as a Function of Sonication	9.15
9.8.	Pre-Sonication PSD for Group 6 S-Saltcake Solids Sample G6-IW-D as a Function of Flow Rate	9.16
9.9.	Post-Sonication PSD for Group 6 S-Saltcake Solids Sample G6-IW-D as a Function of Flow Rate	9.17
9.10.	PSD for Group 6 S-Saltcake Solids Sample G6-W-H as a Function of Sonication.	9.19
9.11.	Pre-Sonication PSD for Group 6 S-Saltcake Solids Sample G6-W-H as a Function of Flow Rate.....	9.20
9.12.	Post-Sonication PSD for Group 6 S-Saltcake Solids Sample G6-W-H as a Function of Flow Rate	9.21
9.13.	Effect of Oxidative Leaching on the Measured PSD for Group 6 S-Saltcake Solids Parametric Testing Samples.....	9.22

<u>No.</u>	<u>Figure Caption</u>	<u>Page</u>
9.14.	XRD Pattern of Caustic Leached Group 6 S-Saltcake Solids with Rutile (TiO ₂) Internal Standard.....	9.23
9.15.	XRD Pattern of Oxidatively Leached Group 6 S-Saltcake Solids.....	9.24
9.16.	SEM Images of the Caustic-Leached and Washed Group 6 S-Saltcake Solids.....	9.25
9.17.	SEM-EDS Images of Group 6 S-Saltcake Caustic-Leached Solids	9.26
9.18.	SEM Image of the Caustic Leached and Washed Group 6 S-Saltcake Solids with EDS Analysis and Map.....	9.27
9.19.	SEM Images of Group 6 S-Saltcake Solids Following Oxidative Leaching and Washing	9.28
9.20.	SEM-EDS Imaging and Analysis of Group 6 S-Saltcake Oxidatively Leached Solids.....	9.29
9.21.	SEM-EDS Image of Group 6 S-Saltcake Oxidatively Leached Solids with Na, Al, Si, P, Ca, Cr, Mn, Fe, Cu, Pb, and U Maps.....	9.30
9.22.	STEM and EDS Analyses of Regions in G6-IW-F (Group 6 S-saltcake sample following caustic-leaching).....	9.31
9.23.	TEM Images of Amorphous Aggregates in G6-IW-F (Group 6 S-saltcake sample following caustic leaching).....	9.32
9.24.	Energy-Filtered Image of G6-IW-F (Group 6 S-saltcake sample following caustic leaching)	9.32
9.25.	Low and High Magnification TEM Images of Manganese (Group 6 S-saltcake sample following oxidative leaching).....	9.33
9.26.	Cumulative Distribution Function that Describes the Probability of Particle Size from a Series of TEM Images of Manganese Particles (Group 6 S-saltcake following oxidative leaching).....	9.34
9.27.	Energy-Filtered Images of G6-W-G Showing the Presence of a Nano-Particle of Uranium (Group 6 S-saltcake sample following oxidative leaching).....	9.34
9.28.	STEM and EDS Analysis of Regions in G6-W-G (Group 6 S-saltcake sample following oxidative leaching).....	9.35
9.29.	TEM Images from G6-W-G (Group 6 S-saltcake sample following oxidative leaching)	9.35

Tables

<u>No.</u>	<u>Table Caption</u>	<u>Page</u>
S.1.	Test Objectives	ix
S.2.	Results and Performance Against Success Criteria	xi
S.3.	R&T Test Conditions.....	xiv
1.1.	Hanford Tank Waste Component Mass (Metric Tons) Inventory Summary.....	1.4
1.2.	Water-Insoluble Component Mass (Metric Tons) Inventories as Functions of Waste Type.....	1.5
1.3.	Projected Distribution (Weight Percent) of Water-Insoluble Components in the Tank Waste Groupings	1.6
2.1.	Selection of Group 5 REDOX Sludge Tanks	2.3
2.2.	Group 5 REDOX Sludge Selected Samples and Targeted Masses from 222S Archive.....	2.4
2.3.	Selection of Group 6 S-Saltcake Tanks	2.5
2.4.	Group 6 S-Saltcake Selected Samples and Targeted Masses from 222S Archive.....	2.6
3.1.	Group 5- REDOX Sludge Sample Masses	3.2
3.2.	Net Sample Masses, Slurry Volumes, and Settled-Solids Volumes for Group 5 Homogenized REDOX Sludge Aliquots.....	3.9
3.3.	Group 6- S-Saltcake Sample Masses	3.11
3.4.	Net Sample Masses, Slurry Volumes, and Settled Solids Volumes for Group 6 S-Saltcake Homogenized Samples	3.18
3.5.	Sub-Sampling of the Group 6 S-Saltcake Combined Solids Slurry.....	3.19
4.1.	Vane and Cup and Rotor Measuring System Dimensions.....	4.6
4.2.	Optical Properties Applied To Test Materials	4.12
4.3.	Prototypic Particle-Size Analysis Test Matrix.....	4.12
5.1.	Physical Property Measurements of Homogenized Group 5 REDOX Sludge	5.1
5.2.	Shear Strength of Group 5 REDOX Sludge Initial Characterization Settled Solids.....	5.2
5.3.	Best Fit of Select Rheological Models to Group 5 REDOX Sludge Flow Curve Data	5.5
5.4.	Apparent Viscosity of Group 5 REDOX Sludge Sample G5-RH-2 at 33 s-1	5.6
5.5.	Radionuclide Characterization of the Group 5 REDOX Sludge.....	5.8
5.6.	Chemical Characterization of the Group 5 REDOX Sludge.....	5.9
5.7.	Phase Distribution of Selected Analytes in Group 5 REDOX Sludge.....	5.11
5.8.	Summary of Results for Group 5 REDOX Sludge Particle-Size Analysis.....	5.12
5.9.	Weight Percent of Group 5 REDOX Sludge Mineral Phases, Best Estimate.....	5.16
6.1.	Physical-Property Measurements of Group 6 S-Saltcake Composited Solids.....	6.2

<u>No.</u>	<u>Table Caption</u>	<u>Page</u>
6.2.	Newtonian Viscosities for Group 6 S-Saltcake Slurry Sample TI490-G6-AR-RH	6.5
6.3.	Apparent Viscosity of Group 6 S-Saltcake Slurry Sample TI490-G6-AR-RH at 33 s ⁻¹	6.7
6.4.	Viscosity of Group 6 S-Saltcake Supernate Sample TI488-G6-AR-J2 as a Function of Temperature	6.9
6.5.	Radionuclide Characterization of the Group 6 S-Saltcake Washed Solids.....	6.10
6.6.	Chemical Characterization of the Group 6 S-Saltcake Washed Solids.....	6.11
6.7.	Phase Distribution of Selected Analytes in Group 6 S-Saltcake	6.13
6.8.	Group 6 S-Saltcake Solids Particle-Size Analysis Summary	6.14
6.9.	Weight Percent of Crystalline Phases of Group 6 S-Saltcake Washed Solids, Best Estimate.....	6.18
7.1.	Group 5 Caustic Leaching Conditions.....	7.2
7.2.	Oxidative Leaching Conditions for Group 6 S-Saltcake Caustic-Leached Solids.....	7.7
8.1.	Time to Achieve 95 Wt% Al Reduction in Group 5 REDOX Sludge	8.5
8.2.	Initial Al (Boehmite) Dissolution Rates	8.8
8.3.	Boehmite Dissolution Rate Constants	8.12
8.4.	Comparison of Cr(VI) and Total Cr Concentrations	8.18
8.5.	Group 5 REDOX Sludge Leaching Final Aqueous Phase Conditions	8.19
8.6.	Solids Wash Solution Composition	8.20
8.7.	Group 5 REDOX Sludge Leached Solids Composition and Leach Factors (Dry Mass Basis)	8.21
8.8.	Group 5 REDOX Sludge Caustic Leached Sample Particle-Size Analysis Summary	8.24
8.9.	Estimated Weight Percent of Mineral Phases in the Caustic-Leached and Washed Group 5 REDOX Sludge Solids.....	8.31
9.1.	Group 6 S-Saltcake Solids Caustic Leach Supernatant and Wash Compositions	9.2
9.2.	Density Measurements of Aqueous Fractions Following Caustic Leaching	9.3
9.3.	Solids Composition of Group 6 S-Saltcake (Water-Insoluble Solids) Before and After Caustic-Leaching	9.3
9.4.	Group 6 S-Saltcake Equilibrium Aqueous Phase Conditions Following Oxidative Leaching	9.9
9.5.	Group 6 S-Saltcake Solids Wash Composition Following Oxidative Leaching.....	9.10
9.6.	Leached Solids Composition and Leach Factors of Group 6 S-Saltcake (Water-Insoluble Solids).....	9.11
9.7.	Summary of Results for Group 6 S-Saltcake Solids Parametric Testing Particle Size Analysis....	9.14
10.1.	Summary of Major Properties and Analytes of Group 5 REDOX Sludge and Group 6 S-Saltcake	10.3
10.2.	Initial Al (Boehmite) Dissolution Rates	10.4
10.3.	Composition of Caustic-Leached Solids from Group 5 REDOX Sludge with Leach Factors of Selected Analytes (3 M NaOH, 90°C, 170 hrs).....	10.4

<u>No.</u>	<u>Table Caption</u>	<u>Page</u>
10.4.	Composition of Leached Solids from Group 6 S-Saltcake with Leach Factors of Selected Analytes (caustic leach at 3 M NaOH and 100°C; oxidative leach at 1.25 M NaOH, 25°C, 24 hrs, Mn/Cr mole ratio of 1).....	10.5

Abbreviation/Acronym List

ASO	Analytical Support Organization
ASR	Analytical Service Request
ATL	Advanced Technologies and Laboratories, International Inc.
BBI	Best Basis Inventory
BET	(Brunauer, Emmett, and Teller) surface area analysis technique
BNI	Bechtel National, Incorporated
BS	blank spike
CAR	corrective action report
CCD	charged coupled device
CCN	corporate correspondence number (BNI)
CF	concentration factor
CUF	cell unit filter
CWP	PUREX cladding waste
CWR	REDOX cladding waste
DI	deionized (water)
DOE	U.S. Department of Energy
DTA	differential thermal analysis
EDS	energy-dispersive spectroscopy
EELS	electron energy-loss spectroscopy
EFRT	external flowsheet review team
EFTEM	energy-filtered transmission electron microscopy
EQL	estimated quantitation limit
FTIR	Fourier transform infrared
GEA	gamma energy analysis
GIF	Gatan Imaging Filter
HAADF	high-angle annular dark-field detector
HDPE	high-density polyethylene
HLRF	High-Level Radiochemistry Facility
HLW	high-level waste
IC	ion chromatography
ICDD	International Centre for Diffraction Data
ICP	inductively coupled plasma
KPA	kinetic phosphorescence analysis
LAW	low activity waste
LCS	laboratory control sample
LEPS	low-energy photon spectroscopy
M&TE	measuring and test equipment
MDL	minimum detection limit
MS	matrix spike
NIST	National Institute for Standards and Technology
OES	optical emission spectrometry
ORP	Office of River Protection
PB	preparation blank

PNNL	Pacific Northwest National Laboratory
PSD	particle size distribution
PTF	pretreatment facility
PUREX	plutonium-uranium extraction
QA	quality assurance
QAP	Quality Assurance Plan
QAPjP	quality assurance project plan
QARD	Quality Assurance Requirements and Description
QC	quality control
R&T	research and technology
REDOX	reduction-oxidation
RI	refractive index
RIR	relative intensity ratio
RPD	relative percent difference
RPL	Radiochemical Processing Laboratory
RPM	revolutions per minute
RPP	River Protection Project
RSD	relative standard deviation
SBMS	Standards-Based Management System
SEM	scanning electron microscopy
SEM	scanning electron microscopy
SORWT	Sort on Radioactive Waste Type
STEM	scanning transmission electron microscopy
TBP	tributyl phosphate
TDS	total dissolved solids
TEM	transmission electron microscopy
TG	thermal gravimetric
TGA	thermogravimetric analysis
TIC	total inorganic carbon
TOC	total organic carbon
TP	test plan
TWINS	Tank-Waste Information Network System
UDS	undissolved solids
UV	ultraviolet
UV/vis	ultraviolet visible
WCS	wet centrifuged solids
WTP	Hanford Tank Waste Treatment and Immobilization Plant
XPS	X-ray photoelectron spectroscopy
XRD	X-ray diffraction

References

- Agnew SF. 1997. *Hanford Tank Chemical and Radionuclide Inventories: HDW Model Rev. 4*. LA-UR-96-3860, Los Alamos National Laboratory, Los Alamos, NM.
- Barnes HA, and NQ Dzuy. 2001. "Rotating Vane Rheometry - A Review." *Journal of Non-Newtonian Fluid Mechanics* 98(1):1-14.
- Falcoiola L, PR Mussini, T Mussini, S Pozzi, and S Rondinini. 2003. "A Thermodynamic Study of the Aqueous (Sodium Chloride + Sodium Hydroxide) Electrolyte Using Sodium Amalgam and Thallous Chloride Electrode Cells." *J. Chem. Thermodynamics* 35:405-416.
- Farinato RS, and Dubin PL. 1999. *Colloid-Polymer Interactions: From Fundamentals to Practice*. John Wiley & Sons, Inc., New York, NY.
- Fedoseev AM, NA Budantseva, AB Yusov, VP Shilov, and CH Delegard. 2002. "Selective Recovery of Chromium from Precipitates Containing d Elements and Actinides: I. Effect of O₂." *Radiochemistry* 44(4):318-324.
- Garvie LAJ, and AJ Craven. 1994. "Use of Electron-Energy Loss Near Edge Fine Structure in the Study of Minerals." *American Mineralogist* 79:411-425.
- Gong X, Z Nie, M Qian, J Liu, LA Pederson, DT Hobbs, and NG McDuffie. 2002. *Gibbsite to Boehmite Transformation in Strongly Caustic and Nitrate Environments*. WSRC-MS-2002-00850, Westinghouse Savannah River Company, Aiken, SC.
- Hill JG, and BC Simpson. 1994. *The Sort On Radioactive Waste Type Model: A Method to Sort Single Shell Tanks into Characteristic Groups*. PNL-9814, Pacific Northwest Laboratory, Richland, WA.
- Hunt RD, JL Collins, and CW Chase. 1998. *Water Washes and Caustic Leaches of Sludge from Hanford Tank S-101 and Water Washed of Sludge from Hanford Tank C-103*. ORNL/TM-13655, Oak Ridge National Laboratory, Oak Ridge, TN.
- Kaminski MD, NM Dimitrijevic, CJ Mertz, and MM Goldberg. 2005. "Colloids from the aqueous corrosion of uranium nuclear fuel." *Journal of Nuclear Materials* 347:77-87.
- Klug HP, and LE Alexander. 1974. *X-Ray Diffraction Procedures for Polycrystalline and Amorphous Materials*. John Wiley & Sons, Inc., New York, NY.
- Lumetta GJ and BM Rapko. 1999. "Removal of Chromium from Hanford Tank Sludges." *Sep. Sci. Technol.* 34:1495-1506.
- Lumetta GJ, BM Rapko, J Liu, DJ Temer, and RD Hunt. 1998. *Washing and Caustic Leaching of Hanford Tank Sludge: Results of FY 1998 Studies*. PNNL-12026, Pacific Northwest National Laboratory, Richland, WA.
- Lumetta GJ, BM Rapko, MJ Wagner, J Liu, and YL Chen. 1996. *Washing and Caustic Leaching of Hanford Tank Sludges: Results of FY 1996 Studies*. PNNL-11278, Rev.1, Pacific Northwest National Laboratory, Richland, WA.

Lumetta GJ, I Burgeson, MJ Wagner, J Liu, and YL Chen. 1997. *Washing and Caustic Leaching of Hanford Tank Sludge: Results of FY1997 Studies*. PNNL-11636, Rev 1, Pacific Northwest National Laboratory, Richland, WA.

Lumetta GJ, KJ Carson, LP Darnell, LR Greenwood, FV Hoopes, RL Sell, SI Sinkov, CZ Soderquist, MW Urie, and JJ Wagner. 2001. *Caustic Leaching of Hanford Tank S-110 Sludge*. PNNL-13702, Pacific Northwest National Laboratory, Richland, WA.

Lumpkin GR, KL Smith, MG Blackford, R Giere, and CT Williams. 1994. "Determination of 25 Elements in the Complex Oxide Mineral Zirconolite by Analytical Electron Microscopy." *Micron* 25:581-587.

Malvern Instruments Ltd. 1997. *Sample Dispersion and Refractive Index Guide*. MAN 0079, Version 3.1. Worcestershire, England.

Meacham JE. 2003. *Aluminum Wash and Leach Factors*. RPP-11079, Rev. 0, CH2MHill Hanford Group, Richland, WA.

Music S, Dstrok. Dragcevic, S Popovic, and N Vdovic. 1998. "Microstructural Properties of Boehmite Formed Under Hydrothermal Conditions." *Materials Science and Engineering B* 52(2-3):145-153.

Panias D, P Asimidis, and I Paspaliaris. 2001. "Solubility of Boehmite in Concentrated Sodium Hydroxide Solutions: Model Development and Assessment." *Hydrometallurgy* 59(1):15-29.

Rapko, BM, GJ Lumetta, JR Deschane, and RA Peterson. 2007. *Process Development for Permanganate Addition During Oxidative Leaching of Hanford Tank Sludge Simulants*. PNNL-16794 (WTP-RPT-164) Battelle—Pacific Northwest Division, Richland, WA. (WTP Doc. No. 24590-QL-HC9-WA49-00001-03-00002.)

Rapko BM, GJ Lumetta, JD Vienna, and SK Fiskum. 2005. *Oxidative Alkaline Leaching of SX-101 and SY-102 and Its Impact on Immobilized High Level Waste*. PNWD-3600 (WTP-RPT-137), Battelle—Pacific Northwest Division, Richland, WA. (WTP Doc. No. 24590-101-TSA-W000-0004-168-00002 Rev. 00A.)

Rapko, BM, JGH Geeting, SI Sinkov, and JD Vienna. 2004. *Oxidative-Alkaline Leaching of Washed 241-SY-102 and 241-SX-101 Tank Sludges*. PNWD-3512 (WTP-RPT-117), Battelle—Pacific Northwest Division, Richland, WA. (WTP Doc. No. 24590-101-TSA-W000-0004-99-00012 Rev. 00A.)

Rapko BM and JD Vienna. 2002. *Selective Leaching of Chromium from Hanford Tank Sludge 241-U-108*. PNNL-14019, Pacific Northwest National Laboratory, Richland, WA.

Rapko BM, JD Vienna, SI Sinkov, J Kim, and AJ Cisar. 2002. *Alkaline Leaching of Key, Non-Radioactive Components from Simulants and Hanford Tank Sludge 241-S-110: Results of FY 01 Studies*. PNNL-14018, Pacific Northwest National Laboratory, Richland, WA.

Rapko BM. 1998. *Oxidative Alkaline Dissolution of Chromium from Hanford Tank Sludges: Results of FY 98 Studies*. PNNL-11908, Pacific Northwest National Laboratory, Richland, WA.

Scotford RF, and JR Glastonbury. 1971. "Effect of Temperature on the Rates of Dissolution of Gibbsite and Boehmite." *Can. J. Chem. Eng.* 49:611-616.

Steffe JF. 1996. *Rheological Methods in Food Process Engineering*. Freeman Press, East Lansing, MI.

Tingey JM, JD Berg, KD Keefer, AS Lea, DR Rector, JW Virden, and S Stenkamp. 1999. *Final Report: Colloidal Agglomerates in Tank Sludge: Impact on Waste Processing*. Environmental Management Science Program, Project No. 54628.

Tromans D and JA Meech. 2002. "Enhanced Dissolution of Minerals: Conjoint Effects of Particle Size and Microtopography." *Minerals Eng.* 15:263-269.

Testing Summary

A testing program evaluating actual tank waste was developed in response to Task 4 from the M-12 External Flowsheet Review Team (EFRT) issue response plan^(a) and Test Specification 24590-PTF-TSP-RT-06-003 Rev. 1.^(b) The test program was subdivided into logical increments. The bulk water-insoluble solid wastes that are anticipated to be delivered to the Waste Treatment and Immobilization Plant (WTP) were identified according to type such that the actual waste testing could be targeted to the relevant categories. Eight broad waste groupings were defined. Samples available from the 222S archive were identified and obtained for testing. The actual waste-testing program included homogenizing the samples by group, characterizing the solids and aqueous phases, and performing parametric leaching tests.

Two of the eight defined groups—reduction-oxidation (REDOX) sludge (Group 5) and S-saltcake (Group 6)—are the subjects of this report. The Group 5 waste was anticipated to be high in boehmite, whereas the Group 6 waste was anticipated to contain a significant fraction of water-insoluble chromium. Thus the focus of the Group 5 testing was on determining the behavior of Al dissolution during caustic leaching and the focus of the Group 6 testing was the oxidative removal of Cr. The waste-type definition, archived sample conditions, homogenization activities, characterization (physical, chemical, radioisotope, and crystal habit), and caustic leach behavior (Group 5) and oxidative leach behavior (Group 6) as functions of time, temperature, and hydroxide concentration are discussed in this report. Testing was conducted according to TP-RPP-WTP-467.^(c)

Objectives

The test objectives are summarized in Table S.1 along with a discussion of how the objectives were met. Several objectives (in gray shading lighter than header shading) did not specifically apply to the scope provided in this report; they will be reported in companion reports as indicated in the controlling test plan.

Table S.1. Test Objectives

Test Objective	Objective Met? (Y/N)	Discussion
1) Determine the physical and chemical characteristics (summarized in Section 6.2.2 of the test plan) relevant to leaching and ultrafiltration behaviors of actual waste samples required for the validation of simulants.	Y	The following characterizations were conducted on the washed solids for Group 5 and Group 6: <ul style="list-style-type: none"> • solids chemical composition • mineral composition • particle-size distribution • crystal habit and morphology • slurry density • slurry rheology, flow curve, and shear strength

- (a) SM Barnes, and R Voke. 2006. “Issue Response Plan for Implementation of External Flowsheet Review Team (EFRT) Recommendations - M12: Undemonstrated Leaching Process.” 24590-WTP-PL-ENG-06-0024 Rev. 0.
- (b) PS Sundar. 2006. *Characterization and Small Scale Testing of Hanford Wastes to Support the Development and Demonstration of Leaching and Ultrafiltration Pretreatment Processes.* 24590-PTF-TSP-RT-06-003 Rev. 1.
- (c) SK Fiskum. 2007. *Characterization and Small Scale Testing of Hanford Wastes to Support the Development and Demonstration of Leaching and Ultrafiltration Pretreatment Processes.* TP-RPP-WTP-467, Rev. 0, 2/2/07 and Rev. 1, 7/31/07. 24590-QL-HC9-WA49-00001-02-00006.

Test Objective	Objective Met? (Y/N)	Discussion
		<ul style="list-style-type: none"> settling rate (for Group 6 only), fraction of settled solids, fraction of centrifuged solids. The results are summarized in Sections 5 and 6.
2) Determine the dissolution rate of aluminum in the actual waste samples, present predominantly as gibbsite, as a function of temperature, free hydroxide concentration, and over a range of sodium concentrations of interest to the caustic leaching process.	NA	This is not applicable for Groups 5 and 6 because gibbsite is not a major component of these wastes. The gibbsite dissolution parameters will be provided in the Group 3 (plutonium-uranium extraction [PUREX] Cladding Waste) and Group 4 (REDOX Cladding Waste) report.
3) Determine the dissolution rate of aluminum in the actual waste samples, present predominantly as boehmite, as a function of temperature, free hydroxide concentration, and over a range of sodium concentrations of interest to the caustic leaching process.	Y	Group 5 is a high-Al waste type, primarily boehmite. Parametric leach testing was conducted on small (~1-g) aliquots of this waste to determine the boehmite dissolution rate. Variable parameters included temperature (80, 90, and 100°C), time (through 170 h), sodium nitrate concentration (1 and 5 M added to 3 M sodium hydroxide matrix), and hydroxide concentration (1, 3, and 5 M). Dissolution kinetics are also discussed. Results are summarized in Section 8.
4) Determine the dissolution rate of chromium and the extent of dissolution of plutonium and other safety related constituents (U, Fe, Mn, Ni, and Zn) in the actual waste samples as functions of temperature and over a range of NaOH concentrations of interest for oxidative leaching. (The NaMnO ₄ dosage will be predetermined for the oxidation of the chromium in the waste solids.)	Y	Group 6 is a high-chromium waste. Parametric leach testing was conducted on small (~0.53-g) aliquots of this waste following initial caustic leaching. Variable parameters included temperature (25 and 50°C), permanganate dosage (0.75, 1.0, and 1.25 Mn:Cr mole ratio), oxidation time (through 24 h), and hydroxide concentration (0.25, 1.25, and 3 M). The Cr dissolution rate and Pu mobilization are reported as functions of these parameters. The mobilization of other safety-related components, including U, Fe, Mn, Ni, Cd, and B, was also evaluated and reported. Results are summarized in Section 9.
5) Determine the dissolution/reaction rate of phosphates in the actual waste samples as a function of temperature and over a range of NaOH concentrations of interest for the caustic leaching process as well as the extent of dissolution during post-leaching wash.	NA	The wastes tested in this report were not high phosphate wastes. The phosphate dissolution parametric testing will be generated from a different waste type and reported in the appropriate waste-specific report.
6) Determine ultrafiltration flux before and after caustic and oxidative leaching over the operating range of solids concentrations during the leaching processes at 25°C when sufficient actual waste sample is	NA	The filtration testing will be reported separately.

Test Objective	Objective Met? (Y/N)	Discussion
available for testing of the filtration behavior.		
7) Scanning electron microscopy (SEM), transmission electron microscopy (TEM), energy dispersive spectroscopy (EDS) and X-ray diffraction (XRD) will be used to determine the primary mineral forms present for Al, Cr, and P and provide information to enable the correlation of these mineral forms to dissolution behavior.	Y	The primary mineral form of Al in the Group 5 waste was determined from the XRD analysis as boehmite. More details are provided in Section 5. The primary form of Cr in the Group 6 caustic-leached and washed solids was assessed using thermogravimetric analysis as Cr ₂ O ₃ . Details are provided in Appendix D. Phosphorus was not a primary form of these two wastes types.

Test Exceptions

No test exceptions applied to this work.

Results and Performance Against Success Criteria

The test plan delineated several success criteria, which are listed in Table S.2. Selected criteria were relevant to the test scope included in this report; the other criteria that are outside of the reported scope are shaded.

Table S.2. Results and Performance Against Success Criteria

List Success Criteria	Explain How the Tests Did or Did Not Meet the Success Criteria
1) A summary (letter report format) of the available information (including published literature) is provided on the characteristics (both known characteristics and those needed to be determined) relevant to leaching and filtration behaviors of the tank farm waste groupings identified for testing.	Letter report number RPP-WTP-07-705 (J. G. Lumetta and R. T. Hallen, WTP-RPT-151, <i>Review of Caustic Leaching Testing With Hanford Tank Waste Sludges</i>) which addressed this success criterion, was delivered to WTP on 1/24/2007.
2) The physical and chemical characteristics for each of the actual waste-sample composites selected for testing are provided (including a format in conformance with the presentation protocols [24590-WTP-GPG-RTD-001]). The relevant physical and chemical characteristics are elaborated in Test Conditions, Section 6.0, of the test plan.	All physical and chemical characterization testing as defined in the test plan was completed. This included extensive physical and chemical characterization of the homogenized slurry materials and extensive chemical characterization of selected leach solids. The analytical results for each test group are reported in the appropriate report sections.
3) The dissolution rate and the extent of dissolution of aluminum present predominantly as gibbsite in actual waste solids are determined as a function of temperature, free-hydroxide, and sodium	NA

List Success Criteria	Explain How the Tests Did or Did Not Meet the Success Criteria
concentrations. The associated uncertainties in test results are provided.	
4) The dissolution rate and the extent of dissolution of aluminum present predominantly as boehmite in actual waste solids are determined as a function of temperature, free-hydroxide, and sodium concentrations. The associated uncertainties in test results are provided.	<p>The boehmite dissolution rate was evaluated on the Group 5 washed solids by measuring the Al in the leach solution as a function of time (1, 4, 8, 24, 72, and 170 h). The effects of free hydroxide concentration and temperature were assessed. Testing was conducted at three free hydroxide concentrations (1, 3, and 5 M) and at three temperatures (80, 90, and 100°C). One test condition (3 M free hydroxide at 90°C) was conducted in triplicate to assess overall test precision. The effect of NaNO₃ concentration on boehmite leaching was evaluated by adding NaNO₃ to two additional samples by testing at 3 M free hydroxide and at 90°C.</p> <p>Boehmite dissolution-rate constants at each test temperature were calculated, and the activation energy at each free hydroxide concentration was calculated. Results are summarized in Section 8.0.</p>
5) The dissolution rate and the extent of dissolution of chromium in the actual waste solids are determined as a function of temperature and over a range of NaOH concentrations of interest to oxidative leaching. The NaMnO ₄ dosage will be predetermined for the oxidation of the chromium in the waste solids. The associated uncertainties in the test results are provided.	<p>Chromium dissolution was evaluated on the caustic-leached and rinsed Group 6 solids by measuring the Cr in the leach solution as a function of time (0.5, 1, 2, 4, 6, and 24 h). The effects of permanganate oxidant dosage, free hydroxide concentration, and temperature were assessed. Testing was conducted at three Mn:Cr mole ratios (0.75, 1.0, and 1.25) each at three free hydroxide concentrations (0.25, 1.25, and 3 M). The effect of temperature (25 and 50°C) was evaluated at two hydroxide concentrations (0.25 and 3 M) and the three oxidant dosages. One test condition (1.25 M free hydroxide, Mn:Cr mole ratio of 1 at 25°C) was conducted in triplicate to assess overall test precision. Results are summarized in Section 9.0.</p>
6) The dissolution rate and the extent of dissolution of phosphates in the actual waste solids are determined as a function of temperature and NaOH concentration along with the uncertainty in these estimates.	NA
7) The ultrafiltration flux before and after caustic and, as applicable, oxidative leaching (reconcentration, if sufficient solids are available) over the operating range of solids concentrations with the actual waste samples at 25°C is defined when available sample size is adequate for the testing.	NA
8) Determination of the primary mineral forms present for Al, Cr, and P, and a qualitative correlation of the dissolution behavior of these	Two phases of Al were identified in the Group 5 sludge, and two additional phases were conjectured based on chemistry. Approximately 90% of the Al mass was

List Success Criteria	Explain How the Tests Did or Did Not Meet the Success Criteria
waste elements to the mineral forms identified.	<p>present as boehmite in the Group 5 sludge. The dissolution behavior of the Al in Group 5 was largely attributed to boehmite. This is discussed in Section 8.0.</p> <p>The Cr mineral form in the Group 6 solids was more difficult to discern. Thermogravimetric analysis indicated it was probably an amorphous form of Cr₂O₃. This formulation was supported by the mass-balance evaluation of the washed solids data from initial characterization.</p> <p>The phosphorus form was not the subject of these two waste groupings; it will be addressed in the bismuth-phosphate sludge and saltcake evaluation.</p> <p>The dissolution rate of the boehmite and chromium were addressed in Success Criteria #5.</p>

Quality Requirements

Pacific Northwest National Laboratory (PNNL) is operated by Battelle for the U.S. Department of Energy. PNNL implements a Quality Assurance Program that is based upon the requirements as defined in the U.S. Department of Energy (DOE) Order 414.1C, Quality Assurance and 10 CFR 830, Energy/Nuclear Safety Management, Subpart A—Quality Assurance Requirements. PNNL has chosen to implement the requirements of DOE Order 414.1C and 10 CFR 830, Subpart A by integrating them into the laboratory’s management systems and daily operating processes. The procedures necessary to implement the requirements are documented through the laboratory’s Standards-Based Management System (SBMS).

PNNL implemented the RPP-WTP quality requirements by performing work in accordance with the *River Protection Project – Waste Treatment Plant Support Program (RPP-WTP) Quality Assurance Plan (RPP-WTP-QA-001, QAP)*. Work was performed to the quality requirements of NQA-1-1989 Part I, Basic and Supplementary Requirements, NQA-2a-1990, Part 2.7, and DOE/RW-0333P, Rev 13, *Quality Assurance Requirements and Descriptions (QARD)*. These quality requirements were implemented through the *River Protection Project – Waste Treatment Plant Support Program (RPP-WTP) Quality Assurance Manual (RPP-WTP-QA-003, QAM)*. The analytical requirements were implemented through RPP-WTP’s Statement of Work (RPP-WTP-QA-005) with the Radiochemical Processing Laboratory (RPL) Analytical Service Operations (ASO).

A matrix that cross-references the NQA-1, NQA-2a, and QARD requirements with the procedures for RPP-WTP work was provided in the test plan TP-RPP-WTP-467. It included justification for those requirements not implemented.

Experiments that were not method-specific were performed in accordance with RPP-WTP’s procedures QA-RPP-WTP-1101 “Scientific Investigations” and QA-RPP-WTP-1201 “Calibration Control System”

so that sufficient data were taken with properly calibrated measuring and test equipment (M&TE) to obtain quality results.

RPP-WTP addressed internal verification and validation activities by conducting an Independent Technical Review of the final data report in accordance with RPP-WTP’s procedure QA-RPP-WTP-604. This review verified that the reported results were traceable, that inferences and conclusions were soundly based, and the reported work satisfied the Test Plan objectives. This review procedure is part of PNNL’s *RPP-WTP Quality Assurance Manual*.

R&T Test Conditions

The R&T test conditions, as defined in the Test Specification,^(a) are summarized in Table S.3.

Table S.3. R&T Test Conditions

List R&T Test Conditions	Were Test Conditions Followed?
1) Selection of actual wastes for testing: the waste samples selected for testing will be from the groupings identified in the resolution of Issue M4.	Yes. Two of the eight waste groupings identified in resolution to Issue M4 were tested: Group 5, REDOX Sludge, and Group 6, S-saltcake.
2) Physical and chemical characterization properties shall be stated and carried out according to the Guideline document 24590-WTP-GPG-RTD-001.	Yes. Physical characterizations, including specific gravity (density), rheology, volume-percent settled solids, and volume-percent centrifuged solids, were determined for both test groups according to the requirements document. The settling rate was only determined for the Group 6 solids slurry; the Group 5 solids composite contained ~85 vol% settled solids, which precluded an appropriate settling test. Chemical characterization was conducted on the supernatant (water used to dissolve and slurry the solids into a workable homogenized composite) on the solids rinsed with three contacts of 1:1 volume ratios of 0.01 M NaOH and on the rinse solution composite.
3) Actual determinations of waste leach kinetics will be carried out in well-mixed conditions. A test matrix will be forwarded to the R&T M12 Issue manager for concurrence before testing. Residual leached and washed solids will be characterized.	Yes. Test matrices for both the boehmite waste (Group 5) caustic leach and chromium waste (Group 6) oxidative leach were forwarded to and approved by the research and technology (R&T) M12 Issue Manager. Actual test conditions are given in Section 7.0 and were compliant with the test matrices.
4) Testing for filtration behavior will be performed.	Not applicable. Filtration testing is not in the scope of this report. It will be reported separately.

(a) PS Sundar. Nov. 2006. *Characterization and Small Scale Testing of Hanford Wastes to Support the Development and Demonstration of Leaching and Ultrafiltration Pretreatment Processes*. 24590-PTF-TSP-RT-06-003, Rev. 1.

Simulant Use

The testing used actual Hanford tank wastes; simulant usage does not apply.

Discrepancies and Follow-on Tests

None.

1.0 Introduction

This is one in a series of reports that define the characterization, parametric leaching, and filtration testing of actual Hanford tank wastes in support of the Hanford Waste Treatment and Immobilization Plant (WTP) pretreatment process development and demonstration. The tests reported here were conducted according to TP-RPP-WTP-467,^(a) which was written in response to Test Specification 24590-PTF-TSP-RT-06-003 Rev. 1.^(b)

1.1 Tank Waste Pretreatment Operations at the WTP

The tank wastes are anticipated to be delivered to WTP largely as slurries of sludge and supernatant. The low-activity waste (LAW) liquid stream will be removed from the solids phase by ultrafiltration in the Pretreatment Facility (PTF). The concentrated high-level waste (HLW) solids may be pretreated using caustic and oxidative leaching processes to dissolve and remove materials (aluminum, chromium, phosphates, and sulfates) that would otherwise limit HLW loading in the immobilized waste glass. During pretreatment, the concentrated HLW solids will be caustic leached, washed, and in the case of high Cr wastes, oxidatively leached and washed once more. The caustic leaching will be conducted to solubilize the aluminum, phosphorus, and sulfur in the HLW solids; the oxidative leaching will be conducted to oxidize the chromium [from Cr(III) to Cr(VI)] using a sodium permanganate (NaMnO_4) solution and dissolve chromate in a mild caustic solution. The HLW solids will be re-concentrated after each leach and wash operation in the ultrafilter.

The current design of the PTF was based on the results for aluminum dissolution (leach factors) from earlier small, bench-scale, caustic leaching tests that were supplied to Bechtel National, Incorporated (BNI) by the U.S. Department of Energy's (DOE's) Office of River Protection (ORP). These studies included small-scale aluminum leaching from tank waste (S-101) previously reported by Hunt et al. (1998) and Lumetta et al. (1997). Only a limited number of small bench-scale oxidative leaching tests using two selected actual waste tank samples (SX-101 and SY-102) with the preferred oxidant NaMnO_4 were carried out to estimate the oxidant dosage and the efficacy of the oxidative leaching process (Rapko et al. 2004; Rapko et al. 2005), but a number of previous studies demonstrated the technical feasibility of the oxidative leaching process (Rapko 1998, Lumetta and Rapko 1999, Rapko and Vienna 2002, Rapko et al. 2002). The testing with actual radioactive wastes has been generally limited to small-scale testing (typically 1 to 10 g) because of limited sample availability and personnel safety associated with sample handling.

1.2 Issues Identified by the External Flowsheet Review Team

A team of foremost experts from industry, national laboratories, and universities (referred to as the External Flowsheet Review Team or EFRT) was assembled by BNI in October of 2005 to conduct an in-

(a) SK Fiskum, TP-RPP-WTP-467, Rev. 0, 2/2/07 and Rev. 1, 7/31/07, *Characterization and Small Scale Testing of Hanford Wastes to Support the Development and Demonstration of Leaching and Ultrafiltration Pretreatment Processes*.

(b) PS Sundar. 2006. 24590-PTF-TSP-RT-06-003 Rev. 1, *Characterization and Small Scale Testing of Hanford Wastes to Support the Development and Demonstration of Leaching and Ultrafiltration Pretreatment Processes*.

depth review of the process flowsheet supporting the design of the WTP. The EFRT identified several issues from the critical review of the process flowsheet,^(a,b) including

- Issue M4: The WTP has not demonstrated that its design is sufficiently flexible to reliably process all of the Hanford tank farm wastes at the design throughputs.
- Issue M12: Neither the caustic leaching nor the oxidative leaching process has been demonstrated at greater than bench scale. The small-scale experiments are capable of defining the leaching chemistry. However, they are limited in their capability to predict the effectiveness of these processes without a scale-up demonstration.
- Issue M13: For wastes requiring leaching, a combination of inadequate filter flux and area will likely limit throughput to the HLW or LAW vitrification facilities.

The work scope defined in the TP-RPP-WTP-467 represented the initial portion of the actual waste-testing portion of Task 4 from the M-12 EFRT issue response plan.^(c) The actual tank waste testing work interfaced with responses developed to resolve EFRT Issue M4. In this case, a family of waste groupings representing the behavior of ~75 wt% of the tank-farm water-washed^(d) solids Al, Cr, and phosphate inventory was developed to assist in the design of subsequent testing that will assess the adequacy of the overall flowsheet design to treat the tank-farm wastes. These waste groupings were the basis for selecting actual wastes for the current scope of testing.

Additional EFRT-defined issues were identified that were likely to benefit from the actual waste testing reported herein, including:

- Issue M1: Piping that transports slurries will plug unless it is properly designed to minimize this risk. This design approach has not been followed consistently, which will lead to frequent shutdowns due to line plugging.
- Issue M2: Large, dense particles will accelerate erosive wear in mixing vessels. The effects of such particles on vessel life must be re-evaluated.
- Issue M3: Issues were identified related to mixing-system designs that will result in insufficient mixing and/or extended mixing times. These issues include a design basis that discounts the effects of large particles and of rapidly settling Newtonian slurries. There is also insufficient testing of the selected designs.

(a) WTP Doc. No. 24590-WTP-PL-ENG-06-0008, Rev 0, "Hanford Waste Treatment and Immobilization Plant (WTP) Project Response Plan for Resolution of Issues Identified by the Comprehensive Review of the WTP Flowsheet and Throughput." Lucas, L., March 2006.

(b) WTP Project Doc. No. CCN 132846 "Comprehensive Review of the Hanford Waste Treatment Plant Flowsheet and Throughput - Assessment Conducted by an Independent Team of External Experts." March 2006, chartered by the Hanford Waste Treatment and Immobilization Plant Project at the Direction of the US Department of Energy, Office of Environmental Management, Washington DC.

(c) Barnes, S. M and Voke, R, September 2006, 24590-WTP-PL-ENG-06-0024 Rev. 0, "Issue Response Plan for Implementation of External Flowsheet Review Team (EFRT) Recommendations - M12: Undemonstrated Leaching Process."

(d) Water-washed solids masses were determined from the application of the tank- and component-specific BBI water-wash factor.

- Issue M6: Many of the process operating limits have not been defined. Further testing is required to define process limits for WTP unit operations. Without this more complete understanding of each process, it will be difficult or impossible to define a practical operating range for each unit operation.

1.3 Waste Groupings

The tank waste complexity and history does not lead to easily-discernable targeted groupings. Hill and Simpson (1994) created the Sort on Radioactive Waste Type (SORWT) model that groups the single-shell tank wastes into broad sub-groups according to waste type. Agnew (1997) presented waste forms in tanks based on process history and modeling. The tank waste Best Basis Inventory (BBI) delineates tank waste source identifications as well as specific analytical results according to tank, core, and segment sample. These sources were consulted in an attempt to establish appropriate groupings from which tank waste samples could be selected for testing.

The tank waste groupings derived from the BBI presented the most workable solution to the categorization by tank waste type and component quantity. The BBI information was obtained through the Tank Waste Information Network System.^(a) Components of interest were defined as Al, Cr, phosphate, and sulfate. Oxalate was evaluated because it will recycle (dissolve then re-precipitate) in the pretreatment plant causing extra duty for the filtration unit. Fluoride was included because it could enhance the precipitation of phosphates (as fluorophosphates) during pretreatment operations. Iron was also evaluated because of the issues related to filtration of iron hydroxide. Sodium, although dominant in the sludge and supernatant, was not considered since most of the sodium is present as water-soluble salts.

The BBI categorizes waste in three phases: supernatant, saltcake, and sludge. Table 1.1 provides a summary of the quantities of each of the components of interest in each primary waste phase relative to the entire tank waste inventory.

The BBI also provides wash and leach factors for each component within a tank with no distinction as to the applicability to the actual waste phase. Wash factors are based on the component fraction remaining after contact with water. The leach factors are based on the component fraction remaining after leaching water-washed solids with 3 M NaOH typically at 100°C (Meacham, 2003). The water wash and leach factors appeared to be derived from sludge testing and may not necessarily be applicable to the saltcake. These factors were applied to each waste phase on a tank-by-tank basis to estimate the residual component masses after water washing and after caustic leaching (see Table 1.1). The water-soluble components will likely dissolve during waste retrieval or feed blending. As such, these were not considered in the development of the waste groupings.

The Cr, F, oxalate, and sulfate components are clearly significantly concentrated in the saltcake phase. The Al and Fe are dominant components in the sludge phase. Phosphorus is distributed between the saltcake and sludge, but the majority of the water-insoluble fraction is expected to be in the sludge phase.

(a) BBI was queried on 10/17/07 to generate the reported values.

Table 1.1. Hanford Tank Waste Component Mass (Metric Tons) Inventory Summary

Waste Phase		Al	Cr	F	Fe	Oxalate	Phosphate	Sulfate
Supernatant	Total	1,239	51	48	6	94	299	434
Saltcake	Total	3,060	412	785	217	1,194	2,812	2,887
	After Washing	1,277	282	117	210	756	420	124
	After Leaching ^(a)	578	223	--	208	--	261	94
Sludge	Total	4,442	132	448	1,055	245	2,060	459
	After Washing	3,594	83	109	1,042	128	884	26
	After Leaching ^(a)	1,479	60	--	1,034	--	178	18
"--" indicates no leach factor was provided in BBI. (a) Caustic leaching conditions: 3 M NaOH typically at 100°C (Meacham 2003).								

The BBI-defined saltcake is generally divided into six main categories as a function of waste source: A, B, BY, R, S, and T. There are many more categories for sludge; however, over 70 wt% of the sludge in the tanks is represented by five main groups: 1) bismuth phosphate wastes (1st and 2nd cycle), 2) cladding waste (CWP and CWR), 3) reduction-oxidation (REDOX) waste, 4) tributyl phosphate (TBP) waste, and 5) ferrocyanide waste (FeCN).^(a) Table 1.2 provides a summary of the calculated water-insoluble quantities of each component (after applying the tank-specific and component-specific BBI-defined wash factors) from each of these waste groups. In most cases, the balance of the sludge-component inventory was described as NA^(b) in the BBI.

The S-saltcake accounts for the largest single source of chromium (~46% of the insoluble chromium) and bismuth phosphate saltcakes (BY and T) account for another ~18% of the chromium inventory. The Al inventory is dominated by the REDOX waste and followed by the cladding wastes (CWP and CWR). The REDOX waste type is of particular interest because a significant fraction contains Al as boehmite (a component difficult to leach) whereas much of the other Al inventory is present as gibbsite (easily leached in sodium hydroxide solution). Phosphate is dominated by the bismuth phosphate sludge followed by the TBP waste type.

-
- (a) The ferrocyanide waste grouping was included as a separate category because of its projected high iron content. Iron hydroxide is a particularly difficult matrix for cross-flow filtration, and the extent that the FeCN wastes behave as Fe(OH)₃ is not known. The FeCN sludge has not yet been tested in the cell unit filter (CUF) operations.
- (b) The BBI waste was designated as "NA" if the waste did not correspond to a defined waste type or if the waste layer was a mixture of waste types.

Table 1.2. Water-Insoluble Component Mass (Metric Tons) Inventories as Functions of Waste Type

Waste Type	Al	Cr	F	Fe	Oxalate	Phosphate	Sulfate
Total	4,871	365	226	1,252	884	1,304	149
<i>Saltcake Category</i>							
A	32	35	16	26	166	25	19
B	80	3	45	26	7	37	21
BY	237	46	52	41	269	145	28
R	170	11	<0.1	4	6	1	0.3
S	366	166	1	47	242	58	20
T	384	20	2	65	59	151	35
Balance of salt cake	7	1	<0.1	1	5	4	0.4
<i>Sludge Category</i>							
Bismuth phosphate	218	14	51	280	4	473	11
CWP	815	3	3	57	9	25	1
CWR	471	4	<0.1	17	4	2	<0.1
REDOX	1,433	23	0.1	53	25	9	1
TBP	41	1	1	92	1	228	5
FeCN	54	3	1	93	7	84	1
Balance of sludge	562	36	53	450	77	64	8

The actual tank waste leach testing program was limited to eight groups that would account for the majority of the material to be processed at the WTP. The saltcake categories were limited to two and included waste types that would provide useful Cr leaching data. The sludge groupings keyed in on the Al, sulfate, and phosphate leaching challenges. The groupings and water-washed component distributions are provided in Table 1.3. These eight groups represent ~75 wt% of the materials of interest in the expected feeds to the WTP with respect to leaching (Al, Cr, phosphate, and sulfate). The tank waste groups represent ≥ 50 wt% of the fluoride and oxalate in the inventory; the saltcakes are the most significant source of these materials and in particular, the bismuth phosphate saltcake.

1.4 Simulant Development

BNI plans to carry out process development and scale-up testing to demonstrate the design effectiveness of both the caustic and the oxidative-leaching processes over the entire applicable range of Hanford tank farm wastes.^(a) Scale-up testing will require substantial volumes of feed. Therefore, the development of simulants that mimic the chemical, leaching, and ultrafiltration behaviors over the range observed for actual waste groups is necessary to the process development and demonstration. The characterization and leaching performance data obtained from the actual waste testing will serve as benchmarks for defining the simulant characteristics and behaviors and as a basis for revising the parameters used in evaluating WTP process performance using the appropriate process models.

(a) WTP Doc. No. 24590-WTP-PL-ENG-06-0008, Rev 0, "Hanford Waste Treatment and Immobilization Plant (WTP) Project Response Plan for Resolution of Issues Identified by the Comprehensive Review of the WTP Flowsheet and Throughput." Lucas, L., March 2006.

Table 1.3. Projected Distribution (Weight Percent) of Water-Insoluble Components in the Tank Waste Groupings

Group ID	Type	Al	Cr	F	Fe	Oxalate	Phosphate	Sulfate
1	Bi Phosphate sludge	4	4	22	22	0.5	36	7
2	Bi Phosphate saltcake (BY, T)	13	18	24	8	37	23	42
3	CWP, PUREX Cladding Waste sludge	17	1	1.3	5	1	2	0.4
4	CWR, REDOX Cladding Waste sludge	10	1	<0.1	1	0.4	0.1	<0.1
5	REDOX sludge	29	6	0.1	4	3	1	0.4
6	S - Saltcake (S)	8	46	0.6	4	27	4	14
7	TBP Waste sludge	1	0.4	0.5	7	0.1	17	3
8	FeCN Waste sludge	1	1	0.4	7	1	6	1
	Balance	17	24	51	41	30	10	32
Note: The component values were rounded off; therefore the sums may not add to exactly 100%.								

1.5 Testing of Groups 5 and 6

The characterization and parametric leaching of two of the eight defined groups, REDOX sludge (Group 5) and S-Saltcake (Group 6), are the subject of this report. Aluminum in the tank waste is expected to be largely composed of gibbsite and boehmite, with additional minor phases that include, but are not limited to, sodium aluminosilicate and cancrinite. The Group 5 testing was focused on the boehmite Al phase to better characterize the leaching chemistry of boehmite as found in actual tank waste. Chromium is another component in the solids phase that can limit the HLW loading in the vitrified glass product. The Group 6 testing focused on studying the oxidative leaching of Cr that did not mobilize to the aqueous phase after caustic leaching.

The waste-type definition, sample identification, archived sample conditions, and homogenization activities are discussed. The caustic leaching behavior (Group 5) with specific reference to boehmite and oxidative leaching behavior (Group 6) with specific reference to Cr dissolution as functions of time, temperature, and hydroxide concentration are provided. The physical, chemical, radioisotope, and crystal morphology characterization in the waste before and after leach processing are discussed.

Results from these tests are expected to refine the knowledge base of the tank waste chemical and mineralogical characteristics. Parametric leach testing will 1) provide the leaching behavior of boehmite and insoluble Cr in these specific water-washed waste composites, 2) support follow-on leach and filtration testing, and 3) support simulant component selection.

2.0 Test Sample Selection

The tank waste sample materials representative of the REDOX sludge (high in boehmite) and S-Saltcake (high in Cr) waste groupings were selected from the sample archive located in the 222S building of the Hanford Site. (Retrieval of new sample materials from the tanks would have been prohibitively expensive and was not considered.) Specific sample identification and selection was conducted in a step-wise process as described in this section.

2.1 Group 5—REDOX Sample Selection

REDOX tank waste sludge with a predominant boehmite component was targeted for testing to support the Group 5 boehmite leaching studies. The REDOX wastes that had been subjected to high temperatures as a result of the in-tank storage condition were identified as most likely to contain Al predominantly in the boehmite phase.

The decision process flowchart for selecting tank waste samples is summarized in Figure 2.1(a). The Tank-Waste Information Network System (TWINS) database was queried to identify the tanks containing >90 vol% REDOX waste type. Although S-101 and S-107 are not listed as REDOX tanks in the TWINS database, a large component of the aluminum has been determined to be boehmite (Lumetta et al. 1998 and Lumetta et al. 1996, respectively). Hill and Simpson (1994) have defined these two waste tanks as “REDOX sludge” and “evaporator bottoms” with the sludge component largely associated with REDOX.

The identified tanks were evaluated relative to the historic tank-temperature history. Tanks that were known to have boiled were selected whereas those that did not have a history of boiling were de-selected. The high-temperature storage condition favored boehmite formation (Gong et al. 2002).

The 222S archive sample inventory^(a) was searched for samples from the identified tanks and defined as sludge matrices. The samples were then cross-referenced to the TWINS database to determine if analytical data from the specific samples were available; samples identified as containing >100,000 µg Al per g sludge (wet mass basis) were carried forward in the selection process. Of these samples, those with <5 g material were omitted. The final list of samples was submitted to staff^(b) at CH2MHill for a two-step evaluation process: 1) the samples were confirmed to represent the REDOX waste stream based on the tank strata, core segment, and corresponding characterization results, and 2) the samples were not held for other activities and could be released from the archive.

(a) Personal communication of the inventory database, file “Vials May18,” provided from P Brackenbury, Bechtel, June 2006.

(b) David Place and Bruce Higley, Process Engineers, Process Analysis Organization, CH2MHill.

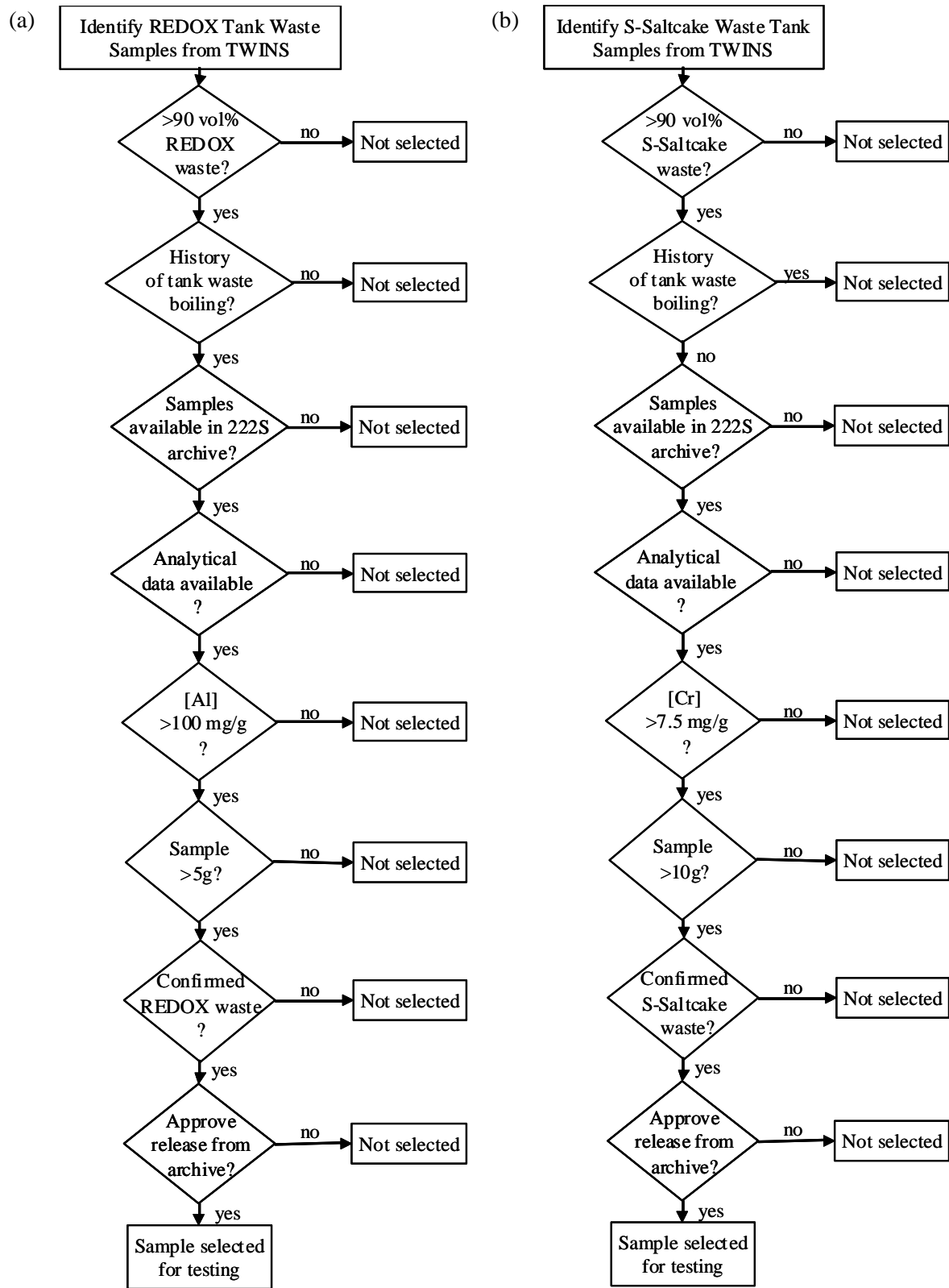


Figure 2.1. Sample Selection Decision Process (a) REDOX Sludge (Group 5), and (b) S-Saltcake (Group 6)

Table 2.1 summarizes the evaluated REDOX tank sources and shows the selection criteria. Samples obtained from tanks identified in bold highlight were those determined to meet all the selection criteria.

Table 2.1. Selection of Group 5 REDOX Sludge Tanks

Tank	REDOX Sludge, kL	Total Sludge, kL	Fraction REDOX Sludge	History of in-tank boiling	222S Archive		
					Available Samples	Identified as Sludge	Analytical Results
241-S-101	(b)	890	(b)				
241-S-102	71	71	1			no ^(a)	
241-S-103	34	34	1		no		
241-S-104	409	500	0.82			no ^(a)	
241-S-105	8	8	1			no ^(a)	
241-S-107	462	1211	0.38^(d)				
241-S-108	19	19	1			no ^(a)	
241-S-109	49	49	1			no ^(a)	
241-S-110	288	364	0.79				
241-S-111	207	245	0.84	no	no		
241-S-112	5	5	1			no ^(a)	
241-SX-101	545	545	1	no		no ^(a)	
241-SX-102	209	209	1	no		no ^(a)	
241-SX-103	294	294	1				
241-SX-104	515	515	1		no		
241-SX-105	238	238	1	no			no
241-SX-107	356	356	1		no		
241-SX-108	280	280	1				(c)
241-SX-109	251	251	1		no		
241-SX-110	184	184	1		no		
241-SX-111	369	369	1		no		
241-SX-112	283	283	1		no		
241-SX-114	478	478	1		no		
241-SX-115	16	16	1		no		
241-TX-101	265	280	0.95				no
241-TX-104	130	130	1	no			
241-TX-106	15	19	0.79		no		no
241-U-101	87	87	1		no		
241-U-102	163	163	1			no ^(a)	
241-U-103	42	42	1			no ^(a)	

(a) TWINS lists samples as “saltcake” or “mix saltcake/sludge”, i.e., not sludge.
(b) Prior testing with S-101 indicated Al is present as boehmite (Lumetta et al. 1998).
(c) Samples <100 mg/g Al.
(d) Prior testing with S-107 indicted Al is present as boehmite (Lumetta et al. 1996).

Table 2.2 summarizes the samples selected from the archive that met the selection criteria. These samples had been in storage at 222-S for ~9 to 12 years. The long storage time could result in alteration of sample characteristics relative to the as-retrieved sample condition through aging and drying.

Table 2.2. Group 5 REDOX Sludge Selected Samples and Targeted Masses from 222S Archive

Tank Sample Date	Jar #	Tank	Core	Segment	Estimated Al, µg/g	Matrix	Net Sample Weight (g)
3/26/1996	9718	S-101	138	6	100,000	Sludge	80.3
	9719	S-101	138	6	100,000	Sludge	97.1
	16905	S-101	138	6	100,000	Sludge	38.7
	9899	S-101	138	7	110,000	Sludge	80.7
	9898	S-101	138	7	110,000	Sludge	76.8
	16953	S-101	138	7	110,000	Sludge	88.2
	15899	S-101	138	7	110,000	Sludge	54.3
	9564	S-101	138	8	120,000	Sludge	72.28
	9815	S-101	138	8	120,000	Sludge	68.09
	9900	S-101	138	9	120,000	Sludge	63.4
	9901	S-101	138	9	120,000	Sludge	61.4
	16914	S-101	138	9	120,000	Sludge	59.1
4/3/1996	9875	S-101	142	6	100,000	Sludge	83.95
	9876	S-101	142	6	100,000	Sludge	61.08
	16673	S-101	142	6	100,000	Sludge	43.2
	16908	S-101	142	6	100,000	Sludge	77.9
	9877	S-101	142	7	110,000	Sludge	84.72
	9878	S-101	142	7	110,000	Sludge	63
	16921	S-101	142	7	110,000	Sludge	95.8
	16925	S-101	142	7	110,000	Sludge	80.6
	9880	S-101	142	8	130,000	Sludge	65.7
	9879	S-101	142	8	130,000	Sludge	49
	15608	S-101	142	8	130,000	Sludge	21.5
9/25/1995	8009	S-107	110	6	100,000	Sludge	60.8
	8010	S-107	110	6	100,000	Sludge	76.2
	13450	S-107	110	6	100,000	Sludge	105.65
9/19/1995	7993	S-107	105	8	100,000	Sludge	7.39
	7995	S-107	105	8	100,000	Sludge	38.2
	13075	S-107	105	8	100,000	Sludge	79.3
6/3/1998	14730	S-110	241	7	200,000	Sludge	48.4
	14727	S-110	241	7	200,000	Sludge	38.7
	14558	S-110	241	7	200,000	Sludge	80.8
	14632	S-110	241	7	200,000	Sludge	129.1
	15000	S-110	241	8	200,000	Sludge	68.4
	14998	S-110	241	8	200,000	Sludge	32.2
5/26/1998	14972	S-110	240	9	120,000	Sludge	16.6
	14601	S-110	240	10	120,000	Sludge	50.4
	14999	S-110	240	10	120,000	Sludge	55.3
	14639	S-110	240	10	120,000	Sludge	9.3
4/28/1998	14468	SX-103	235	11	100,000	Sludge	83.1
	14444	SX-103	235	12A	240,000	Sludge	19.2
5/5/1998	14479	SX-103	239	12	215,000	Sludge	73.2
Sum							2,639

2.2 S-Saltcake Sample Selection

Salt cake tank wastes high in chromium concentration were targeted for testing.

The decision process flowchart for selecting tank waste samples is summarized in Figure 2.1(b). The TWINS database was queried to identify the tanks containing >95 vol% S-Saltcake waste type. The temperature history of the identified tank was evaluated; tanks that had boiled were excluded from consideration to minimize the complexity of removing Al from the matrix as boehmite. The 222S archive sample inventory was searched for samples from the identified tanks; those defined as a saltcake matrix were retained for consideration. These samples were then cross-referenced to the TWINS database to determine if analytical data from the specific samples were available; samples containing >7.5 mg Cr/g saltcake were carried forward. Of these samples, those with >10 g material were selected. The final list of samples was submitted to staff at CH2M Hill for a two-step evaluation process: 1) the samples were confirmed to represent the S-Saltcake waste based on strata from tank and corresponding characterization results, and 2) the samples were not held for other activities and could be released from the archive.

Table 2.3 summarizes the evaluated S-Saltcake tank sources and shows the selection criteria. Samples obtained from tanks identified in bold highlight were those determined to meet all the selection criteria.

Table 2.3. Selection of Group 6 S-Saltcake Tanks

Tank	S-Saltcake, kL	Total Saltcake, kL	S-Saltcake Fraction	History of in-tank boiling?	222S Archive	
					Available Samples	Samples >7.5 mg Cr/g
241-S-101	442	442	1	yes		
241-S-103	858	858	1		no	
241-S-105	1528	1528	1			no
241-S-106	1723	1723	1			
241-S-108	2063	2063	1		no	
241-S-109	1968	1968	1		no	
241-S-110	1109	1109	1	yes		
241-S-111	1152	1152	1			
241-S-112	14	14	1			no
241-SX-102	1083	1083	1			
241-SX-105	1184	1184	1			
241-SX-106	1501	1501	1			
241-SY-101	893	893	1			no
241-SY-103	1203	1203	1			
241-U-103	1366	1366	1			
241-U-106	638	638	1		no	
241-U-108	1531	1531	1			
241-U-109	1249	1249	1			no
241-U-111	742	742	1		no	

Table 2.4 summarizes the samples selected from the archive that met the selection criteria. These samples had been in storage at 222-S for ~7 to 11 years.

Table 2.4. Group 6 S-Saltcake Selected Samples and Targeted Masses from 222S Archive

Tank Sample Date	Jar #	Tank	Core	Segment	Matrix	Estimated Cr, µg/g	Net Sample Weight (g)
2/12/1997	12110	S-106	183	8	Salt	8,700	64.33
4/8/1998	14255	S-111	237	5	Salt	14,900	95.2
	14232	S-111	237	9 (LH)	Salt	8,200	80.55
	14441	S-111	237	9 (LH)	Salt	8,200	47.7
6/30/1998	14644	SX-102	243	2	Salt	8,790	84.3
6/30/1998	14653	SX-102	244	3	Salt	10,600	57.2
2/25/1998	14044	SX-105	229	11	Salt	10,500	117
	14045	SX-105	229	11	Salt	10,500	106.41
	11855	SX-105	229	11	Salt	10,500	49.3
10/13/1997	12895	SX-106	223	7	Salt	9,800	106.6
	12907	SX-106	223	7	Salt	9,800	51.95
	13504	SX-106	223	7	Salt	8,200	97.2
	13505	SX-106	223	7	Salt	8,200	93.42
10/15/1997	19056	SX-106	224	6	Salt	8,300	26.3
	19093	SX-106	224	6	Salt	8,300	22.4
	13642	SX-106	224	6	Salt	8,000	104
	13643	SX-106	224	6	Salt	8,000	85.6
	13645	SX-106	224	8	Salt	7,500	49.68
	13644	SX-106	224	8	Salt	7,500	100.3
	12922	SX-106	224	8	Salt	7,500	111.96
	13646	SX-106	224	9	Salt	8,600	95.1
	19121	SX-106	224	9	Salt	8,600	33.5
3/7/2000	15959	SY-103	280	11	Salt	8,000	231.9
9/30/1996	19292	U-103	182	1	Salt	12,000	13
	19290	U-103	182	1	Salt	12,000	41.7
4/26/1996	10203	U-108	145	9	Salt	7,900	56.9
Sum							2,024
Note: LH indicates lower half of segment.							

3.0 Compositing, Homogenization, and Subdivision

This section summarizes the as-received sample conditions, combination of individual samples into the REDOX Group 5 composite and the S-Saltcake Group 6 composite, homogenization, and composite subdivision.

3.1 REDOX Sludge Group 5

Advanced Technologies and Laboratories, International Inc. (ATL) was contracted to locate, weigh, and package the 42 selected REDOX sludge samples for delivery to the Radiochemical Processing Laboratory (RPL). ATL also evaluated the history of each sample such that the received sample weight could be evaluated relative to the initial mass and interim subsampling activities.^(a)

Table 3.1 provides a summary condition for each sample as follows:

- originating tank
- sample IDs (jar number)
- overall mass loss during storage (accounting for sub-sampling activities) as determined by ATL
- as-received sample condition
- planned net sample masses, based on the 2002 inventory summary^(b)
- documented masses removed from the sample set following the 2002 inventory evaluation
- net masses measured at the 222S facility in 2007
- masses actually transferred to the homogenizer at the RPL.

Three of the selected samples, two from S-107 (#7993 and #13450, combined 113.1 g) and one from S-110 (#14999, 55.3 g) were not available from the 222S archive; they had either been depleted from other sampling activities, or the jars had broken, resulting in loss of sample. Two SX-105 samples (#14468 and 14479) had been sub-sampled after the 2002 inventory, resulting in a depletion of an additional 75 g. After subtracting the masses of the missing and depleted samples, a total mass of 2396 g was expected to be available; the total mass received, 2084 g, was lower than expected by 312 g (13%). The sample-specific difference between the planned mass and the actual mass transferred is provided in terms of grams and as a percentage of the planned mass. Most of this mass loss was attributed to water evaporation from the sample storage jars. Unrecorded sub-sampling events might account for additional sample loss.

(a) Letter from GP Ritenour, March 8, 2007. Reissue 1: Final Report for the Transfer of Group 5 REDOX Samples from the 222S Laboratory Sample Archive to the Radiochemical Processing Laboratory, to LK Jagoda.

(b) Excel file "Vials May 18" provided by P. Brackenbury, personal communication.

Table 3.1. Group 5- REDOX Sludge Sample Masses

Hanford Tank ID	222-S Jar #	Mass Loss During Storage (%)	Sample Condition	Planned Net Mass	Post 2002 Sub- Sampling	2007 Net Mass	Mass to Homogenizer	Difference Between Expected and Transferred Mass	
				(g)	(g)	(g)	(g)	(g)	(%)
S-101	9718	27	ss	80.3	0	62	58.65	21.6	27
S-101	9719	17	ss	97.1	0	90.9	85.62	11.5	12
S-101	16905	8	ss	38.7	0	35.7	33.22	5.5	14
S-101	9899	11	d, f	80.7	0	74	69.98	10.7	13
S-101	9898	16	ss	76.8	0	56.8	53.76	23.0	30
S-101	16953	27	d, c	88.2	0	64.7	63.00	25.2	29
S-101	15899	6	d, c	54.3	0	56.4	40.99	13.3	25
S-101	9564	15	d, c	72.28	0	66.3	63.05	9.23	13
S-101	9815	28	h, d, c	68.09	0	62.4	61.33	6.76	10
S-101	9900	36	d	63.4	0	51.7	51.47	11.9	19
S-101	9901	31	d	61.4	0	57.2	55.92	5.5	9
S-101	16914	17	d, c	59.1	0	49.5	49.23	9.9	17
S-101	9875	11	ss	83.95	0	78	77.16	6.79	8
S-101	9876	16	ss	61.08	0	53.2	52.69	8.39	14
S-101	16673	23	d, c	43.2	0	35.2	32.78	10.4	24
S-101	16908	8	ss	77.9	0	74.8	78.48	-0.6	-1 ^(e)
S-101	9877	20	ss	84.72	0	70.4	62.02	22.70	27
S-101	9878	35	h, d, c	63	0	57.3	54.64	8	13
S-101	16921	10	d	95.8	0	86.5	85.33	10.5	11
S-101	16925	30	h, d	80.6	0	62.2	60.13	20.5	25
S-101	9880	34	h, d, c	65.7	0	53	47.80	17.9	27
S-101	9879	35	h, d, c	49	0	44.2	42.9	6	13
S-101	15608	58	d, c	21.5	0	9.3	2.85	18.6	87
S-107	7993		(c)	7.39	7.39	0	0	0	NA
S-107	7995	27	d	38.2	0	28.3	24.67	13.5	35

Table 3.1 (Contd)

Hanford	222-S	Mass Loss During Storage	Sample	Planned Net Mass	Post 2002 Sub- Sampling	2007 Net Mass	Mass to Homogenizer	Difference Between Expected and Transferred Mass		
								Tank ID	Jar #	(%)
	S-107	13075	22	d, c	79.3	0	65.2	64.19	15.1	19
	S-107	8009	7	d	60.8	0	59.3	56.84	4.0	7
	S-107	8010	2	d	76.2	0	74.6	66.85	9.4	12
	S-107	13450		--	105.65	105.65 ^(a)	0	0	0	NA
	S-110	14972	39	d, p	16.6	0	16.8	15.82	0.8	5
	S-110	14601	28	d, p	50.4	0	53.4	33.76	16.6	33
	S-110	14999		--	55.3	55.3 ^(a)	0	0	0	NA
	S-110	14639	60	d, p	9.3	0	9.4	6.46	2.8	30
	S-110	14730 ^(b)	27	d, c	48.4	0	39.3	38.89	9.5	20
	S-110	14727	21	d, c, f	38.7	0	39.8	39.06	-0.4	-1 ^(e)
	S-110	14558	25	ss	80.8	0	75.8	75.38	5.4	7
	S-110	14632	9	ss	129.1	0	117.5	114.60	14.5	11
	S-110	15000	34	h, d, c	68.4	0	50.3	49.83	18.6	27
	S-110	14998	30	d, c	32.2	0	30.6	23.40	8.8	27
	SX-103	14468	42	d, p	83.1	40	28.3	27.79	15.3	36
	SX-103	14444	30	d, p	19.2	0	17.8	17.44	1.8	9
	SX-103	14479	44	d, c	73.2	35	26 ^(d)	33.11	5.1	13
Sum					2639	243	2084	1971.1	424	18

c = chunk(s); sample was dried into one or more chunks
d = dry solid sample; water was added to soak sample so it could be broken up and removed from the jar for addition to the homogenizer
h = hard
f = foreign material such as pieces of Teflon liner, caps, and rocks present in the sample; foreign material was removed to extent possible before compositing
p = powder consistency
ss = semi-solid, in all cases, the material was extremely viscous
Highlighted and bolded values indicate mass loss exceeding 30%.
(a) The entire sample was removed in prior sampling events.
(b) Sample had been moved from jar #14730 had been re-packed into jar #19884.
(c) Sample #7993 jar broke during preparation for shipping. Sample was lost.
(d) The 2007 net sample mass was suspected to be biased low from replacement of a jar lid.
(e) Negative values were attributed to the uncertainty associated with mass measurement.

Most samples from this group had dried into monolithic chunks during the 7 to 12 years of storage. The average overall mass loss during the storage interval was 25%. Several samples, however, were still moist but very viscous. Photographs of as-received solids are shown in Figure 3.1, Figure 3.2, and Figure 3.3 along with the sample jar number and originating tank identifier. In several cases, jar lid debris was observed on top of the sample material (especially evident in Figure 3.3 #14727). The jar lids succumb to radiolytic degradation during storage. To the extent possible, lid debris was removed before compositing began.

For the most part, the masses transferred into the homogenizer corresponded well with the received masses from 222S. Four samples were associated with large (>30%) mass differences between expected and transferred masses to the homogenizer (see highlighted cells in table). Sample #15608 (S-101) appeared to result in large incremental losses between the expected mass, shipped mass, and transferred mass to the homogenizer—no explanation for the differences was evident. Mass losses associated with the planned mass and the mass transferred to the homogenizer were largely attributed to water evaporation during the long storage period. The sludge residuals that could not be successfully sluiced from the sample jar contributed only a minor fraction to the mass difference.

From the initial planned composite mass of 2.64 kg, a final total mass of 1.97 kg was successfully transferred to the compositing vessel. The tank-basis mass fractionation is shown in Figure 3.4; the masses relate to those measured in the High-Level Radiochemistry Facility (HLRF). The predominant waste source in this composite is tank S-101 at 65 wt%, followed by tank S-110 at 20 wt%.

A step-wise process was applied to transfer the samples to the compositing vessel or the homogenizer.^(a) The dried samples were scraped out into a stainless steel pan and crushed. All materials were then passed through a 1/8-in.-pore-size stainless steel mesh screen fitted to the top of the homogenizer to capture large materials (e.g., gravel). All tank waste materials successfully passed through the screen. Deionized water was used to aid the transfer and hydrate the solids; ~4 liters DI water were added to the solids.

(a) The compositing and homogenization activities were conducted according to Test Instruction TI-RPP-WTP-477, *Group 5 REDOX Hanford Tank Waste Sample Compositing, Homogenization, and Sub-Division*, SK Fiskum, February 5, 2007.

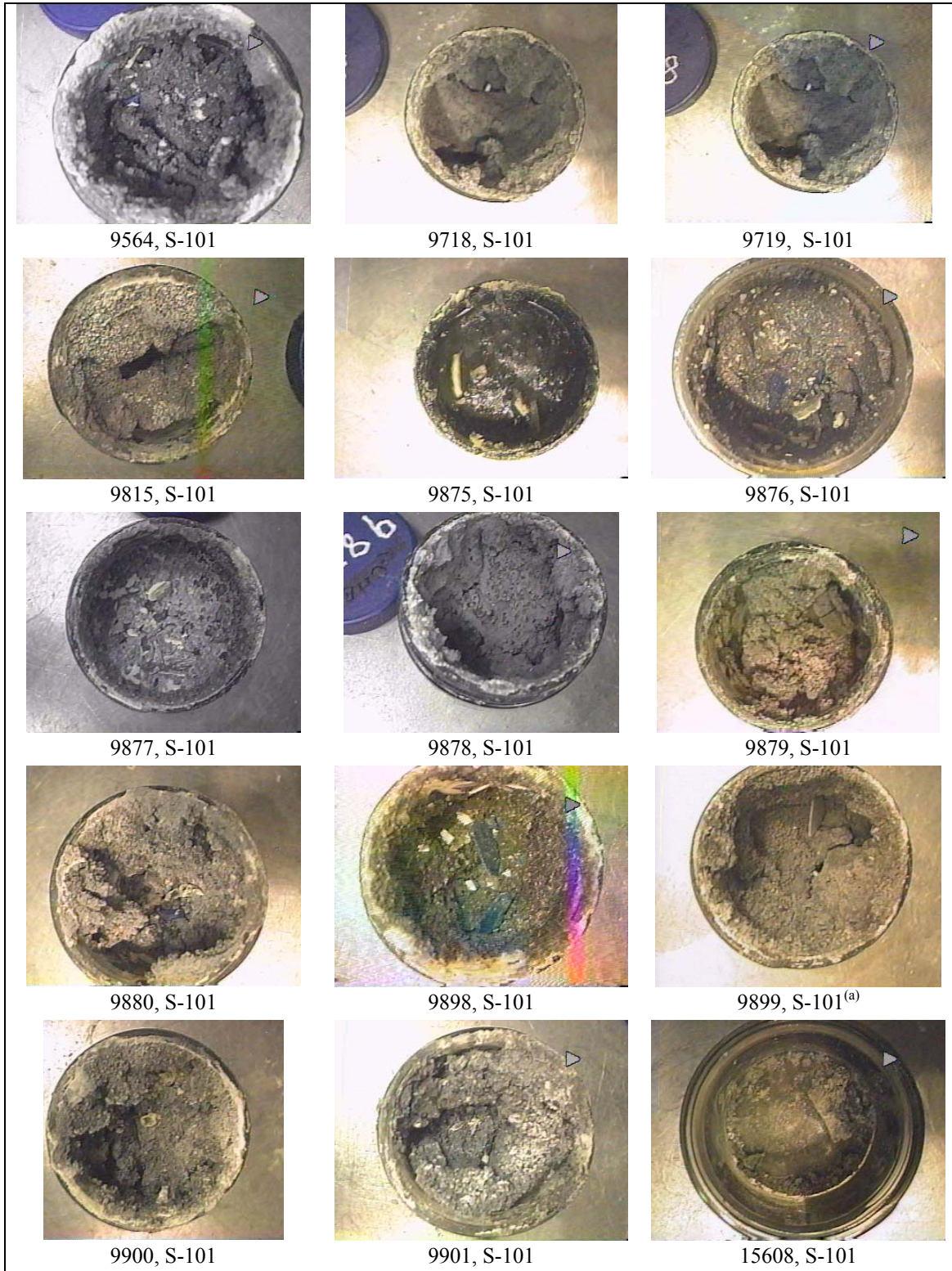


Figure 3.1. Photographs of Group 5 REDOX Sludge S-101 As-Received Samples

(a) Note that photos of sample jars 16953 and 9899 appear identical; it could not be determined which photo was accurate.

(Looking Down into the Jar)

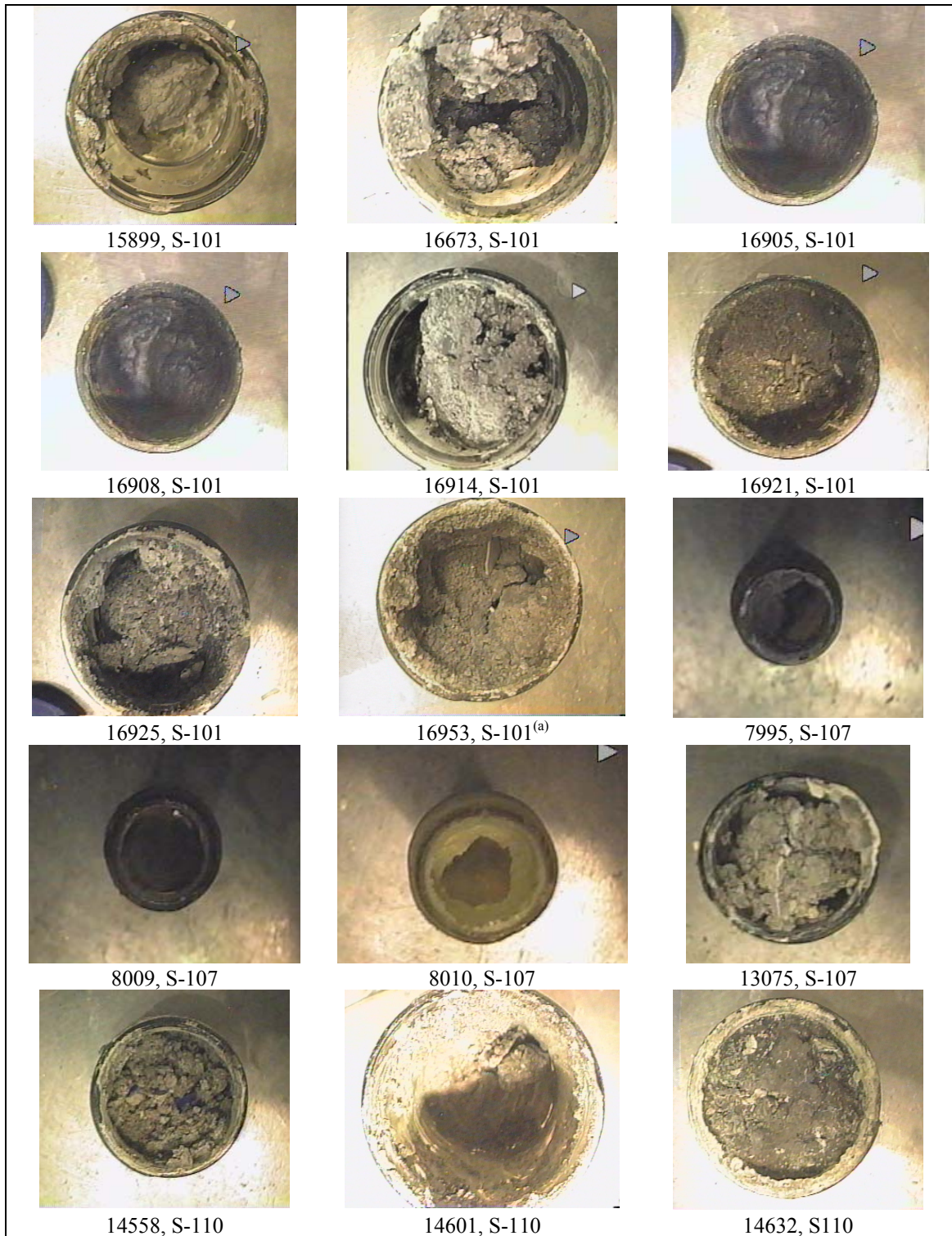


Figure 3.2. Photographs of Group 5 REDOX Sludge S-101, S-107, and S-110 As-Received Samples (Looking Down into the Jar)

(a) Ibid., page 3.5.

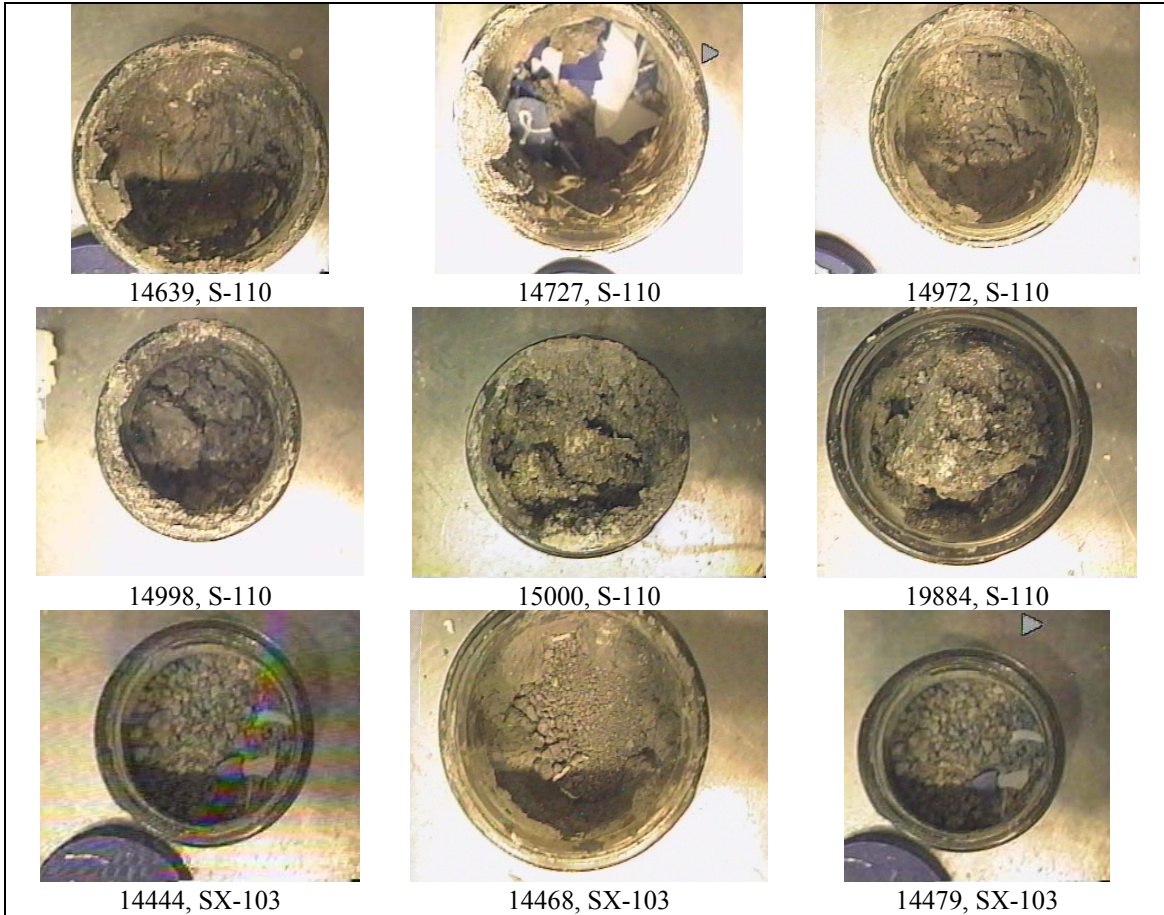


Figure 3.3. Photographs of Group 5 REDOX Sludge S-110 and SX-103 As-Received Samples (Looking Down into the Jar)

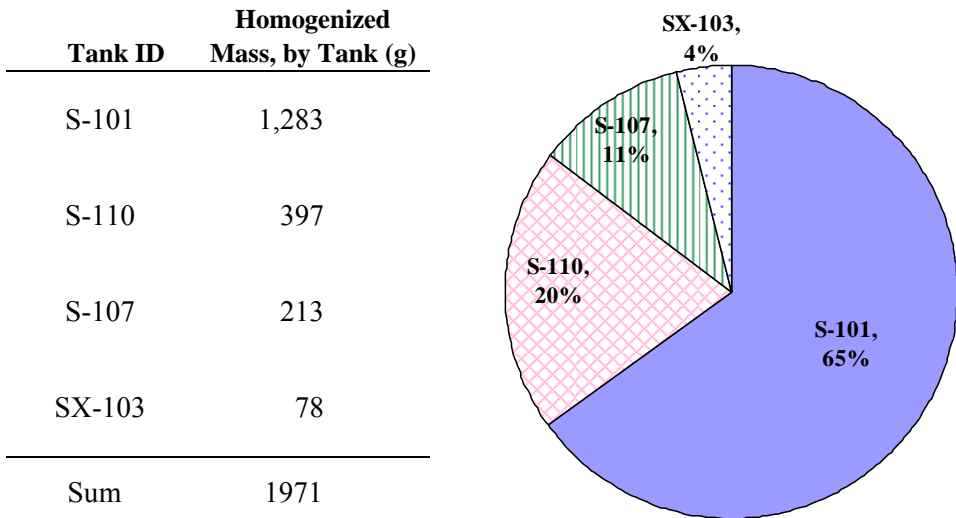
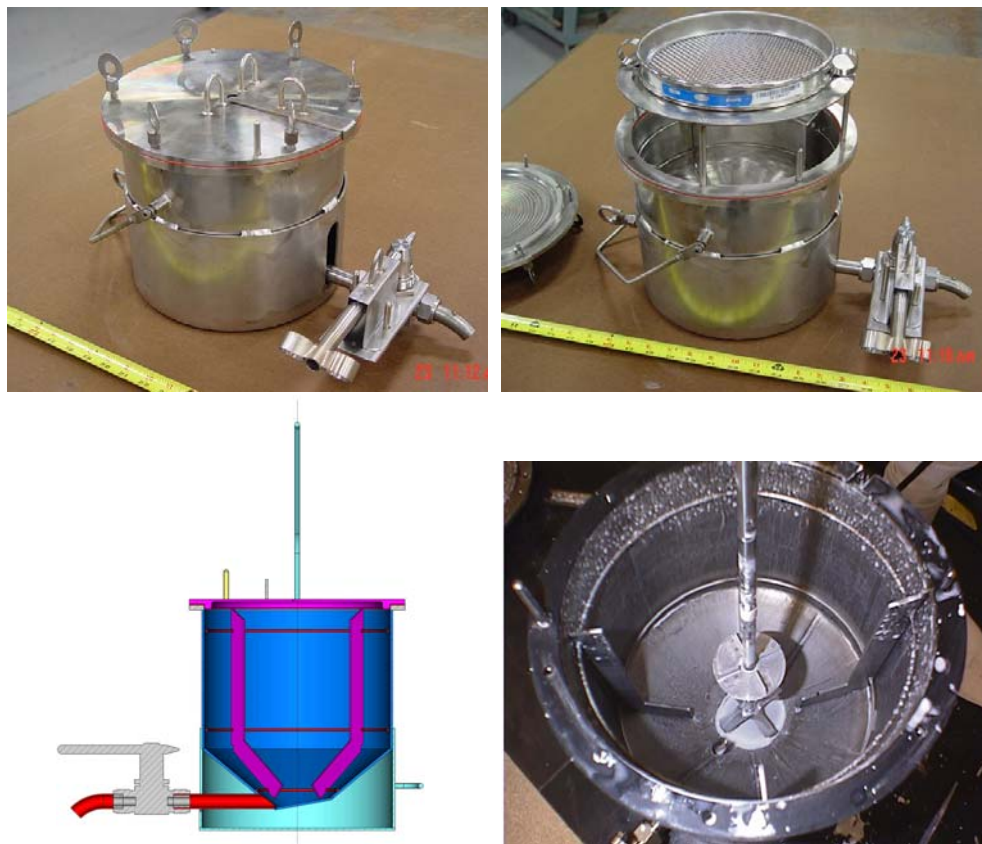


Figure 3.4. Tank Source Distribution of Group 5 REDOX Sludge Composite

The homogenizer, pictured in Figure 3.5, was a 5-L stainless steel baffled vessel equipped with an overhead double-bladed impeller. It was designed to maximize mixing effectiveness of slurry volumes from 1.5 to 5 L in volume. The homogenized slurry was sampled from an opening at the bottom of the homogenizer that was connected to a spigot fitted with a valve.

The wetted solids were mixed 1 h and then allowed to hydrate overnight (~21 h) in the covered homogenizer. (Note that many of the samples had dried during the archival period and a hydration period of ~20 h was considered prudent.) The following morning the mixer was turned back on and the composite was mixed for more than an hour. Material present in the sampling port was then purged by flowing slurry through the port and recycling it back to the top of the tank. The sample port purge was repeated in triplicate just before the start of the sample subdivision. The hydrated solids were then subdivided into sample jars in the order shown in Table 3.2. The net slurry masses, densities, and volume % settled solids after a 5-day settling period are also shown in Table 3.2. The slurry sub-sample densities agreed within 3%, and the volume-percent settled solids averaged 90% with a relative standard deviation of 4%. A total of 4,281 g of slurry (hydrated solids) was recovered after the compositing, homogenization, and sub-sampling processes. The Group 5 sludge composite was a thick, gray slurry with a minimal separable aqueous layer (see Figure 3.6).



Clockwise from top left: with lid in place, with screen in place, cross-section schematic, interior view.

Figure 3.5. RPL Homogenizer

Table 3.2. Net Sample Masses, Slurry Volumes, and Settled-Solids Volumes for Group 5 Homogenized REDOX Sludge Aliquots

Targeted Test	Jar ID	Net Slurry Mass (g)	Total Slurry Volume (mL)	Slurry Density (g/mL)	5-Day Settled Solids Volume %
CUF	TI477-G5-AR-J1 ^(a)	518.85	410	1.28	nm
Phys. Prop.	TI477-G5-AR-S1	21.14	17.8	1.19	90
CUF	TI477-G5-AR-J2	482.89	385	1.25	94
CUF	TI477-G5-AR-J3	495.86	395	1.26	95
Phys. Prop.	TI477-G5-AR-S2	18.30	16.0	1.14	88
Rheology	TI477-G5-AR-RH1	91.22	~75	1.22	87
Chem. analysis	TI477-G5-AR-C1	37.57	29.7	1.26	88
Chem. analysis	TI477-G5-AR-C2	33.74	27.0	1.25	85
Archive	TI477-G5-AR-Arch1	28.36	22.5	1.26	89
CUF	TI477-G5-AR-J4	475.28	375	1.27	94
Parametric leach	TI477-G5-AR-P1 ^(b)	160.30	nm	nm	nm
CUF	TI477-G5-AR-J5	472.19	375	1.26	94
CUF	TI477-G5-AR-J6	451.30	365	1.24	95
CUF	TI477-G5-AR-J7	450.02	365	1.23	95
CUF	TI477-G5-AR-J8	444.17	355	1.25	86
Phys. Prop.	TI477-G5-AR-S3	20.32	16.0	1.27	89
CUF	TI477-G5-AR-J9 ^(c)	79.67	nm	nm	nm
Sum		4281.18	--	Avg.: 1.24	Avg: 91

(a) 1 volume graduation marks were obscured.
 (b) P1 did not contain volume graduation.
 (c) J9 volume was less than the first volume graduation mark.
 nm = not measured



Figure 3.6. Sample TI477-G5-AR-J6

3.2 S-Saltcake Group 6

Advanced Technologies and Laboratories, International Inc. (ATL) was contracted to conduct the Group 6 sample compositing, homogenization, and sub-division.^(a) ATL performed the work according to Pacific Northwest National Laboratory (PNNL) test procedure TPR-RPP-WTP-489^(b) and test instruction TI-RPP-WTP-488^(c) at the 222-S Radiological Hot Cell Facility. The hands-on work for this test instruction was carried out by ATL staff under the direct supervision of PNNL staff during April 2007. ATL provided the sample-specific pedigree summarizing all sub-sampling activities.

Table 3.3 provides a summary condition for each sample as follows:

- sample IDs (jar number)
- originating tank
- overall mass loss during storage (accounting for sub-sampling activities) as determined by ATL^(d)
- as-retrieved sample condition
- planned net sample masses, based on the 2002 inventory summary^(e)
- documented masses removed from the sample set following the 2002 inventory evaluation
- net masses corrected for post-2002 sub-sampling events
- masses actually transferred to the homogenizer at 222S.

(a) Contract was according to PNNL Statement of Work 37270.

(b) LK Jagoda, Procedure for Supervision of Work at 222-S, April 12, 2007.

(c) SK Fiskum, Group 6 S-Saltcake Hanford Tank Waste Sample Compositing, Homogenization, and Sub-Division, April 2007.

(d) HL Anastos and JR Ritenour, Final Report for the Compositing and Transfer of Group 2 Bismuth Phosphate and Group 6 S-Saltcake Samples from the 222S Laboratory to the Radiochemical Processing Laboratory, ATL International Inc., Richland WA, June 26, 2007.

(e) Excel file "Vials May 18" provided by P. Brackenbury, personal communication.

Table 3.3. Group 6- S-Saltcake Sample Masses

Hanford Tank ID	222-S Jar #	Mass Loss During Storage (%)	Sample Condition	Planned Net Mass (g)	Post 2002 Sub-Sampling Mass (g)	Recalculated Expected Net Mass (g)	Mass to Homogenizer (g)	Difference Between Expected and Transferred Mass	
								(g)	(%)
S-106	12110	12	d	68.2	29.9	38.3	30.34	8.0	21
S-111	20103 ^(a)	14	d	30.7	0	30.7	26.44	4.3	14
S-111	14232	32	d	103.6	40.1	63.5	30.19	33.3	52
S-111	14441	23	d	52.7	21.2	31.5	19.57	11.9	38
SX-102	14644	13	w	110.6	20.0	90.6	76.31	14.3	16
SX-102	14653	6	ss; f	79.9	20.0	59.9	55.17	4.8	8
SX-105	11855	3	d	185	132.1	53	46.56	6	11
SX-105	14044	15	ss	123	0	123	105.16	18	15
SX-105	14045	0	depleted	106.4	106.4	0	0	0	NA
SX-106	12895	3	ss	214.9	105.1	109.8	102.68	7.1	6
SX-106	12907	4	d; f	179.4	124.6	54.8	47.63	7.2	13
SX-106	13504	2	w	97.6	0	97.6	95.31	2.3	2
SX-106	13505	2	w	93.9	0	93.9	91.64	2.3	2
SX-106	13642	1	w	104.5	0	104.5	103.06	1.4	1
SX-106	13643	16	ss	113.9	0	113.9	96.15	17.8	16
SX-106	19056	-3 ^(b)	w	23.6	0	23.6	24.36	-0.8	-3 ^(b)
SX-106	19093	2	w	22.4	0	22.4	22.00	0.4	2
SX-106	12922	4	w	245.2	127.8	117.4	106.74	10.7	9
SX-106	13644	<1	w	100.4	0	100.4	99.71	0.7	<1
SX-106	13645	1	ss	49.6	0	49.6	49.06	0.5	1
SX-106	13646	1	w	95.1	0	95.1	94.14	1.0	1
SX-106	19121	2	ss	33.5	0	33.5	32.80	0.7	2
SY-103	15959	4	w	288.4	50.9	237.5	227.31	10.2	4
U-103	19290	2	ss; f	41.7	0	41.7	40.75	1.0	2
U-103	19292	2	ss; f	13.0	0	13.0	12.63	0.4	3

Table 3.3 (Contd)

Hanford Tank ID	222-S Jar #	Mass Loss During Storage (%)	Sample Condition	Planned Net Mass (g)	Post 2002 Sub-Sampling Mass (g)	Recalculated Expected Net Mass (g)	Mass to Homogenizer (g)	Difference Between Expected and Transferred Mass	
								(g)	(%)
U-108	10203	8	d	70.5	10	60	55.08	5	8
Debris removed	--		--				-5.67		
Net	mass			2648	788	1860	1685.12	175	9

ss=semi-solid sample, added directly to the homogenizer.
d = dry solid sample; water was added to soak sample so it could be broken up and removed from the jar for addition to the homogenizer.
w = wet sample, supernatant was clearly visible, added directly to the homogenizer.
f = foreign material such as pieces of Teflon liner, caps, and rocks present in the sample; foreign material was removed to extent possible before compositing.
Highlighted and bolded values indicate mass loss exceeding 30%.
(a) This sample jar contained tank waste sample originally listed as jar 14255.
(b) The negative values were attributed to the uncertainty associated with mass measurement.

One SX-105 sample (106 g) was missing from the archive. Sub-samples had been removed from several samples since the documented summary. The planned^(a) 2.6 kg of S-Saltcake was reduced by 788 g from various documented sub-sampling events that occurred since the 2002 inventory basis.

All samples retrieved from the 222-S inventory were weighed and the contents visually inspected; pertinent observations are shown in Table 3.3 under the heading “Sample Condition.” Most samples were still wet (indicated as “w”). Foreign materials such as pieces of broken caps (indicated as “f”) were removed with stainless steel tweezers from four samples. Deionized water was added to the dry samples (indicated as “d”) enabling hydration of the salts after an overnight soak period. These initially dry salts were sufficiently fluidized or softened to allow effective mobilization. The sample jars were opened and photographed looking down into the jars. Sample photographs are shown in Figure 3.7 through Figure 3.9 (note that saltcakes can appear very dark when transition metal oxides are present even in low concentrations).

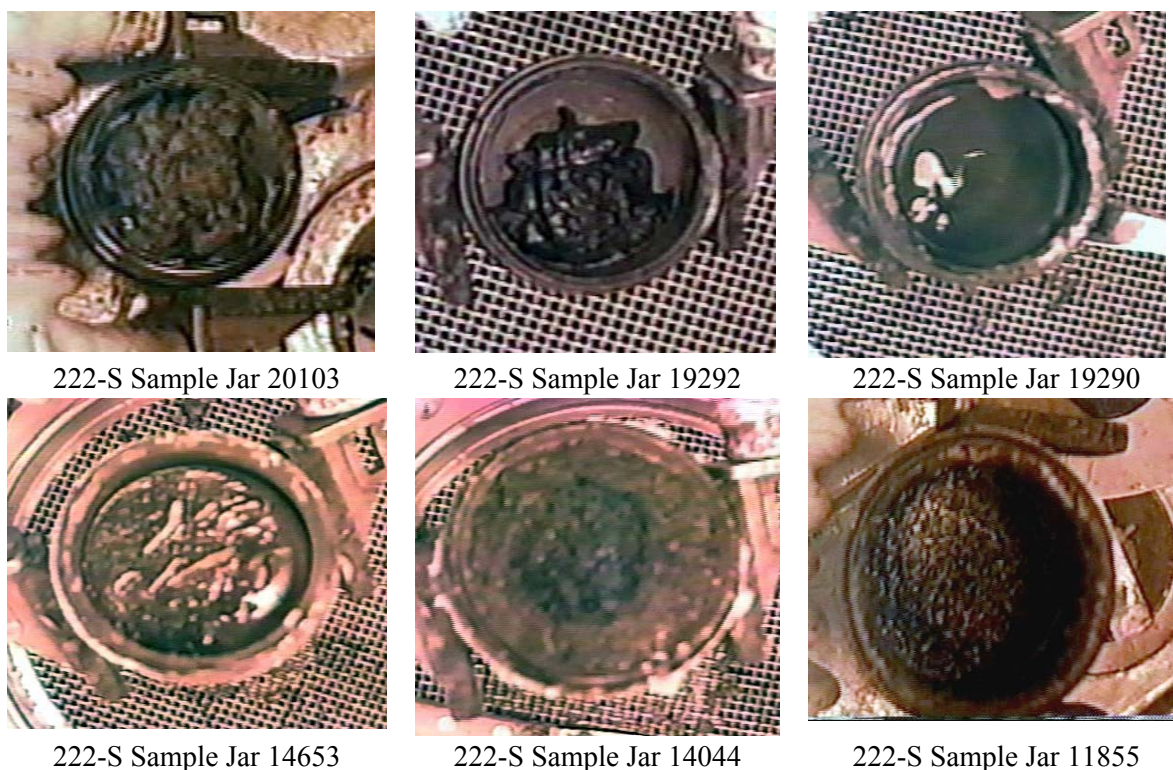
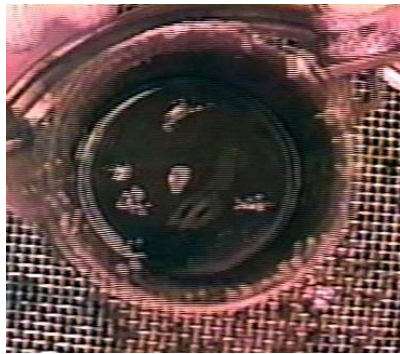
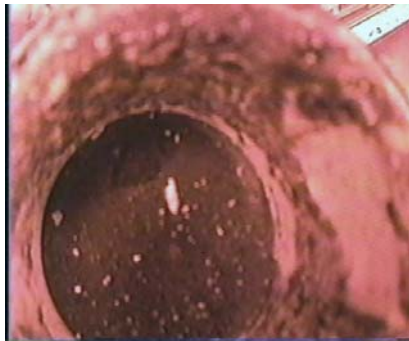


Figure 3.7. Photographs of Group 6 S-Saltcake Samples

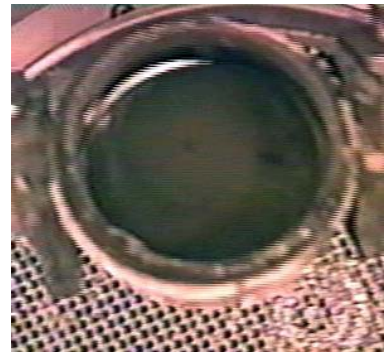
(a) Letter RPP-WTP-07-696 to S Barnes from GH Beeman, December 18, 2006.



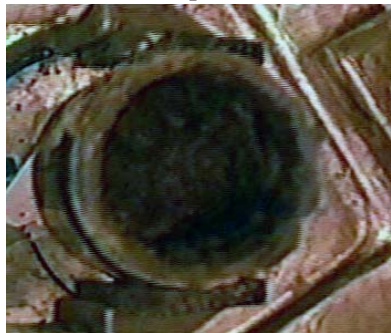
222-S Sample Jar 12895



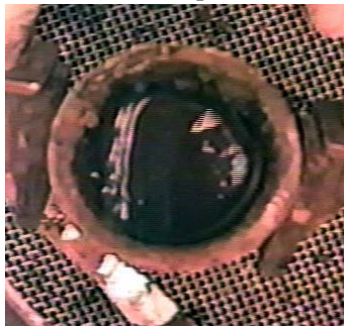
222-S Sample Jar 12907



222-S Sample Jar 14644



222-S Sample Jar 12110



222-S Sample Jar 12110
(water added)



222-S Sample Jar 13646



222-S Sample Jar 19121



222-S Sample Jar 19056



222-S Sample Jar 19093



222-S Sample Jar 14232



222-S Sample Jar 14232
(water added)

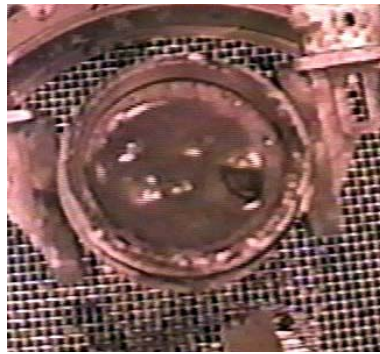


222-S Sample Jar 14441

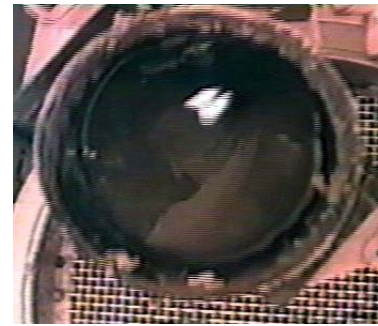
Figure 3.8. Photographs of Group 6 S-Saltcake Samples



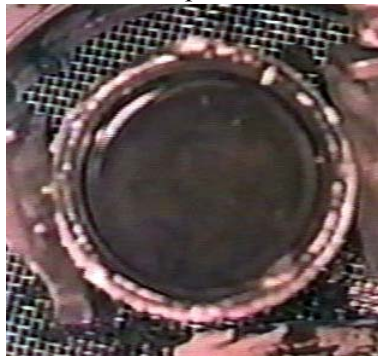
222-S Sample Jar 13504



222-S Sample Jar 13505



222-S Sample Jar 15959



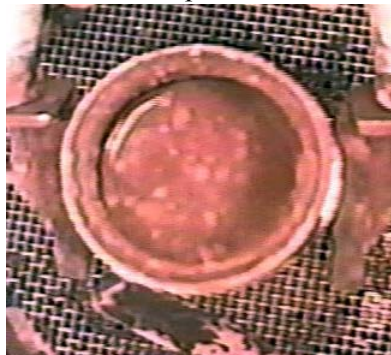
222-S Sample Jar 13642



222-S Sample Jar 13643



222-S Sample Jar 10203



222-S Sample Jar 10203
(water added)



222-S Sample Jar 13645



222-S Sample Jar 13644



222-S Sample Jar 12922

Figure 3.9. Photographs of Group 6 S-Saltcake Samples

The samples were thoroughly mixed with a stainless steel spatula to a consistency such that most of the contents could be poured or scraped out. The remaining residues in the jars were removed by a process of scraping and rinsing with deionized (DI) water. Nearly all residues were successfully removed from the sample jars and transferred to the homogenizer. The sample jars were air-dried and reweighed, and the net transferred mass was calculated. Small jar pieces (lids and glass) that chipped or broke off during manipulations were collected and weighed as a composite (4.28 g net mass).

The nominal tank waste mass distribution of the composite was calculated and is shown in Figure 3.10. The SX-106 tank waste dominated this composite.

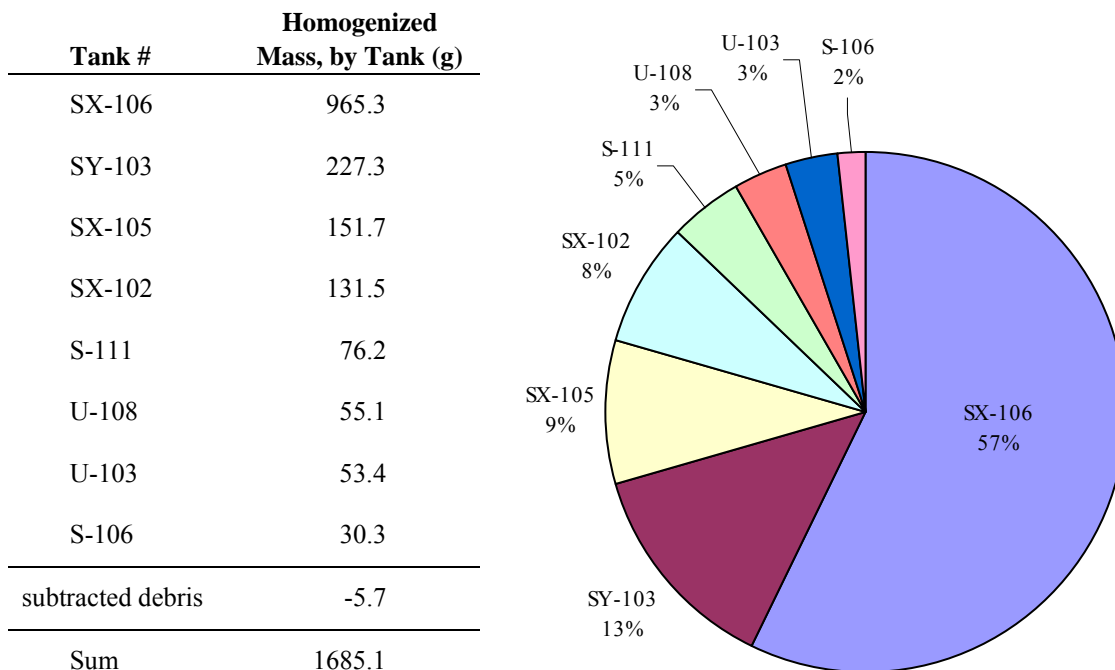


Figure 3.10. Nominal Mass Distribution of S-Saltcake Tank Wastes in the Group 6 Composite

Before placement in the homogenizer, the sample materials were passed through a stainless steel sieve ($\frac{1}{8}$ -in. pore size) fitted to the top of the homogenizer. Agglomerated material greater than $\sim\frac{1}{8}$ inch were trapped on the sieve. Solids (or semi-solids) retained on the sieve were forced through the openings by grinding with a stainless steel pestle. Most materials passed through the sieve; however, several small pieces of material did not pass the sieve. These appeared to be small pieces of gravel and broken glass (Figure 3.11). During the process of removing the sieve from the top of the tank, one of the small particles retained on the sieve bounced off and fell into the homogenizer tank. This object was likely a small piece of gravel. The remaining particles were collected into the sample jar TI488-G6-AR $>\frac{1}{8}$ (1.39 g net mass).

The sample masses actually transferred to the homogenizer are shown in Table 3.3 along with the differences between the expected masses and the transferred masses. A small part of the mass difference was associated with the collected debris, including bottle pieces (net mass of 4.28 g) and gravel (net mass of 1.39 g). The total mass loss was 163.1 g, which is equivalent to 9% of the expected mass. The mass loss was attributed to water evaporation during the archival period. In two cases, the sample mass

differences exceeded 30%; it is not clear if this was solely due to evaporation or the result of an unidentified sub-sampling activity. The total net mass of Group 6 S-Saltcake added to the homogenizer was 1685 g.

The homogenizer was a 5-L stainless steel tank previously available in-cell from other processing activities at the 222S facility. It was thoroughly cleaned before processing the S-Saltcake. The bottom of the homogenizer was conical with a ½-in. drain valve centered in the bottom. The homogenizer contained baffles and was equipped with an overhead stirrer. The stirrer supported a stainless steel shaft and a triple impeller assembly. The tank was covered with a lid during stirring and settling times to minimize evaporation and splattering losses. The hot cell temperature was ~27°C during processing activities.

After sample slurry transfer to the homogenizer, sufficient DI water was added to the tank to bring the volume up to approximately the 3-liter level such that the supernatant would be reasonably close to 5 M Na. The impeller and lid were positioned, and mixing was ramped up. Mixing continued for 2 h. After the solution had been mixed ~50 min, mixing was briefly stopped, and ~100-mL slurry was removed from the drain line. The collected slurry was returned to the homogenizer through the topside opening, and mixing was restarted. (This removed solids initially collected in the bottom neck of the homogenizer tank during the compositing process.) All solids were well-contacted with solution, allowing all soluble species to dissolve under the given conditions.

After mixing was completed, the impeller was removed, and the blades were rinsed with water; the rinse water was collected in the homogenizer. Solids were allowed to settle overnight.^(a) The slurry was then subdivided by sampling from the bottom valve sequentially into 16 volume-graduated 250-mL jars. The settled solids volumes were recorded after a 3-day settling period. The settled solids were dark brown, and the supernatant was bright yellow. The net sample mass, slurry volume, and settled-solids volume are provided in Table 3.4 in the order that they were collected. These samples and the rocky debris (sample TI488-G6-AR>1/8) were shipped to the RPL May 2, 2007.



Figure 3.11. Group 6 S-Saltcake Waste Debris Collected on the Sieve (cm scale)

(a) The goal of creating the Group 6 composite material was to dissolve all water-soluble components in DI water and collect the insoluble solids into one composite container. Therefore, sub-sampling of the combined slurry into uniform distributions was not required.

Table 3.4. Net Sample Masses, Slurry Volumes, and Settled Solids Volumes for Group 6 S-Saltcake Homogenized Samples

Jar ID	Net Slurry Mass (g)	Total Slurry Volume (mL)	3-Day Settled Solids Volume (mL)
TI488-G6-AR-J1	216.37	165	100
TI488-G6-AR-J2	243.20	190	120
TI488-G6-AR-J3	232.47	190	100
TI488-G6-AR-J4	250.43	200	70
TI488-G6-AR-J5	245.45	200	42
TI488-G6-AR-J6	247.72	200	30
TI488-G6-AR-J7	240.27	200	15
TI488-G6-AR-J8	245.54	200	13
TI488-G6-AR-J9	229.92	200	14
TI488-G6-AR-J10	245.35	200	11
TI488-G6-AR-J11	238.96	200	12
TI488-G6-AR-J12	243.43	200	10
TI488-G6-AR-J13	247.28	200	11
TI488-G6-AR-J14	245.98	200	10
TI488-G6-AR-J15	268.88	220	10
TI488-G6-AR-J16	150.44	120	16
Sum	3791.69	3085	584

The undissolved solids components were transferred from the 16 individual composite collection jars and combined into a 1-L glass bottle at the RPL using supernatant solution to effect the quantitative transfer.^(a) The bulk of the supernatant (2630 g) was re-distributed into the sample jars for eventual use in filtration testing. The consolidated slurry of 1133 g (volume ~840 mL) had a settled solids fraction of ~63 vol%.^(b) The solids were suspended using an overhead paddle stirrer, and sub-samples were removed for chemical and physical property testing as shown in Table 3.5. The effectiveness of the sample split was evaluated from comparing the gross densities and the volume percent settled solids after a brief 1-day settling time. The slurry sub-sample densities agreed within 2%, and the volume percent settled solids averaged 60% with a standard deviation of 6.5%. The sample split settled solids and total slurry volumes summation agreed well with the starting volumes.

(a) Processing was conducted according to TI-RPP-WTP-490, Initial Characterization of Group 6 Tank Waste: S-Saltcake, SK Fiskum, April 23, 2007.

(b) At 14.7 wt% total undissolved solids (see Section 6), the consolidated slurry was calculated to represent 166 g undissolved solids. Therefore, from the original 1,685 g of Group 6 S-Saltcake retrieved from the 222S archive, 166 g (9.8 wt%) was water-insoluble solids. Therefore, 90 wt% of the material was either already aqueous or water soluble.

Table 3.5. Sub-Sampling of the Group 6 S-Saltcake Combined Solids Slurry

Test Material	Sample ID	Slurry mass (g)	Slurry Volume (mL)	Settled Solids Volume (mL)	Slurry Density (g/mL)	Vol %Settled Solids
Initial slurry	TI490-G6-AR (start)	1132.76	840	525	1.35	63
Phys. Properties	TI490-G6-AR-S1	11.49	8.5	5.5	1.35	65
Chem. analysis	TI490-G6-AR-C	22.84	17.5	10	1.31	57
Phys. Properties	TI490-G6-AR-S2	11.01	8.35	5.3	1.32	63
Rheology	TI490-G6-AR-RH	193.07	142	80	1.36	56
Archive	TI490-G6-AR-ARCH	20.81	15.5	8.0	1.34 ^(a)	52 ^(a)
Phys. Properties	TI490-G6-AR-S3	11.95	9.0	5.15	1.33	57
Final slurry	TI490-G6-AR (end)	853.26	640	410	1.33	64
Sums and averages		1124.43 ^(b)	841 ^(b)	524 ^(b)	1.34 ^(c)	61 ^(c)
<p>(a) High uncertainty in volume measurement. (b) Sum of the final composite slurry and the sample aliquots masses and volumes. (c) Average of all samples. Note: Samples were collected in the given order.</p>						

4.0 Characterization Methods

This section describes the characterization methods used to determine rheological properties, physical properties, chemical and radiochemical composition, particle size, surface area, and crystal form and habit.

The initial characterization activities of the Group 5 REDOX sludge and Group 6 S-Saltcake materials included physical-property testing and chemical analysis. Particle characterization was limited to evaluating the washed solids. Washing was considered crucial to better understand the nature of the solids, free of complications associated with supernatant entrainment. The initial sample processing and characterization activities are summarized in Figure 4.1.

4.1 Physical Properties

The physical-property characterization was conducted according to procedure RPL-COLLOID-02, Rev. 1, *Measurement of Physical and Rheological Properties of Solutions, Slurries and Sludges*, which is consistent with the WTP guidelines document.^(a) Physical-properties characterization samples were taken in triplicate near the beginning (S1), middle (S2), and end (S3) of the aliquoting activity following slurry homogenization. Samples sizes were generally between 10 and 15 mL. The samples were collected in volume-graduated, glass centrifuge tubes. The REDOX samples were tested in 40-mL tubes (Kimble-Kontes product number 45200-40, Vineland, New Jersey), and the S-saltcake samples were tested in 10-mL tubes (Kimble-Kontes product number 45200-10).

The 3-day settling study was omitted for the REDOX sludge because of the slow and minimal solids settling behavior manifested during the homogenization assessment where only ~90 vol% settled solids were obtained after a 5-day settling time. The S-saltcake samples were agitated thoroughly in the centrifuge tubes and allowed to settle for 3 days with periodic volume measurements.

The samples were centrifuged at ~1000 G for 1 hour. The total sample volume and solids volume were recorded to assess the vol% wet centrifuged solids (WCS). After centrifuging, the S2 REDOX sample centrifuge tube broke, releasing the sample on the cell floor; the sample was not recoverable. The supernatants were decanted and transferred to tared graduated cylinders; the net solution masses and volumes were determined. The remaining WCSs were weighed in the centrifuge tubes to assess gross densities. The supernatant samples were transferred to tared glass vials. Both the supernatant fractions and the residual solids fractions (containing interstitial supernatant) were air-dried and then transferred to a 105°C oven for continued drying until constant mass was attained.

(a) 24590-WTP-GPG-RTD-001, Rev 0, "Guidelines for Performing Chemical, Physical, and Rheological Properties Measurements," G. L. Smith and K. Prindiville, May 2002.

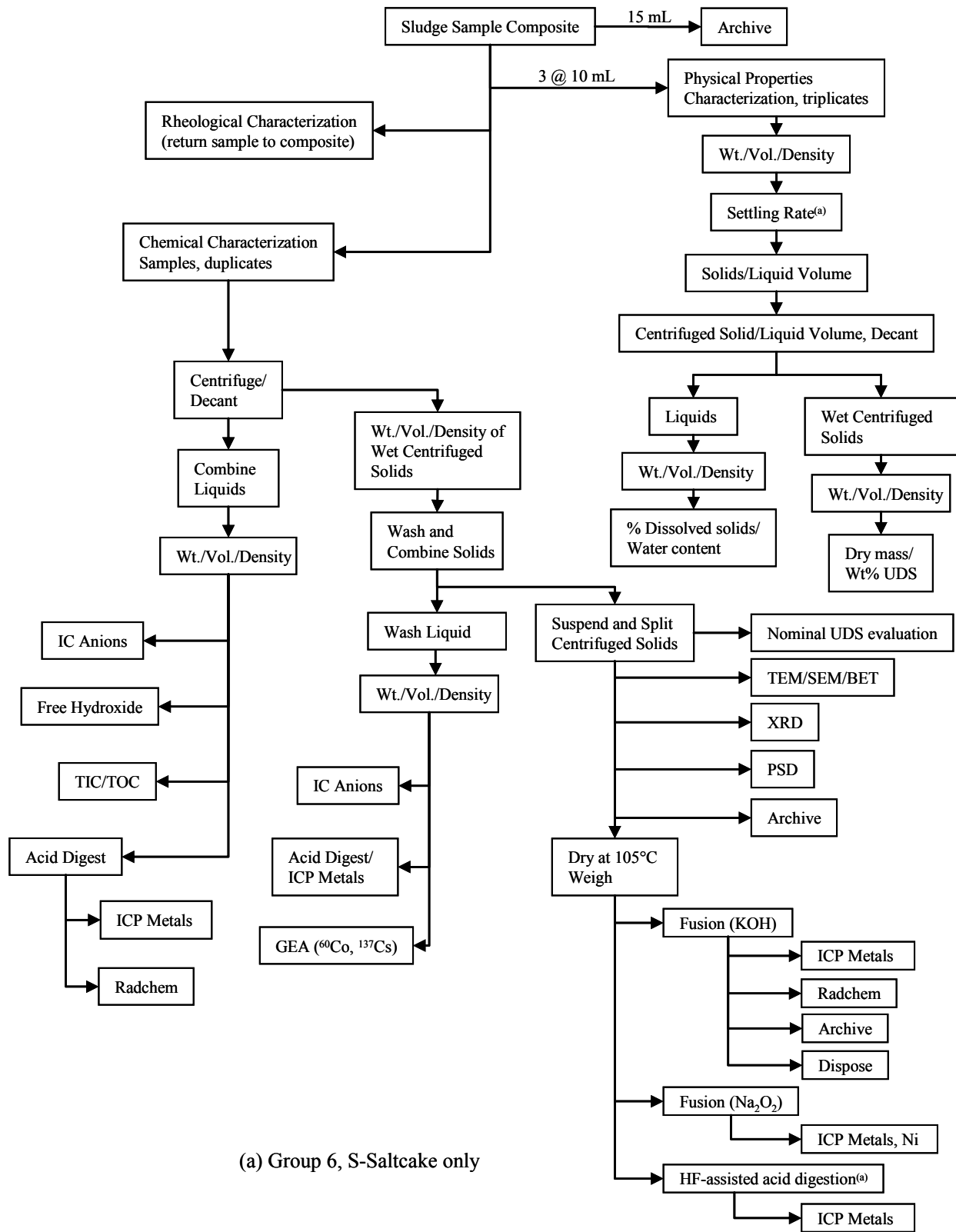


Figure 4.1. Composite Group Analysis Scheme

The collected data were processed as described by Smith and Prindiville^(a) to determine the volume and weight percent of wet solids (total, settled, and centrifuged), densities, total undissolved solids, and dissolved solids content.

4.2 Rheology

Rheological testing was conducted on the solids in contact with the supernatant generated as part of the homogenization process. Testing was conducted according to RPL-COLLIOD-02, *Measurement of Physical and Rheological Properties of Solutions, Slurries and Sludges*, which conforms to established guidelines.^(a) For the current study, two regions of tank waste flow behavior are considered: 1) incipient motion in settled tank waste solids (shear strength) and 2) non-elastic flow of tank waste slurries and supernates (flow curve).

4.2.1 Shear-Strength Testing

For tank waste slurries, a finite stress must be applied before the material will begin to flow. The stress required to transition the material from elastic deformation to viscous flow is referred to as the shear strength, and its origin can be attributed to static and kinetic friction between individual particles and/or aggregates, strength of the matrix supporting the coarse fraction (i.e., the interstitial fluid), and sludge cohesion arising from interparticle adhesive forces such as van der Waals forces.

The shear strength was measured using the vane method. For the vane technique, the stress required to begin motion is determined by slowly rotating a vane immersed in the test sample's settled solids while continuously monitoring the resisting torque as a function of time. A material's static shear strength is then associated with the maximum torque measured during the transition from initial to steady-state vane rotation.

The maximum torque required for incipient motion is dependent on vane geometry. To account for vane geometry affects, shear strength is expressed in terms of the uniform and isotropic stress acting over the surface area of the cylinder of rotation swept out by the vane. The shear strength is related to the maximal torque during incipient motion according to Equation 4.1 (Barnes and Dzuzy 2001):

$$\tau_{ss} = \frac{M_{max}}{4\pi R^3 \left(\frac{H}{2R} + \frac{1}{3} \right)} \quad (4.1)$$

Here, τ_{ss} is the shear strength [N/m²], M_{max} is the maximum torque [N·m], and R and H are the radius and height of the cylinder of rotation swept out by the vane [m]. Because the shear band observed upon slow rotation of the vane does not extend appreciably beyond the vane paddles, R and H are taken to be the dimensions of the vane itself.

(a) 24590-WTP-GPG-RTD-001 Rev 0, "Guidelines for Performing Chemical, Physical, and Rheological Properties Measurements," G. L. Smith and K. Prindiville, May 2002.

4.2.2 Flow-Curve Testing

Non-elastic flow of tank waste slurries and supernates is characterized with rotational viscometry. The typical result of such testing is a set of flow curve data, which shows the stress response of a material to a range of applied rates-of-deformation. Specifically, flow-curve testing allows characterization of a material's shear stress, τ , and response as a function of applied shear rate, $\dot{\gamma}$. Once measured, flow curve data can be interpreted with several constitutive equations for the viscous stress/rate-of-strain relationship. Such analysis allows the flow behavior over a broad range of conditions to be described with just a few rheological descriptors such as viscosity, yield stress, consistency, and flow index.

A concentric cylinder rotational viscometer operated in controlled-rate mode was used for flow-curve testing of tank waste slurries and supernates. Rotational viscometers operate by placing a given volume of test sample into a measurement cup of known geometry. A cylindrical rotor attached to a torque sensor is then lowered into the sample until the slurry is even with, but does not cover, the top of the rotor. A single-point determination of a fluid's flow properties is made by spinning a rotor at a known rotational speed, Ω , and measuring the resisting torque, M , acting on the rotor. The torque acting on the rotor can be directly related to the shear stress at the rotor using the equation,

$$\tau = \frac{M}{2\pi HR_l^2} \quad (4.2)$$

Shear stress has units of force per area [N/m²]. The rotational rate is related to the shear rate. However, calculating the fluid shear rate at the rotor is complicated by the fact that shear rate depends on both the measurement system geometry and the fluid rheological properties. For the simplest fluids (i.e., Newtonian fluids), the shear rate of the fluid at the rotor can be calculated given the geometry of the cup rotor shear by using the equation,

$$\dot{\gamma} = \left(\frac{2R_o^2}{R_o^2 - R_l^2} \right) \Omega \quad (4.3)$$

Here, shear rate has units of inverse seconds [s⁻¹]. Calculating shear rate for materials showing more complex shear stress versus shear rate behavior (i.e., non-Newtonian fluids) requires estimates of yield stress and degree of shear-thinning or shear-thickening. As the goal of rheological testing is to determine and quantify such behavior, these values are typically not known. This requirement can be circumvented by using a cup and rotor system with a small gap (~1 mm) for fluid shear. For fluid flow in small gap cup and rotor systems, shear-rate effects introduced by fluid properties are minimized such that Equation 4.3 provides an accurate determination of shear rate for non-Newtonian materials. Shear rates examined in this study spanned the range from 1 to 1000 s⁻¹.

The resistance of a fluid to flow is often described in terms of the fluid's apparent viscosity, η_{app} , which is defined as the ratio of the shear stress to shear rate:

$$\eta_{app} = \frac{\tau}{\dot{\gamma}} \quad (4.4)$$

For Newtonian fluids, the apparent viscosity is independent of shear rate. For non-Newtonian fluids, the apparent viscosity will vary as a function of shear rate. The units of apparent viscosity are Pa·s, although it is typically reported in units of centipoise (cP; where 1 cP = 1 mPa·s).

Flow-curve data are usually combined plots of τ and η_{app} as a function of $\dot{\gamma}$. As stated above, flow-curve data can be interpreted with several constitutive equations (i.e., flow curves), allowing characterization of that data with just a few rheological descriptors. The behavior of tank waste sludges, slurries, and supernates can be described by four common flow-curve equations:

- **Newtonian**—Newtonian fluids flow as a result of any applied stress and show constant viscosity over all shear conditions. The flow curve for Newtonian fluids is,

$$\tau = \eta \dot{\gamma} \quad (4.5)$$

where η is the Newtonian viscosity.

- **Ostwald (Power Law)**—Power-law fluids flow as a result of any applied stress and have viscosities that either increase or decrease with increasing shear rate. They are described by,

$$\tau = m \dot{\gamma}^n \quad (4.6)$$

where m is the power-law consistency index, and n is the power-law index. Power-law fluids with $n < 1$ are referred to as pseudoplastic (shear-thinning), whereas power-law fluids with $n > 1$ are referred to as dilatant (shear-thickening).

- **Bingham Plastic**—Bingham plastics are fluids that show finite yield points. A finite stress (i.e., the yield stress), must be exceeded before these types of materials flow. Once flow is initiated, the stress response of the material is Newtonian over the rest of the shear-rate range. Bingham plastics are described by,

$$\tau = \tau_O^B + k_B \dot{\gamma} \quad (4.7)$$

where τ_O^B is the Bingham yield index, and k_B is the Bingham consistency index.

- **Herschel-Bulkley**—Fluids that behave in accordance with a Herschel-Bulkley model show a finite yield followed by power-law behavior over the rest of the shear-rate range. They are described by,

$$\tau = \tau_O^H + k_H \dot{\gamma}^b \quad (4.8)$$

where τ_O^H is the Herschel-Bulkley yield index, k_H is the Herschel-Bulkley consistency index, and b is the Herschel-Bulkley power-law index.

Power-law fluids, Bingham plastics, and Herschel-Bulkley fluids are examples of non-Newtonian fluids. In general, liquids without internal and/or interconnected structures (such as tank waste supernates) are Newtonian. Sludges and slurries are typically non-Newtonian, but their exact behavior depends on the concentration of solids and suspending phase chemistry. Sufficiently dilute slurries may show Newtonian behavior.

4.2.3 Rheology Instrumentation

Rheological characterization was accomplished using a Rotovisco® RV20 Measuring System M equipped with an M5 measuring head sold by HAAKE Mess-Technik GmbH u. Co. (now the Thermo Electron Corporation, Madison, WI). The M5 measuring head is a “Searle” type viscometer capable of producing rotational speeds up to 500 revolutions per minute (RPM) and measuring torques up to 0.049 N·m. The minimum rotational speed and torque resolution achievable by this measuring head are 0.05 RPM and 0.49 mN·m, respectively.

Specific measurement tools, such as cup and rotor assemblies and shear vanes, are attached to measure selected rheological properties. Shear-strength measurements employed an 8-mm × 16-mm (R × H) shear vane tool. Flow-curve measurements employed an MV1 stainless steel measuring cup and rotor. The dimensions of the MV1 and vane measuring systems are listed in Table 4.1.

Table 4.1. Vane and Cup and Rotor Measuring System Dimensions

Measuring System	Vane/Rotor Radius, mm	Vane/Rotor Height, mm	Cup Radius, mm	Gap Width, mm
Vane Tool	8	16	> 16	> 8
MV1	20.04	60	21	0.96

The temperature was controlled with a combination of the standard measuring system M temperature jacket and a Cole-Parmer® Polystat® Temperature-Controlled Recirculator, Model Number C-12920-00. The temperature jacket provided a heat-transfer area between the cup and the recirculating fluid. The jacket temperature was monitored using a Type-K thermocouple (Omega Model TJ36-CASS-116-G-6-CC). Temperature control was employed only for flow-curve measurements. The shear strengths were measured at ambient temperature (~30°C in the hot cells).

The rheometer was controlled and data were acquired with a remote computer connection using the RheoWin Pro Job Manager Software, Version 2.96. During measurement, the software automatically collects and converts rotor torque readings into shear stresses based on Equation 4.1 (for vane testing) or Equation 4.2 (for flow-curve testing). Likewise, the software also automatically converts the rotational rate readings into shear rates based on Equation 4.3.

4.2.4 Rheology Materials and Methods

No sample treatment was performed before analysis with the exception of the mechanical agitation required to mix and sub-sample selected waste jars.

4.2.4.1 Shear-Strength Testing

Before testing, the tank waste slurries provided for shear-strength testing were mixed thoroughly and subsequently allowed to settle for at least 48 to 72 h. When possible, the shear strength was measured by immersing the 8×16 mm vane tool to a depth of 15 mm into the settled solids. The vane was slowly rotated at 0.3 RPM for 180 s. For the entire duration of rotation, the time, rotational rate, and vane torque were continuously monitored and recorded. At the end of the measurement, shear stress versus time data were parsed, and the maximum measured shear stress (i.e., the material's shear strength) was determined.

4.2.4.2 Flow-Curve Testing

Each flow curve was measured over a 15-min period and split into three 5-min intervals. Over the first 5 min, the shear rate was smoothly increased from zero to 1000 s^{-1} . For the second 5 min, the shear rate was held constant at 1000 s^{-1} . For the final 5 min, the shear rate was smoothly reduced back to zero. During this time, the resisting torque and rotational rate were continuously monitored and recorded.

Before each test, the sample was left undisturbed in the measuring system for 5 min to allow temperature equilibration. The sample was then mixed for 3 min using the measuring system rotor to re-disperse any settled solids and to pre-shear slurries before measurement.

Flow-curve tests were run at 25, 40, and 60°C . Because of limited sample volume, all three temperature tests were performed on the same sample. To combat the effects of sample evaporation, a moisture barrier was installed over the opening at the top of the temperature jacket during testing, and after each test, the cup was raised so that fresh sludge/slurry filled the measurement gap.

4.3 Sample Preparation for Chemical Characterization

The samples taken for chemical characterization (refer to Figure 4.1) were centrifuged at 1000 G for 1 hr, similar to the physical property testing samples; then the supernatants were decanted. The solids were washed with three successive additions of 0.01 M NaOH.^(a) After adding each wash solution, the sample was agitated for 15 min, centrifuged 30 min at 1000 G, and then the liquid phase was removed. The three wash solutions were combined into a composite and passed through 0.45-micron pore size nylon filter. The supernatant and wash solution densities were determined by measuring the masses of 1-mL volume deliveries four times per sample.

More 0.01 M NaOH was added to the washed solids so that the slurry could be easily mixed using a Teflon-coated stirbar, and the solids suspended. Aliquots of the suspended-solids slurries were taken for chemical/radiochemical analysis, particle-size distribution (PSD), Brunauer, Emmett, and Teller (surface area analysis technique) (BET), scanning electron microscopy (SEM), transmission electron microscopy (TEM), and X-ray diffraction (XRD) analyses. The washed solid slurry sample aliquots taken for chemical analysis were dried to constant mass at 105°C ; the solids chemical analysis was based on the dry sample mass. The supernatant and the filtered solids wash solution were provided directly for chemical characterization.

(a) Specific wash volumes are provided in the context of the results discussion.

4.4 Chemical and Radioisotope Characterization

The following sections describe procedures used to support the chemical and radiochemical characterization of the solids and aqueous samples. Aqueous samples were distributed directly to the free hydroxide, ion chromatography (IC), and total inorganic carbon/total organic carbon (TIC/TOC) analytical workstations as indicated in Figure 4.1. The solids and liquids required a digestion step before distribution to the inductively coupled plasma-optical emission spectroscopy (ICP-OES) and radiochemistry workstations.

4.4.1 Free Hydroxide

The free hydroxide was determined using potentiometric titration with standardized HCl according to procedure RPG-CMC-228, *Determination of Hydroxyl (OH) and Alkalinity of Aqueous Solutions, Leachates, and Supernates and Operation of Brinkman 636 Auto-Titrator*. The free hydroxide was defined as the first inflection point on the titration curve. Quality control (QC) samples were generated at the analytical workstation and included a sample replicate determination, process blank, blank spike (BS), and matrix spike (MS).

4.4.2 Anions

Anions were determined by ion chromatography using a Dionix ICS-2500 IC system equipped with a conductivity detector according to procedure RPG-CMC-212, *Determination of Common Anions by Ion Chromatography*. Additional sample dilutions from 100× to 25,000× were required to accurately measure the analytes. QC samples were generated at the analytical workstation and included a sample replicate determination, process blank, BS, and MS.

4.4.3 TIC/TOC

The TIC was determined by using silver-catalyzed hot persulfate (HP) oxidation according to procedure RPG-CMC-385, *Carbon Measured in Solids, Sludge, and Liquid Matrices*. The hot persulfate wet oxidation method was used. This method takes advantage of acid decomposition of the carbonate (TIC measure) followed by oxidation of organic carbon (TOC measure) using acidic potassium persulfate at 92 to 95°C. QC samples were generated at the analytical workstation and included a sample replicate determination, process blank, BS, and MS.

4.4.4 Acid Digestion

Aqueous samples were digested with acid according to procedure PNL-ALO-128, *HNO₃-HCl Acid Extraction of Liquids for Metals Analysis Using a Dry-Block Heater*. The acid-digested solutions were brought to a nominal 25-mL volume (resulting in a nominal 25× dilution where the initial sample size was 1-mL); absolute volumes were determined based on final solution weights and densities. The supernatant sample was processed in duplicate. As part of the analytical preparation batch, the ASO processed a digestion preparation blank (PB), a BS, and an MS. The spike solution contained a broad suite of stable elements; radionuclides were not included in the digestion preparation. Aliquots of the BS, MS, and PB, along with the sample aliquots, were delivered to the ICP-OES workstation for analysis; sample and PB aliquots were delivered to the radiochemical workstations for separations supporting specific radioisotope analysis.

4.4.5 KOH Fusion

The potassium hydroxide (KOH) fusion was conducted in the shielded analytical facility (hot cells) according to PNL-ALO-115, *Solubilization of Metals from Solids using KOH-KNO₃ Fusion*. A nominal sample size of 0.1 to 0.2 g dry solids was combined with a KOH/KNO₃ flux mixture and fused at 550°C for 1 hour in a nickel crucible. The fused material was acidified with HNO₃, taken to a 100-mL volume with DI water, and then split for metals and radionuclide analysis. The sample was prepared in duplicate along with a fusion blank and an LCS (SRM-2710, Montana Soil, purchased from the National Institute for Science and Technology [NIST]).

4.4.6 NaOH/Na₂O₂ Fusion

The NaOH/Na₂O₂ fusion was conducted in the shielded analytical facility (hot cells) according to PNL-ALO-114, *Solubilization of Metals from Solids using a Na₂O₂-NaOH Fusion*. A nominal sample size of 0.1 to 0.2 g dry solids was combined with a NaOH/Na₂O₂ flux mixture and fused at 550°C for 1 hour in a zirconium crucible. The fused material was acidified with HNO₃, taken to a 100-mL volume with DI water, and then split for metals analysis. The sample was prepared in duplicate along with a fusion blank and a laboratory control sample (LCS) (SRM-2710, Montana Soil).

4.4.7 HF-Assisted Acid Digestion

The HF-assisted acid digestion was conducted in the Sample Receiving and Preparation Laboratory according to PNL-ALO-138, *HNO₃-HF-HCl Acid Digestion of Solids for Metals Analyses Using a Dry Block Heater*. A nominal sample size of 0.1 to 0.2 g dry solids was contacted with a mixture of concentrated HF and HNO₃ and evaporated to dryness in a Teflon[®] reaction tube. Concentrated HCl was then added, and the sample was evaporated to dryness a second time. Additional concentrated HNO₃ and HCl were added, the reaction tube was capped tightly, and the mixture was heated in a dry-block heater at 95°C for 6.5 h. The digestate was cooled, brought to a 50-mL volume, and then split for metals analysis. The sample was prepared in duplicate along with a fusion blank and an LCS (SRM-2710, Montana Soil).

4.4.8 Metals Analysis by ICP-OES

Metals were measured by ICP-OES according to procedure RPG-CMC-211, *Determination of Elemental Composition by Inductively Coupled Argon Plasma Optical Emission Spectrometry (ICPOES)*. The preparative QC samples (duplicate, PB, BS, MS) were processed along with analytical workstation QC (post digestion spike and serial dilution).

4.4.9 U (KPA)

Uranium was determined directly from samples prepared by KOH fusion using a Chem Chek Instruments KPA according to procedure RPG-CMC-4014, Rev. 1, *Uranium by Kinetic Phosphorescence Analysis*. The LCS did not contain U, so preparative QC was limited to the duplicate and PB. A post-digestion spike was conducted at the analytical workstation.

4.4.10 Gamma Energy Analysis

Gamma energy analysis was performed with direct or diluted samples that were prepared from acid digestion, fusion, or neat (see Figure 4.1). Sample counting was conducted according to procedure RPG-CMC-450, *Gamma Energy Analysis (GEA) and Low-Energy Photon Spectroscopy (LEPS)*, using high-purity germanium detectors. Extended count times (up to 20 h) were employed as needed to achieve low

detection limits. In many cases, the Compton background from the high ^{137}Cs activity (661 keV) limited the achievable detection limit of lower-energy gamma emitters (e.g., ^{241}Am at 59 keV). The QC associated with the GEA analysis was composed of the sample duplicate and PB; because this is a direct analysis, no additional QC samples were required.

4.4.11 Gross Alpha and Gross Beta

The gross alpha and beta activities were measured from aqueous samples prepared by acid-digestion, and washed-solids samples prepared by KOH/ KNO_3 fusion. Prepared sample aliquots were plated directly onto stainless steel planchets according to procedure RPG-CMC-4001, *Source Preparation for Gross Alpha and Gross Beta Analysis*. The mounts prepared for gross alpha analysis were counted with Ludlum alpha scintillation counters. The gross alpha analysis tends to be confounded by the dissolved solids in the sample matrix. The solids can absorb the alpha particles, decreasing the intensity relative to the detector, which biases the results low. The sources prepared for gross beta analysis were counted with an LB4100 gas-proportional counter. In both cases, counting operations were conducted according to procedure RPG-CMC-408, Rev.1, *Total Alpha and Total Beta Analysis*. The preparative QC included the sample duplicates and the preparation blank. The BS and MS were prepared at the analytical workstation on sample dilutions.

4.4.12 Pu Isotopes: ^{238}Pu and $^{239+240}\text{Pu}$

The ^{238}Pu and $^{239+240}\text{Pu}$ activities were measured from aqueous samples prepared by acid-digestion and washed solids samples prepared by KOH/ KNO_3 fusion. Radiochemical separations were conducted according to procedure RPG-CMC-4017, *Analysis of Environmental Water Samples for Actinides and Strontium-90* (analyte purification using ion exchange); source preparation was conducted according to RPG-CMC-496, *Coprecipitation Mounting of Actinides for Alpha Spectroscopy* (co-precipitation of PuF_3 with LaF_3); and alpha counting was conducted according to RPG-CMC-422, Rev.1, *Solutions Analysis: Alpha Spectrometry*. The preparative QC included the sample duplicates and the preparation blank. The BS and MS were prepared at the analytical workstation on sample dilutions.

4.4.13 Strontium-90

The ^{90}Sr activities were measured from aqueous samples prepared by acid-digestion, and washed-solids samples were prepared by KOH/ KNO_3 fusion. Radiochemical separation was conducted according to procedure RPG-CMC-476, *Strontium-90 Separation Using Eichrom Strontium Resin*; source preparation and beta counting were conducted according to RPG-CMC-474, *Measurement of Alpha and Beta Activity by Liquid Scintillation Spectrometry*.

4.4.14 Chromate

The Cr(VI) concentration was determined from the major optical absorbance band of chromate (CrO_4^{2-}) with a maximum at 372 nm in selected leachate samples. Determination of chromate concentration in diluted leachates was based on the linear relationship between optical absorbance of the sample at the peak maximum (A_{372}) and concentration of Cr(VI) in the analyzed solution (C_{chromate}) as illustrated below:

$$A_{372} = \epsilon_{372} \cdot C_{\text{chromate}} \cdot l \quad (4.9)$$

where ϵ_{372} is the molar absorptivity of the chromate peak at 372 nm (expressed in $\text{M}^{-1}\text{cm}^{-1}$), and l is the optical path length of a spectrophotometric cell (expressed in cm) used to contain the analyzed sample.

The linearity of the Equation 4.9 was verified in a calibration experiment using a series of solutions with a known concentration of chromate (prepared from 0.1043N $K_2Cr_2O_7$, Aldrich Chemical Co., Milwaukee, WI) in a 0.24-M NaOH matrix. The calibration curve showed good linearity ($R^2 = 0.9994$) with a slope equal to $\epsilon_{372} \cdot l = 5312 \pm 43 \text{ M}^{-1}$ in the dynamic range of 0.0069 mM to 0.42 mM of chromate.

The same spectrophotometric cell was used in all subsequent experiments in the determination of sample chromate concentrations. For this reason, it was not necessary to determine the actual optical pathlength of the cell. Therefore, the chromate concentration was calculated simply as the ratio of A_{372} and the slope of the calibration curve

$$C_{\text{chromate}} = A_{372}/\text{slope} \quad (4.10)$$

Most of the samples submitted for chromate analysis were too concentrated in chromate to be measured directly. In these cases, the samples were diluted with 0.24 M NaOH to lower the chromate concentration to less than 0.2 mM so as to have optical readings within the linearity range of the calibration plot. Applying 0.24 M NaOH instead of water verified that the Cr(VI) in the diluted solutions was present exclusively as the chromate species.

The UV-visible measurements were made on a 400 Series charge-coupled device array spectrophotometer (Spectral Instruments Inc, Tucson, AZ) with a 200- to 950-nm scanning range. The solutions were held in PLASTIBRAND[®] 1-cm cuvettes. The 0.24 M NaOH solution (diluent) was used to obtain the baseline reading before measuring the chromate-containing samples. Because NIST-traceable standards were not used, the calculated chromate concentrations are reported for information only.

4.5 Particle-Size Attributes

Particle attributes, including size distribution and surface area, are discussed in the following sections.

4.5.1 Particle-Size Distribution

Particle sizes were characterized according to procedure RPL-COLLOID-01, Rev. 1, *Particle Size Analysis Using Malvern MS2000*. This procedure uses a Mastersizer 2000 (Malvern Instruments, Inc., Southborough, MA 01772 USA) with a Hydro μ P wet dispersion accessory. Malvern lists the Mastersizer particle-size measurement range as nominally 0.02 to 2000 μm . The actual PSD measurement range is dependent on the accessory used as well as the properties of the solids being analyzed. When coupled with the Hydro μ P wet dispersion accessory, the nominal listed measuring range is reduced to 0.02 to 150 μm . The Malvern 2000 uses laser diffraction technology to define PSD.

The Hydro μ P wet-dispersion accessory consisted of a 20-mL sample flow cell with a continuous variable and independent pump and ultrasound. Both flow and sonication can be controlled and altered during measurement. PSD measurements were made before, during, and after sonication, allowing determination of the influence of each on the sample PSD. The primary measurement functions of the Malvern analyzer were controlled through Mastersizer 2000 software, Version 5.1 [Malvern Instruments, Ltd. Copyright[©] 1998-2002]. The optical properties applied to the test samples are summarized in Table 4.2.

The PSD measurements were conducted on the washed solids in a 0.01-M NaOH dispersion solution matrix. The sample dispersion was added drop-wise to the instrument (while the pump was active) until

an ~10% obscuration was reached. For all samples, less than 10 mg of solids was required to reach the desired obscuration in the 20-mL flow cell.

Table 4.2. Optical Properties Applied To Test Materials

Test	Material Selected for Optical Properties	Refractive Index (RI)	Absorption
Initial Characterization			
Group 5	Boehmite ^(a)	1.655	1.0
Group 6	Boehmite ^(a)	1.655	1.0
Parametric			
Group 5	Uranium Oxide ^(b)	2.4	1.0
Group 6	Chrome Oxide ^(a)	2.5	1.0
All/Suspending Phase	Water ^(a)	1.33	n/a
(a) See reference Malvern Instruments Ltd., April 1997.			
(b) See reference Kaminski et al., 2005.			

The size distributions of particles were measured under varying flow conditions before, during, and after sonication. A typical test matrix is shown in Table 4.3. Not all conditions were tested for some samples (e.g., initial characterization samples only employed pump speeds of 3000 RPM). For each condition, three successive 12-second measurements of PSD were taken. An average of these measurements was then generated by the analyzer software. Both individual measurement and average were saved to the analyzer data file. Once measurements were complete, the sonic power for the next condition was set, the sample was given 30 to 60 seconds to equilibrate, and the next set of measurements was taken.

Table 4.3. Prototypic Particle-Size Analysis Test Matrix

Condition No.	Pump Speed (RPM)	Sonic Power	Comment
1	3000	0%	pre-sonic measurement
2	2000	0%	pre-sonic measurement
3	4000	0%	pre-sonic measurement
4	3000	25%	sonicated measurement
5	3000	50%	sonicated measurement
6	3000	75%	sonicated measurement
7	3000	0%	post-sonic measurement
8	2000	0%	post-sonic measurement
9	4000	0%	post-sonic measurement

4.5.2 Surface Area (BET)

Samples were prepared for surface-area measurements in an effort to minimize solidification into a monolith upon drying. To this end, the solids were rinsed twice with ethanol and twice again with ethyl ether according to procedure TPR-RPP-WTP-486, *Procedure for BET Sample Preparation Using Ethanol and Ethyl Ether as Drying Agents*. Each rinse was conducted in a centrifuge tube. The solids were well suspended in the rinse solution, and then the phases were separated by centrifuging and decanting. The

final ethyl ether rinse was used to transfer the solids slurry to the sample cell. The ethyl ether was then evaporated at room temperature directly from the sample cell.

The sample was further dried and out-gassed using the Quantachrome Instruments Monosorb Model MS-21 (Boynton Beach, FL) outgassing station. This entailed pre-flushing nitrogen through the sample cell for ~10 min and then heating and flushing for overnight (>10 h) at 110°C.

The surface-area measurements were conducted according to OCRWM-BET-01, *Surface Area Measurement with a Monosorb Gas Analyzer*, which is consistent with ASTM method D5604-96, Test Method B (Single-Point Surface Area by Flowing Gas Apparatus). The flow gas used in the measurement mode was composed of 30% nitrogen in helium. The system was calibrated per manufacturer instructions. The system performance was assessed using a 29.9 ± 0.75 m²/g carbon surface area standard Lot D-6 obtained from Micromeritics (Norcross, GA).

4.6 Crystal Form and Habit

The solids crystal characteristics were determined on small aliquots of the washed solids. In all cases, the solids sample fractions were allowed to air dry at room temperature in preparation for analysis. This effort was intended to minimize morphological changes that might occur upon heating. The methods applied for XRD, SEM, and TEM evaluations are discussed in the following sections.

4.6.1 X-Ray Diffraction

The sample mounts for XRD determination were prepared from the dried solids according to procedure RPL-PIP-4, *Preparing Sealed Radioactive Samples for XRD and Other Purposes*. Specimens were pulverized to a powder with a boron carbide mortar and pestle, mixed with an internal standard (rutile, TiO₂, or alumina, Al₂O₃), and mounted on a glass slide. In some cases, the internal standard was omitted in an effort to provide better clarity of the sample diffraction pattern free from potential interference from the internal standard diffraction pattern. The XRD examination was conducted according to procedure PNNL-RPG-268, *Solids Analysis, X-Ray Diffraction Using RGD #34*. Process parameters included examination of the X-ray 2-theta range from 5 to 65 degrees with a step size of 0.02 degrees and a dwell time of 20 seconds.

Phase identification was performed with JADE, Version 8.0 (Materials Data Inc., Livermore, CA) software search and peak match routines with comparison to the ICDD (International Centre for Diffraction Data) database PDF-2, Version 2.0602 (2006). The ICDD database included the ICSD (Inorganic Crystal Structure Database) maintained by Fachinformationszentrum, Karlsruhe, Germany. Phase identification incorporated chemistry restrictions based on the elements determined from chemical analysis.

4.6.2 Scanning Electron Microscopy

A small sample was transferred with a wooden Q-tip stem onto carbon tape supported by an aluminum pedestal mount. The sample was analyzed using the radiation-shielded Amray Model 1610T SEM according to RPL-611A-SEM, *Scanning Electron Microscope Examinations*. In selected cases, the mount was carbon-coated. Selected sample areas were evaluated by energy dispersive X-ray spectroscopy (EDS) for qualitative elemental composition.

4.6.3 Transmission Electron Microscopy

The TEM samples were prepared in a two step methanol rinsing process. A small amount of the sludge slurry was mixed and transferred into methanol; a drop of the methanol slurry was transferred into a second vial containing methanol; then a drop of this second solution was deposited onto a lacey carbon TEM grid. The particles were air-dried on the lacey grid. Note that the sample drying process may induce changes in the morphology of the particle agglomerates. However, the objective of the TEM investigation was to look at the fundamental characteristics and sizes of individual particle crystallites that are not dependent on drying effects.

The observations were performed on an FEI Tecnai G2-30 (FEI Inc., Hillsboro, OR) with a field emission filament operating at 300 keV equipped with a Scanning Transmission Unit and High-Angle Annular Dark-Field Detector (HAADF), energy dispersive x-ray detector, and a Gatan Imaging Filter (GIF), model GIF2000 (Gatan Inc., Pleasanton, CA). Particle or area analysis was performed by identifying the composition with X-ray energy dispersive spectroscopy (EDS) and electron energy-loss spectroscopy (EELS). Images were obtained with either the scanning transmission electron microscopy (STEM) system or normal bright-field imaging. Energy-filtered images were also obtained with the image filter to produce element-specific area maps.

4.6.4 Electron Energy-Loss Spectroscopy

For the chromium oxidation study, two Group 6 samples were examined—G6-Cr-TEM (rigorously caustic-leached sample) and G6-IW (initial sample caustic-leached sample)—together with two mineral standards (Cr_2O_3 and PbCrO_4). The standards were crushed with a mortar and pestle, and a few particles were deposited onto a lacy carbon film. This type of film provided many thin regions where there was no carbon interference.

The EELS spectra were obtained using a 0.6-mm entrance aperture and an energy dispersion of 0.1 eV/channel. Low-loss spectra (including the zero loss peak) were acquired with an integration time of <0.2 s and core-loss spectra between 2 and 5 s. To reduce potential beam reduction, the acquisition time was kept as small as possible. The spectra were collected in the imaging mode of the transmission electron microscope and were corrected for dark current and channel-to-channel gain variation of the charge coupled device (CCD) detector.

The energy resolution was about 0.8 to 1.0 eV or better. By lowering the extraction voltage, it was possible to obtain an energy resolution of close to 0.7 eV. However, this resolution did not provide sufficient spectral intensity. Garvie and Craven (1994) have reported EELS data on the Cr-L_{2,3} edge for a series of minerals using a cold-field emission gun instrument. Although they obtained better energy resolution (0.35 eV) than that obtained in this study, the spectra generated by Garvie and Craven were useful for understanding the features present on the chromium edge.

The core-loss regime was energy calibrated, and the energy drift was measured while data were being acquired by collecting zero-loss spectra before or after core-loss spectra were collected. The position of the C-K (1s) peak at 284 eV (arising from transitions to the π^* molecular orbital) from the TEM lacy carbon support film was used to evaluate the energy calibration and as a means of roughly checking that the energy resolution was sufficient for collecting data.

Two methods were adopted for determining the chemical state of chromium in the sludge samples. In the first method, we obtained the following ratio defined as:

$$I - \text{ratio} = \frac{I(L_3)}{I(L_2)} \quad (4.11)$$

L_2 and L_3 are the intensities of background-corrected Cr-absorption edges. The second method was to look at the O:Cr ratio as an indication of oxygen content.

4.7 Quality Assurance and Quality Control

The following sections describe the quality assurance (QA) program and QC measures applied to the conduct of work.

4.7.1 Application of WTPSP Quality Assurance Requirements

PNNL's QA program is based on requirements defined in DOE Order 414.1C, Quality Assurance, and 10 CFR 830, Energy/Nuclear Safety Management, Subpart A—Quality Assurance Requirements (a.k.a., the Quality Rule). PNNL has chosen to implement the requirements of DOE Order 414.1C and 10 CFR 830, Subpart A by integrating them into the laboratory's management systems and daily operating processes. The procedures necessary to implement the requirements are documented through PNNL's Standards-Based Management System.

PNNL implemented the RPP-WTP quality requirements by performing work in accordance with the *River Protection Project – Waste Treatment Plant Support Program (RPP-WTP) Quality Assurance Plan (RPP-WTP-QA-001, QAP)*. Work was performed to the quality requirements of NQA-1-1989 Part I, Basic and Supplementary Requirements, NQA-2a-1990, Part 2.7, and DOE/RW-0333P, Rev 13, *Quality Assurance Requirements and Descriptions (QARD)*. These quality requirements are implemented through the *River Protection Project – Waste Treatment Plant Support Program (RPP-WTP) Quality Assurance Manual (RPP-WTP-QA-003, QAM)*.

A matrix that cross-references the NQA-1, NQA-2a, and QARD requirements with PNNL's procedures for this work was given in the test plan, TP-RPP-WTP-467.^(a) It included justification for those requirements not implemented. The QA requirements of DOE/RW-0333P, Rev 13, Quality Assurance Requirements and Descriptions (QARD) and DOE Order 414.1C were not identified as a requirement for this work in the test specification.

4.7.2 Conduct of Experimental and Analytical Work

Experiments that were not method-specific were performed in accordance with PNNL's procedures QA-RPP-WTP-1101 "Scientific Investigations" and QA-RPP-WTP-1201 "Calibration Control System," verifying that sufficient data were taken with properly calibrated measuring and test equipment (M&TE) to obtain quality results.

(a) SK Fiskum, TP-RPP-WTP-467, Rev. 0, 2/2/07 and Rev. 1, 7/31/07, *Characterization and Small Scale Testing of Hanford Wastes to Support the Development and Demonstration of Leaching and Ultrafiltration Pretreatment Processes*, Pacific Northwest National Laboratory, Richland, WA.

As specified in the supporting Test Specification, 24590-PTF-TSP-RT-06-0001, Rev. 0, BNI's Quality Assurance Project Plan (QAPjP), PL-24590-QA00001, was not applicable because the work was not performed in support of environmental/regulatory testing, and the data will not be used as such.

Balances are calibrated annually by a certified contractor, QC Services, Portland, Oregon. A balance performance check was conducted each day the balance was used.

The Analytical Services Operation (ASO) conducted analytical testing according to the Statement of Work RPP-WTP-QA-005, Rev. 2, *Analytical Support by the PNNL RPL Analytical Support Operation*. The analytical results and raw data are traceable through the project files according to the Analytical Services Request (ASR) number and RPL number.

4.7.3 Internal Data Verification and Validation

PNNL addressed internal verification and validation activities by conducting an independent technical review of the final data report in accordance with PNNL's procedure QA-RPP-WTP-604. This review verified that the reported results were traceable, that inferences and conclusions were soundly based, and the reported work satisfied the Test Plan objectives. This review procedure is part of PNNL's RPP-WTP Quality Assurance Manual.

5.0 Initial Characterization Results for REDOX Sludge Group 5

This section reports and discusses the analytical results for the Group 5 REDOX sludge slurry composite. Sample handling and processing steps are summarized in Figure 4.1. The supernatant results represent the equilibrated aqueous phases in contact with the solids; the solids characterization results were obtained after washing with 0.01 M NaOH (as described in Section 4.3).

5.1 Physical Properties of the Composite Slurry

Physical-property results for the REDOX sludge are summarized in Table 5.1 along with the propagated 1- σ error, average, and relative percent difference between S1 and S3 (the glass centrifuge tube holding S2 broke). Good precision was obtained for the sample set. Because the Group 5 material contained such a large fraction of settled solids (90%), the settling test was omitted.

Table 5.1. Physical Property Measurements of Homogenized Group 5 REDOX Sludge

Description	AR-S1	AR-S2	AR-S3	Nominal 1 σ error	Avg.	S1 and S3 RPD ^(a) (%)
Bulk Sample						
Density (g/mL)	1.24	1.22	1.27	0.08	1.24	2.1
Total Solids (wt%)	34.6%	--	35.1%	0.02%	34.9%	1.6
Total Undissolved Solids (wt%)	18.2%	--	18.9%	0.02%	18.5%	3.6
Settled Solids						
Density (g/mL)	1.25	--	1.28	0.09	1.26	2.1
Vol%	87.5%	86.7%	87.5%	8%	87.2%	0.0
Wt%	88.8%	--	88.2%	8%	88.5%	0.70
Total Undissolved Solids (wt%)	21.9%	--	21.4%	2%	21.6%	2.2
Wet Centrifuged Solids						
Density (g/mL)	1.38	--	1.36	0.08	1.37	1.3
Vol%	50%	--	53%	4%	52%	6.1
Wt%	55.8%	--	57.1%	0.02%	56.5%	2.4
Total Undissolved Solids (wt%)	34.7%	--	33.9%	5%	34.3%	2.4
Total Solids (wt%)	46.0%	--	46.3%	0.02%	46.1%	0.58
Supernatant						
Density (g/mL)	1.183	--	1.200	0.009	1.192	1.4
Total Dissolved Solids (wt%)	19.9%	--	19.8%	0.03%	19.8%	0.35
Water Content (g/g)	0.8015	--	0.8021	0.0004	0.8018	0.09
(a) RPD = relative percent difference						

5.2 Rheology of the Composite Slurry

Multiple Group 5 slurry samples were available for rheology testing. Shear-strength testing employed settled solids in five Group 5 sample jars. These jars were designated as TI477-G5-AR-J4 to -J8. Flow-curve testing employed a single Group 5 test sample, designated G5-RH-2 that was sub-sampled from Group 5 sample jar TI477-G5-AR-J6. All test samples contained 18.5 wt% UDS (see Table 5.1). Rheology measurements produced the following reportable data for the Group 5 initial characterization samples:

- a single measurement of settled-solids shear strength after 48 to 72 h
- four measurements of settled-solids shear strength after an indefinite period of time (~1 to 2 months)
- flow-curve data at 25°C, 40°C, and 60°C
- Power-law, Bingham Plastic, and Herschel-Bulkley flow-curve descriptors at 25°C, 40°C, and 60°C.

5.2.1 Shear Strength

The shear-strength test results are shown in Table 5.2. The single observation at 52 hrs of settling time indicates a shear strength of 72 Pa. The average of four observations of settled-solids shear strength at an indefinite settling time of one month or greater is 360 ± 60 Pa. In more familiar terms, 72 Pa is similar to the stress required to initiate flow in mustard, whereas 360 Pa is about twice the force required to initiate flow in mayonnaise (cf. Section 6.7 in Steffe 1992).

Table 5.2. Shear Strength of Group 5 REDOX Sludge Initial Characterization Settled Solids

Test Sample	Settling Time	Shear Strength [Pa]
TI477-G5-AR-J4	> 1 month	290
TI477-G5-AR-J5	> 1 month	430
TI477-G5-AR-J6	52 hrs	72
TI477-G5-AR-J7	> 1 month	350
TI477-G5-AR-J8	> 1 month	360
Ambient hot-cell temperature (~30°C) 18.5 wt% total undissolved solids.		

The variability in the repeat long-time measurements can be a result of either granular phenomena, such as particle-particle stick-slip and lithostatic pressure, or differences in the actual settling times between each sample jar. Although the variability in the 52-hr measurement is unknown, the results suggest that the shear strength increases significantly over long settling times. An increase in static shear strength typically occurs as a result of increased particle-particle contact, friction, cohesion as the solids settle and compact, gelation, or a combination thereof. Knowledge of the sample settling rate in relation to the rate of shear strength increase may provide additional insight into the mechanism of increase. However, it is difficult to accurately estimate the rate of increase given shear strength data for only two settling times.

5.2.2 Flow Curve

The results of flow-curve measurements for sample G5-RH-2 are shown in Figure 5.1. Over shear rates of 0 to 100 s⁻¹, shear stress was observed to increase rapidly as a function of shear rate for all temperatures. The rate of increase appeared to decrease with increasing temperature, with the 60°C showing the slowest response. Beyond 100 s⁻¹, all flow curves leveled out and showed a much slower increase in shear stress with shear rate. Over 100 to 1000 s⁻¹, shear stress increases at 25°C were linear, whereas both 40 and 60°C measurements showed slight-to-moderate downward curvature, indicative of a shear thinning fluid.

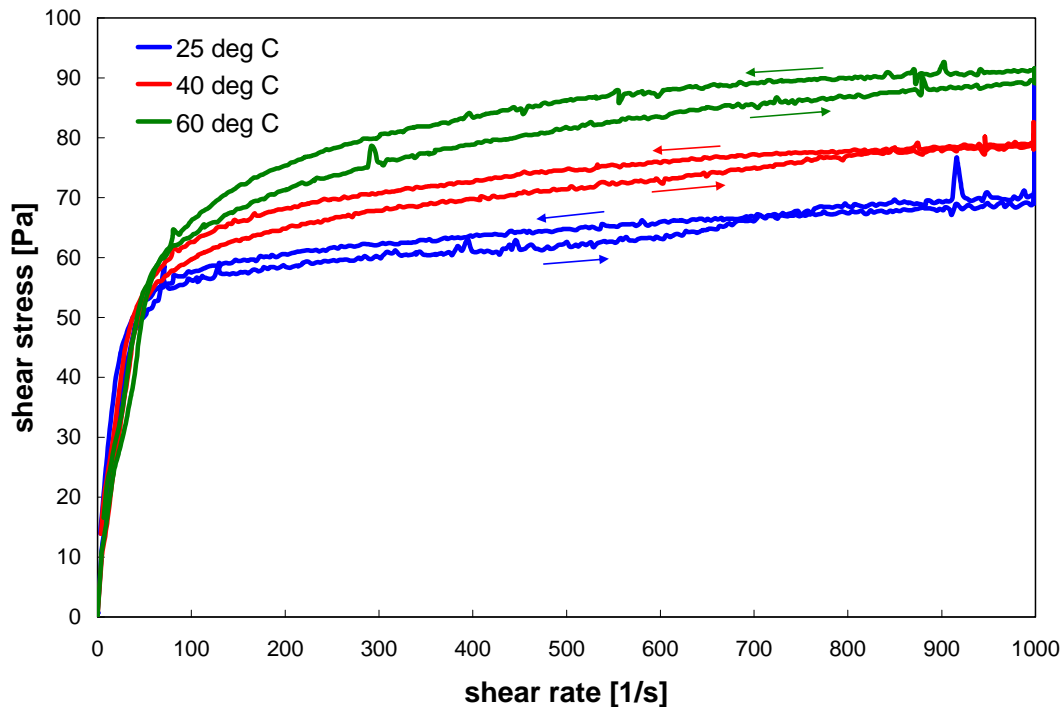


Figure 5.1. Shear Strength Versus Shear Rate for Group 5 REDOX Sludge Initial Characterization Sample G5-RH-2 at 25°C, 40°C, and 60°C (18.5 wt% UDS), Measured Using the MV1 Smooth Cup and Rotor. The arrows indicate the direction of the shear/rotational rate ramp.

The flow curves showed hysteresis for all temperatures. Specifically, the shear stress measured during the ramp up to 1000 s⁻¹ was always lower than that measured on the ramp back down to zero. Flow-curve-data hysteresis occurs as a result of sample alteration brought about by shear, chemical processes (such as precipitation), settling, or evaporation. Even though the sludge was sheared before being measured to mix the sample and eliminate structure, continued shearing of the sludge throughout each of the 15-min flow-curve tests could have continued to alter the sample. However, shearing tends to break-up and eliminate particle aggregates, which in turn lowers the force required to maintain fluid motion. As such, the observation of increased shear stress on all flow-curve down-ramps was not consistent with the expected shear-induced hysteresis effects typically seen with tank waste. Settling effects were also unlikely because the sludge was mixed immediately before testing to re-suspend settled solids and because phase separation was not observed when transferring the sample to the measurement cup.

Although chemical changes were also unlikely (as the jars from which the sample had been taken had at least 1 month to reach chemical equilibrium), it was possible that heating the sample could have altered particle-particle interactions. Particle-size measurements of Group 5 initial characterization samples did show sample instability (see Section 5.4). Specifically, applying sonic energy appeared to cause particle coagulation as it was accompanied by an increase in the fraction of coarse particles and particle aggregates. This could be consistent with the observations in Figure 5.1, as the formation of particle aggregates tends to increase the force required for fluid motion. Although particle coagulation can explain the shear-stress hysteresis, the evaporation of liquid (and the resulting increase in solids concentration it causes) was the most likely cause of the observed hysteresis. This was supported by the fact that separation between up-ramp and down-ramp stress curves increased with increasing temperature.

The measured range of shear stresses $>100 \text{ s}^{-1}$ uniformly increased with increasing temperature. For example, an increase of $\sim 20 \text{ Pa}$ was observed between the 25°C and 60°C measurements at 1000 s^{-1} . Like flow-curve hysteresis, the increase in measured shear stress with temperature may be attributed to either the coagulation of particles or evaporation. Because of volume limitations, the same Group 5 waste material was repeatedly tested. As such, evaporation was the most likely cause for the observed shear-stress increase.

The flow-curve behavior observed in Figure 5.1 is difficult to characterize. Altogether, the curves look highly pseudo-plastic. However, the sharp transition in slope that occurs around $\sim 100 \text{ s}^{-1}$ is not well-captured by the Ostwald equation (see Section 4.1) as shown in Figure 5.2. Although Figure 5.2 is restricted to flow-curve data at 40°C , Ostwald fits of 25° and 60°C data show similar problems. The unusual stress versus strain-rate behavior over 0 to 100 s^{-1} might be an artifact caused by the slip between the test sample and sensor surfaces.

When attempting to analyze the data using Bingham-Plastic and Herschel-Bulkley models, flow-curve data in the 0 to 100 s^{-1} region skewed the curve fits at higher shear rates. To overcome this problem, regression analysis for Bingham-Plastic and Herschel-Bulkley models was limited to the 200 to 1000 s^{-1} shear-rate region. The results of regression analysis for sample G5-RH-2 are shown in Table 5.3. Figure 5.2 shows the Bingham-Plastic and Herschel-Bulkley model fits for 40°C ; similar fits were obtained at 25° and 60°C . Based on the reported correlation coefficient, R , all models provided roughly equivalent fits of the data. All fits of the flow-curve data suggested a finite yield point. For the Ostwald (power-law) fit of the 40°C data, the dramatic change in slope as the shear rate approaches zero forms an apparent yield stress that falls between 30 and 40 Pa. The Bingham Plastic and Herschel-Bulkley fits of the 40°C data suggest yield points of ~ 65 and $\sim 45 \text{ Pa}$, respectively.

Because none of the fitting parameters and corresponding equations provided an accurate representation of the low-shear region, care must be taken when interpreting them. A general representation of how the flow-curve behavior changes with temperature may be derived from the Bingham-Plastic model parameters. Here, the apparent yield stress increased from 57 to 74 Pa as the temperature increased from 25° to 60°C . Likewise, the consistency of the fluid increased slightly from 13 cP to 17 cP. Whether these numbers are actually representative of the actual yield stress and consistency cannot be ascertained from the flow-curve measurements alone.

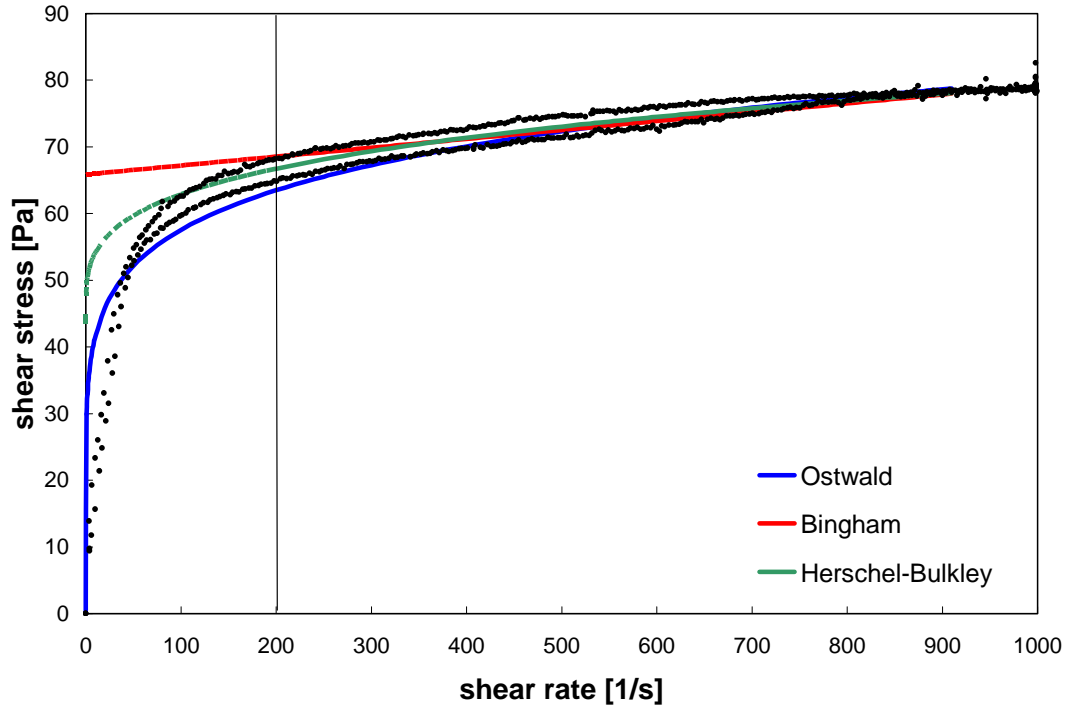


Figure 5.2. Flow Curve Fits for Group 5 REDOX Sludge Sample G5-RH-2 at 40°C (18.5 wt% UDS)

Note: Filled circles are flow curve data. The Ostwald fit (blue line) is applied over 0 to 1000 s^{-1} , whereas the Bingham-Plastic and Herschel-Bulkley fits (red and green lines, respectively) are applied over 200 to 1000 s^{-1} . The Bingham Plastic and Herschel-Bulkley fits are extrapolated down to 0 from 200 s^{-1} (shown as dashed lines).

Table 5.3. Best Fit of Select Rheological Models to Group 5 REDOX Sludge Flow Curve Data

Temperature [°C]	Model	Yield Stress [Pa]	Consistency [Pa·s ⁿ]	Flow Index	R ^(a)
25	Ostwald (Power-Law)	n/a	30	0.12	0.94
40	Ostwald (Power-Law)	n/a	30	0.14	0.95
60	Ostwald (Power-Law)	n/a	28	0.17	0.95
25	Bingham-Plastic	57	0.013	n/a	0.94
40	Bingham-Plastic	66	0.013	n/a	0.95
60	Bingham-Plastic	74	0.017	n/a	0.92
25	Herschel-Bulkley	56	0.044	0.83	0.94
40	Herschel-Bulkley	44	5.8	0.26	0.96
60	Herschel-Bulkley	26	19	0.18	0.94

(a) R is the correlation coefficient of the fit.

On the other hand, the flow-curve fits provide reasonable bounds for the material yield stress for Group 5 wastes. Neglecting the unusual behavior between 0 and 100 s^{-1} , examining the fits in Figure 5.2 suggests that the Bingham-Plastic model overestimates the material yield point. As such, the yield stress for this

model can be used to place a conservative upper bound on the actual material yield stress. The lower bound for material yield in Figure 5.2 is less clear because of slip; however, the Herschel-Bulkley yield stress typically provides a conservative lower bound. The Ostwald equation is usually neglected because it does not incorporate a yield stress (although for the fit shown in Figure 5.2, it does suggest an apparent yield of 30 Pa). Based on the information in Table 5.3, it is possible to bound the actual material yield stress for Group 5 initial characterization samples between 20 and 74 Pa, depending on temperature.

The apparent viscosity at 33 s^{-1} was derived from each measurement as a point of reference; results are provided in Table 5.4. For each temperature, this reference point was determined from measurement data and from the fitting parameters provided in Table 5.3. Viscosities at 33 s^{-1} can be found in previous PNNL waste rheology characterizations (and still serve as a useful standard point of comparison). In terms of physical significance, 33 s^{-1} is indicative of shear rates that exist in pulse-jet mixing systems and process pumps at startup. The measurement data at all three temperatures showed high shear stress (~30 to 75 Pa); thus, the apparent viscosities at 33 s^{-1} were on the order of 1000 cP. Because the consistency of the material was low, apparent viscosities dropped off rapidly.

Table 5.4. Apparent Viscosity of Group 5 REDOX Sludge Sample G5-RH-2 at 33 s^{-1}

Temperature [°C]	η_{app} (cP) from measurement data	η_{app} (cP) from fitting parameters		
		Power-Law	Bingham Plastic	Herschel- Bulkley
25	1320	1400	1750	1720
40	1250	1490	2010	1760
60	1060	1550	2260	1870

5.2.3 Chemical and Radiochemical Composition

The two samples taken for chemical characterization were evaluated for volume percent centrifuged solids as part of the initial phase separation. In this case, the volume percent centrifuged solids duplicated well at 46% but was slightly less than the 52% centrifuge solids found with the physical-property testing samples. Centrifuging conditions were the same in each case; however, the centrifuge cones were constructed of different materials: polypropylene for the characterization samples and glass for the physical-property test samples.

The gray centrifuged solids appeared uniform top to bottom (see Figure 5.3). The supernatant was yellow, most likely because of the presence of chromate ion. The supernatant density was determined to be 1.16 g/mL ($T = 24^\circ\text{C}$) based on the average masses of four 1-mL volume deliveries. This compared well with the density determined as part of the physical-property testing procedure (density = 1.19 g/mL).

The specific washing scheme for the redox sludge is provided in Figure 5.4. With each successive washing step, the CS packing was more easily disturbed during the course of supernatant removal with the transfer pipet. The hydroxide concentration in the final wash solution was estimated to be 0.05 M after incorporating the sequential dilution of the entrained supernatant. The difference between the total input wash volume (60.7 mL) and the collected wash plus entrained supernatant volume (58 mL) was attributed to residual fluid above the final washed solids. The combined volume of washed centrifuged

solids was ~23 mL, representing a total centrifuged-solids volume loss of ~3 mL or ~12% by volume. The CS volumes were estimated based on the centrifuge-tube graduations.

The average radioanalytical results for the supernatant, composited wash solution, and washed solids are provided in Table 5.5 along with the applicable relative percent differences (RPD, measure of precision between duplicates). The gross-beta results showed good agreement with the sum of beta emitters: ^{137}Cs and ^{90}Sr (in secular equilibrium with ^{90}Y) thus indicating that no other major source of beta-gamma activity was present. The gross alpha activity in the supernatant liquid was below the method detection limit. The gross alpha activity measured in the solids agreed reasonably well with the summation of alpha emitters (^{238}Pu , $^{239+240}\text{Pu}$, and ^{241}Am) (the latter generally provides a better estimate of total alpha activity). The duplicate GEA results from the KOH fusion preparation resulted in a large scatter of the GEA data; therefore, the reported values in Table 5.5 were taken from the NaOH/ Na_2O_2 fusion preparation. The washed solids GEA analysis showed the presence of ^{54}Mn . This isotope has a 312-day half-life and will no longer be present in the tank waste as a result of processing activities associated with the waste production. It was most probably a contaminant from homogenization processing in the HLRF where concurrent work with irradiated fuel assemblies was conducted. For initial characterization purposes, its presence can be ignored.



Figure 5.3. Chemical Characterization Sample of Group 5 REDOX Sludge Centrifuged Solids

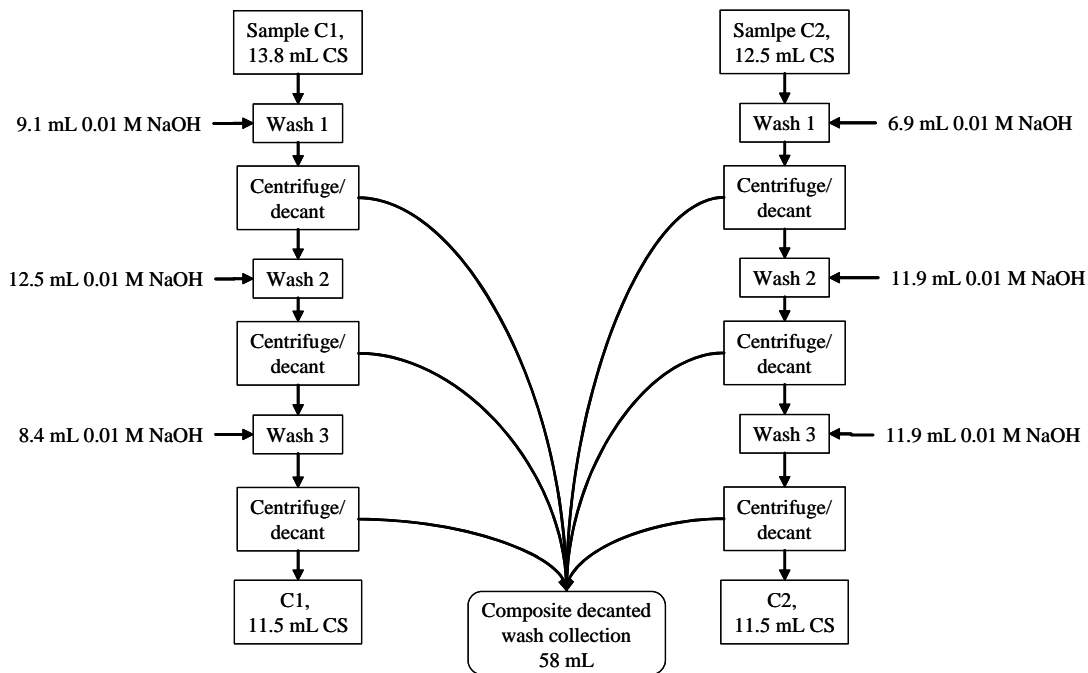


Figure 5.4. Wash Sequence of Group 5 REDOX Sludge Supporting Initial Characterization (CS = centrifuged solids)

Table 5.5. Radionuclide Characterization of the Group 5 REDOX Sludge

Sample ID>	Supernatant		Wash composite		Washed solids	
	07-00365		07-00366		07-00367	
Analyte	μCi/mL	RPD	μCi/mL	RPD	μCi/g ^(a)	RPD
¹³⁷ Cs	3.73E+1	0.27	1.06E+1	2.8	5.33E+1 ^(b)	1.7
⁶⁰ Co	<2.E-4	na	<2.E-5	na	1.23E-2 ^(b)	4.1
²⁴¹ Am	<4.E-2	na	<2.E-3	na	2.90E-1 ^(b)	16
²³⁸ Pu	1.35E-6	63	n/a	na	2.27E-2	3.5
²³⁹⁺²⁴⁰ Pu	1.95E-5	13	n/a	na	8.83E-1	9.0
⁹⁰ Sr	2.66E-2	3.8	n/a	na	6.62E+2	0.15
Gross alpha	<2.E-4	na	<2.E-4	na	8.77E-1	35
Sum of alpha	2.08E-5	8.4	n/a	na	1.22E+0	4.1
Gross beta	3.89E+1	7.5	11.1	^(c)	1.52E+3	0.66
Sum of beta	3.73E+1	0.27	n/a	na	1.38E+3	0.88
<i>Opportunistic</i>						
⁵⁴ Mn	n/a	na	n/a	na	9.16E-3 ^(d)	31.4
¹⁵⁴ Eu	<7.E-4	na	<1.E-4	na	1.23E-1	2.4
¹⁵⁵ Eu	<1.E-2	na	<2.E-3	na	<5.E-2	na
ASR 7874 Reference date is March 1, 2007. (a) Analyte concentrations are calculated on a dry-mass basis. (b) The ¹³⁷ Cs, ⁶⁰ Co, and ²⁴¹ Am in the solids were determined from a sample prepared by NaOH/Na ₂ O ₂ fusion. (c) This sample was not required to be run in duplicate; therefore, an RPD was not calculated. (d) Probable contaminant from processing in the HLRF. Notes: na = not applicable; n/a = not analyzed						

The chemical composition of the washed Group 5 solids is provided in Table 5.6. As expected, the sludge consisted primarily of aluminum with significant sodium and uranium components. The supernatant was primarily sodium salts (nitrate, nitrite, carbonate, and hydroxide). The anionic and cationic charge balance was evaluated for the supernatant, resulting in a 2.4% difference, well within analytical uncertainties.

The fractional distribution of selected analytes in the supernatant, wash, and solids phases is shown in Table 5.7 and Figure 5.5. A large portion (70 to 84%) of the Na, P, Cr, and S partitioned to the aqueous phase. Washing did not mobilize any significant additional quantities. The Al remained primarily in the solids phase. Analyte water wash factors were calculated from the mass distribution in the combined supernatant and wash solutions relative to the total analyte mass according to Equation 5.1.

$$F_i = \frac{\sum S_i + W_i}{S_i + W_i + UDS_i} \quad (5.1)$$

where S_i is the analyte mass in supernatant fraction, W_i is the analyte mass in combined wash solution, and UDS_i is the analyte mass in the undissolved solids.

Table 5.6. Chemical Characterization of the Group 5 REDOX Sludge

	Supernatant			Wash Composite			Washed Solids	
Sample ID>	07-00365			07-00366			07-00367	
Analyte	µg/mL	M	RPD	µg/mL	M	RPD	µg/g ^(a)	RPD
Al	2,595	9.62E-2	2.70	704	2.61E-2	na	326,500	2
B	45.8	4.23E-3	3.72	[18]	[1.7E-3]	na	[81]	[7]
Bi	<2	<1.E-5	na	<2	<1.E-5	na	<70	na
Cd	<0.3	<2.E-6	na	<0.2	<2.E-6	na	<3	na
Cr	1,225	2.36E-2	2.45	342	6.58E-3	na	2,110	0
Fe	<2	<4.E-5	na	<2	<4.E-5	na	7,265	13
K	487	1.24E-2	2.26	142	3.63E-3	na	<10,000	na
Mn	<0.2	<4.E-6	na	<0.2	<4.E-6	na	4,500	2
Na	73,700	3.21E+0	2.99	21,400	9.31E-1	na	55,200	0
Ni	<0.6	<1.E-5	na	<0.6	<1.E-5	na	308	1.9
S	[235]	7.3E-3	4.26	[59]	[1.8E-3]	na	<300	na
Si	54	1.9E-3	7.41	21	7.48E-4	na	8,760	8
Sr	[0.039]	4.5E-7	10	<0.02	<2.E-7	na	1,165	1
U	<9	<4.E-5	na	<9	<4.E-5	na	19,700	2
Zn	<0.6	<9.E-6	na	<0.6	<9.E-6	na	[76]	[52]
Zr	<0.8	<9.E-6	na	<0.8	<9.E-6	na	[140]	[0]
U KPA	n/a						20,200	3
nitrite	24,500	5.33E-1	0.82	6,980	1.52E-1	1.15	na	
nitrate	89,600	1.45E+0	0.00	25,300	4.08E-1	0.79	na	
phosphate	1,165	1.23E-2	2.58	354	3.73E-3	2.3	na	
sulfate	702	7.31E-3	0.57	193	2.01E-3	0	na	
oxalate	873	9.91E-3	0.57	270	3.07E-3	0	na	
free hydroxide	na	2.35E-1	4.3	no data				
TOC as C	420	3.5E-2	0					
TIC as C	5,100	4.25E-1	0					
Opportunistic								
fluoride	59.7	3.14E-3	0.67	10.9	6.21E-4	15	na	
Ag	<0.4	<4.E-6	na	<0.4	<4.E-6	na	<7	na
As	<7	<1.E-4	na	<20	<2.E-4	na	<100	na
Ba	<0.4	<3.E-6	na	[0.35]	[2.5E-6]	na	[105]	[10]
Be	[0.014]	[1.5E-6]	na	[0.023]	[2.6E-6]	na	<0.4	na
Ca	[5.7]	[1.4E-4]	25	[3.5]	[8.7E-5]	na	1,270	14
Ce	<1	<9.E-6	na	<1	<9.E-6	na	<90	na
Co	[0.50]	[8.5E-6]	na	<0.4	<7.E-6	na	<9	na
Cu	<0.5	<8.E-6	na	<0.5	<8.E-6	na	[39]	[72]
Dy	<0.4	<2.E-6	na	<0.4	<2.E-6	na	<20	na
Eu	<0.1	<7.E-7	na	<0.1	<7.E-7	na	<70	na

Table 5.6 (Contd)

Sample ID>	Supernatant			Wash composite			Washed solids	
	07-00365			07-00366			07-00367	
Analyte	µg/mL	M	RPD	µg/mL	M	RPD	µg/g	RPD
La	<0.1	<1.E-6	na	[0.14]	[9.8E-7]	na	[38]	[0]
Li	<0.6	<8.E-5	na	<0.6	<8.E-5	na	<10	na
Mg	<0.7	<3.E-5	na	[1.4]	[5.8E-5]	na	[245]	4
Mo	14.6	1.52E-4	10	[4.9]	[5.1E-5]	na	<10	na
Nd	<2	<1.E-5	na	<2	<1.E-5	na	<100	na
P	364	1.17E-2	0.28	107	3.45E-3	na	[675]	[1]
Pb	<4	<2.E-5	na	[3.80]	[1.8E-5]	na	<40	na
Pd	<1	<1.E-5	na	<1	1.21E-05	na	<80	na
Rh	[2.66]	[2.6E-5]	na	<3	<3.E-5	na	<50	na
Ru	[2.25]	[2.2E-5]	na	<0.8	<8.E-6	na	<20	na
Sb	[3.39]	[2.8E-5]	na	<3	<3.E-5	na	<80	na
Se	[5.85]	[7.4E-5]	na	<5	<6.E-5	na	<100	na
Sn	[3.0]	[2.5E-5]	na	<2	<2.E-5	na	<100	na
Ta	<1	<8.E-6	na	<1	<8.E-6	na	<30	na
Te	<3	<3.E-5	na	<3	<3.E-5	na	<100	na
Th	[2.3]	[9.9E-6]	na	[1.8]	[7.8E-6]	na	<80	na
Ti	<0.1	<2.E-6	na	[0.18]	[3.8E-6]	na	[32]	[10]
Tl	<7	<3.E-5	na	<7	<3.E-5	na	<90	na
V	[1.45]	[2.8E-5]	na	[0.66]	[1.3E-5]	na	<6	na
W	17.7	9.60E-5	14	<5	<3.E-5	na	<40	na
Y	<0.09	<1.E-6	na	<0.09	<1.E-6	na	<9	na

(a) Analyte concentrations are calculated on a dry-mass basis.
ASR 7489.
Analyte uncertainties were typically within $\pm 15\%$ (2-s); results in brackets indicate that the analyte concentrations were greater than the minimum detection limit (MDL) and less than the estimated quantitation limit (EQL), and uncertainties were $>15\%$.
Opportunistic analytes are reported for information only; QC requirements did not apply to these analytes.

The water-wash factors obtained from the current testing were compared with the weighted mean of the water-wash factors obtained from the TWINS database. The weighting factors were obtained from the relative masses of tank waste that were used to create the composite. The experimental Na and P wash factors resulted in fairly good correspondence with the TWINS water-wash factors. The experimental Cr- and Al-wash factors varied from the TWINS factor by ~0.5 to 4. The experimental S wash factor was compared to the TWINS sulfate wash factor since the S wash factor was not provided in TWINS. Direct cross comparison for these factors was confounded by the specific sample selection process. Samples high in Al were selected for testing, and these did not necessarily represent the tank composite.

Table 5.7. Phase Distribution of Selected Analytes in Group 5 REDOX Sludge

Analyte	Supernatant wt%	Wash Solution wt%	Water-Wash Factor wt%	TWINS Water-Wash Factor ^(a) wt%	Solids wt%
Cr	70	0.37	70	38	30
Al	3	0.02	3	11	97
Na	84	0.46	85	86	15
P	69	0.38	69	89 ^(b)	31
S	[75]	[0.36]	>75	99 ^(c)	<25

(a) The water-wash factor represents the weighted mean of the four represented tank-waste sources from the TWINS database.
 (b) TWINS reported a phosphate water-wash factor.
 (c) Reported in TWINS as sulfate; sulfur water wash factor was not available.
 Results in brackets indicate that the analyte concentrations were >MDL and <EQL.

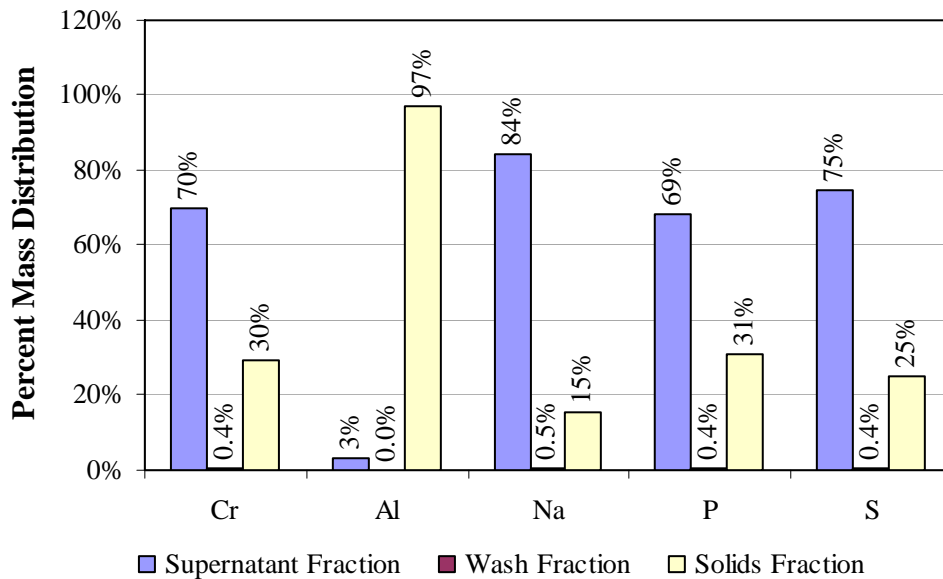


Figure 5.5. Selected Analyte Phase Distribution for Group 5 REDOX Sludge

5.3 Particle Size

Table 5.8 summarizes the particle-size measurements for primary and duplicate samples of Group 5 washed solids. The diameters listed correspond to the 10%, 50%, and 90% volume/weight fractiles and are listed as a function of the test condition.

The d(50) ranged from 4.3 to 8.2 μm , the d(10) ranged from 1.0 to 1.9 μm , and the d(90) ranged from 16 to 19 μm . The listed fractiles did not appear to be strongly affected by sonication. However, there was a slight increase in the measured d(50) upon the application of sonic power to both Group 5 primary and duplicate samples.

The influence of sonication on the measured distribution was difficult to evaluate when expressed as diameters corresponding to specific cumulative undersize fractions (as above). Figure 5.6 and Figure 5.7 show the PSDs before, during, and after sonication for Group 5 primary and duplicate samples, respectively. The “during sonication” PSDs corresponded to the test conducted at 75% sonic power. Both samples showed similar size ranges and behavior over the various test conditions. Before sonication, both samples showed a broad and relatively continuous distribution of sizes ranging from 0.3 μm up to $\sim 50 \mu\text{m}$. The primary sample showed two maxima at 2.5 and 8 μm ; however, these were less distinct in the duplicate sample.

The application of sonic power to the Group 5 samples distinctly altered the PSD. Although the range of particle sizes observed in the distribution remained relatively unchanged, both duplicate and primary samples showed a significant increase in the population of 8- to 10- μm particles and a corresponding decrease in the 1- to 3- μm particles. This was contrary to what would normally be expected, as sonication typically breaks down particle aggregates. The effect on the resulting size distribution was a reduction in the fraction of large particles and an increase in the fraction of small particles. As such, it was difficult to classify this apparent increase in the population of larger fractions without having additional information on the distribution of primary particle sizes (i.e., the size of individual particles). Because the Malvern analyzer is unable to differentiate between single (primary particle) and particle aggregates during measurement, such information was not available from the current analysis.

Table 5.8. Summary of Results for Group 5 REDOX Sludge Particle-Size Analysis

Sample	Sonic Power	Condition	d(10) [μm]	d(50) [μm]	d(90) [μm]
Group 5—Primary	0%	pre-sonic	1.1	4.3	16
	25% (~5 W)	sonicated	0.98	5.9	17
	50% (~10 W)	sonicated	1.0	6.5	17
	75% (~15 W)	sonicated	1.1	6.6	16
	0%	post-sonic	1.0	6.4	16
	0%	post-sonic	1.0	6.6	17
Group 5—Duplicate	0%	pre-sonic	1.1	4.6	19
	25% (~5 W)	sonicated	1.2	6.7	18
	50% (~10 W)	sonicated	1.4	7.9	18
	75% (~15 W)	sonicated	1.7	8.1	18
	0%	post-sonic	1.9	8.2	18

Note: The diameters corresponding to the 10%, 50%, and 90% volume/weight fractiles are given [d(10), d(50), and d(90), respectively].

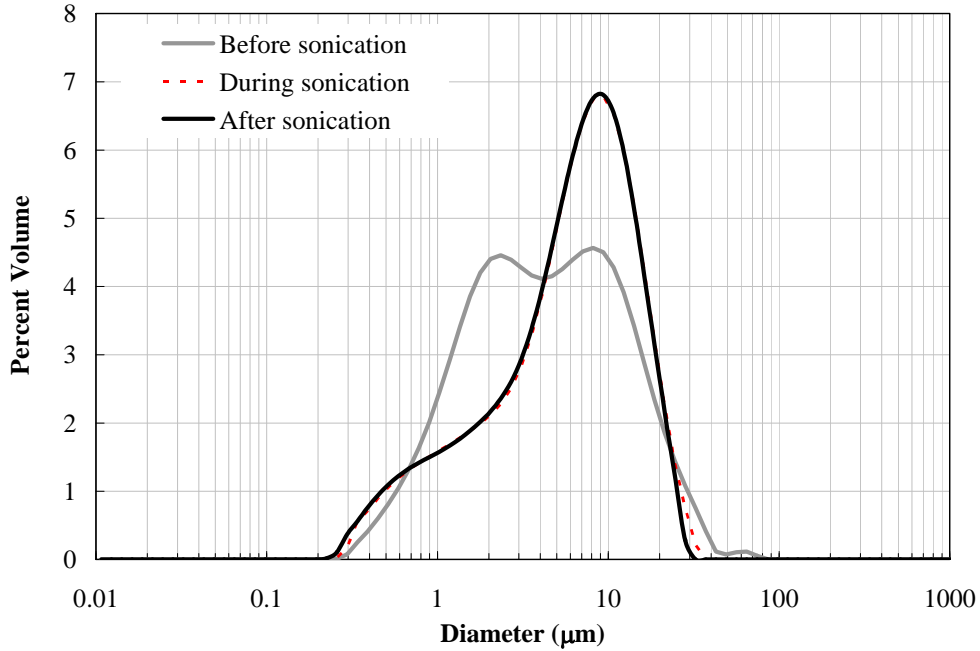


Figure 5.6. Group 5 REDOX Sludge Primary Sample PSDs (volume/weight basis) Before, During, and After Sonication

(Note: The analyzer flow cell was operated at 3000 RPM and at a maximum sonic power of 75% [~ 15 W]).

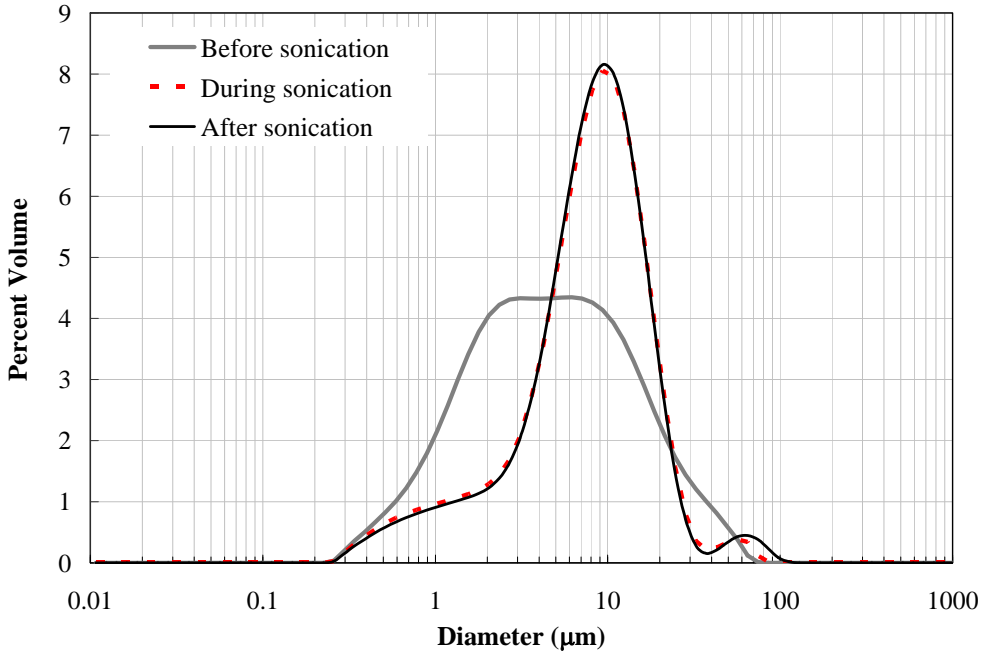


Figure 5.7. Group 5 REDOX Sludge Duplicate Sample PSDs (volume/weight basis) Before, During, and After Sonication

(Note: The analyzer flow cell was operated at 3000 RPM and at a maximum sonic power of 75% [~ 15 W]).

Although the increase in 8- to 10- μm particle population was contrary to what was expected, there is a reasonable physical basis for this observation. The pre-measurement treatment of these samples involved a significant alteration of the suspending phase chemistry during the compositing of the tank waste samples and subsequent washing and re-suspension activities. The consequence of this alteration was that a stable state of particle aggregation from earlier sample conditions may have been preserved as a semi-stable state in the subsequent conditions. This can occur because of energy barriers to aggregate restructuring that derive from strong interparticle forces. Although dispersion and mixing events may have not been sufficient to overcome this energy barrier, the application of sonic energy is highly disruptive and could have been sufficient to allow agglomerate restructuring.

Post-sonication measurements of both primary and duplicate samples compared well (i.e., show no significant difference) with size distributions taken during sonication. This suggests that the aggregate restructuring that occurred upon sonication was not reversible over the period of post-sonication observation (roughly 7 min for the primary sample and 3 min for the duplicate).

5.4 Surface Area

A single 0.14-g sample tested for surface area resulted in 26 m^2/g . (Duplicate samples were tested but the sample masses were small and resulted in high uncertainty.)

5.5 Crystal Form and Habit

The XRD pattern for Group 5 is provided in Figure 5.8; the background-subtracted XRD pattern with stick-figure phase identification is shown in Figure 5.9. The XRD pattern was dominated by boehmite with minor contributions from gibbsite, iron oxide, sodium nitrate, and sodium uranium oxide. A small amount of talc was found in the sample and was traced to contamination from the powdered gloves used in the sample preparation.

An indication of the relative concentrations of boehmite and gibbsite were obtained from Whole Pattern Fitting analysis using Relative Intensity Ratio (RIR) values. The average gibbsite-to-boehmite phase ratio from seven sample preparations was 0.077.

The boehmite peak at 14° $2\text{-}\theta$ was very broad for peaks in this region. The broadening was affected by one or two circumstances: other phases (sodium uranium oxide and nickel hydrogen phosphate hydrate) were contributing to this peak, and/or the crystallite size of boehmite was unusually low. The nominal boehmite crystallite size was estimated to be 203 Å based on the attribution of the 14° $2\text{-}\theta$ peak only to boehmite and application of a simplistic crystallite size evaluation.^(a)

(a) The Jade operating software applied the Scherrer equation to estimate the crystallite size (Klug and Alexander 1974, pp. 687-690).

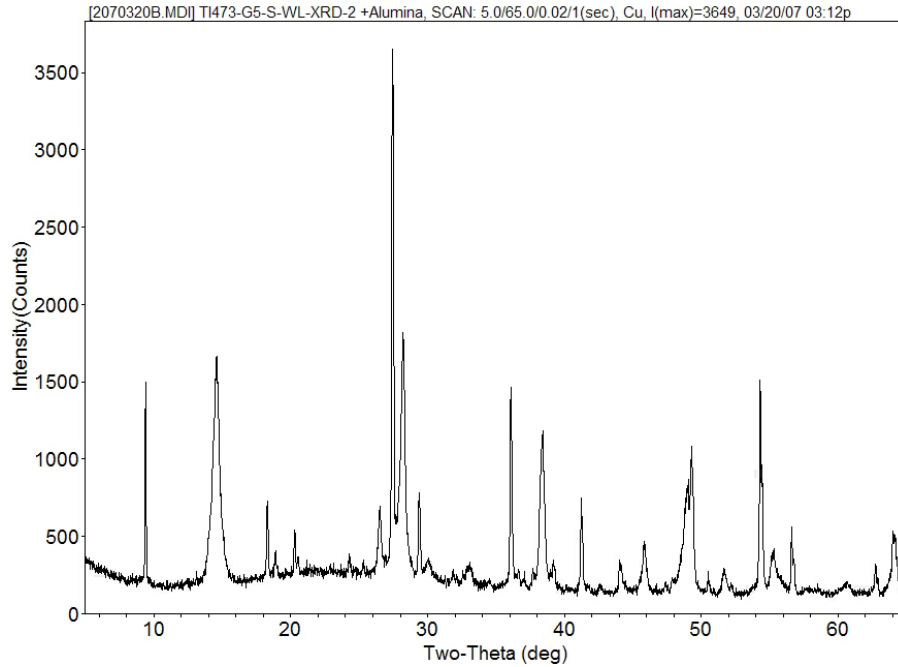


Figure 5.8. XRD Pattern of Washed Group 5 REDOX Sludge with Rutile (TiO₂) Internal Standard

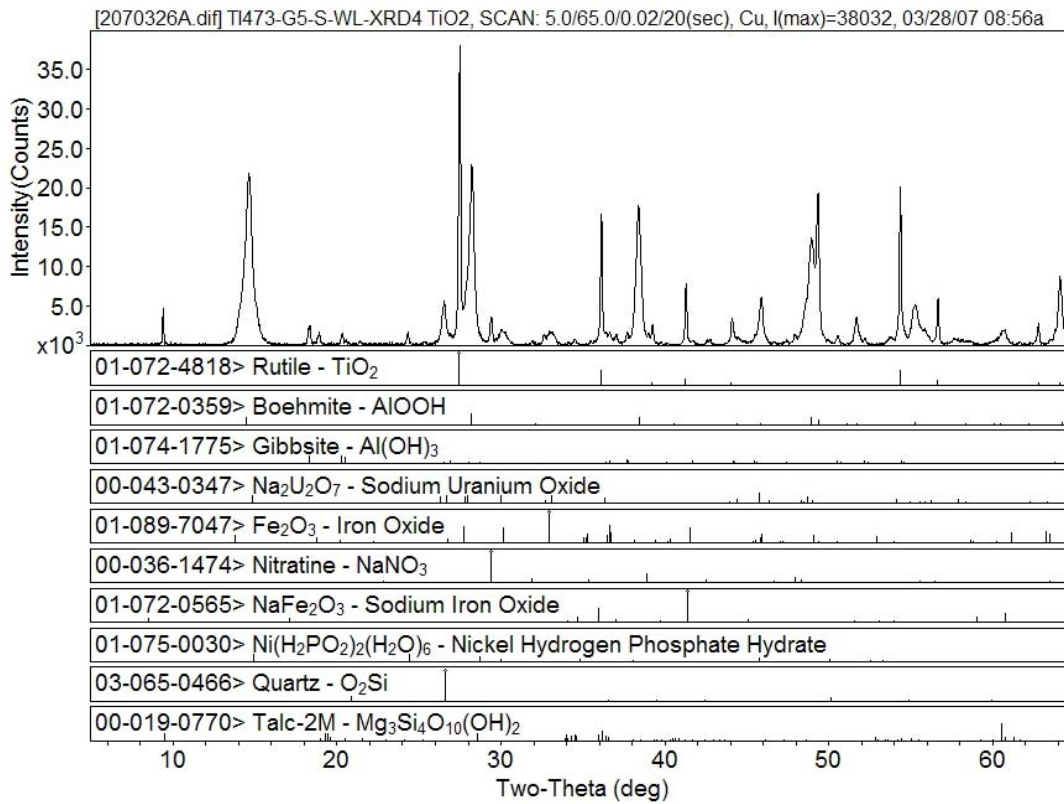


Figure 5.9. XRD Pattern of Washed Group 5 REDOX Sludge, Background-Subtracted with Stick-Figure Peak Identification

The XRD pattern was consistent with the chemical analysis. The approximate mass percent of chemical phases was determined by evaluating the crystalline species in conjunction with the elemental concentrations. Table 5.9 summarizes the mass percent of phases in the solids. Phases were listed as “observed” if recognized in the XRD pattern. Two phases containing Al were “assigned” based on chemical analysis, assumptions about the tank chemistry, and STEM-EDS analysis; these potentially comprised a small fraction of the waste form, ~4.8 wt%. The entrained-salts component was determined from the calculated dilution of entrained supernatant in the wet centrifuged solids. The three sequential washings at ~1:1 liquid-to-solids phase ratio were not sufficient to remove all of the supernatant. As intended, the Group 5 waste sample was clearly dominated by boehmite.

Figure 5.10 shows the phase ratio breakdown after correcting for the entrained supernatant salts from the composition. Boehmite comprises 74% of the mass fraction of well-washed solids.

Figure 5.11 provides a SEM-EDS map of selected elements. As expected, Al dominated the composition, consistent with the chemical analysis. Other elements (Na, U, Cr, Fe, Mn, and Si) were mapped but showed no distinct phase boundaries.

Table 5.9. Weight Percent of Group 5 REDOX Sludge Mineral Phases, Best Estimate

Crystalline Phase	Chemical Structure	Weight %	Basis ^(a)
Boehmite	AlOOH	66.8	Observed
Gibbsite	Al(OH) ₃	5.1	Observed
Zeolite A (prototypic and bounding based on [Si])	NaSiAlO ₄	3.1	Assigned
Sodium uranium oxide	Na ₂ U ₂ O ₇	2.6	Observed
Cancrinite (prototypic and bounding based on [Ca])	Na ₆ Ca ₂ Al ₆ Si ₆ O ₂₄ (CO ₃) ₂	1.7	Assigned
Iron oxide	Fe ₂ O ₃	1.0	Observed
Unknown or amorphous Cr, Mn, Ni, Sr	Cr, Mn, Ni, Sr	0.8	Chem analysis
Unaccounted sodium	Na	2.0	Assigned
Entrained Na salts from supernatant	various	9.6	Observed and calculated
Assumed counter ions	oxides, hydroxides, etc.	7.3	Balance
Sum		100	
<p>(a) <i>Observed</i> indicates that the characteristic crystal diffraction pattern of the identified crystalline phase was observed in the sample XRD pattern.</p> <p><i>Assigned</i> indicates that the characteristic crystal diffraction pattern of the identified crystalline phase was not observed in the sample XRD pattern, and its listing is based on assumptions about tank waste chemistry, chemical analysis, or TEM-EDS; therefore, the assigned crystalline phase should be considered with caution.</p> <p><i>Calculated</i> indicates that the mass associated with supernatant entrainment was calculated based on the supernatant dilution factor during solids washing.</p>			

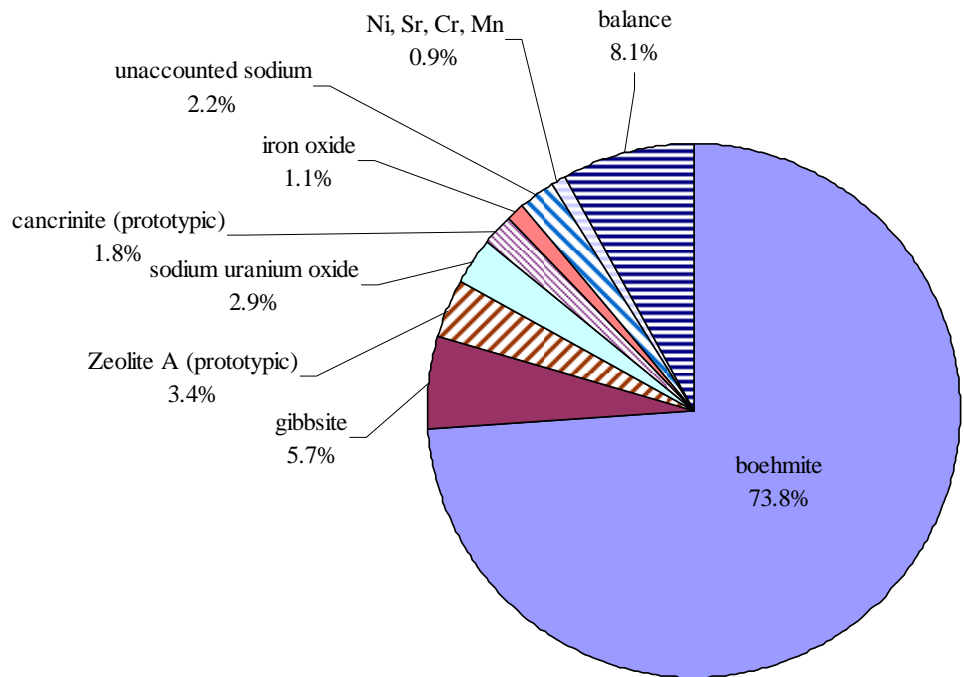


Figure 5.10. Washed Group 5 REDOX Sludge Phase Composition (Entrained Supernatant Removed), Best Estimate

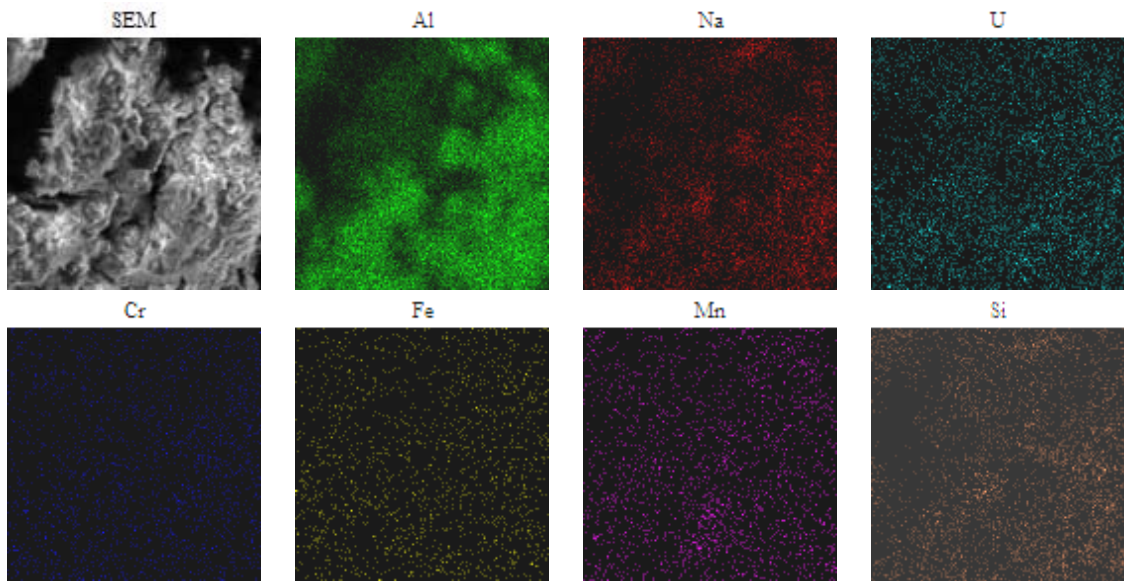


Figure 5.11. SEM-EDS Image of Washed Group 5 REDOX Sludge with Al, Na, U, Cr, Fe, Mn, and Si Maps

Several SEM images of the washed solids are shown in Figure 5.12. The sample is dominated by aggregates of small particles. The small particle size indicated the material will have a large surface area. These images support the PSD analysis where the particle diameters were largely on the order of 10 μm with a range of 0.2 to 40 μm . One SEM view (c) showed crystal block shapes up to 20 microns on a side. In view (f), elongated prismatic structures are also seen.

The TEM micrographs of the solids phase are shown in Figure 5.13, and STEM micrographs with EDS are shown in Figure 5.14. Some STEM images obtained were not in sharp focus because of the thickness of the particles on the TEM grid, and thus specific crystalline properties could not be discerned. The material had a relatively high surface area with small particles, was dominated by Al phases, and the specific particle morphology of Al phases was identified as boehmite (identified by its rhombohedral platelet-like morphology). Spherical and elongated particles also were evident that appeared to be associated with more dense material consistent with U, Mn, and Fe species.

The boehmite phase was identified by its rhombohedral platelet-like morphology. Boehmite is sometimes observed to be fibrous or acicular, so such observations are not always diagnostic. In the presence of nitrate, boehmite is known to precipitate as hexagonal plates (Music et al. 1998). The morphology of gibbsite crystals evolves from thin, rounded hexagons and faceted lozenges into faceted plates and blocks with well-formed basal prismatic faces. Caustic conditions, not just reaction time, are known to lead to the formation of larger crystals.

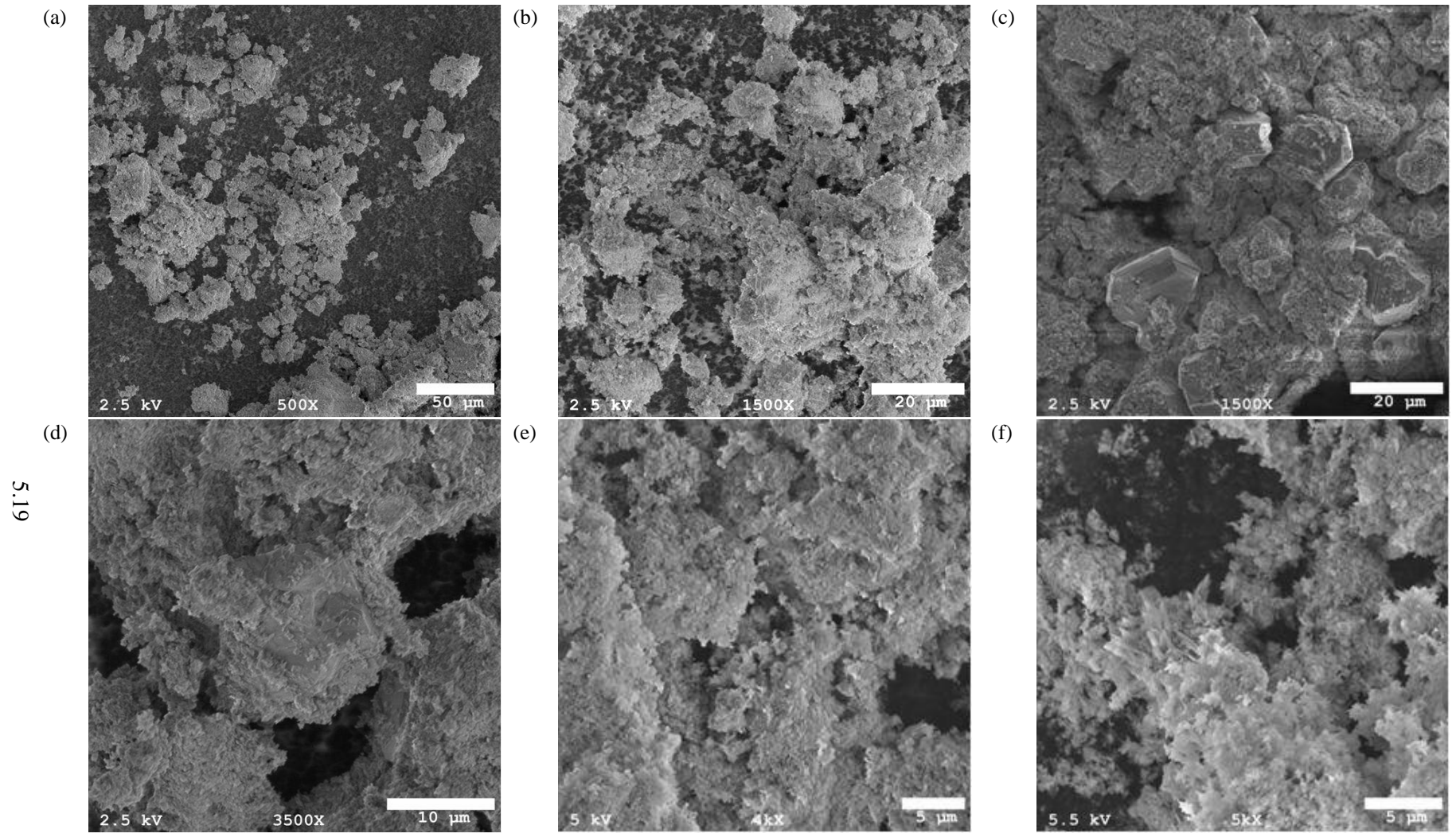


Figure 5.12. SEM Images of Washed Group 5 REDOX Sludge, Various Magnifications and Views

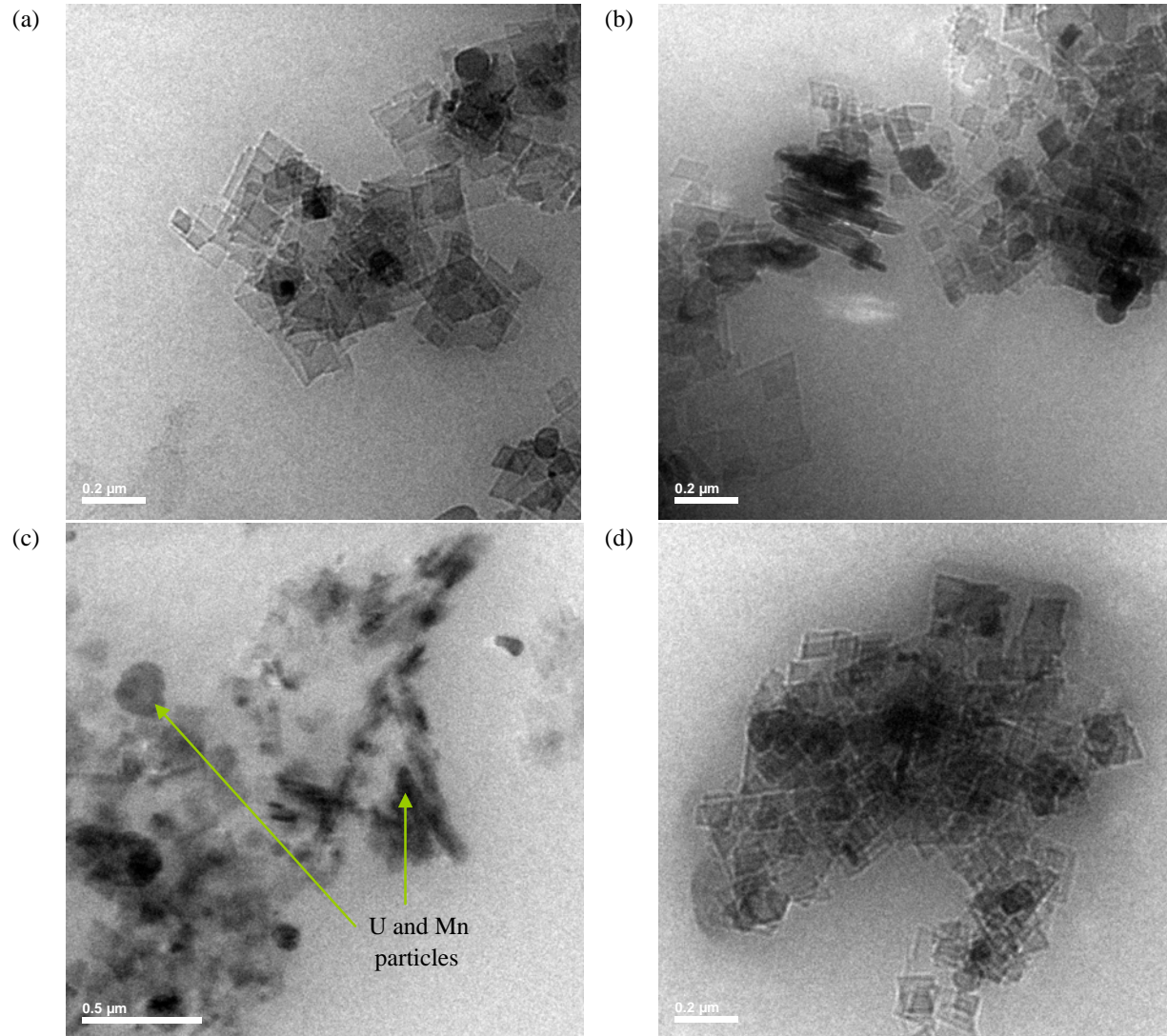


Figure 5.13. TEM Images of Washed Group 5 REDOX Sludge

When boehmite is present in excess, dispersion and re-agglomeration processes “fluff-up” agglomerates, whereas when gibbsite is in excess, the small boehmite particles can become attached to the larger particles and will not contribute to changing the density of the solids (Tingey et al. 1999).

Additional images of the Group 5 solids are presented in Section 8. These samples had been more extensively washed in preparation for parametric leach testing and were mounted on a different type of grid (lacey carbon).

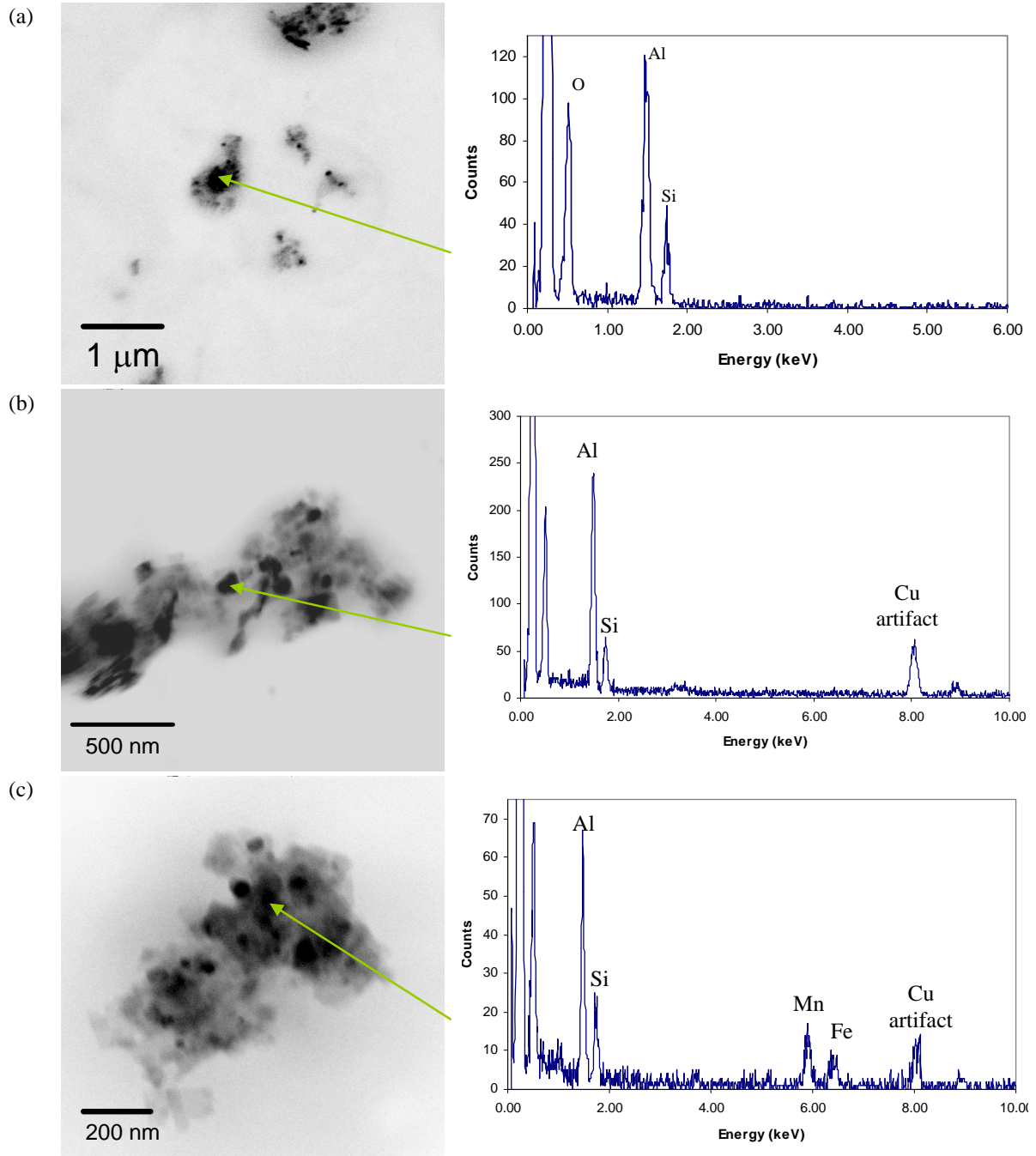


Figure 5.14. STEM Images of Washed Group 5 REDOX Sludge

6.0 Initial Characterization Results for S-Saltcake Group 6

The following sections report on and discuss the analytical results for the S-Saltcake slurry composites. Sample handling and processing steps are summarized in Figure 4.1. The supernatant results represent the equilibrated aqueous phase in contact with the solids; the solids results were obtained after washing with 0.01 M NaOH (as described in Section 4.3).

6.1 Physical Properties of the Solids Slurry

Two of the physical-property testing samples from the composited solids are shown in Figure 6.1. The solids were uniform, finely-divided, and had a dark mahogany coloration; the clear supernatant liquid was yellow, characteristic of dissolved chromate.

The settling curves of the triplicate samples of S-saltcake composited solids are shown in Figure 6.2. Results are shown in two ways: 1) volume percent settled solids as a function of time and 2) height of settled solids as a function of time. Observation of a clarified supernatant was not apparent until 1 hr had elapsed. Settling was essentially complete after 30 hr.

The physical-property results for the triplicate S-Saltcake samples (S1, S2, and S3) are summarized in Table 6.1 along with the propagated 1- σ error, average, and relative standard deviation of the triplicate values. Excellent precision was obtained for the sample set.



Figure 6.1. Group 6 S-Saltcake Solids Composite

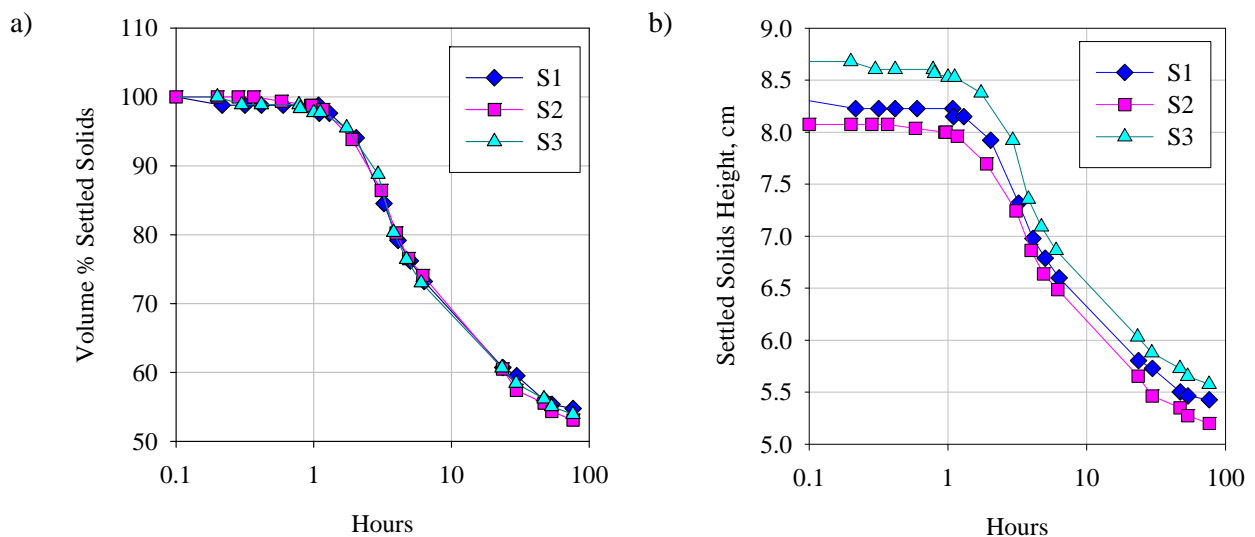


Figure 6.2. Group 6 S-Saltcake Solids Settling Test

Table 6.1. Physical-Property Measurements of Group 6 S-Saltcake Compositeds Solids

Description	S1	S2	S3	Nominal 1- σ error	Avg.	RSD ^(a) (%)
Bulk Sample						
Density (g/mL)	1.38	1.38	1.37	0.057	1.38	0.38
Total Solids (wt%)	39.9	39.3	39.2	0.055	39.5	1.0
Total Undissolved Solids (wt%)	15.0	14.6	14.6	0.056	14.7	1.8
Settled Solids						
Density (g/mL)	1.43	1.45	1.46	0.1	1.45	1.0
Vol%	55.4	53.8	55.2	4.7	54.8	1.6
Wt%	60.3	58.2	59.8	5.4	59.5	1.8
Total Undissolved Solids (wt%)	24.9	25.0	24.4	2.3	24.8	1.3
Wet Centrifuged Solids						
Density (g/mL)	1.65	1.85	1.75	0.20	1.75	5.6
Vol%	28.9	27.5	28.2	3.3	28.2	2.5
Wt%	35.5	37.5	36.2	0.046	36.4	2.9
Total Undissolved Solids (wt%)	41.0	42.1	41.0	6.6	41.4	1.6
Total Solids (wt%)	59.1	56.4	57.4	0.10	57.6	2.4
Supernatant						
Density (g/mL)	1.23	1.24	1.23	1.23	0.037	0.49
Total Dissolved Solids (wt%)	29.1	28.8	28.6	0.06	28.8	0.91
Water Content (g/g)	0.7088	0.7125	0.7139	0.0009	0.7117	0.37
(a) RSD = relative standard deviation						

6.2 Rheology of the Composite Slurry

Initial characterization of Group 6 rheology examined both waste-slurry concentrate at 14.7 wt% UDS and supernate samples.

6.2.1 Shear Strength

Because the volume of settled solids for Group 6 was limited, it was not possible to immerse the vane 16 mm (as required by RPL-COLLOID-02 for a 16 mm vane tool) without contacting the bottom of the container. For Group 6 slurry testing, it was decided to maximize the distance between vane blades and the bottom of the container. As such, the vane was immersed until the top of the blades were just below the surface of the settled solids.

The single Group 6 shear-strength observation at 66 hrs of settling time indicated a shear strength of 20 Pa. This shear strength was less than that of food products such as tomato ketchup and spaghetti sauce (cf. Section 6.7 in Steffe 1992). Figure 6.3 shows the shear stress versus time curve measured for the Group 6 initial-characterization sample as part of shear-strength testing. No repeat measurements were

taken for Group 6 shear strength, and as such, the measurement uncertainty cannot be quantified. Since only one settling period for shear strength was observed, neither the rate of shear-strength increase nor the potential for continued increase can be evaluated. That a maximum existed in the shear-stress versus time curve observed during incipient motion indicates that granular forces, both frictional and cohesive, occurred in settled solids for Group 6. Because of the limited volume of Group 6 test sample, the geometric constraints required to eliminate the container effects of vane testing could not be satisfied. As such, the measurement of shear strength given here may not be independent of container geometry.

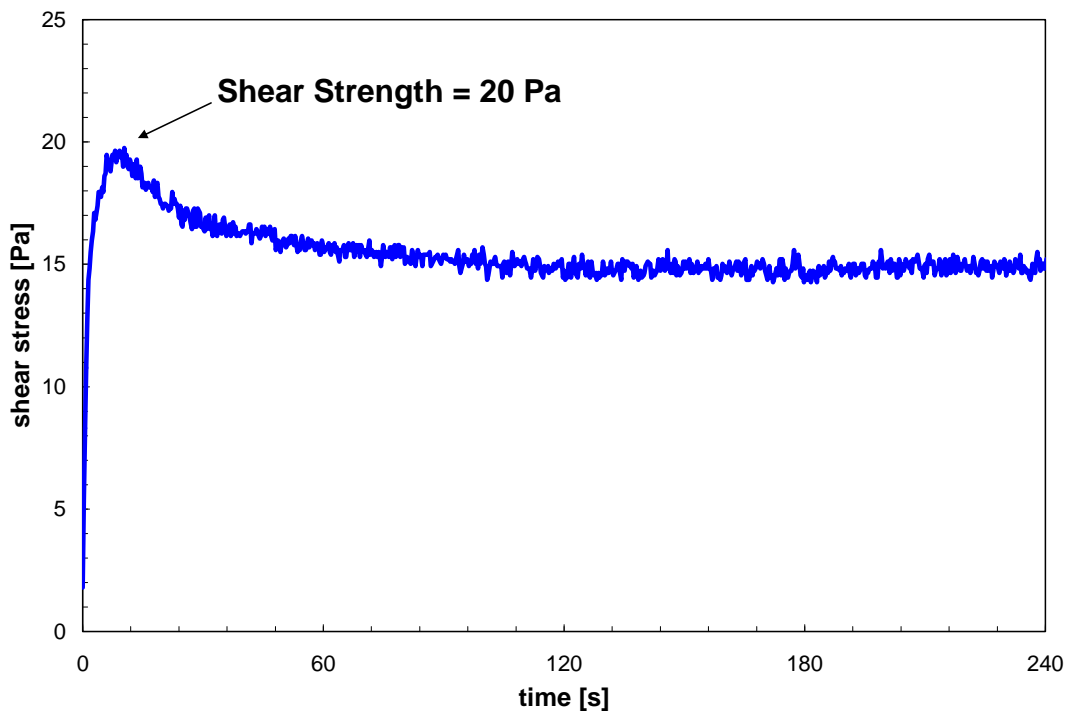


Figure 6.3. Shear-Strength Measurement for Group 6 S-Saltcake Initial-Characterization Slurry TI490-G6-AR-RH Settled Solids 66 Hours After Mixing (14.7 wt% UDS). Data show the shear stress acting on an 8×16 mm (R×H) vane tool as a function of time. The maximum in the curve corresponds to the settled-solids shear strength.

6.2.2 Flow Curve

For Group 6 slurries, the initial mixing step was used to provide an additional measurement of viscosity, which was determined by averaging the apparent viscosity measured during constant rotation over the 3-min mixing period. Likewise, flow-curve measurements for Group 6 supernatants were supplemented by a single post-measurement viscosity determination using constant rotation. These measurements will be hereafter referred to as “mixing” or “constant rotation” viscosities.

6.2.2.1 Results of Flow Curve Testing—Group 6 Slurry

Flow curve testing results for the Group 6 slurry sample, TI490-G6-AR-RH, are shown in Figure 6.4. The 25° and 40°C measurements show Newtonian behavior (i.e., a linearly increase shear stress with shear rate and a zero intercept) over the entire measurement range of 0 to 1000 s⁻¹. The up-ramp of the 25°C measurement suggests a small non-zero intercept; however, given the noise in the adjacent measurement data and possible inertial effects of the rotor, this intercept does not appear to be

significantly different than zero. The 60°C measurement data showed a slight downward curvature up to 600 s⁻¹, but the curvature was not so severe that the behavior could not be characterized as Newtonian. At 600 s⁻¹, there was a well-defined increase in the slope of the 60°C flow curve. The sudden nature of this increase and its reproducibility on the flow curve down-ramp were consistent with turbulent slurry flow in the gap between the rotor and cup wall.

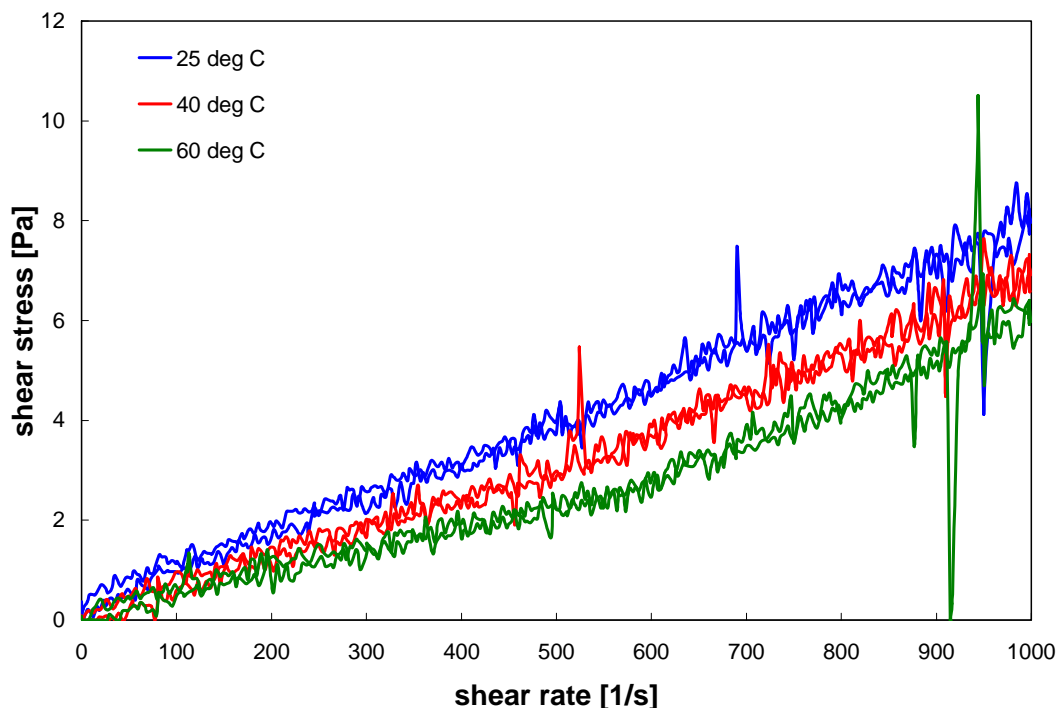


Figure 6.4. Flow Curve (shear stress versus shear rate) for Group 6 S-Saltcake Initial Characterization Slurry Sample TI490-G6-AR-RH at 25°C, 40°C, and 60°C (14.7 wt% UDS) as Measured Using the MV1 Cup and Rotor. Note: the second repeat measurement for 25°C is shown here, as it is the closest to the 40° and 60°C measurements in time.

Rotational viscometry operates under the assumption of laminar flow. Because most rotational viscometers employ small gap sizes (~1 mm) and because most test fluids are non-Newtonian or are Newtonian with high viscosity (i.e., greater than 10 cP), flow conditions within the gap are typically laminar. However, turbulent flow conditions will be realized during flow-curve measurement for low-viscosity fluids. For example, flow-curve measurements of water (which has a viscosity of 1 cP) in the MV1 measurement cup system show a transition from laminar to turbulent flow around 200 s⁻¹. This transition point scales approximately with viscosity, such that transition points for higher viscosity fluids can be predicted simply by multiplying 200 s⁻¹ by the ratio of the current viscosity to that of water. Thus, 5 cP fluids should have a transition point around 1000 s⁻¹, which is the measurement limit for the flow curves discussed herein. As such, laminar-to-turbulent flow transitions should not be observed for fluids with viscosities greater than 5 cP.

Turbulent flow dissipates more energy than laminar flow. As a result, more force is required to maintain constant rotation of the measurement systems in turbulent flow. This is observed in flow curve measurements as an increase in the slope of the shear-stress versus shear-rate curve (like observed in

Figure 6.4). This increase is not predictable and cannot be analyzed to extract the actual viscosity of the test fluid. Thus, any flow-curve data beyond the transition point are usually discarded.

Based on the observations above, Newtonian viscosities for each flow-curve measurement taken for the Group 6 slurry were calculated. The results are shown in Table 6.2 and indicate a slurry viscosity between 4 and 8 cP. Both initial and repeat measurements are shown for 25°C. In addition, a separate measurement of viscosity at each temperature was derived by taking the average of the apparent viscosity measured during constant rotation mixing of the slurry before measurement. These measurements will be hereafter referred to as “mixing” viscosities.

Table 6.2. Newtonian Viscosities for Group 6 S-Saltcake Slurry Sample TI490-G6-AR-RH. Reported viscosities are determined by least-squares analysis of flow curve data over 0-1000 s⁻¹ unless noted otherwise.

Temperature [°C]	Model	Viscosity [cP]	R ^(a)
25 (measurement 1 of 2)	Average (constant rotation) ^(b)	6.3 ± 0.2	n/a
25 (measurement 2 of 2)	Average (constant rotation) ^(b)	7.6 ± 0.2	n/a
40	Average (constant rotation) ^(b)	5.7 ± 0.3	n/a
60	Average (constant rotation) ^(b)	4.2 ± 0.1	n/a
25 (measurement 1 of 2)	Newtonian	6.5	0.996
25 (measurement 2 of 2)	Newtonian	8.0	0.994
40	Newtonian	6.9	0.991
60	Newtonian ^(c)	4.6	0.972
(a) R is correlation coefficient of the fit.			
(b) Viscosity determined by averaging apparent viscosity during constant rotor rotation at 470 s ⁻¹ .			
(c) Least-squares analysis restricted to 0-600 s ⁻¹ .			

Repeat rheology measurements for Group 6 waste slurries show a time-dependent increase in viscosity. In particular:

- The second measurement of viscosity at 25°C (8.0 cP) is significantly higher than the first (6.5 cP).
- Comparison of the flow curve data at 25°C also shows a uniform increase at all shear rates on the second measurement (see Figure 6.5).
- Newtonian viscosities derived from flow-curve data are always greater than the mixing viscosities determined from the period of constant rotation immediately before flow-curve testing at all temperatures. For example, the average of the apparent viscosities measured during the mixing at 60°C indicates a viscosity of 4.2 ± 0.1 cP. The flow curve measured immediately after mixing found a best-fit Newtonian viscosity of 4.6 cP. While this observed difference may be a result of experimental error, viscosity measurements at all other temperatures mirror this increase.

The consistency of viscosity increase between each “repeat” measurement strongly suggests that this increase is potentially caused by a macroscopic change in the slurry sample. As discussed for the Group 5 initial-characterization rheology samples, an actual increase in the viscosity of the slurry can occur as a result of sample alteration brought about by shear, chemical processes (such as precipitation), settling, or evaporation.

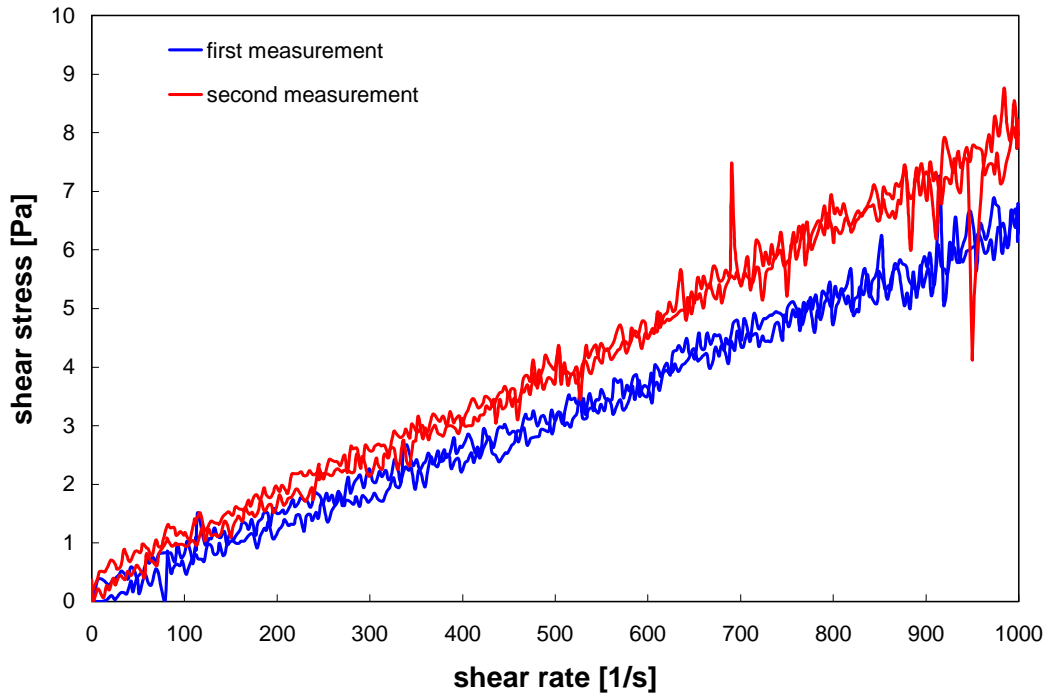


Figure 6.5. Two Repeat Measurements of the Flow Curve (shear stress versus shear rate) for Group 6 S-Saltcake Initial Characterization Slurry Sample TI490-G6-AR-RH at 25°C (14.7 wt% UDS) as Measured Using the MV1 Cup and Rotor

The viscosity increase was difficult to attribute to either macroscopic changes in the sample or changes to the measuring system. Shear effects, which typically lower tank waste viscosity, are not consistent with the increase in shear stress observed for Group 6 wastes. Settling effects did not appear to be the cause as 1) the sludge was mixed immediately before testing to re-suspend settled solids, 2) phase separation was not observed when transferring the sample to the measurement cup, and 3) no hysteresis between the up- and down-ramps of the flow curve was observed. Chemical changes were not likely because the slurry was aged 1 month before testing and the stress increase was observed at low-temperature. Although the time-dependent increase in slurry viscosity was consistent with slurry evaporation, significant evaporation should also be accompanied by flow-curve hysteresis. Figure 6.4 and Figure 6.5 show little to no hysteresis, even at higher temperatures where evaporation is expected to be more severe.

Viscosity increase as a result of slurry evaporation was the most likely of the potential causes listed. An explanation for the lack of flow-curve hysteresis is that slurry evaporation occurs only between flow-curve measurements when the moisture barrier has been removed from the system. However, if evaporation only occurs when the moisture barrier is removed from the system, the mixing and flow-curve viscosities shown in Table 6.2 should be similar (as flow-curve measurements immediately follow mixing). Because of this inconsistency and lack of flow-curve hysteresis, evaporation cannot be definitively listed as the cause of slurry viscosity increase.

With regard to the temperature dependence of the flow curves, the measured slurry viscosity decreased with increasing temperature. Taking the three closest chronological measurements, the Newtonian

viscosity decreased from 8.0 cP to 6.9 cP to 4.6 cP as the temperature was increased from 25° to 40° to 60°C, respectively. The viscosities measured by constant rotation showed similar behavior. The decrease in slurry viscosity was consistent with the expected behavior. That is, dilute slurries typically show a decrease in apparent viscosity as a result of a decrease in the viscosity of the slurry’s suspending phase. Given that evaporation appeared to increase viscosity in repeat measurements, the results in Table 6.2 most likely underestimate the magnitude of viscosity decrease with temperature.

As a point of reference, the apparent viscosity at 33 s⁻¹ was derived from each measurement. The results are provided in Table 6.3. For each temperature, this reference point was determined from measurement data alone, as the apparent viscosity predicted by the Newtonian model was independent of shear rate. The apparent viscosities provided in Table 6.3 are unreliable because 33 s⁻¹ occurs on the lower end of the shear-rate range, and the shear stresses measured there are close to the RV20-M5 measuring system’s lower torque limit. As such, the measurements are strongly affected by rotor noise and inertia. It is not recommended that these values be used for any engineering or design calculations. Instead, engineering design should employ the Newtonian viscosities reported in Table 6.2.

Table 6.3. Apparent Viscosity of Group 6 S-Saltcake Slurry Sample TI490-G6-AR-RH at 33 s⁻¹

Temperature [°C]	η_{app} (cP) from up-ramp	η_{app} (cP) from down-ramp
25	15	5
25	23	13
40	7	2
60	10	2

6.2.2.2 Results of Flow-Curve Testing—Group 6 Supernate

Flow-curve testing results for the Group 6 supernate sample, TI488-G6-AR-J2, are shown in Figure 6.6. With regard to the shear-stress versus shear-rate behavior, flow curves for 25, 40, and 60°C show a sharp increase in slope at 400 s⁻¹. As discussed in the previous section, such increases in the flow-curve slope are indicative of a transition from laminar to turbulent flow in the gap between the measurement rotor and cup. Data at shear rates beyond the transition point are not usable.

Group 6 supernate is expected to behave as a Newtonian fluid given the lack of undissolved or dissolved species capable of forming internal structure. The flow-curve data below 400 s⁻¹ appear to support this assertion. Specifically, the flow curves show zero yield stress and no significant curvature. Based on the transition point alone, a rough estimate of supernate viscosity is 2 cP. Although apparent viscosity and shear-stress data before the transition point are valid, the large uncertainty in shear stress from operating near the sensing limit of the measuring head and the large hysteresis between the flow-curve up- and down-ramp resulting from rotor inertia prevent accurate determination of fluid viscosity from least-squares analysis and the apparent viscosity at 33 s⁻¹. As such, neither will be reported herein. An alternative measurement strategy to the standard 15 minute flow employed to obtain estimates for Group 6 supernatant viscosity.

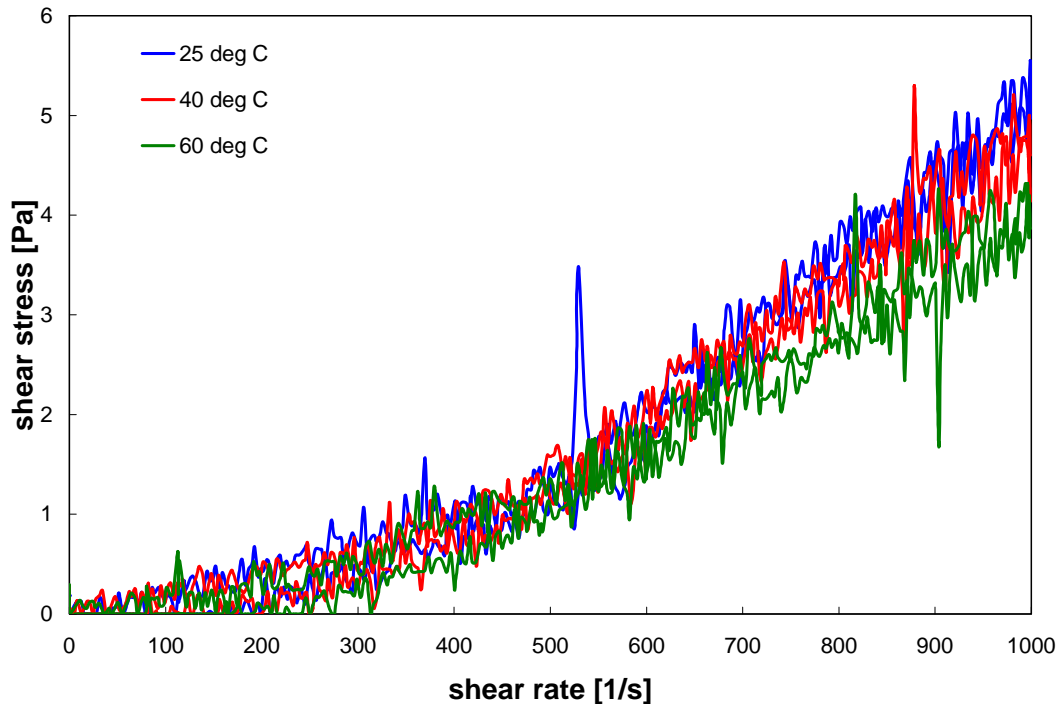


Figure 6.6. Flow Curve (shear stress versus shear rate) for Group 6 S-Saltcake Initial Characterization Supernate Sample TI488-G6-AR-J2 at 25° C, 40° C, and 60°C as Measured Using the MV1 Cup and Rotor

To determine the viscosity of the Group 6 supernate samples, a series of constant rotation viscosity determinations were performed. Here, the shear stress required to maintain rotation of the measurement system was monitored over an extended period of time. Inertial hysteresis effects are avoided because rotation is constant (as opposed to the accelerating/decelerating rates used for flow-curve measurements herein). In addition, the measured apparent viscosity can be time averaged to smooth out any variation in shear-stress measurements. Measurements were taken at 25, 40, and 60°C. For 25 and 60°C, a total of 20 apparent viscosity measurements were taken over a period of 20 seconds. For 40°C, a total of 60 measurements were taken over 60 seconds. At the end of each measurement period, results were averaged to determine a representative measure of viscosity at the given temperature. The results of this analysis (see Table 6.4) show the expected decrease in supernatant viscosity with increasing temperature and are consistent with the decrease in slurry viscosity with temperature (see Table 6.2). However, given the large uncertainty (reported as the standard deviation of the sample) associated with each supernatant viscosity measurement, the decrease observed therein is not statistically significant even though it is both expected and consistent with Group 6 slurry behavior.

6.3 Pretreatment for Chemical Characterization

The sample taken for chemical characterization was centrifuged at 1000 G for 1 hr, similar to the physical-property testing samples, to effect a phase separation. The volume-percent centrifuged solids was also determined; in this case, the volume-percent centrifuged solids was 28.6%, virtually equivalent to the 28.2% centrifuge solids found with the physical-property testing samples. The solids appeared similar to the physical-property testing samples.

The specific washing scheme for the S-Saltcake solids is provided in Figure 6.7. As previously observed with the Group 5 sludge processing, the packing of the WCS was more easily disturbed with each successive wash. The final hydroxide concentration in the final wash solution was estimated at 0.06 M after incorporating the sequential dilution of the entrained supernatant. The final volume of washed centrifuged solids was 4.0 mL, representing a total centrifuged-solids volume loss of ~1 mL or ~20% by volume.

Table 6.4. Viscosity of Group 6 S-Saltcake Supernate Sample TI488-G6-AR-J2 as a Function of Temperature. Viscosity determined by averaging apparent viscosity during constant rotor rotation at 300 s⁻¹.

Temperature [°C]	Model	Viscosity [cP]
25	Average (constant rotation)	1.5 ± 0.3
40	Average (constant rotation)	1.4 ± 0.2
60	Average (constant rotation)	1.1 ± 0.2

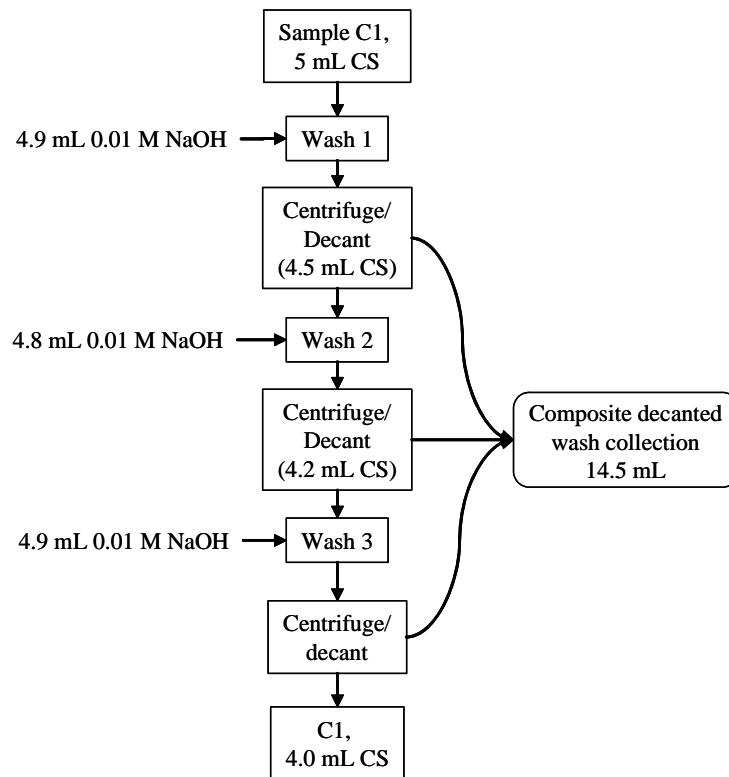


Figure 6.7. Wash Sequence for Group 6 S-Saltcake Solids Supporting Initial Characterization (CS = centrifuged solids)

6.4 Chemical and Radiochemical Composition

The average radioanalytical results and RPDs for the supernatant, composited wash solution, and washed solids are provided in Table 6.5. The gross beta showed good agreement with the sum of beta emitters,

the ^{137}Cs and ^{90}Sr (in secular equilibrium with ^{90}Y) thus indicating that no other major source of beta-gamma activity was present. The gross alpha agreed well with the summation of alpha emitters (^{238}Pu , $^{239+240}\text{Pu}$, and ^{241}Am)—the latter generally provides the better estimate of total alpha activity.

Table 6.5. Radionuclide Characterization of the Group 6 S-Saltcake Washed Solids

Sample ID>	Supernatant		Wash composite		Washed solids	
	07-00739		07-00740		07-00741	
Analyte	$\mu\text{Ci/mL}$	RPD	$\mu\text{Ci/mL}$	RPD	$\mu\text{Ci/g}^{(a)}$	RPD
^{137}Cs	8.34E+1	0.24	1.82E+1	0.55	1.00E+2	2
^{60}Co	<2.E-4	na	<5.E-5	na	6.35E-2	4
^{241}Am	<1.E-2	na	<1.E-2	na	4.57E+0	11
^{238}Pu	<2E-5	na	--	--	1.22E-1	7.4
$^{239+240}\text{Pu}$	8.83E-5 ^(b)	12	--	--	9.23E-1	1.7
^{90}Sr	7.16E-2	5.7	--	--	2.66E+2	2.3
Gross alpha	<5.E-4	na	--	--	5.54E+0	0.54
Alpha sum	1.02E-4	11	--	--	5.61E+0	8.4
Gross beta	7.68E+1	5.1	--	--	6.27E+2	3.7
Beta sum	8.35E+1	0.25	--	--	6.32E+2	2.2
<i>Opportunistic</i>						
^{154}Eu	<1.E-3	na	<3.E-4	na	1.43E+0	4.2
^{155}Eu	<1.E-2	na	<4.E-3	na	5.47E-1	6.4
ASR 7918 Reference date is May 1, 2007. (a) Analyte concentrations are calculated on a dry-mass basis. (b) The $^{239+240}\text{Pu}$ concentration in the PB was 12% of the sample activity. "--" indicates analysis was not conducted.						

The average chemical analytical results and RPDs for the supernatant, composited wash solution, and washed solids are provided in Table 6.6. The solids consisted primarily of aluminum, sodium, and chromium with significant contributions from Fe, Si, and U. The supernatant was primarily sodium salts of nitrate, nitrite, and hydroxide. The charge balance was evaluated for the supernatant, resulting in a 2.0% difference between cationic and anionic species, well within analytical uncertainties. Oxalate had not appreciably dissolved in the supernatant; the dissolution of oxalate was apparently retarded by the high sodium salt content. Therefore, the organic carbon in the supernatant (0.115 M) could not be attributed to dissolved oxalate; other organic species must have been present. Significant quantities of oxalate dissolved during the solids washing steps, concomitant with the decreasing sodium content in the liquid phase.

The fractional distribution of selected analytes in the supernatant, wash, and solids phases is shown in Table 6.7 and Figure 6.8. Sodium, phosphorus and sulfur largely partitioned to the aqueous phase (high salt supernatant). The oxalate remaining with the solids was estimated from the XRD pattern and relative intensity ratios of the sodium oxalate and gibbsite. Oxalate did not dissolve until the sodium concentration in the aqueous phase was significantly reduced. Presumably, additional oxalate would have been removed from the solid phase with more extensive washing of the solids.

Table 6.6. Chemical Characterization of the Group 6 S-Saltcake Washed Solids

Sample ID>	Supernatant			Wash composite			Washed solids	
	07-00739			07-00740			07-00741	
Analyte	µg/mL	M	RPD	µg/mL	M	RPD	µg/g ^(a)	RPD
Al	7,590	2.81E-1	9.7	1,580	5.86E-2	na ^(b)	187,000	2.1
B	30.3	2.80E-3	2.6	[9.4]	[8.7E-4]		<95	na
Bi	<2	<1.E-5	na	<2.3	<1.E-5		474	3.2
Cd	<0.2	<2.E-6	na	<0.24	<2.E-6		139	5.1
Cr	535	1.03E-2	12	138	2.65E-3		92,850	1.8
Fe	<2	<4.E-5	na	<2.1	<4.E-5		14,700	1.4
K	1,140	2.92E-2	12	235	6.01E-3		<180	na
Mn	<0.2	<4.E-6	na	<0.21	<4.E-6		4,680	1.7
Na	117,500	5.11E+0	7.7	33,300	1.45E+0		93,500	1.9
Ni	[2.25]	[3.8E-5]	na	[1.8]	[3.1E-5]		1,035	4.8
P	2685	8.67E-2	11	1710	5.52E-2		2,230	5.4
S	2,615	8.2E-2	8.8	614	1.92E-2		[750]	[48]
Si	90	3.2E-3	10	[9.8]	[3.5E-4]		15,500	2.6
Sr	<0.02	<2.E-7	na	<0.017	<2.E-7		54	2.6
U	<9	<4.E-5	na	<8.5	<4.E-5		6,575	4.1
Zn	<0.6	<9.E-6	na	<0.57	<9.E-6		987	8.8
Zr	<0.8	<9.E-6	na	<0.82	<9.E-6		391	3.8
U KPA	--						4,415	0.7
nitrite	37,650	8.18E-1	1.3	8,070	1.75E-1	0.99	--	
nitrate	119,500	1.93E+0	0.84	26,000	4.19E-1	1.5	--	
phosphate	8,355	8.80E-2	1.3	5,345	5.63E-2	1.7	--	
sulfate	7,965	8.29E-2	0.13	1,800	1.87E-2	1.1	--	
oxalate	<5.8	<6.6E-5	na	7,090	8.06E-2	2.0	--	
free hydroxide	12,200	7.15E-1	1.4	no data				
TOC as C	1,385	1.15E-1	3.6					
TIC as C	6,250	5.21E-1	1.6					
Opportunistic								
fluoride	110	5.79E-3	3.64	413	2.16E-2	1	--	
chloride	3225	9.10E-2	0.31	706	1.99E-2	0	--	
Ag	<0.4	<4.E-6	na	<0.43	<4.E-6	na ^(b)	[24]	[4.3]
As	<7	<1.E-4	na	<7.0	<9.E-5		<102	na
Ba	<0.3	<3.E-6	na	<0.34	<2.E-6		85.6	1.8
Be	[0.029]	<3.E-6	na	[0.034]	[3.8E-6]		3.59	2.0
Ca	26.5	6.61E-4	20	[9.2]	[2.3E-4]		5,365	0.9
Ce	<1	<1.E-5	na	<1.2	<9.E-6		221	0.9
Co	<0.4	<7.E-6	na	<0.39	<7.E-6		[6.2]	[21]
Cu	<0.5	<8.E-6	na	<0.49	<8.E-6		94.6	5.2
Dy	<0.4	<2.E-6	na	[0.80]	[4.9E-6]		<5.1	na

Table 6.6 (Contd)

Sample ID>	Supernatant			Wash composite			Washed solids	
	07-00365			07-00366			07-00367	
Analyte	µg/mL	M	RPD	µg/mL	M	RPD	µg/g	RPD
Eu	<0.1	<7.E-7	na	<0.11	<7.E-7		[5.0]	[8.0]
La	[0.31]	[2.2E-6]	na	[0.13]	[9.4E-7]		211	3.8
Li	<0.6	<8.E-5	na	<0.55	<8.E-5		187	2.7
Mg	[2.35]	[9.7E-5]	na	<0.71	<3.E-5		655	4.0
Mo	34.7	3.61E-4	8	8.10	8.44E-5		<10	na
Nd	<2	<1.E-5	na	<1.7	<1.E-5		443	3.2
P	2,685	8.67E-2	11	1,710	5.52E-2		2,230	5.4
Pb	<4	<2.E-5	na	<3.7	<2.E-5		1,510	6.6
Pd	<1	<1.E-5	na	<1.3	<1.E-5		<18	na
Rh	<2.6	<3.E-5	na	<2.6	<2.E-5		<37	na
Ru	[4.0]	[4.0E-5]	na	[2.7]	[2.7E-5]	na ^(b)	<12	na
Sb	<3.2	<3.E-5	na	<3.2	<3.E-5		<46	na
Se	[6.7]	[8.5E-5]	na	[8.4]	[1.1E-4]		[72]	3.1
Sn	[12]	[1.0E-4]	na	[6.2]	[5.2E-5]		[73]	[59]
Ta	<1.4	<8.E-6	na	<1.3	<7.E-6		<19	na
Te	<3.2	<3.E-5	na	[4.0]	[3.1E-5]		<46	na
Th	<1.4	<6.E-6	na	<1.2	<5.E-6		272	12
Ti	[0.19]	[4.0E-6]	na	[0.16]	[3.3E-6]		54.5	1.7
Tl	<6.7	<3.E-5	na	<6.6	<3.E-5		<95	na
V	[0.96]	[1.9E-5]	na	[1.6]	[3.1E-5]		<4.6	na
W	54.8	2.98E-4	18	17.0	9.25E-5		[35]	[11]
Y	<0.09	<1.E-6	na	<0.085	<1.E-6		63.5	5.2

(a) Analyte concentrations are calculated on a dry-mass basis.
(b) Wash solution was not required to be run in duplicate.
ASR 7918
Analyte uncertainties were typically within ±15% (2-s); results in brackets indicate that the analyte concentration were less than the minimum detection limit (MDL) and greater than the estimated quantitation limit (EQL), and uncertainties were >15%.

Table 6.7. Phase Distribution of Selected Analytes in Group 6 S-Saltcake

Analyte	Supernatant %	Wash solution %	Water Wash Factor %	Solids %
Cr	8	0.5	8.9	91
Al	38	2	40	60
Na	89	6	96	5
P	83	13	96	4
Oxalate	<0.1	23 ^(a)	23 ^(a)	77 ^(b)
S	93	5.4	98	[1.7] ^(c)

(a) Presumably, the oxalate wash factor would have increased with increasing water-wash volume.
 (b) Inferred from the XRD pattern evaluation.
 (c) Bracketed result indicates that the analyte concentration was >MDL and <EQL.

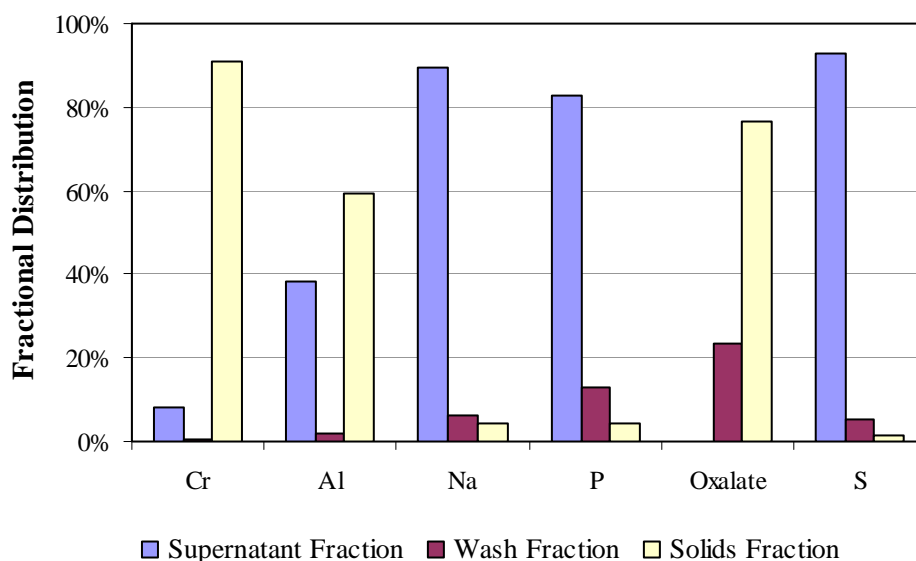


Figure 6.8. Selected Analyte Phase Distribution or Group 6 S-Saltcake

6.5 Particle Size

Table 6.8 provides a summary of the particle-size measurements for the primary and duplicate samples for Group 6. The particle diameters correspond to the 10%, 50%, and 90% volume/weight fractiles and are listed as a function of test condition.

For Group 6, the d(50) ranged from 2.4 to 6.3 μm , the d(10) ranged from 0.66 to 0.89 μm , and the d(90) ranged from 8.7 to 86 μm . For both duplicate and primary samples, pre-sonication d(90)s appeared to be reduced by a factor of two by the application of sonic power. The reduction in size continued throughout the sonication. Immediately after sonic power was shut off, the primary sample showed a dramatic increase in both d(50) and d(90). The duplicate sample showed similar behavior, but to a much lesser degree. Specifically, whereas the primary d(90) jumped from 11 to 86 μm once sonication was stopped,

the duplicate d(90) only increased from 8.7 to 11 μm . With regard to the d(50), the primary sample increases from 3.1 μm up to 6.3 μm while the duplicate only jumped from 2.4 μm to 2.8 μm .

The influence of sonication on the measured distribution was difficult to evaluate when expressed as diameters corresponding to specific cumulative undersize fractions (as above). Figure 6.9. and Figure 6.10 show the particle-size distributions before, during, and after sonication for the primary and duplicate samples, respectively. The “during sonication” PSDs corresponded to the 75% sonic power condition. Both samples showed relatively similar size distributions between 0.3 μm and 20 μm . With regard to this range, the distribution before sonication showed a maximum population around 1.5 μm for both primary and duplicate samples. After this peak, the population gradually decreased until 10 μm , after which a sharp reduction was observed. As observed in the Group 5 particle-size measurements, the application of sonic power increased the fraction of the 8- to 10- μm particles for both primary and duplicate samples. Although the primary sample distribution from 0.3 to 20 μm is more strongly affected than the duplicate distribution in this range, both samples appeared to become slightly bimodal. While the increase could suggest aggregate restructuring, it is more likely a result of the breakdown of the large aggregate peak that was present in the pre-sonication measurement ($\sim 60 \mu\text{m}$) that disappeared during sonication.

Table 6.8. Group 6 S-Saltcake Solids Particle-Size Analysis Summary

Sample	Sonic Power	Condition	d(10) [μm]	d(50) [μm]	d(90) [μm]
Group 6—Primary	0%	pre-sonic	0.77	3.1	40
	25% (~5 W)	sonicated	0.74	3.0	14
	50% (~10 W)	sonicated	0.77	3.3	12
	75% (~15 W)	sonicated	0.71	3.1	11
	0%	post-sonic	0.82	4.7	59
	0%	post-sonic	0.89	6.3	86
Group 6—Duplicate	0%	pre-sonic	0.74	3.1	19
	25% (~5 W)	sonicated	0.70	2.4	9.3
	50% (~10 W)	sonicated	0.69	2.4	9.3
	75% (~15 W)	sonicated	0.66	2.4	8.7
	0%	post-sonic	0.76	2.7	10
	0%	post-sonic	0.69	2.8	11
Note: The diameters corresponding to the 10%, 50%, and 90% volume/weight fractiles are given [d(10), d(50), and d(90), respectively].					

With regard to the upper range of particle sizes, pre-sonication measurements showed a well-defined peak at $\sim 60 \mu\text{m}$ for the primary sample and $\sim 100 \mu\text{m}$ for the duplicate sample. The disappearance of these peaks upon sonication in both cases suggests that these peaks corresponded to particle aggregates. After sonication, the aggregate peak reformed for the primary sample distribution, but did not reform in the duplicate sample distribution.

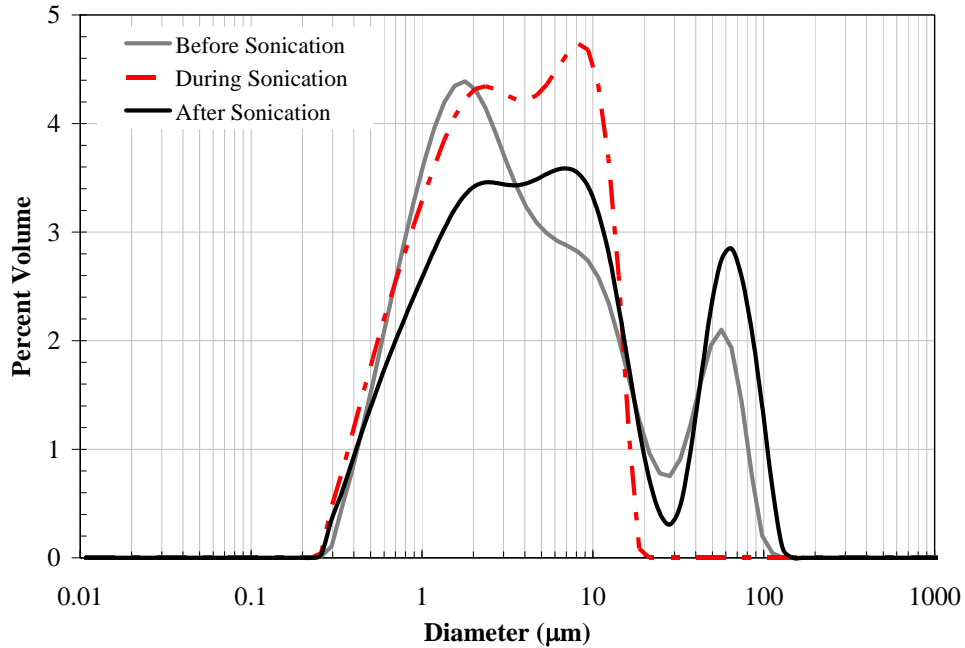


Figure 6.9. Group 6 S-Saltcake Solids Primary Sample Particle Size Distributions (volume/weight basis) Before, During, and After Sonication

Note: The analyzer flow cell was operated at 3000 RPM and at a maximum sonic power of 75% (~15 W).

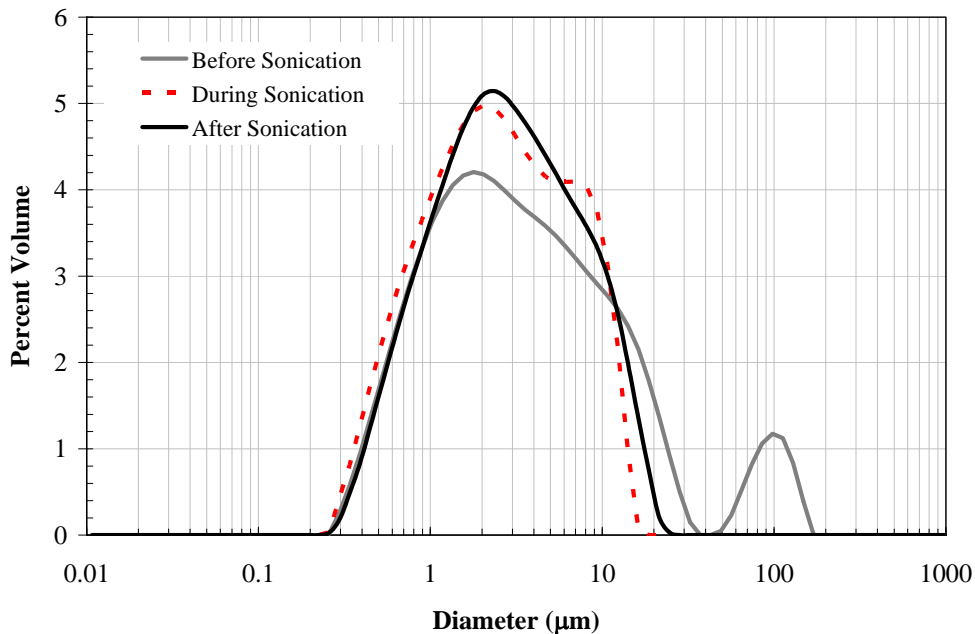


Figure 6.10. Group 6 S-Saltcake Solids Duplicate Sample Particle-Size Distributions (volume/weight basis) Before, During, and After Sonication

Note: The analyzer flow cell was operated at 3000 RPM and at a maximum sonic power of 75% (~15 W).

6.6 Surface Area

Duplicate BET measures were conducted resulting in 95 and 45 m²/g, respectively, averaging 70 m²/g (\pm 36%). The reason for the wide spread between duplicates is not known.

6.7 Crystal Habit

The XRD pattern of the sample alone (no internal standard and no background subtraction) is provided in Figure 6.11. Another sample mount containing alumina (internal standard) is provided in Figure 6.12 along with the stick-figure peak identification. The background had been subtracted in this figure.

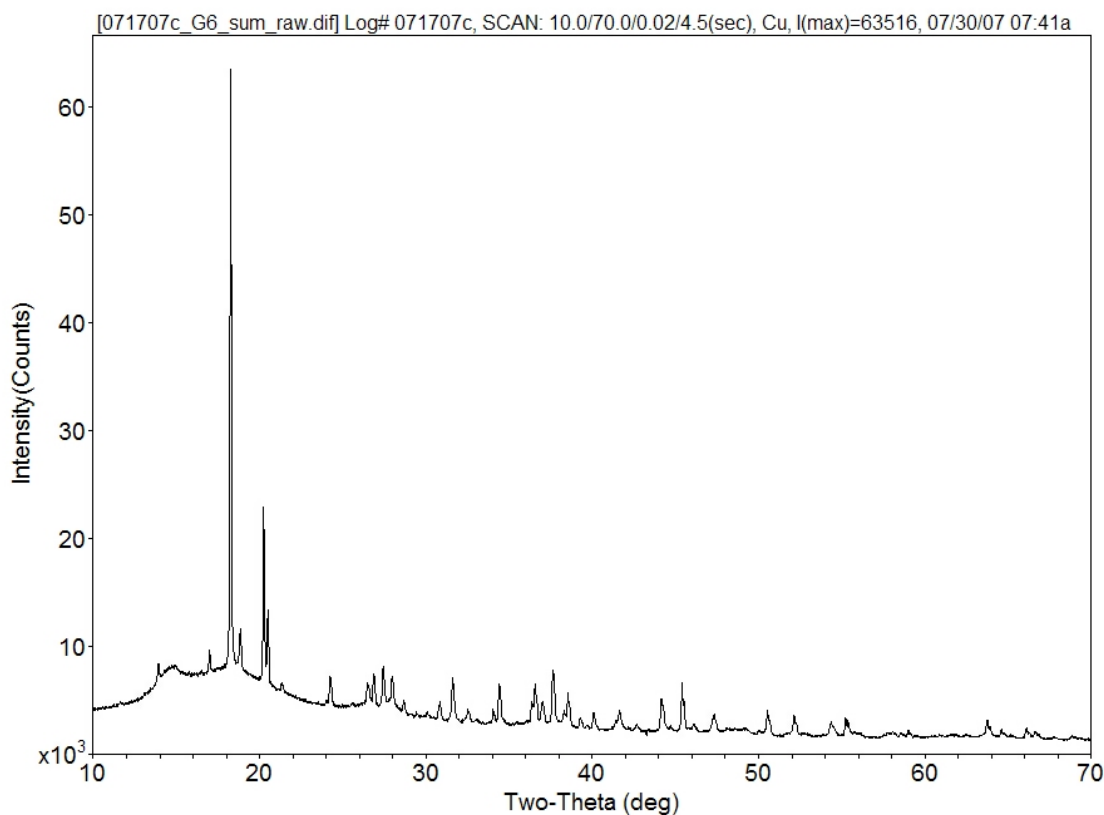


Figure 6.11. Group 6 S-Saltcake Washed Solids XRD Pattern, No Internal Standard

The XRD patterns were dominated by gibbsite with minor contributions from boehmite, sodium oxalate, cancrinite, quartz, and trace sodium uranium oxide. Sodium oxalate is water-soluble but apparently had not been completely removed during the three successive water contacts. The nominal gibbsite crystal size was estimated to be 1,580 Å based on the application of a simplistic evaluation of the crystallite size.^(a)

(a) The Jade operating software applied the Scherrer equation to estimate the crystallite size (Klug and Alexander 1974, pp. 687-690).

Table 6.9 summarizes the best estimate of the weight percent phases in the washed solids. Several crystalline phases were identified by XRD. Other phases were estimated based on the measured metal concentrations, tank waste chemistry, and evaluation of the available SEM-EDS and STEM-EDS spectral results. The relative mass fractions were derived from the chemical analysis, XRD identification, and XRD-determined relative intensity ratios. The amorphous chromium (assigned phase of Cr_2O_3 based on thermogravimetric evaluation of the caustic-leached and washed solids, see Appendix D) was a significant component (13.6%) of the water-washed solids matrix. Sodium oxalate was found at significant quantity (14 wt%). The three sequential contacts in a 1:1 liquid to centrifuge solids volume ratio was insufficient, leaving >70 wt% of the total sodium oxalate with the solids phase. Larger wash volumes, longer contact times, and application of heat would probably successfully remove this component.

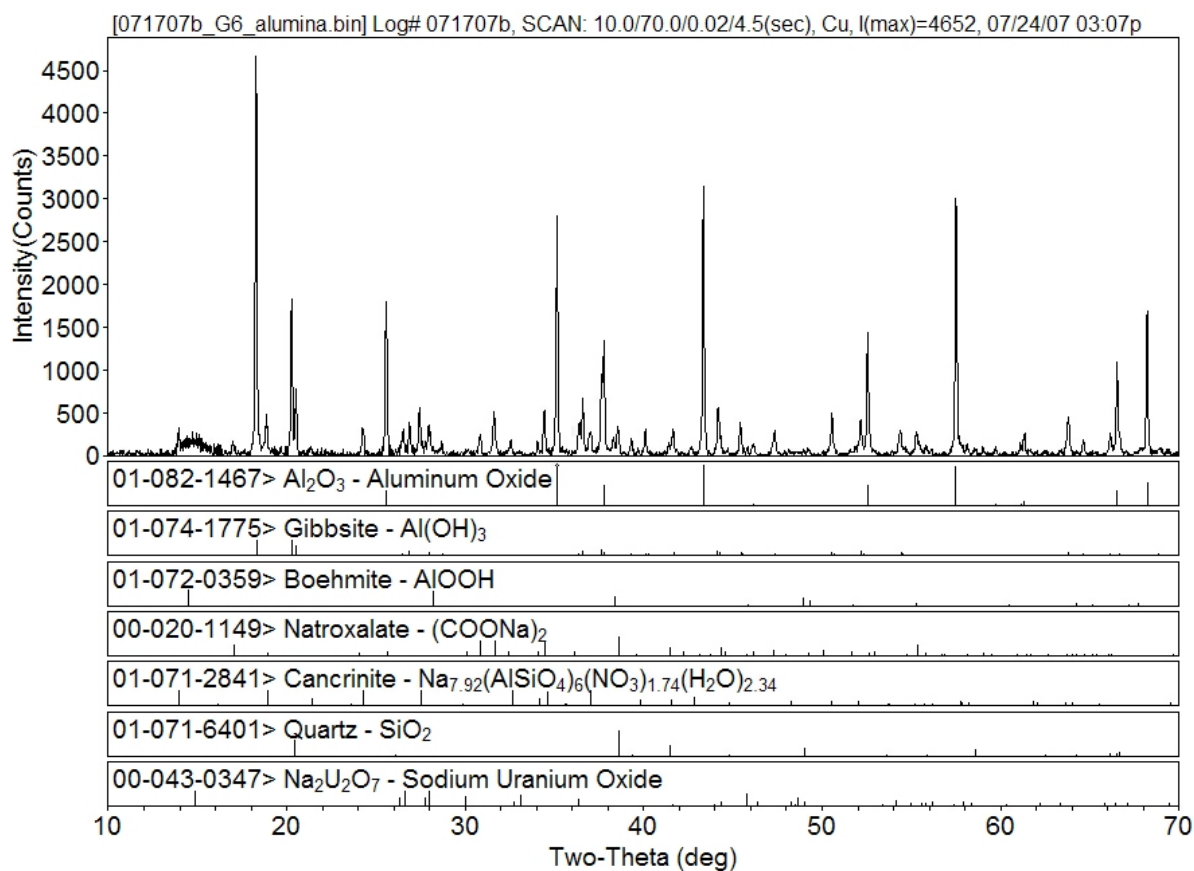


Figure 6.12. Group 6 S-Saltcake Washed Solids XRD Pattern, Background-Subtracted with Alumina Internal Standard and Stick-Figure Peak Identification

The ratios of the solid-phase components were reevaluated by mathematically removing the entrained supernatant and sodium oxalate fractions. The resulting component mass distribution is shown in Figure 6.13. After gibbsite, the Cr_2O_3 component is the most significant fraction at 16 wt%.

The SEM images of the Group 6 washed solids are shown in Figure 6.14 through Figure 6.17. A wide variety of shapes was observed, including tetrahedrons (consistent with boehmite), cubes, and rounded

aggregates (consistent with gibbsite). Most particle diameters were significantly less than 2 μm . Selected scans show EDS results and area maps. The material was dominated by Al; Cr appeared to be scattered throughout the matrix (see element map in Figure 6.15). The EDS map shown in Figure 6.17 indicates easily discernible discrete Cr locations that are coincident with Fe and Mn. A specific shape could not be discerned for the high-Cr species. The particles were too small to be identified by SEM.

Table 6.9. Weight Percent of Crystalline Phases of Group 6 S-Saltcake Washed Solids, Best Estimate

Crystalline Phase	Chemical Structure	Weight %	Basis ^(a)
Gibbsite	Al(OH) ₃	39.4	Observed
Boehmite	AlOOH	8.9	Observed
Sodium oxalate	Na ₂ C ₂ O ₄	14.1	Observed
Cancrinite	Na _{7.92} (AlSiO ₄) ₆ (NO ₃) _{1.7} (H ₂ O) _{2.34}	6.7	Observed
Silicon dioxide	SiO ₂	1.0	Observed
Sodium uranium oxide	Na ₂ U ₂ O ₇	0.6	Observed
Chromium oxide	Cr ₂ O ₃	13.6	TGA
Unknown or amorphous Na	Na	2.3	Chem analysis
Unknown or amorphous Bi, Fe, Mn, Ni, P, Sr, Zn	Bi, Fe, Mn, Ni, P, Sr, Zn	3.0	Chem analysis
Entrained Na salts from supernatant	NaNO ₃ , NaNO ₂ , etc.	3.1	Observed and Calculated
Assumed counter ions	oxides, hydroxides, etc.	7.3	Balance
Total		100	
<p>(a) <i>Observed</i> indicates that the characteristic crystal diffraction pattern of the identified crystalline phase was observed in the sample XRD pattern.</p> <p><i>Chemical analysis</i> indicates that the element mass was determined from the solids chemical characterization.</p> <p><i>TGA</i> indicates that the structure was inferred from the TGA analysis study (see Appendix D).</p> <p><i>Calculated</i> indicates that the mass associated with supernatant entrainment was calculated based on the supernatant dilution factor during solids washing.</p> <p><i>Balance</i> is the mass balance resulting in 100% composition. This mass is probably associated with oxides, hydroxides, etc. associated with the metals (e.g., iron hydroxide).</p>			

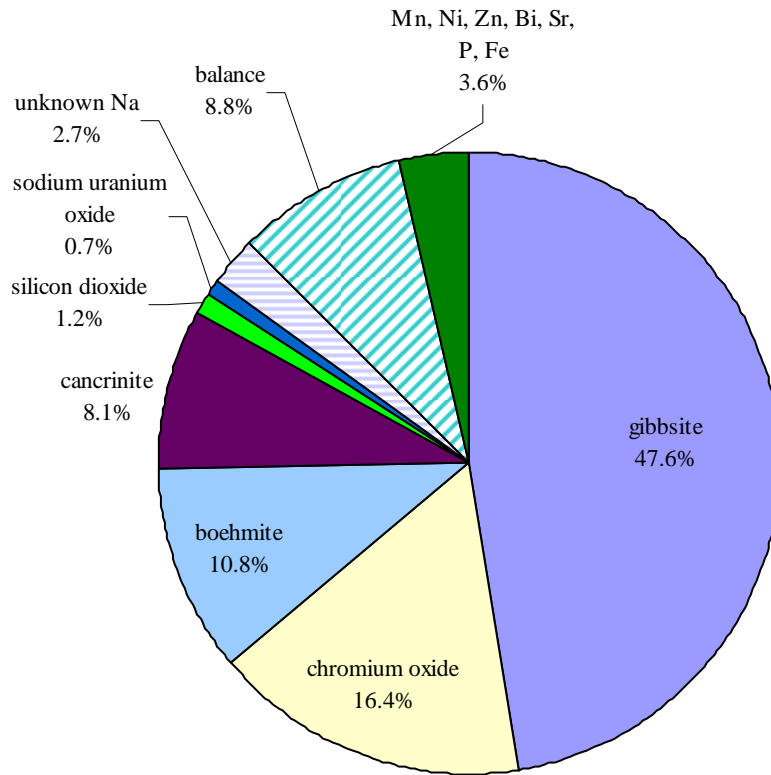


Figure 6.13. Group 6 S-Saltcake Washed-Solids-Phase Identification (Entrained Supernatant and Sodium Oxalate Fractions Removed)

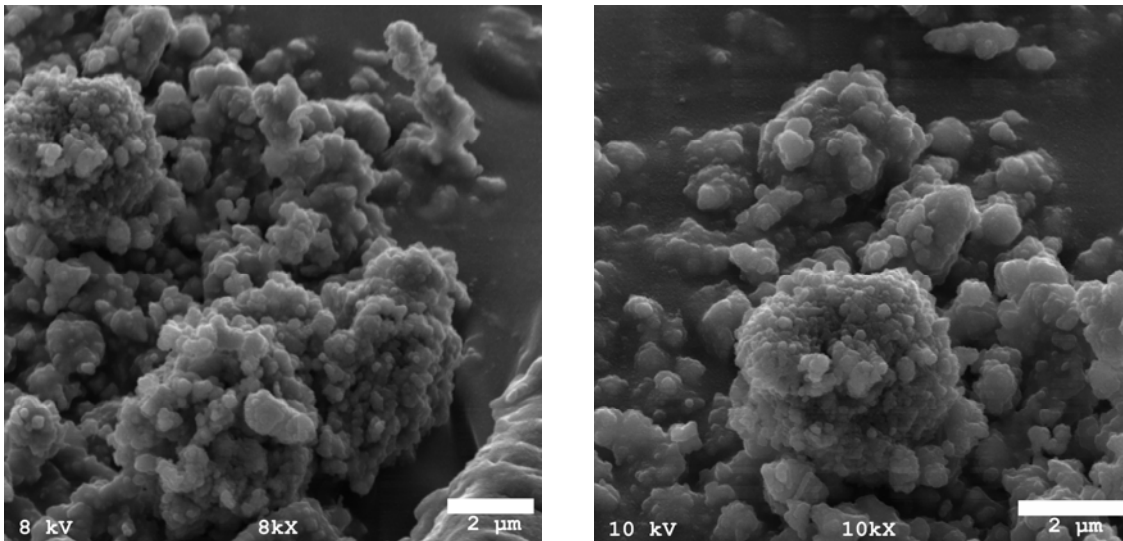


Figure 6.14. SEM Images of Group 6 S-Saltcake Washed Solids, Magnified 8,000× and 10,000×

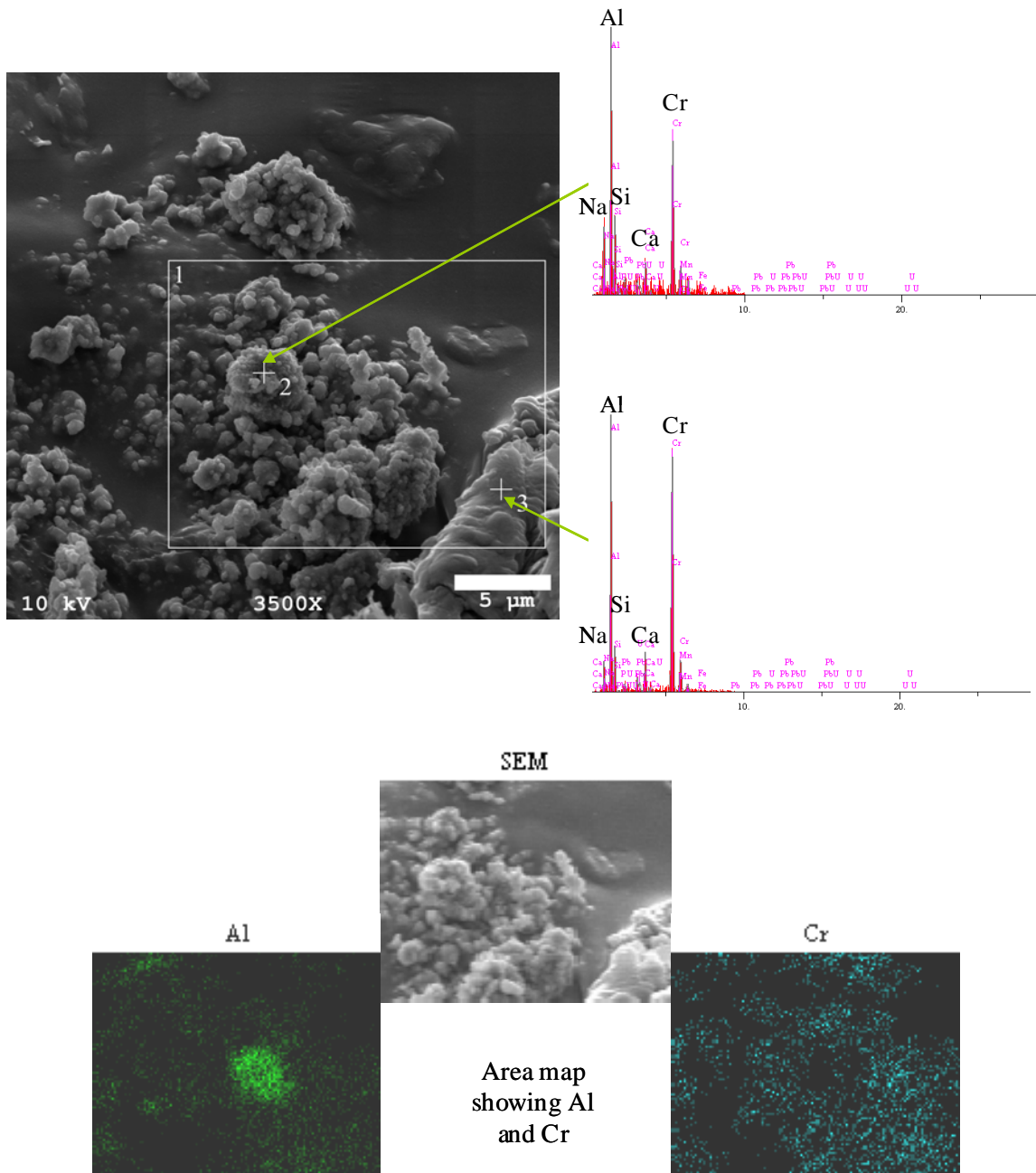


Figure 6.15. SEM Micrographs of Group 6 S-Saltcake Washed Solids with EDS and Area Map

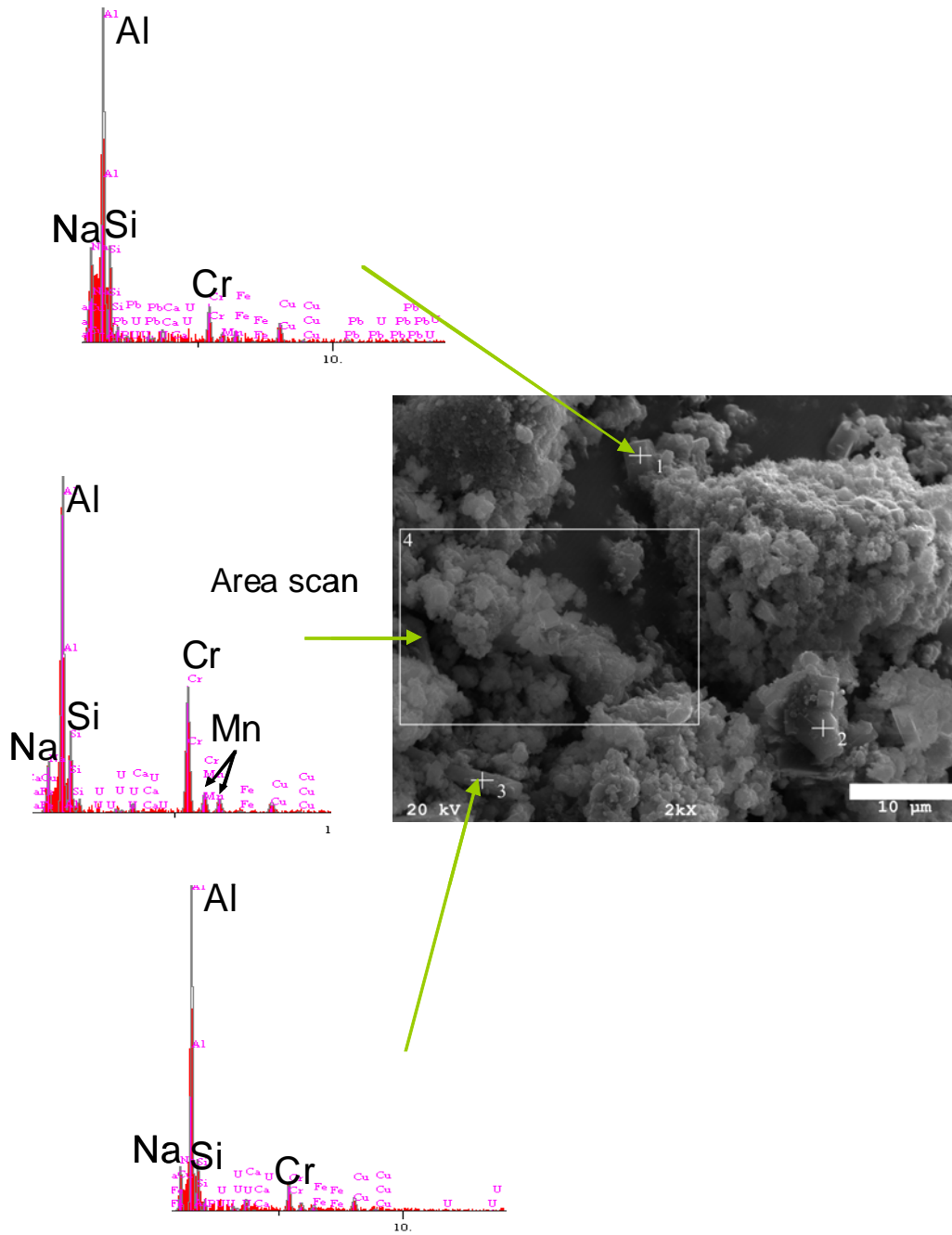


Figure 6.16. EDS Area Maps, Selected Elements in Group 6 S-Saltcake Washed Solids

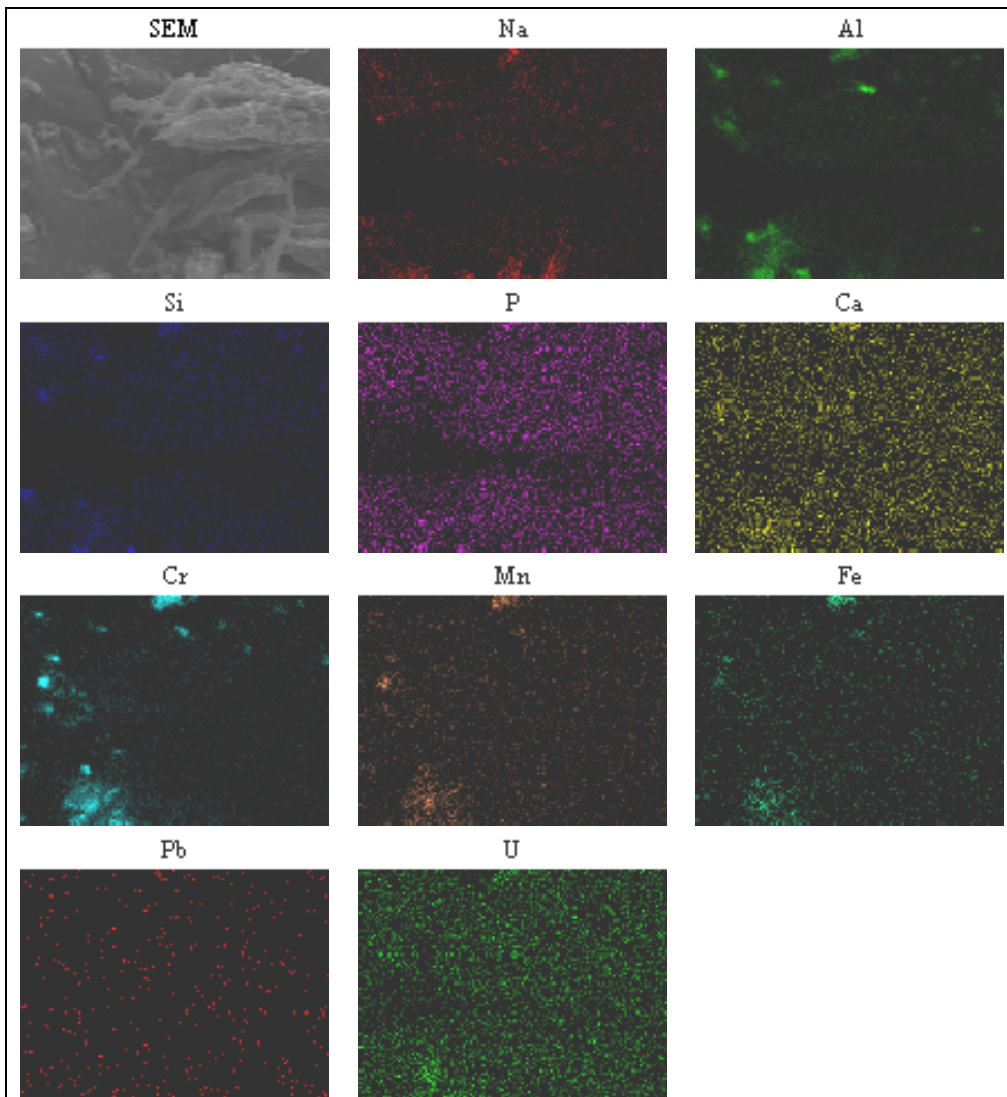


Figure 6.17. EDS Map of Group 6 S-Saltcake Washed Solids

The TEM analysis showed very few discrete particles in the Group 6 washed solids. The Group 6 solids, shown in Figure 6.18, consisted of a mixed amorphous agglomerate material; X-ray analysis showed this material to be an Al-Cr phase (most of the imaged materials were close to the Cu grid, which made analysis difficult). The nature of the individual particle agglomerates can be seen in Figure 6.19a-f. The material clearly possessed a large surface area. A small proportion of boehmite particles was found in the Group 6 solids (see Figure 6.19g-h) supporting the XRD evaluation.

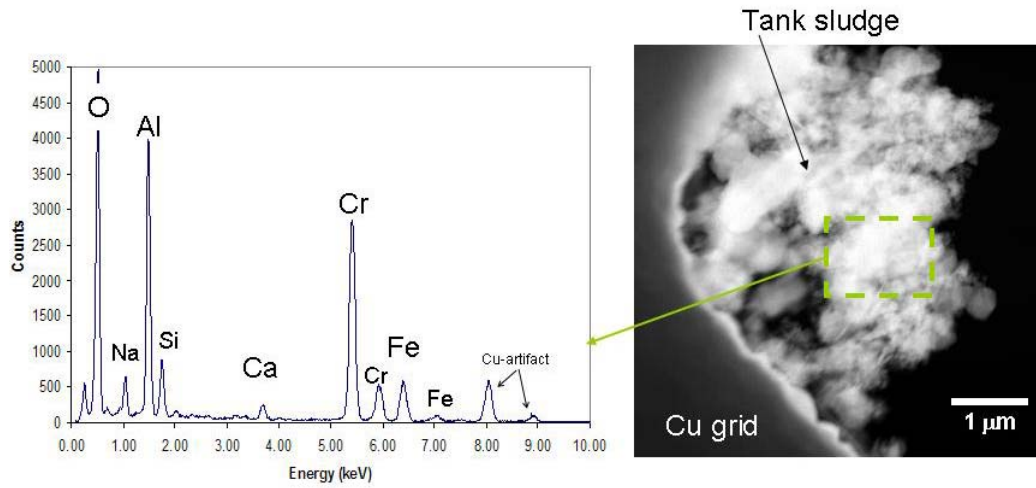


Figure 6.18. EDS Analysis of an Al-Cr Phase in Group 6 S-Saltcake Washed Solids with STEM Image of an Agglomerate

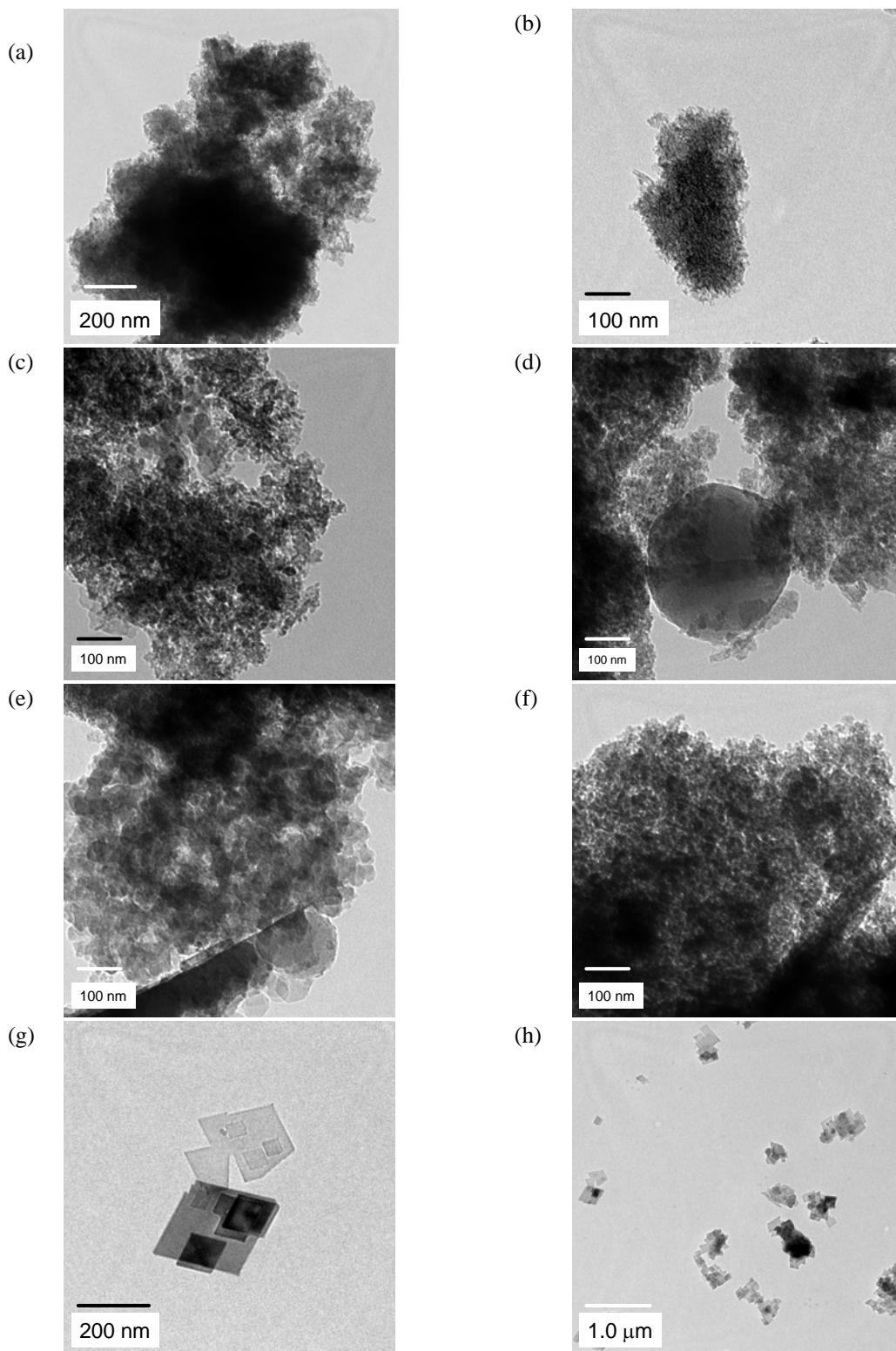


Figure 6.19. TEM Images of Washed Group 6 S-Saltcake Solids (a-f) Showing High Surface Area Material that Dominated G6-S-WL (g-h) Boehmite Particles

A few areas containing heavy elements (uranium) were found using the HAADF detector. One such particle is shown in Figure 6.20 along with the energy dispersive X-ray analysis. The Al and Cr were ubiquitous in this sample, and their appearance on the EDS scan was not necessarily related to the U phase.

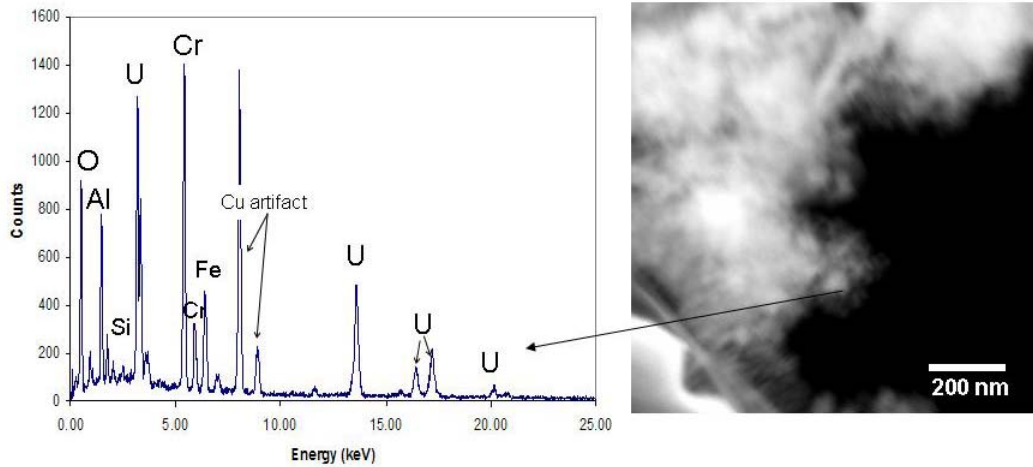


Figure 6.20. EDS and STEM Analysis Showing a Uranium-Rich Phase in the Group 6 S-Saltcake Washed Solids

7.0 Batch Contact Parametric Testing Methodology

This section describes the methods used to conduct the leach testing for Group 5 (parametric caustic leaching of boehmite) and Group 6 (caustic leach and parametric oxidative leaching of Cr) composite materials.

7.1 Group 5 REDOX Sludge

Testing on the Group 5 sludge evaluated boehmite leaching chemistry in actual tank waste. The composite material was rinsed with 0.01 M NaOH, subdivided, and subjected to a parametric test matrix for caustic-leach testing as discussed in the following sections.^(a)

7.1.1 Initial Washing of the Group 5 Solids

A 100-g slurry of the homogenized, Group 5 composite sample was transferred to a 200-mL centrifuge bottle by mixing with an overhead mixer and transferring with a large transfer pipet. At a concentration of 0.17 g of water-insoluble solids per gram of slurry, the 100-g aliquot represented 17 g of water-insoluble solids. The slurry was centrifuged (at ~960 G) for 20 minutes, and the supernatant was removed. The approximate solids volume was estimated to be 37 mL based on volume graduation marks on the bottle. Approximately 110 mL (3× the centrifuged solids volume) of 0.01 M NaOH was added, and the slurry was mixed for 15 minutes using an overhead stirrer. The slurry was centrifuged (at ~960 G) for 10 minutes and the supernatant removed. The washing steps were repeated twice for a total of three washes.

7.1.2 Division of the Washed Group 5 Solids

To conduct a successful sample subdivision, the slurry needed to be thinned extensively.^(b) The slurry was quantitatively transferred to a 1-L polyethylene bottle. Additional DI water was added to the solids, resulting in a final volume of 900 mL (or 17 g solids in 905 g of slurry, equivalent to 1.9 wt% undissolved solids [UDS]).

An overhead mixer equipped with a 3-bladed stainless steel impeller was used to homogenize the thinned slurry. Thirteen ~66.5 g slurry samples were transferred to 125-mL high-density polyethylene (HDPE) bottles using a large disposable polyethylene pipet. Each sample contained ~1.25 g UDS. The samples were removed from the hot cell for follow-on processing at the fume hood workstation.

One additional sample (G5-IW) containing approximately 21.0 g of slurry (equivalent to 0.4 g dry solids) was transferred to a 60-mL HDPE bottle. This sample was sub-divided by mixing and pipetting into sample vials. The samples were submitted for analysis by ICP-OES, XRD, and TEM to establish the starting composition of the washed solids.

(a) Testing was conducted according to TI-RPP-WTP-481, *Parametric Caustic Leach Test of Group 5 Hanford Redox Sludge Waste*, L Snow, March, 2007.

(b) An initial subdivision of slurry at a concentration of 17 g solids in 96 g slurry was not successful.

7.1.3 Caustic Leaching of the Washed Group 5 Solids

The leaching conditions (test matrix) for each of the 13 samples are summarized in Table 7.1. The test matrix evaluated the effects of free hydroxide concentration (1 to 5 M NaOH), temperature (80 to 100°C), and sodium nitrate concentration (1 to 5 M NaNO₃) on boehmite leaching kinetics.

Table 7.1. Group 5 Caustic Leaching Conditions

Bottle ID	Free [OH], M		[Na], M		[NO ₃], M		Temperature, °C ^(b)
	Target	Measured ^(a)	Target	Measured ^(a)	Target	Measured ^(a)	
G5-80-1	1	0.97	1	1.15	NA	NA	80 ^(c)
G5-80-3	3	3.30	3	3.52	NA	NA	80 ^(c)
G5-80-5	5	5.06	5	5.33	NA	NA	80 ^(c)
G5-90-1	1	0.91	1	1.18	NA	NA	90
G5-90-3a	3	2.94	3	3.22	NA	NA	90
G5-90-3b	3	2.90	3	3.21	NA	NA	90
G5-90-3c	3	3.02	3	3.25	NA	NA	90
G5-90-1N-3	3	3.13	4	4.22	1	1.11	90
G5-90-5N-3	3	3.06	8	8.46	5	5.13	90
G5-90-5	5	5.01	5	5.16	NA	NA	90
G5-100-1	1	0.86	1	1.11	NA	NA	100
G5-100-3	3	2.81	3	3.22	NA	NA	100
G5-100-5	5	5.11	5	5.58	NA	NA	100

(a) The measured analyte concentrations represent the equilibrium concentration obtained after a 170-h contact time.
(b) The temperature uncertainty was ±2.5°C.
(c) Loss of temperature control occurred after 72 h process time, see Appendix A.
Note: All analyte concentrations were measured at ambient (~21°C) temperature.
Analytical Service Requests (ASRs): 7904, 7909, 7913, 7917

The contact solution was adjusted in each sample to support the test matrix. Sodium hydroxide (19 M) was pipetted into each aliquot of washed solids slurry in the following amounts: 5.3 mL to yield 1 M NaOH, 15.8 mL to yield 3 M NaOH, and 26.3 mL to yield 5 M NaOH. The leaching mixtures were then diluted to a final volume of 100 mL (estimated uncertainty of 2 mL) with DI water. (The 100-mL volume had been pre-marked on each sample bottle.) Contact time with the concentrated NaOH was brief (<5 min). Solid NaNO₃ was added to two samples in sufficient quantity to meet the target nitrate concentration. The sample bottles were weighed after each addition of reagents (NaOH, water, and NaNO₃). Each leaching vessel was closed with a cap equipped with a tube condenser. The condenser was used to eliminate pressurization, minimize water loss, and minimize the spread of contamination.

The sample slurries were transferred to a temperature-controlled shaker table. The temperature was controlled with an aluminum heating block (J-KEM Scientific, Inc.) equipped with a Type T thermocouple. The heating block was supported on a J-KEM BTS-3500 digital bench-top shaker (Figure 7.1). The shaking speed was digitally controlled to 200 rpm; based on visual inspection, the solids were well suspended in solution. The samples were grouped according to the leaching temperature, and one group was leach-tested at a time. Before leach testing was conducted, the heating block was pre-heated to the appropriate temperature. The temperature control failed during the 80°C test between 72 h

and 170 h leach time (see Appendix A for discussion), and the WTP R&T M12 Issue Manager was notified of the event.^(a)

The leaching mixtures were shaken for 170 hours, and solution samples were withdrawn at 1, 4, 8, 24, 72, and 170 hours. At each sampling time, the shaker was stopped, and the solids were allowed to settle until there was enough clear liquid to conveniently sample. Approximately 2-mL of the clarified leachate were withdrawn with a transfer pipette and filtered through a 0.45- μm pore size nylon syringe filter; the transfer pipette, the syringe filter, and the syringe had been pre-heated in an oven to 100°C before filtering in an effort to minimize temperature changes impacting the sample. One 0.5-mL sample of filtered solution was acidified with 15 mL of 0.3 M HNO_3 for analysis by ICP-OES; another 0.5-mL sample of filtered solution was added to 15 mL of 1×10^{-4} M NaOH for analysis by ion chromatography. The remaining filtered solution was returned to the leaching vessel, and the leaching process was continued. The new liquid level was marked after each sample was taken. Evaporation was minimal during the course of the experiment. As evaporation occurred between sampling times, the sample volume was returned to the previous sample level by adding DI water. After 170 hours, additional leachate samples were taken for determination of the free hydroxide ion concentration, gamma emitters by GEA, and Cr(VI) by UV/vis spectrophotometry.

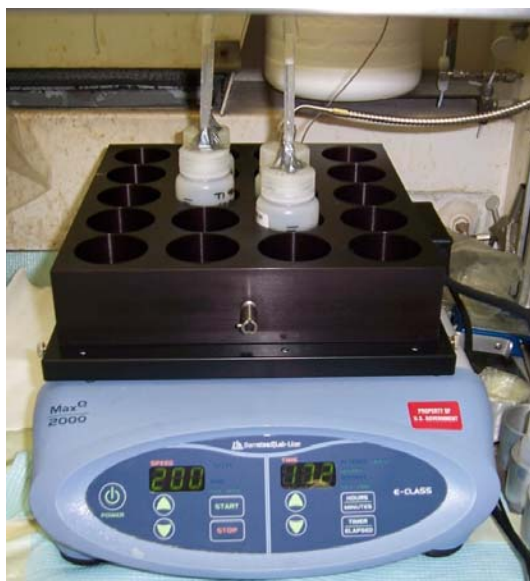


Figure 7.1. Batch Contact Shaker Supporting Parametric Testing

The final concentration values for free hydroxide, sodium, and nitrate are shown in Table 7.1 and were based on results from the samples taken at 170 hours.

After the final sample was taken at temperature, the slurries were removed from the mixing/heating block and cooled to ambient ($\sim 22^\circ\text{C}$) temperature. The slurries were centrifuged, and all but about 10 mL of the leachate was decanted. The solids were transferred to tared 15-mL centrifuge tubes. To the extent possible, all residual solids were transferred from the sample bottles by rinsing with the decanted

(a) A Corrective Action Report (CAR) was submitted to WTP addressing this issue (#21094-4).

leachate. The samples were then centrifuged, the leachate removed, and the centrifuged solids volume determined for each sample. The samples were then weighed, and the wet solids mass was determined.

7.1.4 Washing of Caustic-Leached Group 5 Solids for Analysis

The solids from the triplicate samples (G5-90-3a, -3b, -3c, leached at 90°C in 3 M NaOH, and each consisting of ~0.2 mL centrifuged solids volume) were prepared for characterization as shown in Figure 7.2. Samples were transferred to 15-mL volume-graduated, plastic centrifuge tubes; the volume graduations were used to assess solids volume. One of the solid samples was slurried in 0.01 M NaOH and divided between the remaining two solid samples. These two solid samples were then washed by adding ~5 mL of 0.01 M NaOH (equivalent to a phase ratio ~17 wash solution to centrifuged solids volume) and mixing on a vortex mixer for 5 min. The slurries were centrifuged for 5 min and the supernatant removed. The wash steps were repeated twice more for a total of three washes. After the final wash, the two samples were combined into one centrifuge tube by slurrying in additional 0.01 M NaOH. The sample was centrifuged and the aqueous phase removed. The solids were slurried in ~4 mL of DI water and sub-divided for analysis: PSD, XRD, TEM, SEM, BET surface area, KOH fusion with subsequent analysis for ICP-OES metals, GEA, Pu, total alpha, total beta, ⁹⁰Sr, and U by KPA.

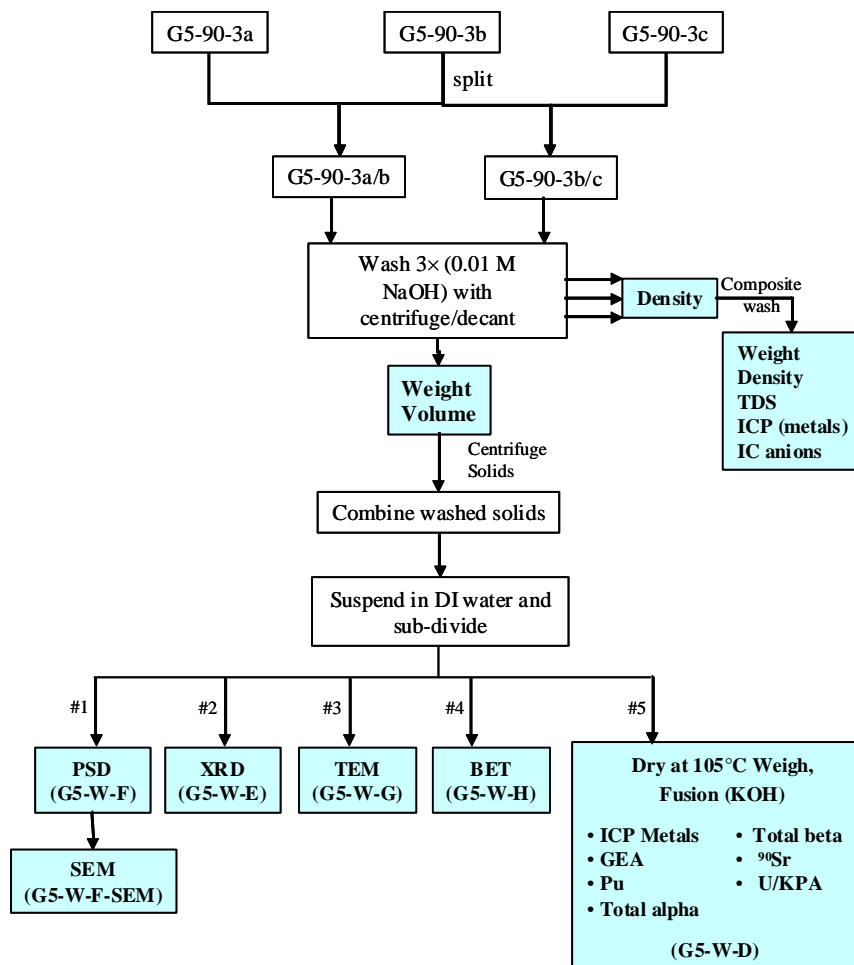


Figure 7.2. Washing, Subdivision, and Analysis Scheme for the Group 5 REDOX Sludge Caustic-Leached Solids

7.2 Group 6 S-Saltcake

Testing on the Group 6 saltcake solids evaluated actual tank waste Cr oxidative leaching chemistry. The Group 6 S-saltcake solids required subdivision from the composited solids, initial caustic leaching under prototypic plant conditions to remove Al, leached solids washing, sub-division into specific test samples, and finally parametric oxidative leaching, followed by analysis.^(a)

7.2.1 Initial Washing of the Group 6 Solids

The Group 6 composite solids slurry sample was mixed using an overhead stirrer fitted with a bladed stainless steel impeller. A 150-g aliquot was removed with a large transfer pipet and transferred to a 200-mL centrifuge bottle. At a concentration of 0.16 g dry water-insoluble solids per gram of slurry, the 150-g slurry contained ~24 g of water-insoluble solids. The slurry aliquot was centrifuged at ~610 G for 15 min,^(b) and then the supernatant was removed. The approximate volume of solids was estimated to be 35 mL based on volume graduations on the sample bottle. Approximately 105 mL (3× the centrifuged solids volume) of 0.01 M NaOH was added to wash the solids, and the slurry was mixed for 5 minutes by shaking. The slurry was centrifuged at ~610 G for 15 min, and then the supernatant was removed. The washing steps were repeated twice for a total of three washes.

7.2.2 Caustic Leaching and Washing of the Group 6 Solids

The washed Group 6 solids were caustic-leached in 100 mL (liquid volume to solid mass phase ratio of 4.2) of 3 M NaOH at ~100°C (boiling water bath) for 8 hours. During the leach processing, the slurry was mixed with a magnetic stir bar; the rotational speed was adjusted to obtain good suspension of the solids in solution. After 8 h, the slurry was removed from the boiling water bath and cooled to ambient temperature. After sitting overnight, the slurry was centrifuged at ~610 G for 15 minutes, and then the leachate was removed. The leachate was analyzed for density, ICP-OES metals (B, Cr, U, Fe, Mn, Ni, and Zn), anions (sulfate, phosphate, and nitrate), Pu, and free hydroxide.

The volume of leached centrifuged solids was determined to be ~20 mL. A 60-mL volume of 0.01 M NaOH (equal to 3× the solids volume) was added, and the slurry was mixed for 5 minutes by shaking. The slurry was centrifuged (at ~610 G for 15 min) and the supernatant removed. The washing was repeated twice more, for a total of three washes. Each wash solution was measured for density, and then the wash solutions were composited and sub-sampled for analysis by ICP-OES, anions, and Pu. The sample handling and analysis of the caustic leached Group 6 solids is summarized in Figure 7.3.

The solids were suspended in 300 mL DI water and two subsamples taken for analysis. One 3.1-g slurry sample (G6-Cr) was submitted for chemical characterization. The wt% UDS was determined from the

-
- (a) Testing was conducted according to TI-RPP-WTP-504, *Preparation of Group 6 Hanford Saltcake Waste for Oxidative Leaching*, L Snow, May 2007, and TI-RPP-WTP-528, *Parametric Oxidative Leach Test of Group 6 Hanford Saltcake Waste*, L Snow, July, 2007.
- (b) Mechanical issues with the in-cell centrifuge prohibited the application of 1000 G force and 1-h centrifuge time. The shorter centrifuging duration at lower centrifugal force resulted in well-compacted solids from which the supernatant could be decanted. Using higher force and time would result in a slightly smaller volume of centrifuged solids. Since the subsequent wash volumes were based on the centrifuged solids volume, the wash volumes might have been larger than required per the test plan, resulting in more complete removal of entrained supernatant. No negative impact was expected on the Cr leach data.

aliquots dried for fusion processing, and the fused sample preparations were then analyzed for ICP-OES metals, Pu, U (KPA), ^{90}Sr , total alpha, and total beta. The measured Cr concentration was used to determine the required amount of NaMnO_4 to be added to each parametric test sample for oxidative leaching.

Another 4.2-g slurry sample was withdrawn for additional analysis. This sample was centrifuged and the supernatant removed. The supernatant was submitted for analysis of free hydroxide, anions, and total inorganic and total organic carbon content. The solids were suspended in water and sub-divided for analysis of particle-size distribution, phase characterization of the insoluble solids by TEM, SEM, and XRD, and surface area of the solids by BET.

7.2.3 Division of Caustic-Leached Group 6 Solids

The slurry was composed of 3.3 wt% UDS. An overhead mixer was used to homogenize the slurry, and 17 slurry samples, each ~16.1 g, were transferred to 125-mL HDPE bottles using a large disposable polyethylene pipet. Each sample was calculated to contain ~0.53 g UDS.

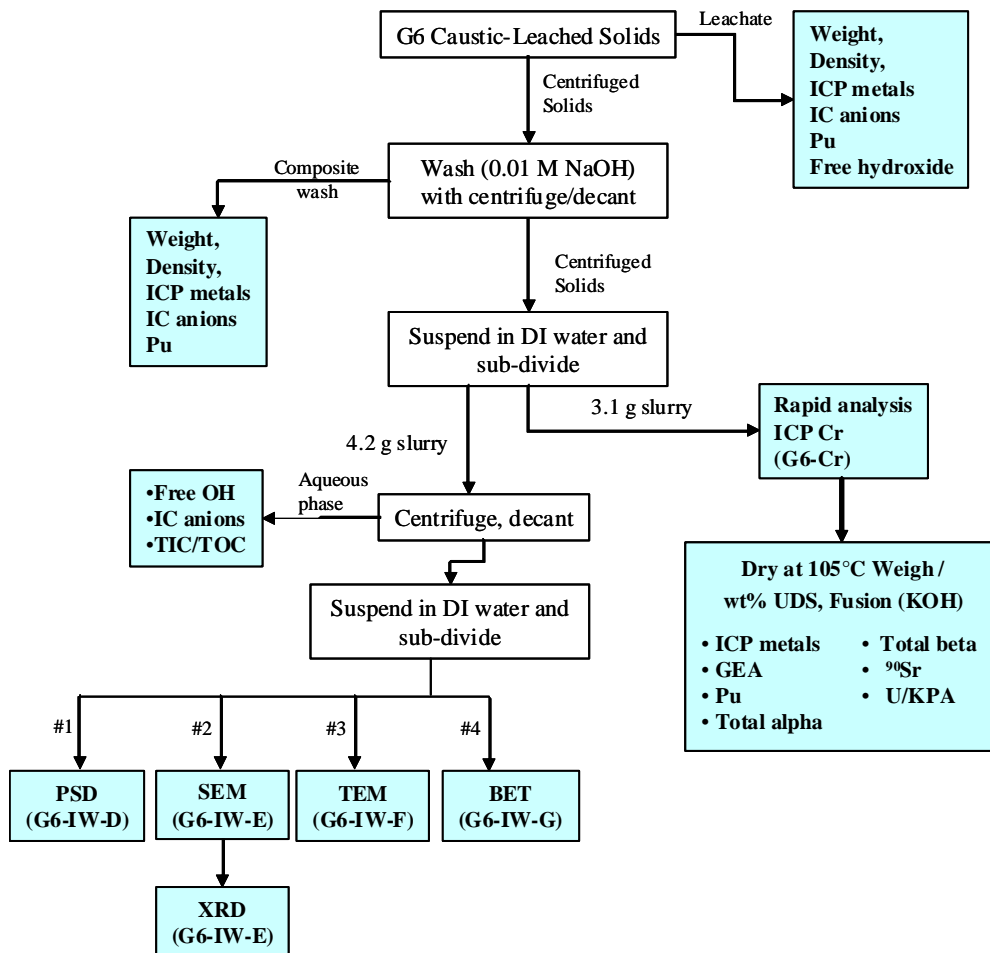


Figure 7.3. Washing, Subdivision, and Analysis Scheme for the Group 6 S-Saltcake Caustic-Leached Solids

7.2.4 Oxidative Leaching of the Caustic-Leached Group 6 Solids

The leaching conditions for each of the 17 samples are summarized in Table 7.2. The aluminum heating block was pre-heated to the appropriate temperature. Sodium hydroxide (19 M) was added to each aliquot of washed solids in the following amounts: 1.3 mL to yield 0.25 M NaOH, 6.6 mL to yield 1.25 M NaOH, and 15.8 mL to yield 3 M NaOH. The slurry mixtures were then diluted to 100 mL with DI water. Contact time with the concentrated NaOH was brief (<5 min). Aliquots of 1 M NaMnO₄ (freshly prepared and filtered) were then added to each sample in the following amounts: 1.3 mL to yield 0.75 Mn/Cr mole ratio, 1.7 mL to yield 1.0 Mn/Cr mole ratio, and 2.2 mL to yield 1.25 Mn/Cr mole ratio. The liquid level was marked on each bottle. The free hydroxide shown in Table 7.2 was measured after at the conclusion of the test.

Table 7.2. Oxidative Leaching Conditions for Group 6 S-Saltcake Caustic-Leached Solids

Bottle ID (Group#-T-[OH]-Mn/Cr)	[NaOH], M		Mn/Cr Mole Ratio	Temperature, °C ^(a)
	Target	Final [OH]		
G6-25-0.25-0.75	0.25	0.22	0.75	25
G6-25-0.25-1	0.25	0.23	1	25
G6-25-0.25-1.25	0.25	0.20	1.25	25
G6-25-1.25-0.75	1.25	1.29	0.75	25
G6-25-1.25-1.25	1.25	1.26	1.25	25
G6-25-1.25-1a	1.25	1.26	1	25
G6-25-1.25-1b	1.25	1.25	1	25
G6-25-1.25-1c	1.25	1.26	1	25
G6-25-3-0.75	3	3.03	0.75	25
G6-25-3-1	3	2.98	1	25
G6-25-3-1.25	3	2.86	1.25	25
G6-50-0.25-0.75	0.25	0.23	0.75	50
G6-50-0.25-1	0.25	0.24	1	50
G6-50-0.25-1.25	0.25	0.21	1.25	50
G6-50-3-0.75	3	3.11	0.75	50
G6-50-3-1	3	3.09	1	50
G6-50-3-1.25	3	3.01	1.25	50

(a) The temperature uncertainty was $\pm 2.5^\circ\text{C}$.
 Note: The hydroxide concentrations were measured at ambient ($\sim 21^\circ\text{C}$) temperature.

The leaching mixtures were shaken for 24 hours at 200 rpm resulting in good suspension of the solids. Samples were withdrawn at 0.5, 1, 2, 4, 6, and 24 hours. One sample, G6-25-0.25-1, was shaken for an additional 24 h with a final sampling at 48 h. At each sampling event, the shaker was stopped, and the solids were allowed to settle for ~6 to 10 min, resulting in sufficient clarification of the aqueous portion to support sampling without solids removal. Then ~4 mL of the leachate were withdrawn from the leaching mixture and filtered through a 0.45- μm pore size nylon syringe filter. For the tests run at 50°C, both the syringe filter and the syringe were pre-heated in an oven to 50°C before filtering. Analytical samples of each filtered leach solution were prepared. One 0.5-mL aliquot was acidified with 15 mL of 0.3 M HNO₃.

for ICP-OES analysis. Another 0.5-mL aliquot was added to 2.5 mL of 2 M HNO₃ for Pu analysis. A 2-mL sample of filtered leachate was analyzed directly using UV/vis for chromate concentration.

After the final samples were taken at temperature, the slurries were removed from the mixing/heating block and cooled to ambient temperature. The slurries were centrifuged, and the leachates were decanted.^(a) Samples of the leachate were filtered for analysis of ICP-OES metals, free hydroxide U (by KPA), and Pu concentration.

The triplicate Group 6 oxidatively leached solids exposed to the 25°C leach temperature and 1.25 M NaOH matrix at a Mn/Cr mole ratio of 1 were composited for characterization. The characterization was conducted similarly to the Group 5 caustic leach solids; the process flow and applied characterizations are summarized in Figure 7.4.

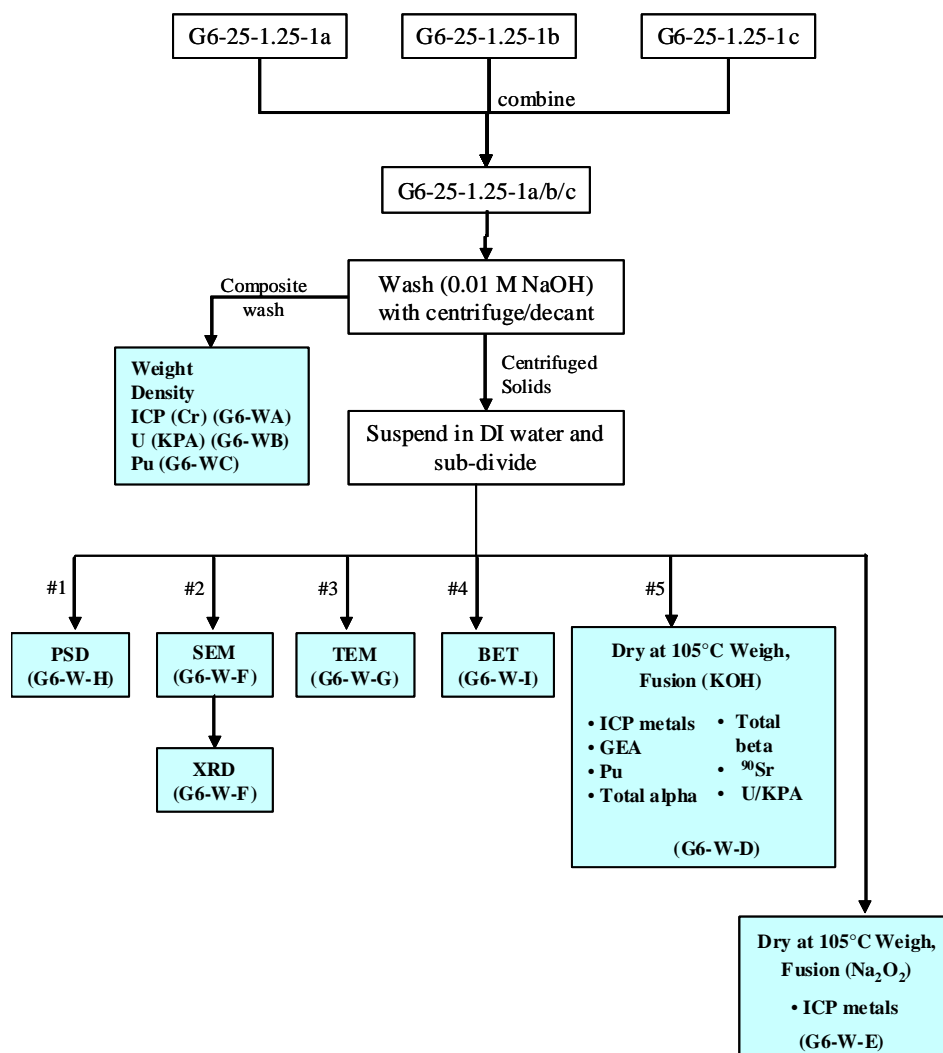


Figure 7.4. Washing, Subdivision, and Analysis Scheme for the Group 6 S-Saltcake Oxidatively Leached Solids

(a) The contact dose rates of the leached solids were too high to safely conduct transfer to volume-graduated centrifuge tubes to assess the volume of centrifuged solids.

8.0 Group 5 REDOX Sludge Parametric Caustic Leaching Test Results

The Al component in the Group 5 waste was ~90 wt% boehmite. The parametric leach testing of this waste sample was directed toward understanding boehmite dissolution in the actual tank waste and thus being able to match the boehmite dissolution properties to a simulant material with minimal confounding of matrix effects. The parametric leaching results and residual solids composition are discussed in the following sections.

8.1 Expected Boehmite Solubility

Panias et al. (2001) demonstrated boehmite solubility as a function of free hydroxide and temperature according to Equation 8.1:

$$C = A_1 \times (1E - 6) \times T^3 + A_2 \times (1E - 3) \times T^2 + A_3 \times (1E - 2) \times T + A_4 \quad (8.1)$$

where C = concentration of Al as Al_2O_3

$$A_1 = -0.0618925 \times C' + 1.36953$$

$$A_2 = 0.02301 \times C' + 0.1707$$

$$A_3 = 2.498E-6 \times C'^3 - 3.106E-4 \times C'^2 + 5.483E-2 \times C' - 1.332$$

$$A_4 = 3.236E-6 \times C'^3 - 7.887E-4 \times C'^2 + 1.584E-1 \times C' - 2.518$$

T = temperature in degrees C

C' = concentration of Na as Na_2O .

Using Equation 8.1, the theoretical boehmite solubility limits in terms of grams Al per liter of solution were derived and are shown in Figure 8.1. The expected trends in boehmite solubility as functions of temperature and free hydroxide concentration are clear; boehmite solubility increases with increasing temperature and NaOH concentration.

The boehmite solubility limits, as shown in Figure 8.1, are useful in interpreting the results obtained from the actual waste testing. The Al present as *boehmite* in the Group 5 sludge was calculated to be ~330 mg/g (dry mass basis, free of residual supernatant).^(a) Based on the 1.25-g sample size and final leach solution volume of 90 mL (accounting for volume loss during sampling), complete dissolution of the boehmite would result in 4.6 mg Al/mL. Two test conditions in the test matrix challenged the expected boehmite solubility:

- 1 M free hydroxide at 80°C; under these conditions, the maximum boehmite dissolution was expected to be 3.8 mg Al/mL.
- 1 M free hydroxide at 90°C; under these conditions, the maximum boehmite dissolution was expected to be 4.6 mg Al/mL.

(a) The XRD analysis of the starting material showed the sample to be ~74% boehmite and only ~5.7% gibbsite (after subtracting the mass of entrained supernatant components).

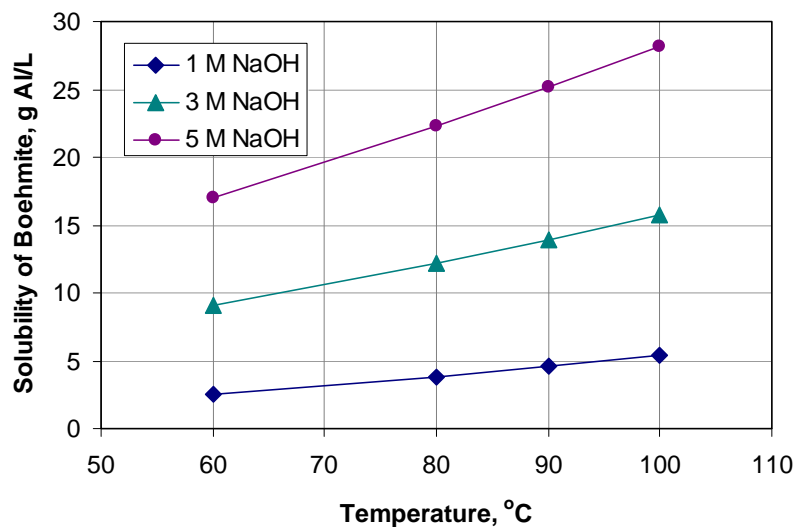


Figure 8.1. Theoretical Boehmite Solubility as a Function of Temperature in 1, 3, and 5 M NaOH Solutions Based on the Literature Model (Panias et al. 2001)

These expected solubilities do not take into account the effect of the gibbsite dissolution (5.8 wt% gibbsite in the washed solids). The Al concentration associated with the gibbsite dissolution is projected to be ~0.28 mg/mL.

8.2 Time, Temperature, and Hydroxide Effects on Aluminum Dissolution

The Al dissolution rates of Group 5 sludge as functions of time, temperature, and free hydroxide concentrations were evaluated. Based on the *total* Al concentration in the solids material (380 mg/g—free of residual supernatant and inclusive of other Al mineral forms such as gibbsite, zeolite, and cancrinite), the complete dissolution of Al would result in a concentration of 5.4 mg Al/mL or 0.20 M.

The leaching data at constant temperature and varying free-hydroxide concentrations are summarized in Figure 8.2 through Figure 8.4. A measure of experimental precision is shown by the triplicate tests conducted at 3 M free hydroxide and at 90°C in Figure 8.3. The scatter in the data was within the analytical characterization uncertainty of ±15%.

Examination of Figure 8.2 indicated that the loss of temperature control during the 80°C test did not have an obvious impact on the dissolution curve; the final equilibrium Al concentrations were consistent with the expected boehmite solubility at the given temperature and NaOH concentrations.

The initial rapid rise in Al concentration was most likely associated with gibbsite dissolution; the subsequent increase in Al concentration was associated with the dissolution of boehmite. Boehmite is known to dissolve much more slowly than gibbsite (Scotford and Glastonbury 1971). Dissolution of the gibbsite fraction alone would result in ~1E-2 M Al in the leachate solution. This Al concentration was

generally reached in <1 hr; only the 1 M free hydroxide at 80°C test condition did not reach this Al concentration at the 1-hr sampling point where 7E-3M was measured.

Approximately 95 wt% of the Al in the Group 5 composite needed to be removed from the sludge to eliminate Al as the limiting factor in waste loading in product glass.^(a) This condition was met after a 28-hr contact time with 5 M NaOH at 100°C. Table 8.1 summarizes the projected hours of leach time required to achieve 95 wt% Al removal as a function of all leach conditions. The projected leach time was based on the simple interpolation between graphed points in Figure 8.2 through Figure 8.7. At the 5 M NaOH leach condition, the 90°C temperature resulted in a longer estimated leach time than that of the 80°C temperature. This effect was an artifact of the crossover in the Al concentrations at 72 h (see Figure 8.7); these two Al concentrations differed by only 5%, well within the analytical uncertainty of ±15%. The 90°C leach temperature is expected to lower the boehmite dissolution time relative to the 80°C leach temperature.

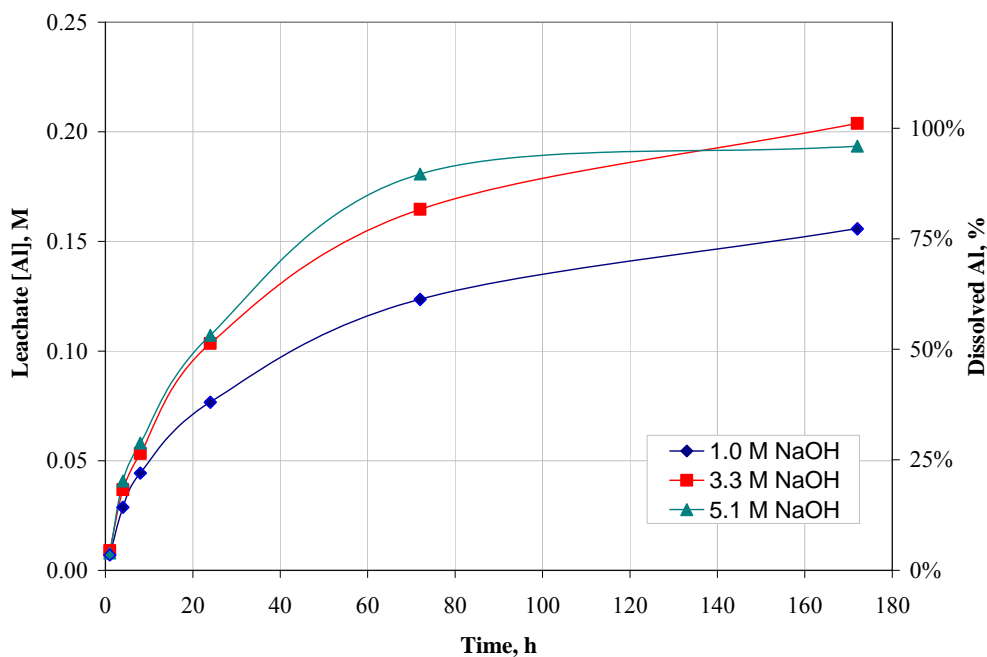


Figure 8.2. Aluminum Concentration Versus Time at 80°C Leach Temperature in 1, 3, and 5 M NaOH Solutions for Group 5, REDOX Sludge

(Note: 170-hr data are presented for indication-only; see Appendix A.)

(a) Note that the 95 wt% Al removal is specific to this particular composite material (which was specifically selected for its high Al content) as well as the glass loading limitation of 0.11 grams Al₂O₃ per gram of glass. Different waste blends and different alumina loading limits will have different requirements for Al removal. As such, this may be considered a worst-case condition.

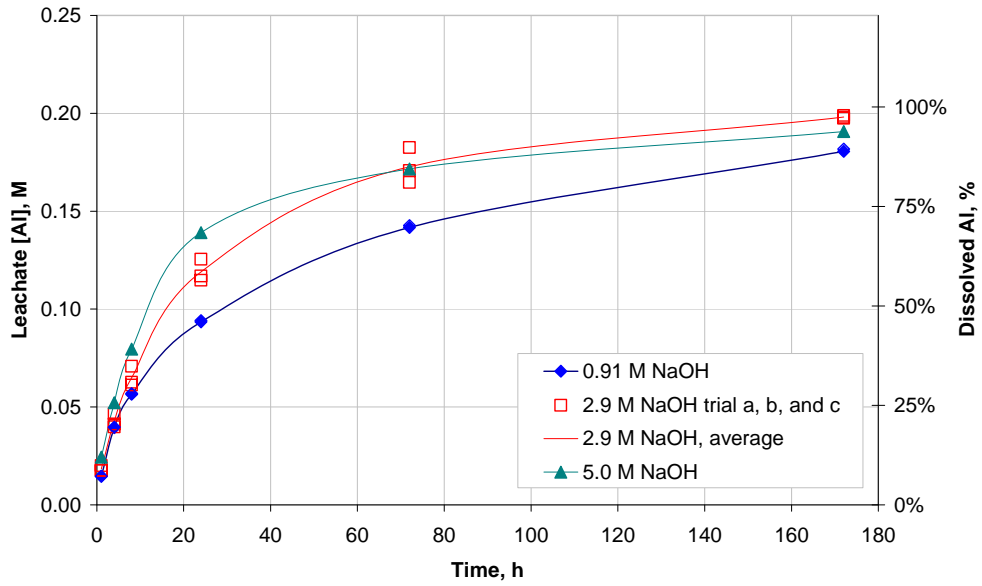


Figure 8.3. Aluminum Concentration Versus Time at 90°C Leach Temperature in 1, 3, and 5 M NaOH Solutions for Group 5, REDOX Sludge

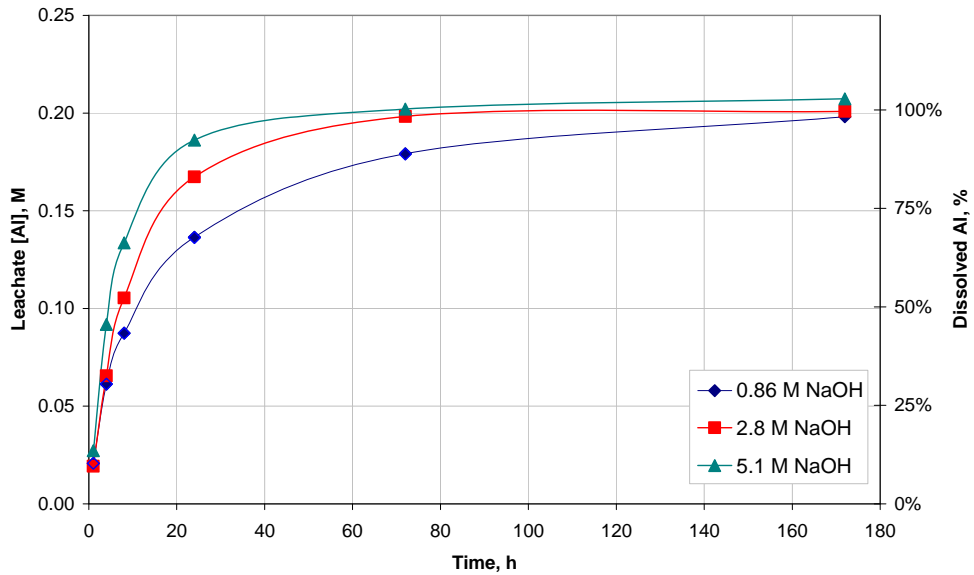


Figure 8.4. Aluminum Concentration Versus Time at 100°C Leach Temperature in 1, 3, and 5 M NaOH Solutions for Group 5, REDOX Sludge

Table 8.1. Time to Achieve 95 Wt% Al Reduction in Group 5 REDOX Sludge

Leach Matrix	Process Temperature, °C		
	80	90	100
1 M NaOH	not achieved	not achieved	116 hr
3 M NaOH	130 hr	130 hr	48 hr
5 M NaOH	110 hr ^(a)	164 hr ^(a)	28 hr

(a) The discrepancy in leach times was attributed to an experimental artifact. As shown in Figure 8.7, the 80°C Al leach result exceeded the 90°C result at 72 hr. Note: The 95 wt% Al removal is specific to this particular composite material (which was specifically selected for its high Al content) as well as the glass loading limit of 0.11 grams Al₂O₃ per gram of glass. Different waste blends and different alumina loading limits will have different requirements for Al removal. As such, this may be considered a worst-case condition.

The same data are re-plotted in Figure 8.5 through Figure 8.7 to show the effect of temperature at constant free-hydroxide concentration. As expected, reducing temperature had a negative effect on the boehmite dissolution rate. At 24-hr and 1 M free hydroxide (Figure 8.5), leaching at 90°C resulted in 0.093 M Al (~46 wt% Al removal) and at 100°C resulted in 0.14 M Al (~68 wt% Al removal). A similar effect was noted for the 3 M and 5 M free-hydroxide matrix conditions.

Temperature dependence is further defined (see Figure 8.8) for two selected test times (8 hrs and 24 hrs) and at the three free-hydroxide test conditions. As temperature increased, the dissolution of boehmite increased. Further discussion of the temperature dependence is provided in Section 8.3.

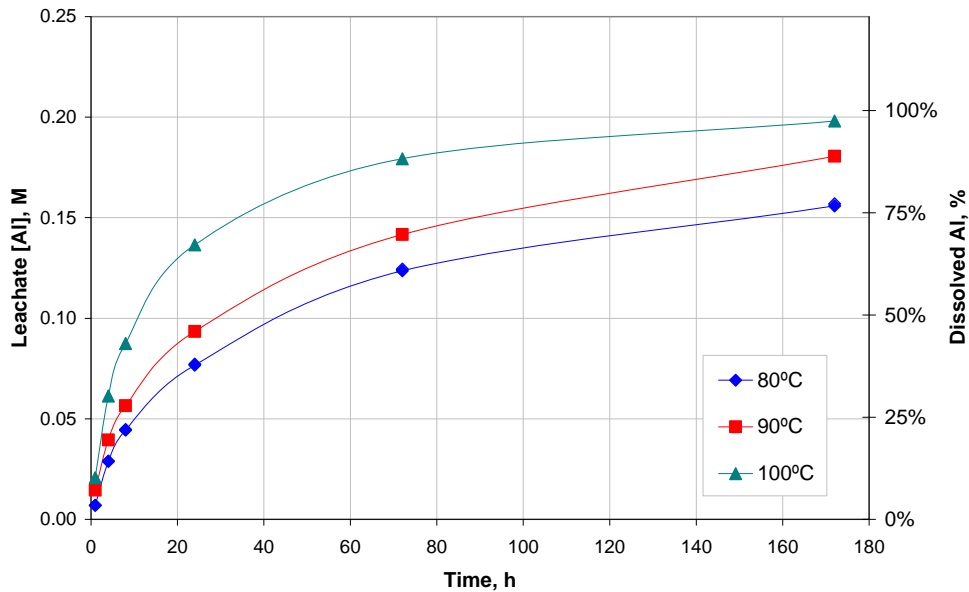


Figure 8.5. Aluminum Concentration and Percent Dissolved in 1 M NaOH for Group 5, REDOX Sludge
(Note: the 80°C 170-hr leach datum is presented for indication-only; see Appendix A.)

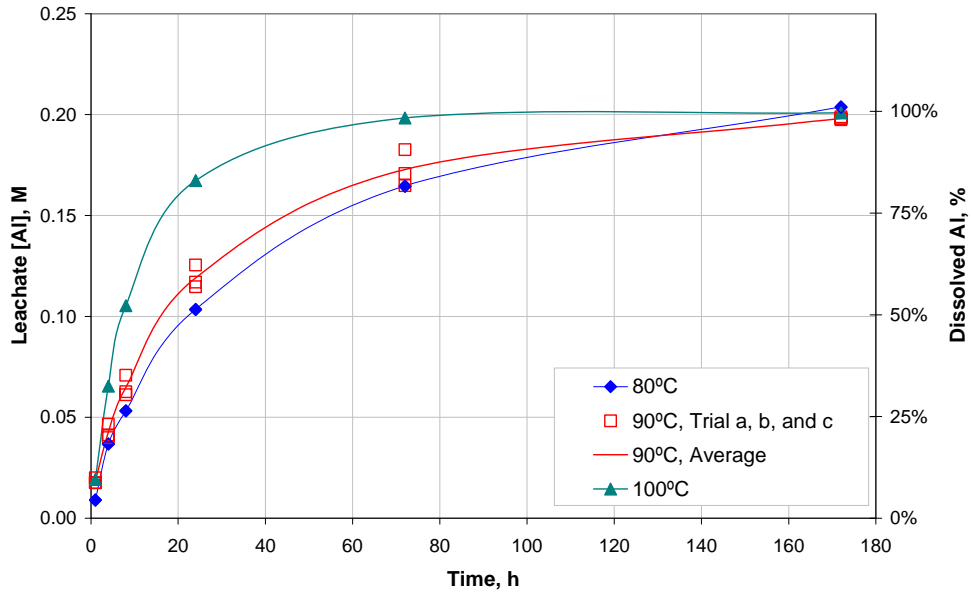


Figure 8.6. Aluminum Concentration and Percent Dissolved in 3 M NaOH for Group 5, REDOX Sludge (Note: the 80°C 170-hr leach datum is presented for indication-only; see Appendix A.)

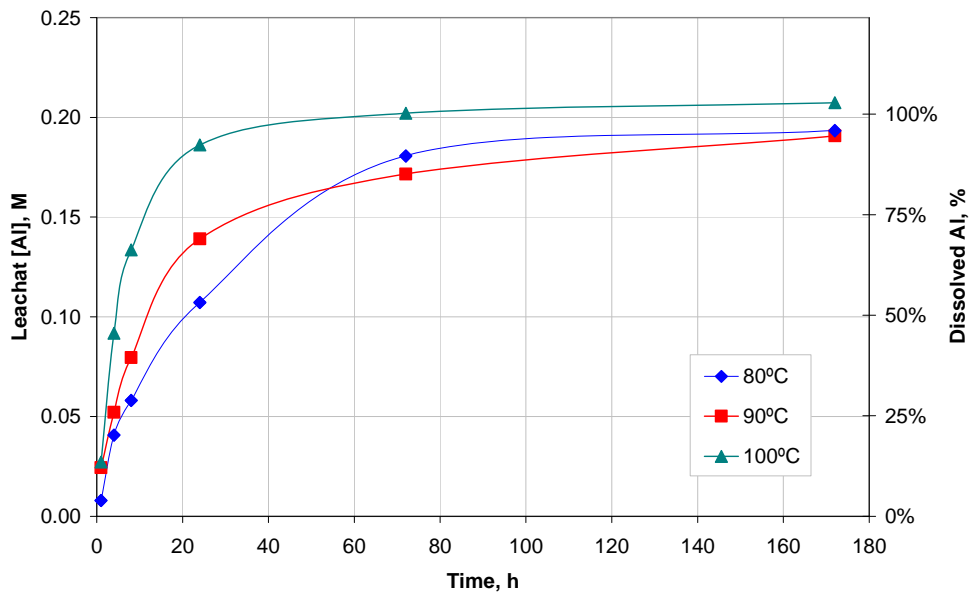


Figure 8.7. Aluminum Concentration and Percent Dissolved in 5 M NaOH for Group 5, REDOX Sludge (Note: the 80°C 170-hr leach datum is presented for indication-only; see Appendix A.)

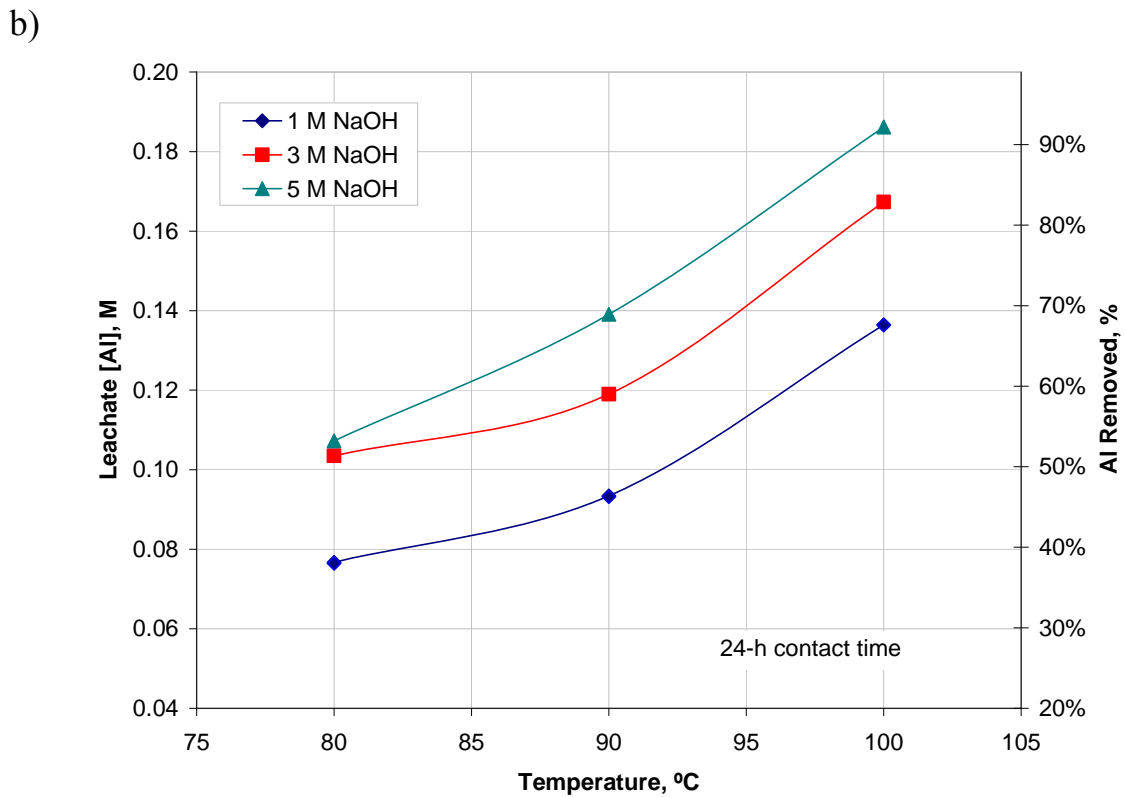
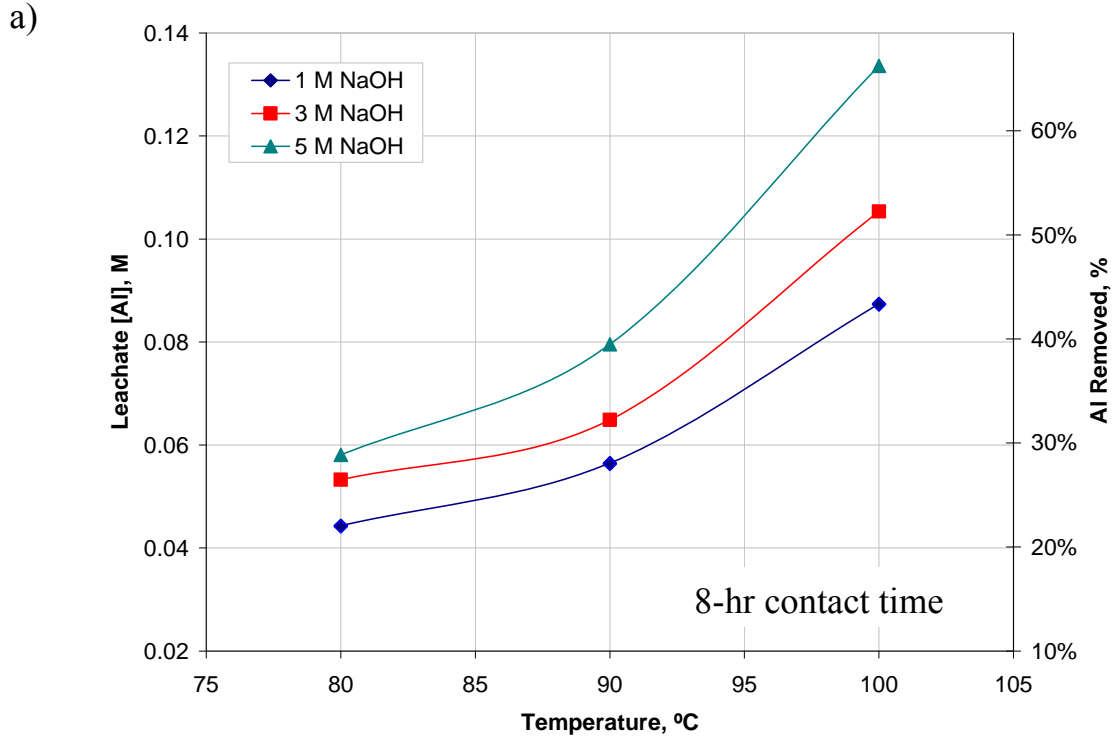


Figure 8.8. Aluminum Concentration in Leach Solution as a Function of Process Temperature (a) 8-hr Contact Time and (b) 24-hr Contact Time for Group 5, REDOX Sludge

8.3 Analysis of Group 5 REDOX Sludge Boehmite Dissolution Kinetics

General kinetic parameters for caustic dissolution of the boehmite phase in the Group 5 REDOX sludge sample were determined to establish a basis of comparison to the caustic dissolution of boehmite materials being evaluated for use in tank waste simulants. To a first approximation, the rate of transfer of Al into the liquid phase can be expressed as:

$$\frac{d(\text{Al})}{dt} = k(\text{OH}^-)^x \quad (8.2)$$

This assumes constant activity of the Al solid phase (e.g., boehmite) and constant activity of water. These assumptions are reasonable early in the dissolution process (time \leq 8 hr). Taking the logarithm of both sides of Equation 1:

$$\log\left[\frac{d(\text{Al})}{dt}\right] = \log k + x \log(\text{OH}^-) \quad (8.3)$$

The hydroxide ion dependence can be determined as the slope of the plot of the $\log\left[\frac{d(\text{Al})}{dt}\right]$ versus $\log(\text{OH}^-)$; and the rate constant k can be derived from the intercept. In these expressions, $\frac{d(\text{Al})}{dt}$ is the initial rate of Al dissolution, or more specifically for this analysis, the rate of Al dissolution from boehmite.

For the experiments performed with the Group 5 tank-sludge sample, determination of the initial boehmite dissolution rate is complicated by the fact that some gibbsite is present in the tank-sludge solids. To remove the influence of gibbsite on the boehmite dissolution kinetics, the first hour of leaching was omitted from the analysis of the data. The Group 5 boehmite Al dissolution rates were determined by plotting the Al concentration versus time and determining the best-fit regression line through the 1-, 4-, and 8-hr data points. Such plots were constructed at the three different temperatures (80, 90, and 100°C) used and the three different NaOH concentrations used. Figure 8.9 through Figure 8.11 present the results, and the initial reaction rates are tabulated in Table 8.2.

Table 8.2. Initial Al (Boehmite) Dissolution Rates

[NaOH], M	d[Al]/dt, mole L ⁻¹ h ⁻¹		
	80°C ^(a)	90°C ^(a)	100°C ^(a)
1	(5.3 ± 0.9)E-3	(5.9 ± 1.1)E-3	(8.2 ± 0.9)E-3
3	(6.2 ± 1.4)E-3	(6.6 ± 0.7)E-3	(1.05 ± 0.03)E-2
5	(7.0 ± 1.8)E-3	(7.8 ± 0.7)E-3	(1.30 ± 0.14)E-2
(a) The reported uncertainties represent the standard errors for the regression lines in Figure 8.9 through Figure 8.11.			

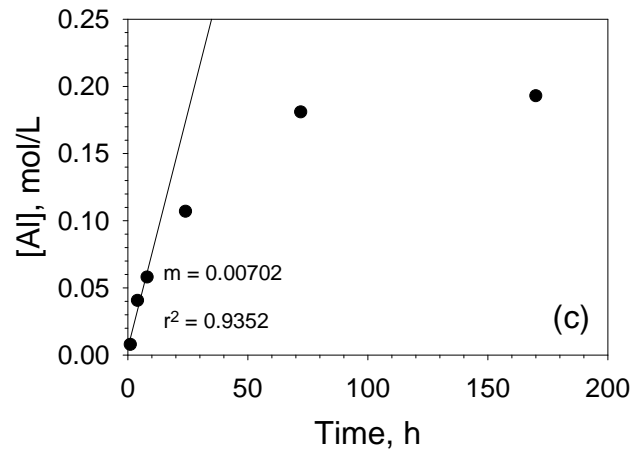
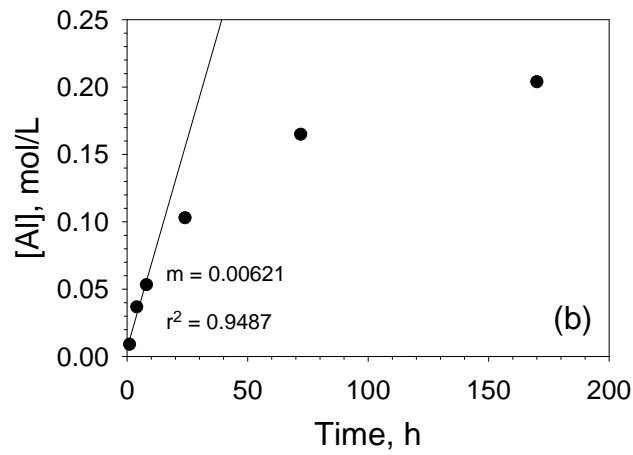
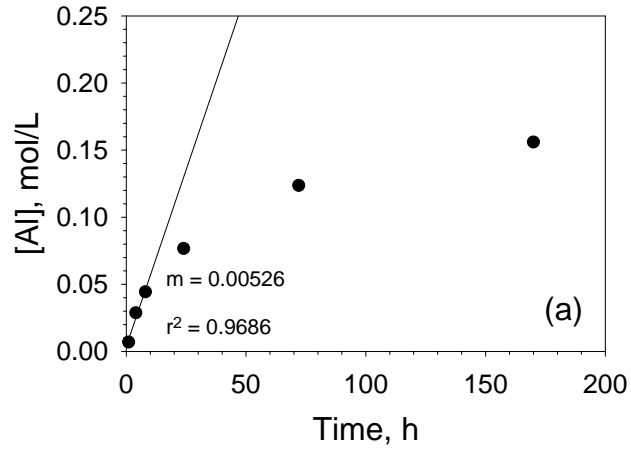


Figure 8.9. Plot of Al Concentration Versus Time for Leaching of Group 5 Solids at 80°C with a) 1 M NaOH, b) 3 M NaOH, and c) 5 M NaOH (Group 5, REDOX Sludge Test Material)

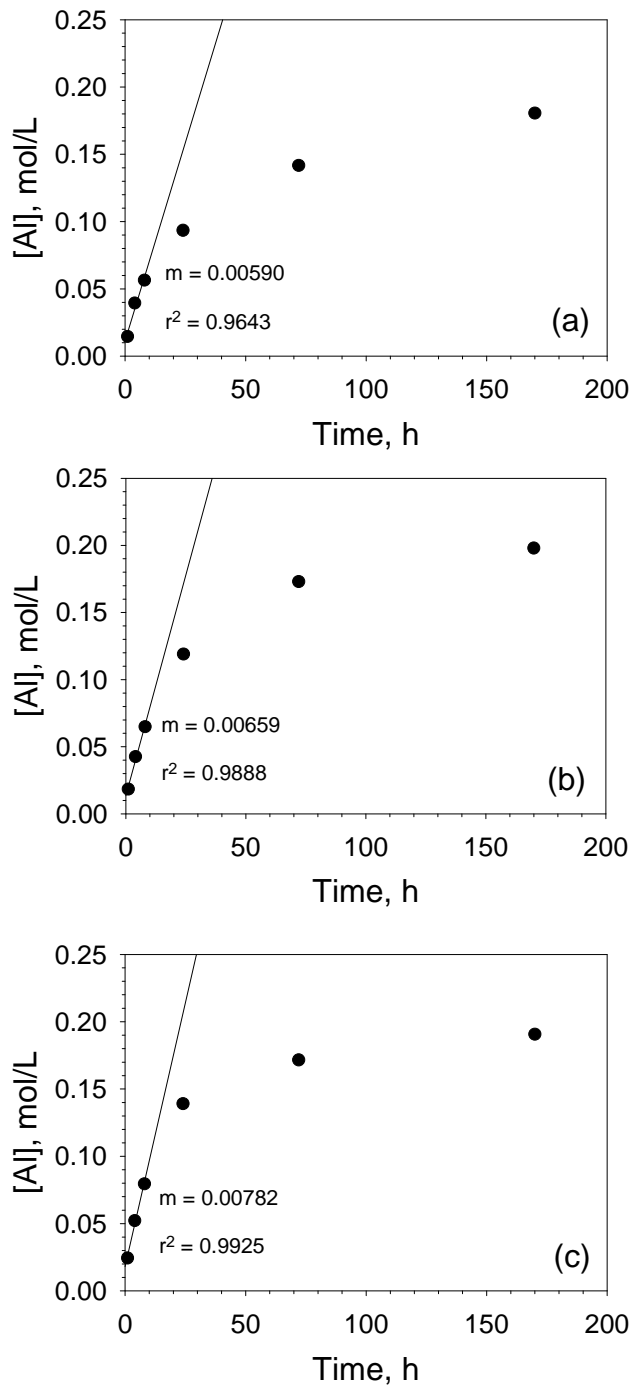


Figure 8.10. Plot of Al Concentration Versus Time for Leaching of Group 5 Solids at 90°C with a) 1 M NaOH, b) 3 M NaOH, and c) 5 M NaOH (Group 5 REDOX Sludge Test Material)

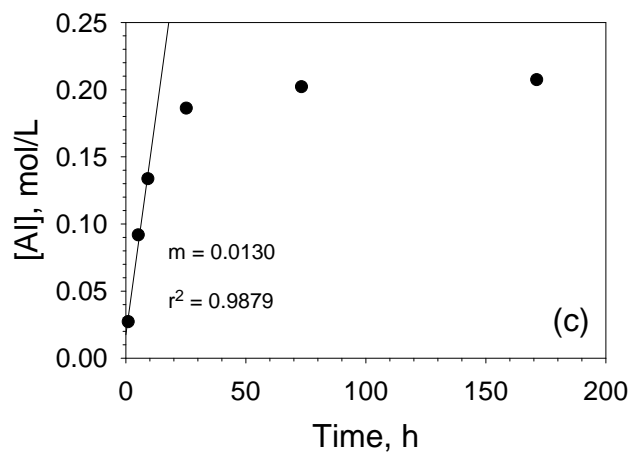
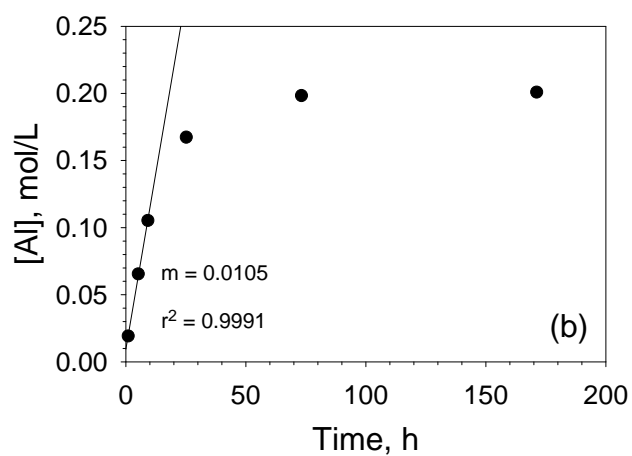
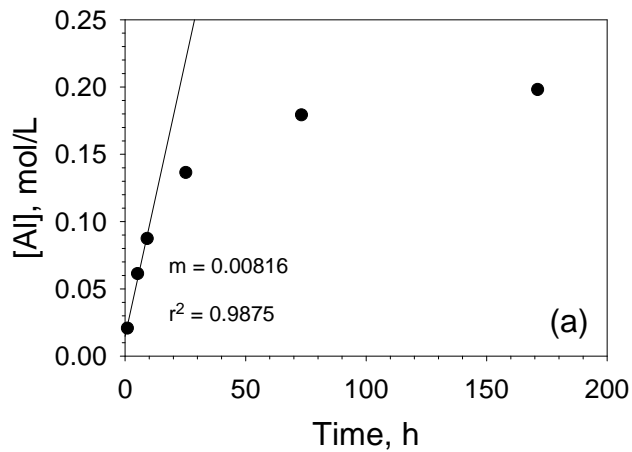


Figure 8.11. Plot of Al Concentration Versus Time for Leaching of Group 5 Solids at 100°C with a) 1 M NaOH, b) 3 M NaOH, and c) 5 M NaOH (Group 5 REDOX Sludge Test Material)

Using Equation 8.3 to determine the dependence of boehmite dissolution on the hydroxide ion concentration, the data in Figure 8.1 were plotted on a logarithmic/logarithmic scale (Figure 8.12). The results indicated a weak dependence in the dissolution rate on the hydroxide ion concentration. At 80°C and 90°C, the hydroxide ion dependence is approximately $1/5^{\text{th}}$ order, while at 100°C, it is approximately $1/4^{\text{th}}$ order. The rate constants (k) can be derived from the intercepts of the regression lines shown in Figure 8.12. Table 8.3 compiles the rate constants at each temperature investigated. Note that these rate constants represent only the initial reaction rates and as such should not be extrapolated to the entire boehmite dissolution reaction. Furthermore, as evidenced by the fractional hydroxide orders, the reaction rate has no mechanistic significance. This model cannot be extrapolated to WTP processing conditions because it does not capture all of the factors that affect kinetics (because it is not a mechanistic model). Again, the initial reaction rates are only expected to be useful for comparison to analogous measurements on commercially available boehmite materials that are candidates for simulant formulation.

Table 8.3. Boehmite Dissolution Rate Constants

T, °C	log k ^(a)	k	ln k
80	-2.29 ± 0.02	5.13E-3	-5.27
90	-2.24 ± 0.03	5.75E-3	-5.16
100	-2.09 ± 0.02	8.13E-3	-4.81
(a) The reported uncertainties represent the standard errors for the regression lines in Figure 8.12.			

The apparent activation energy (ΔE_a) for the boehmite dissolution can be determined from the rate constants using the Arrhenius equation, expressed as:

$$\ln(k) = \ln(A) - \left(\frac{\Delta E_a}{R} \right) \left(\frac{1}{T} \right) \quad (8.4)$$

where A is a constant, R is the gas constant ($8.314 \text{ JK}^{-1} \text{ mol}^{-1}$), and T is the temperature expressed in Kelvin. Figure 8.13 presents the Arrhenius plot for the data from Table 8.3. This analysis of the data yields an apparent activation energy of $25.2 \pm 8.7 \text{ kJ/mol}$. This value is considerably lower than that reported in the literature (123 kJ/mol) for dissolution of pure boehmite in NaOH (Scotford and Glastonbury 1971). The literature value suggests that the reaction rate is controlled by chemical reaction at the boehmite particle surface, whereas the result obtained here suggests that it is controlled primarily by mass transport (i.e., mixing) properties (under the experimental conditions used here). The boehmite material used by Scotford and Glastonbury (1971) consisted of much larger particles (20 to 40 μm with a surface area of $500 \text{ cm}^2/\text{g}$) than those observed in the Group 5 tank waste solids (90 vol% of the particles were less than 20 μm based on the volume distribution; the surface area of the initial washed solids was $26 \text{ m}^2/\text{g}$ or $260,000 \text{ cm}^2/\text{g}$). It is possible that enough surface area was available for the boehmite particles in the Group 5 tank waste that reaction with hydroxide ion at the surface was no longer the controlling factor. The smaller particle size and higher surface area of the Group 5 boehmite particles would presumably have more sharp edge (“step”) sites than the material used by Scotford and

Glastonbury. The edge sites theoretically dissolve more easily (i.e., with lower apparent activation energy) than flat surfaces (“terrace”) sites (Tromans and Meech 2002).^(a)

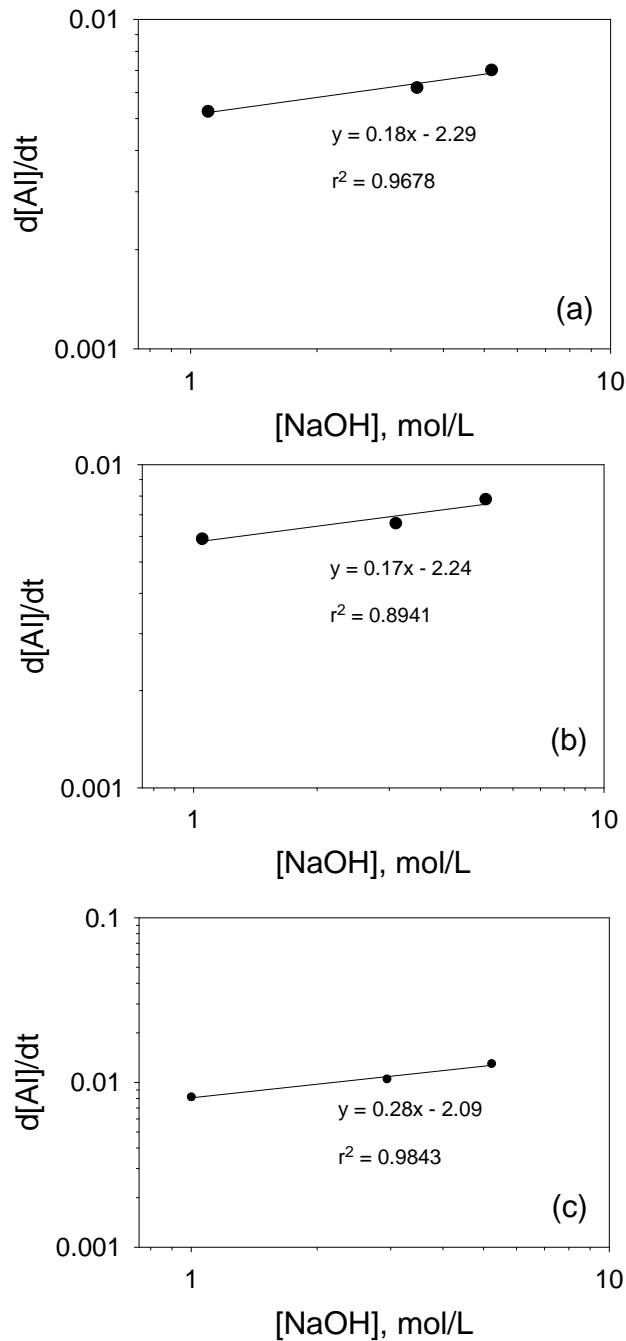


Figure 8.12. Plot of the Initial Al Dissolution Rate Versus the NaOH Concentration During the Leaching of Group 5 Solids at a) 80°C, b) 90°C, and c) 100°C (Group 5 REDOX Sludge Test Material)

(a) Actual waste processing conditions are not expected to necessarily result in a low activation energy for boehmite dissolution since other parameters (such as solids concentration and electrolyte composition) not tested in this study may affect it.

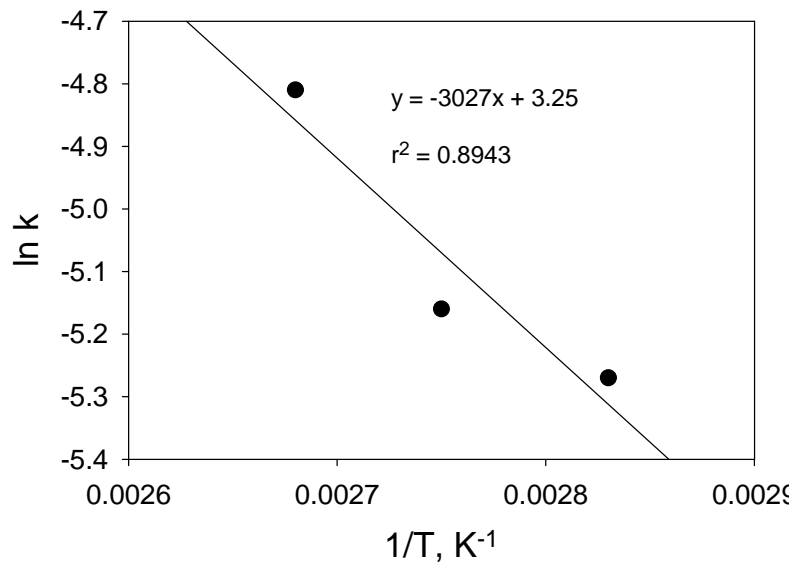


Figure 8.13. Traditional Arrhenius Plot of the Boehmite Dissolution Rate Constant Versus 1/T (Group 5 REDOX Sludge Test Material)

Scotford and Glastonbury (1971) suggested a slightly different approach to applying the Arrhenius equation. They argue that Equation 8.3 suggests that the initial rate and the rate constant are directly proportional at a given hydroxide concentration. It follows that Equation 8.4 can be rewritten as:

$$\ln\left[\frac{d(\text{Al})}{dt}\right] = \ln(A) - \left(\frac{\Delta E_a}{R}\right)\left(\frac{1}{T}\right) \quad (8.5)$$

The construction of the Arrhenius plots presented in Figure 8.14 was based on Equation 8.5 at the three different hydroxide concentrations examined. When analyzed in this manner, the data indicated that the apparent activation energy was dependent upon the hydroxide ion concentration (Figure 8.15). It was not clear why the apparent activation energy would be lower at lower hydroxide ion concentration. Nevertheless, the apparent activation energy was still 4 to 5 times less than that reported by Scotford and Glastonbury, indicating that mass transport is the dominant factor in the rate of boehmite dissolution from the Group 5 solids under the experimental conditions used here.

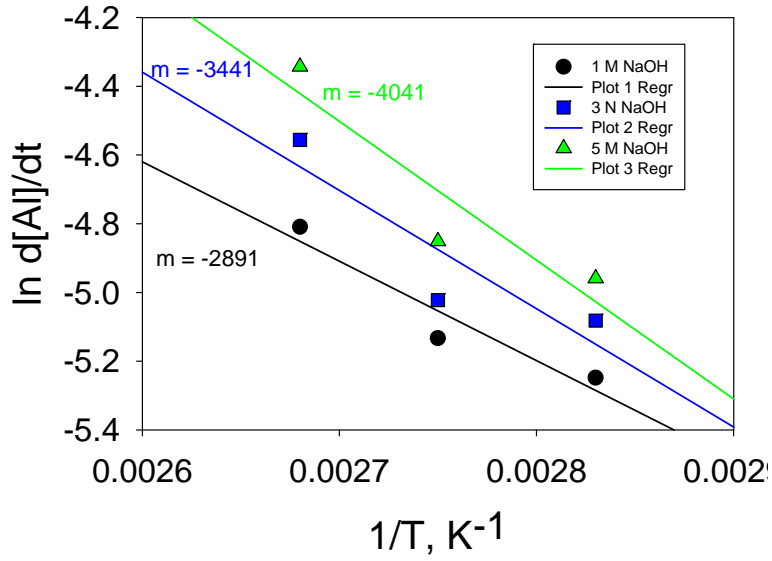


Figure 8.14. Modified Arrhenius Plot of the Boehmite Dissolution Rate Versus $1/T$, Based on Equation 8.5 (Group 5 REDOX Sludge Test Material)

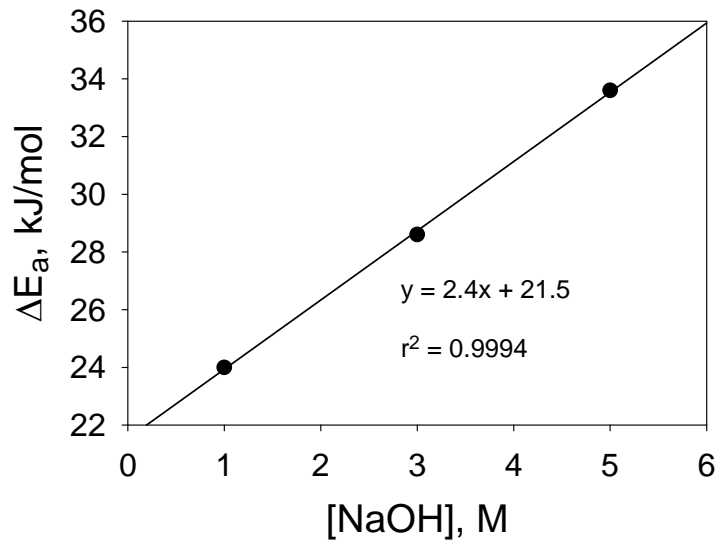


Figure 8.15. Dependence of the Boehmite Dissolution Apparent Activation Energy on the NaOH Concentration (Group 5 REDOX Sludge Test Material)

8.4 Effect of Sodium on Aluminum Dissolution

The effect sodium on the Al dissolution behavior was assessed by increasing the NaNO₃ concentration during leaching of the Group 5 solids in 3 M NaOH at 90°C. The total Na concentrations were increased to 4 M by adding 1 M NaNO₃ and to 8 M by adding 5 M NaNO₃. Figure 8.16 summarizes the results. In the figure, average values are given for the triplicate test conducted 3 M Na (i.e., no added NaNO₃); the error bars represent the standard deviation of the triplicates results. The data suggest a minor effect of sodium nitrate concentration on the Al dissolution behavior from the washed Group 5 solids during leaching with 3 M NaOH at 90°C. The relative rate of Al dissolution is generally greater with an increased concentration of NaNO₃. This should be viewed as strictly an empirical observation. More detailed thermodynamic and kinetic investigations would be required to fully understand the origin of this effect. Other sodium salts potentially present in actual waste leaching mixtures in the WTP might exert different effects.

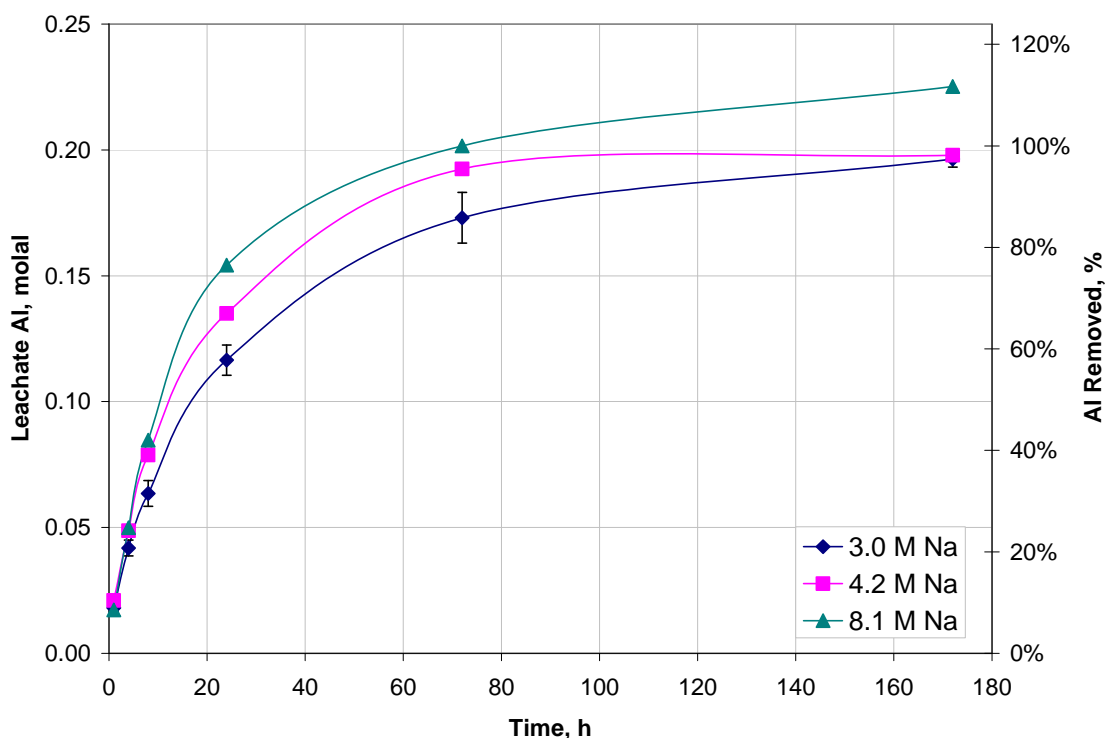


Figure 8.16. Matrix Effect of Na Concentration on Al (Boehmite) Dissolution (Group 5 REDOX Sludge)
Conditions: 3 M free hydroxide at 90°C

8.5 Chromium Leaching Behavior and Speciation

The Cr concentrations in solution were determined opportunistically with the Al. Chromium did leach into solution. Selected Cr dissolution curves are shown in Figure 8.17. The Cr concentrations for all samples are provided in Appendix B. The final Cr concentration in solution would be ~24 µg/mL if all Cr dissolved based on a starting composition of 1733 µg/g. Based on the Cr concentration in the combined solids *following* leaching in 3 M NaOH (see Section 8.8), the total Cr in solution would have

been ~20 µg/mL had it all dissolved. Even under the most rigorous leaching conditions, only ~60 wt% of the Cr was removed from the water-insoluble Group 5 solids. This Cr removal result is somewhat lower than was observed previously for sludge from tank S-110, in which up to ~90 wt% of the Cr could be removed by applying extended (1 week) caustic leaching (Lumetta et al. 2001).

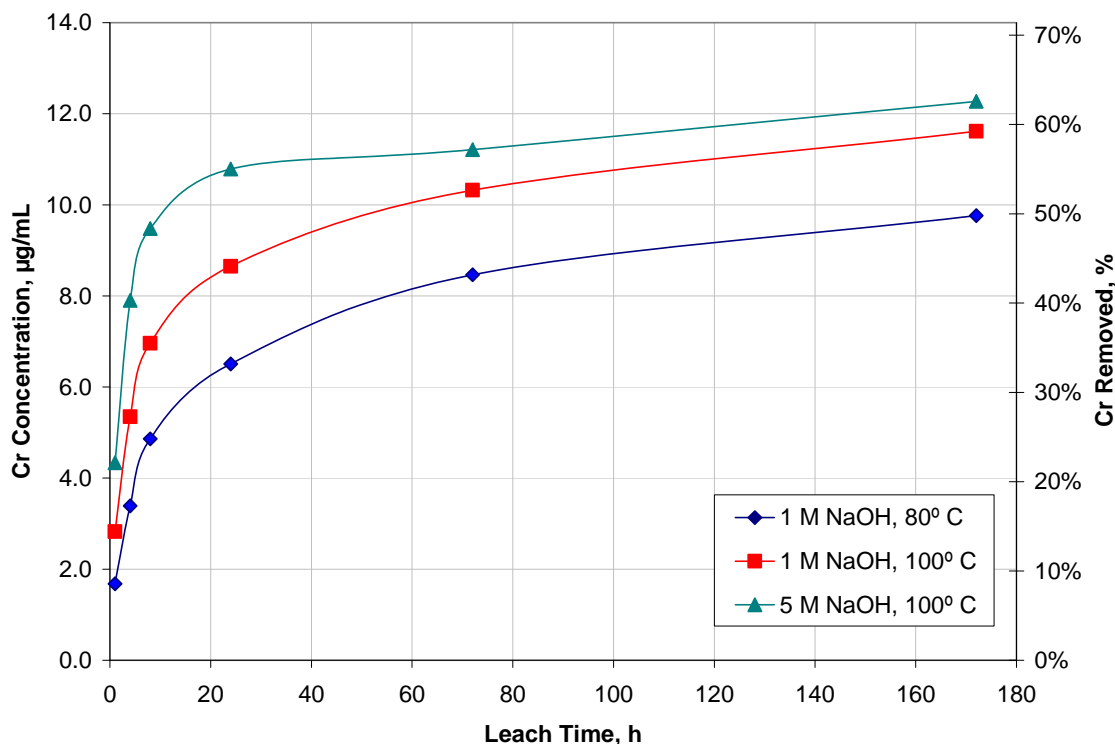


Figure 8.17. Cr Dissolution as a Function of Time and Hydroxide Concentration for Group 5 REDOX Sludge

(Note: the 80°C 170-hr leach datum is presented for indication-only; see Appendix A.)

Table 8.4 shows the CrO_4^{2-} (measured by UV/Vis) and the total Cr concentrations (measured by ICP-OES) at the final equilibrium condition (170-hr leach time). The ratio of Cr(VI)/total Cr is also provided; within the uncertainty of the analytical methods, these concentrations were equivalent. An oxidant was not specifically added to the leach solutions; oxidation of non-chromate species could have been facilitated by oxygen from the air.

The Cr leaching behavior paralleled the Al leaching behavior. The Cr leach rate was reduced with lower leach temperature and lower free-hydroxide concentration. This behavior suggests that a fraction (~60 wt%) of the Cr may be entrained in the boehmite structure. As the boehmite dissolution progressed, the entrained Cr was exposed to the leaching solution and dissolved directly [if the entrained Cr was Cr(VI)] or oxidized to soluble Cr(VI) by adventitious oxygen. Alternatively, it may be that oxidation of Cr(III) by O_2 is dependent upon temperature and $[\text{OH}^-]$ in the same way as Al dissolution. The oxidation of Cr(III) by oxygen gas is also known to increase with increasing NaOH concentration (Fedoseev et al. 2002).

Table 8.4. Comparison of Cr(VI) and Total Cr Concentrations

Nominal Leaching Conditions		Concentration (M)		Cr(VI)/Cr Ratio
Temperature, °C	[NaOH], M	Cr (VI)	Total Cr	
80	1 M	2.30E-04	1.88E-04	1.22
	3 M	2.05E-04	2.22E-04	0.92
	5 M	1.95E-04	2.10E-04	0.93
90	1 M	2.37E-04	2.00E-04	1.19
	3 M, trial a	2.18E-04	2.02E-04	1.08
	3 M, trial b	1.97E-04	2.11E-04	0.93
	3 M, trial c	1.97E-04	2.01E-04	0.98
	3 M, 1 M NaNO ₃	1.94E-04	1.94E-04	1.00
	3 M, 5 M NaNO ₃	1.47E-04	2.00E-04	0.74
	5 M	2.22E-04	2.14E-04	1.04
100	1 M	2.96E-04	2.23E-04	1.33
	3 M	2.41E-04	2.20E-04	1.10
	5 M	2.29E-04	2.36E-04	0.97

8.6 Anions, Phosphorus, Silicon, and Iron Leach Behavior

The concentrations of P and Si were measured opportunistically with Al by ICP-OES. The anionic compositions were also assessed at each sampling period. Anion, P, and Si concentrations in the leachate did not significantly change during the leach testing. The results are summarized in Appendix B.

Iron concentrations were also measured opportunistically by ICP-OES. The Fe concentrations in the leachates were variable. However, they appeared to generally increase relative to the first sampling period at 1 hr ($<5E-5$ M Fe) to the 170-hr sampling period ($\sim 5E-4$ M Fe).

8.7 Assessment of Final Leach Conditions

A summary of the final (170-h) leach solution chemistry and physical parameters is shown in Table 8.5. The final free hydroxide and sodium concentrations were at the targeted values, within the uncertainty of the analytical methods ($\pm 15\%$). The calculated percentage of aluminum that was removed at each leaching condition is also shown. Appendix B summarizes the concentrations of Cr, P, Si, Fe, phosphate, nitrate, and sulfate in the final leach solutions. The GEA results for ⁶⁰Co and ²⁴¹Am were <MDL; the GEA results are also provided in Appendix B.

The tests conducted at 1 M free hydroxide conditions and at 80°C and 90°C were estimated to be at or very near the solubility limits of boehmite (see Section 8.1). The final Al concentrations in the leachates (170-hr sample time) are shown in Figure 8.18 for each hydroxide test condition. The estimated boehmite solubility (Panias et al. 2001) at 3 M free hydroxide and 80°C is 0.45 M, well above the process conditions. The estimated boehmite solubility at 1 M free hydroxide is also shown in Figure 8.18, and its line runs parallel to and just under the line defined by the test conditions at 1 M free hydroxide. The gap between the estimated boehmite solubility and the observed Al concentration in the 1 M free hydroxide

leachate solution at 80°C and 90°C was ~0.013 M Al, consistent with the Al component from gibbsite dissolution.

Table 8.5. Group 5 REDOX Sludge Leaching Final Aqueous Phase Conditions

Temp., °C	Density, g/mL	Free [OH], M	[NO ₃], M	Na, M	[Al], M	Wt % Al Removed	¹³⁷ Cs, μCi/mL
80 ^(a)	1.06	0.97	NA	1.15	0.156	77	0.456
80 ^(a)	1.14	3.30	NA	3.52	0.204	101	0.545
80 ^(a)	1.20	5.06	NA	5.33	0.193	96	0.496
90	1.06	0.91	NA	1.18	0.181	89	0.477
90 trial a	1.13	2.94	NA	3.22	0.198	98	0.453
90 trial b	1.13	2.90	NA	3.21	0.199	98	0.499
90 trial c	1.13	3.02	NA	3.25	0.197	98	0.480
90	1.20	3.13	1.10 ^(b)	4.22	0.189	94	0.328
90	1.30	3.06	5.35 ^(b)	8.46	0.184	91	0.283
90	1.20	5.01	NA	5.16	0.191	94	0.464
100	1.06	0.86	NA	1.11	0.198	98	0.437
100	1.13	2.81	NA	3.22	0.201	100	0.483
100	1.21	5.11	NA	5.58	0.207	103	0.487

(a) For indication-only, see Appendix A.
 (b) Average of six measurements over the entire sampling period.

ASR 7904, 7909, 7913, 7917, 7926
 Reference date for radionuclide: June 7, 2007.
 Analyte uncertainties were typically within ±15% (2-s).

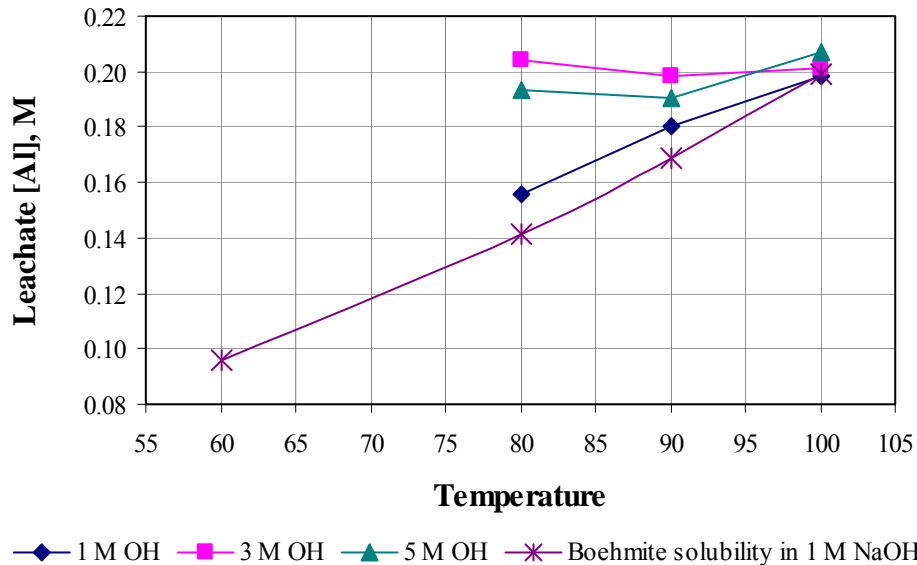


Figure 8.18. Final Al Concentration Versus Temperature, 1, 3, and 5 M Free Hydroxide
 (Note: the 80°C 170-hr leach data are presented for indication-only; see Appendix A.)

8.8 Comparison of Initial and Caustic Leached and Washed Solids Properties

The Group 5 solids that had been caustic leached at 90°C in 3 M NaOH for 170 hrs were combined and washed in preparation for analysis. The wash solution composition and the washed solids chemical, radiochemical, particle size, and crystal habit are discussed.

8.8.1 Leached Solids Wash Solution

The combined volume of wet centrifuged leached solids before washing was ~0.55 mL. The volume was not recorded during the step-wise wash process; however, the final washed wet centrifuged solids volume was ~0.4 mL. Some floating solids were observed after the third wash; the aqueous phase was adjusted to 0.2 M Na to inhibit the float, and the solids were re-centrifuged and the supernatant removed. After the third wash, the wet centrifuged solids mass was 1.13 g.

The densities of the three sequential wash solutions were 1.016g/mL, 1.001 g/mL, and 1.010 g/mL, respectively. The composite wash solution (30 mL volume) density, ICP metals, and anion composition are shown in Table 8.6.

Table 8.6. Solids Wash Solution Composition

Analyte	µg/mL	Analyte	µg/mL	Physical Properties	Value
Al	147	Si	15.0	Density	1.007 g/mL
Cr	[0.394]	nitrate	16.7	TDS ^(a)	0.73 wt%
Na	3610	phosphate	3.5		
P	<4.4	sulfate	2.4		
(a) TDS = total dissolved solids.					

8.8.2 Chemical and Radiochemical Composition

The initial composition of washed solids (before caustic leaching) is provided in Table 8.7 along with selected results from the initial characterization study. The solids from initial characterization had been washed three times, resulting in an estimated 9 wt% salt entrainment from the supernatant phase. The “before leaching” material had been more extensively washed, i.e., no salt entrainment (except for NaOH from the washing liquid) was expected. The two result sets agreed fairly well. The solids composition after leaching in 3 M NaOH at 90°C for 170 hrs and washing is also shown in Table 8.7.

Table 8.7. Group 5 REDOX Sludge Leached Solids Composition and Leach Factors (Dry Mass Basis)

Analyte	Avg. Initial Charac.	Avg. Before Leaching,	Avg. After Leaching,	Observed Leach Factor	BBI Leach factor S-101
	µg/g (ASR 7874)	µg/g (ASR 7926)	µg/g (ASR 7926)		
Al	326,500	388,250	83,675	0.98	0.357
B	[81]	<740	<443	--	
Bi	<70	<694	[1,125]	--	
Cd	<3	<36	<39	--	
Cr	2,110	1,733	9,770	0.54	0.19
Fe	7,265	8,463	73,825	0.29	0.007
Mn	4,500	5,375	62,650	0.06	na
Na	55,200	<55,000	[76,500]	--	
Ni	308	[680]	5,185	0.38	na
P	[675]	<743	<664	--	0.74
S	<300	<3700	[3,921]	--	na
Si	8,760	[15,250]	[17,875]	0.90	0.36
Sr	1,165	1,243	15,125	0.01	
U	19,700	[21,750]	286,750	0	0.02
Zn	[76]	<268	[268]	--	
Zr	[140]	[330]	[1,500]	0.63	
U (KPA)	20,200	26,500	318,000	0.03	
	µCi/g	µCi/g	µCi/g		
⁶⁰ Co	0.0123	0.0232	0.177	0.38	
⁹⁰ Sr	662	719	8,900	0	
¹³⁷ Cs	53.3	39.8	7.63	0.98	
¹⁵⁴ Eu	0.123	<0.03	1.21	--	
¹⁵⁵ Eu	<0.05	<0.1	<0.4	--	
²³⁹⁺²⁴⁰ Pu	0.883	0.898	11.3	0	
²⁴¹ Am	0.290	0.44	3.99	0.26	
total alpha	1.22	1.2	16.7	0	
total beta	1,520	1,300	17,100	0	
Opportunistic	µg/g	µg/g	µg/g		
Ag	<7	<79	<68	--	
As	<100	[1,651]	[1,663]	0.92	
Ba	[105]	<187	[1,525]	--	
Be	<0.4	[16]	<4	0.98	
Ca	1,270	9,100	22,975	0.80	0.03
Ce	<90	<941	<816	--	
Co	<9	<96	<93	--	
Cu	[39]	<453	[618]	--	
Dy	<20	<241	<209	--	
Eu	<7	<77	<67	--	
K	[38]	<168,000	<142,000	--	
La	<10	<50	[153]	--	
Li	<7	<149	[203]	--	

Table 8.7 (Contd)

Analyte	Avg. Initial Charac. $\mu\text{g/g}$ (ASR 7874)	Avg. Before Leaching, $\mu\text{g/g}$ (ASR 7926)	Avg. After Leaching, $\mu\text{g/g}$ (ASR 7926)	Observed Leach Factor	BBI Leach factor S-101
Mg	[245]	<756	[3,400]	--	
Mo	<10	[248]	[275]	0.91	
Nd	<100	<1450	[1,321]	--	
Pb	<40	<420	[1,613]	--	
Pd	<80	[1,884]	<742	0.97	
Rh	<50	<560	<486	--	
Ru	<20	<241	<225	--	
Sb	<80	<797	<691	--	
Se	<100	[1,579]	[1,331]	0.93	
Sn	<100	[1,280]	<1102	0.93	
Ta	<30	<274	<238	--	
Te	<100	<1078	<935	--	
Th	<80	<840	<729	--	
Ti	[32]	<126	[540]	--	
Tl	<90	[1,242]	[1,475]	0.90	
V	<6	<66	<71	--	
W	<40	<461	<371	--	
Y	<9	<92	[188]	--	

Analyte uncertainties were typically within $\pm 15\%$ (2-s); results in brackets indicate that the analyte concentrations were greater than the minimum detection limit (MDL) and less than the estimated quantitation limit (EQL), and uncertainties were $> 15\%$.
 Opportunistic analytes are reported for information only; QC requirements did not apply to these analytes.
 Radionuclide reference date: June 7, 2007 (ASR 7926) and March 1, 2007 (ASR 7874).
 BBI leach factors cited Meacham (2003).

The analysis of the leachate solutions showed that Mn, Sr, and U had not dissolved. The relative concentration factor (CF) of these analytes averaged 12 in the final leached and washed solids, based on the concentration ratio after leaching to before leaching. This term was used to determine the specific analyte leach factors according to Equation 8.6

$$LF = \left(\frac{C_F}{C_I \times 12} \right) \quad (8.6)$$

where LF is the leach factor, C_F is the final analyte concentration, and C_I is the initial analyte concentration.

The calculated leach factors for major and minor constituents are provided with comparison to the BBI leach factors (8-hr leach time) for the primary sludge constituent source: S-101. The Group 5 8-hr Al and Cr leach factors can be estimated from Figure 8.6 and Figure 8.17 to be 0.32 and 0.28, respectively. These were similar to those reported in BBI. Notably, extended (170 hrs) leach times did not mobilize U, Sr, Mn, or Pu to the aqueous phase. Consistent with previous leaching tests with Hanford sludge solids, a significant fraction (98%) of the ^{137}Cs reported to the liquid phase (which would be routed to the LAW

pretreatment facility). The calculated leach factor for ^{241}Am suggests that 26 % of this transuranic radionuclide would also be routed to the LAW facility. However, analysis of the leachate solutions indicated ^{241}Am to be $<2 \times 10^{-4} \mu\text{Ci/mL}$, translating to $< 10\%$ dissolution of ^{241}Am during leaching of the Group 5 solids in 3 M NaOH at 90°C .

As shown in Figure 8.19, approximately 90% of the mass dissolved with a 170-hr leach time. In this case, uranium would be expected to become the limiting component of the glass loading.

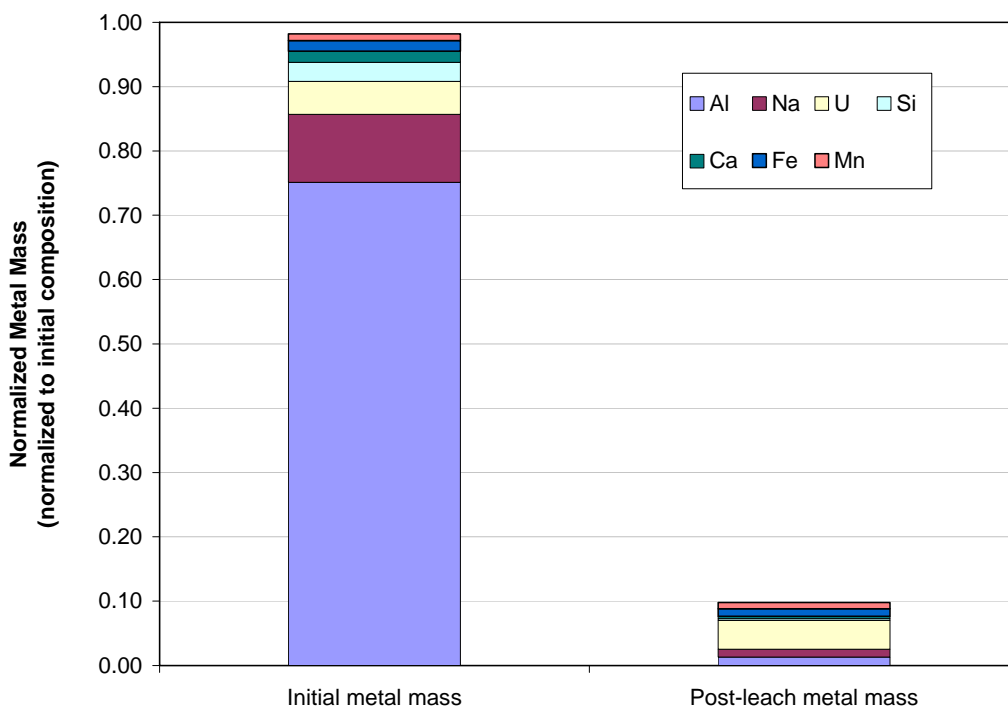


Figure 8.19. Group 5 REDOX Sludge Reduction in Solid Mass with Caustic Leaching

8.8.3 Particle-Size Distribution

Table 8.8 provides a summary of the particle-size measurements for the leached and washed solids (sample ID G5-W-F, analyzed in duplicate). The diameters listed correspond to the 10%, 50%, and 90% volume/weight fractiles [d(10), d(50), and d(90), respectively], and are listed as a function of test conditions.

The measurements indicated d(10)s ranging from 0.9 to 1.6 μm , d(50)s falling between 2.6 and 11.7 μm , and d(90)s spanning 16.5 to 85.9 μm . Neglecting the measurements where entrained bubbles were suspected, the trends with the test condition in the d(10), the d(50), and (with one exception) the d(90) compared well between initial and repeat measurements. In the following paragraphs, the behavior of G5-W-F with respect to sonication and pump speed setting is discussed. For brevity, the discussion will primarily focus on the initial measurement. Toward the end of the discussion, both measurements are compared as a rough measure of result reproducibility.

Table 8.8. Group 5 REDOX Sludge Caustic Leached Sample Particle-Size Analysis Summary

Sample	Pump Speed	Sonication %	d(10) [μm]	d(50) [μm]	d(90) [μm]
G5-W-F Measurement 1/2	3000	0	0.94	2.6	16
	2000	0	1.6	6.4	27
	4000	0	1.2	3.8	30
	3000	25	1.0	8.5	38
	3000	50	1.0	11	52
	3000	75	1.0	12	48
	3000	0	1.1	11	41
	2000	0	1.3	11	43
	4000	0	0.91	5.8	34
G5-W-F Measurement 2/2 (replicate measurement)	3000	0	0.87	3.3	28
	2000	0	1.3	6.3	32
	4000	0	0.90	4.9	48
	3000	25	0.85	5.5	31
	3000	50	0.90	9.3	86
	3000	75	0.91	9.5	68
	3000 ^(a)	0	1.3 ^(a)	10 ^(a)	77 ^(a)
	2000 ^(a)	0	1.7 ^(a)	9.6 ^(a)	79 ^(a)
	4000 ^(a)	0	1.0 ^(a)	7.6 ^(a)	68 ^(a)

(a) Measurement suspected of being altered by bubbles in the flow cell.

The influence of flow rate on the measured distribution was difficult to evaluate when expressed as diameters corresponding to specific cumulative undersize fractions (as above). Lowering of the initial pump speed from 3000 RPM to 2000 RPM increased the apparent size of suspended particles. It is suggested that 1) the particles making up the fine fraction of the distribution were denser than the large fraction, 2) the coarse fractions were loose, low-bulk density flocs that were easily formed at low pump speeds and sheared apart at the higher rates, or 3) a combination of 1) and 2). Out of these explanations, 2) is the most likely. A pump setting of 4000 RPM also exhibited an increased d(10), d(50), and d(90) over 3000 RPM, but the increase was not as dramatic as observed in the 3000 to 2000 RPM transition. The increase observed at 4000 RPM could have been caused by suspension of large dense particles. Based on these observations, a pre-sonication suspension behavior for leached Group 5 can be postulated. At low pump speeds (i.e., 2000 RPM), low-density primary particles and loose particle aggregates constituted the majority of material suspended in the measurement cell. At 3000 RPM, the pump shears apart the loose particle aggregates and may suspend dense, small particles in the waste solids (but not larger particles). At 4000 RPM, the pump was able to suspend dense large particles.

The size range of particles suspended by the pump action can be evaluated by examining the PSD distributions for pre-sonication measurements (shown in Figure 8.20). At 2000 RPM, the size distribution was roughly bimodal with equal population peaks at 3 and 15 μm. The low-pump-setting distribution had small shoulders spanning 0.2 to 0.8 μm and 60 to 200 μm. The upper and lower peaks could have corresponded to primary particles and particle aggregates, respectively. It was also possible that the 100-μm fraction could be caused by bubbles in the flow cell. When the pump speed setting was increased to 3000 RPM, the distribution became dominated by a high population of 2-μm particles. The portion of the distribution ranging from 6 to 200 μm was reduced relative to 2000 RPM. This suggested that the

2- μm peak corresponded to very dense particles that were suspended at 3000 RPM but not at 2000 RPM or to particles created by the shearing apart of larger aggregates with the increased pump speed. Further increase of the pump speed to 4000 RPM increased the 6- to 200- μm fraction of particles relative to 3000 RPM; a corresponding reduction in the 2- μm peak was also observed. Both these observations were consistent with the suspension of larger (perhaps dense) particles or particle aggregates at 4000 RPM. Because the entrainment of air into the system became a problem at 4000 RPM, higher pump settings were not attempted to determine if further alteration of the size distribution occurred.

The application of sonic energy to the suspension appeared to substantially increase the size of material suspended in the flow cell. Indeed, the $d(50)$ and $d(90)$ for 3000 RPM increased by a factor of 3 to 4 between 0% and 75% sonication power. A corresponding increase in the $d(10)$ was not observed, suggesting that the smallest particles were not influenced by sonication. The PSDs corresponding to “before sonication,” “during sonication,” and “after sonication” measurement states are shown in Figure 8.21. Consistent with the initial characterization samples, the application of sonic energy lowered the population of 2- μm particles/aggregates while increasing the population of 10- to 20- μm particles. This behavior was consistent with sonication-induced aggregation and/or aggregate restructuring. Specifically, it appears that the application of sonic energy promoted particle contact and provided sufficient energy to overcome any barriers to aggregation (such as coulombic repulsion of like-charged particles). Based on a slight shift of the center of the 10- μm shoulder before sonication to 15 μm after sonication, it appears that sonication causes the 2- to 3- μm particles to attach to existing 10- to 20- μm particles. When sonic energy was removed, the new state of aggregate appeared to be stable or pseudo-stable, as the 2- μm peak was not reformed during the course of the after-sonication measurement.

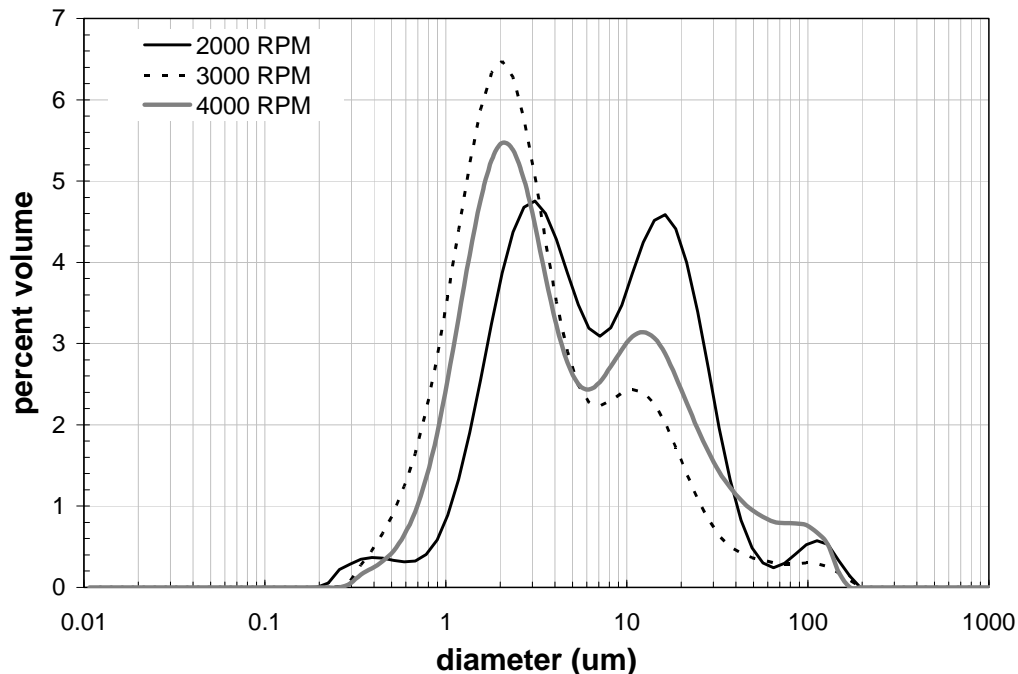


Figure 8.20. Leached Group 5 REDOX Sludge PSD (G5-W-F) as a Function of Pump Speed Before Dispersion Sonication

Post-sonication pump-speed studies provided insight into how sonication altered the total distribution of particles (Figure 8.22). Both the percent of undersize diameters reported in Table 8.8 and the size distribution indicated little difference between post-sonication measurements made at 2000 and 3000 RPM. This could suggest that a significant fraction of the $\sim 2\text{-}\mu\text{m}$ particles previously suspended at 3000 RPM had been incorporated into a larger, but lower, bulk density, aggregate/floc that could be suspended at 2000 RPM. The reappearance of a strong shoulder at $2\ \mu\text{m}$ suggests 1) the suspension of very dense particles or 2) the breakdown of the 10- to $20\text{-}\mu\text{m}$ restructured aggregates under shear. It should be noted that the slight shift of the peak of the population that centered at $15\ \mu\text{m}$ down to $10\ \mu\text{m}$ would be consistent with option 2). That is, it appears that small 2- to $3\text{-}\mu\text{m}$ particles are being sheared off larger $15\text{-}\mu\text{m}$ aggregates. The loss of material reduces the size of the $15\text{-}\mu\text{m}$ aggregates down to $10\text{-}\mu\text{m}$ aggregates (or particles).

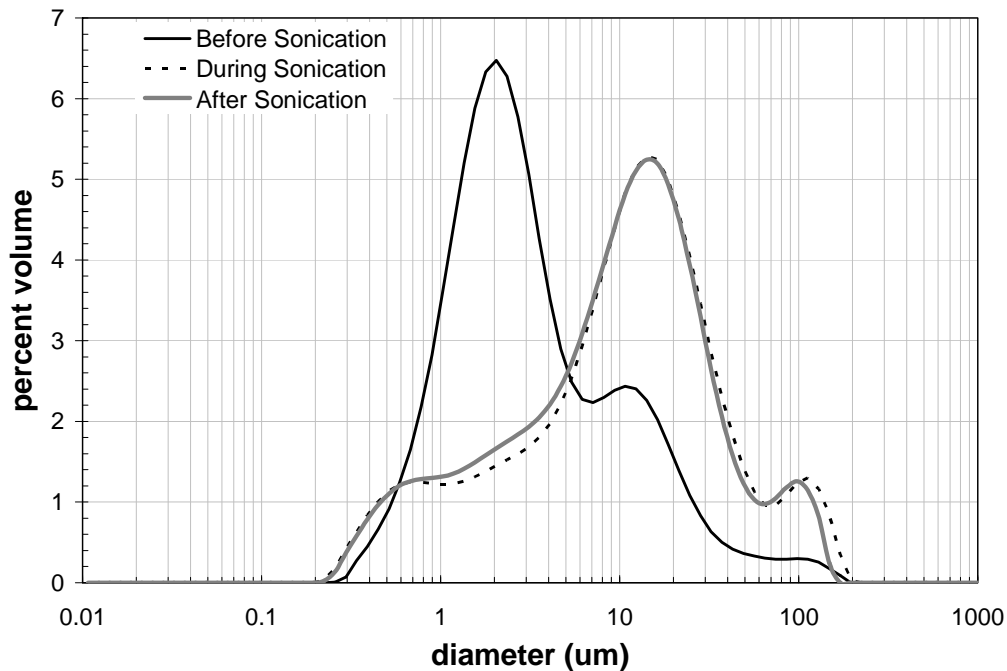


Figure 8.21. Leached Group 5 REDOX Sludge PSD (G5-W-F) as a Function of Applied Sonication

Note: The before-sonication measurement state corresponded to 3000 RPM and 0% sonic power. The during-sonication measurement state corresponded to 3000 RPM and 75% sonic power. The after-sonication measurement state corresponded to 3000 RPM and 0% sonication.

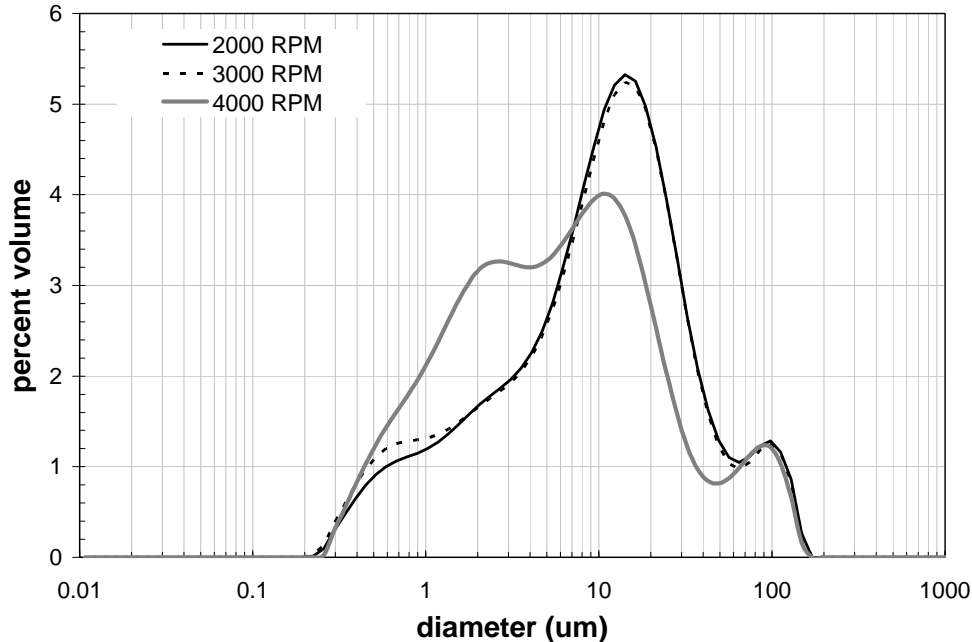


Figure 8.22. Leached Group 5 REDOX Sludge PSD (G5-W-F Measurement 1/2) as a Function of Pump Speed After Dispersion Sonication

Figure 8.23 is a plot of the PSD for the duplicate measurement as a function of sonication. PSDs for the duplicate “before sonication” measurement states compared well. Specifically, distributions for both initial and replicate measurements showed a strong peak at $\sim 2 \mu\text{m}$, a shoulder at 8 to 10 μm , and a gradual decay to zero from 10 to 200 μm . The main difference between pre-sonication measurements was that the shoulder and trailing edges were more pronounced in the replicate. “During sonication” measurements also compared well: a broad distribution of particles from 0.2 to 4 μm led up to a large population peak at 10 to 20 μm . Both during-sonication distributions showed a smaller population peak at 100 μm . In contrast, post-sonication distributions for initial and replicate measurements did not compare well. The “after sonication” replicate showed a much larger peak (nearly equivalent in fractional contribution to the primary 10- to 20- μm peak) as well as a reversal of the aggregate formation. The 100- μm peak was suspected to result from air entrainment into the system as it was similar in magnitude to the 100- μm peak observed in test condition 3 on the first sample measurement. Post-sonication distributions for both initial and replicate samples should be approached with caution because the presence of bubbles in the post-sonication replicate measurements was not confirmed by resetting the pump. Additionally, all G5-W-F measurements showed a peak centered near 100 μm , and it is possible that these peaks resulted from a small amount of entrained air in the flow cell.

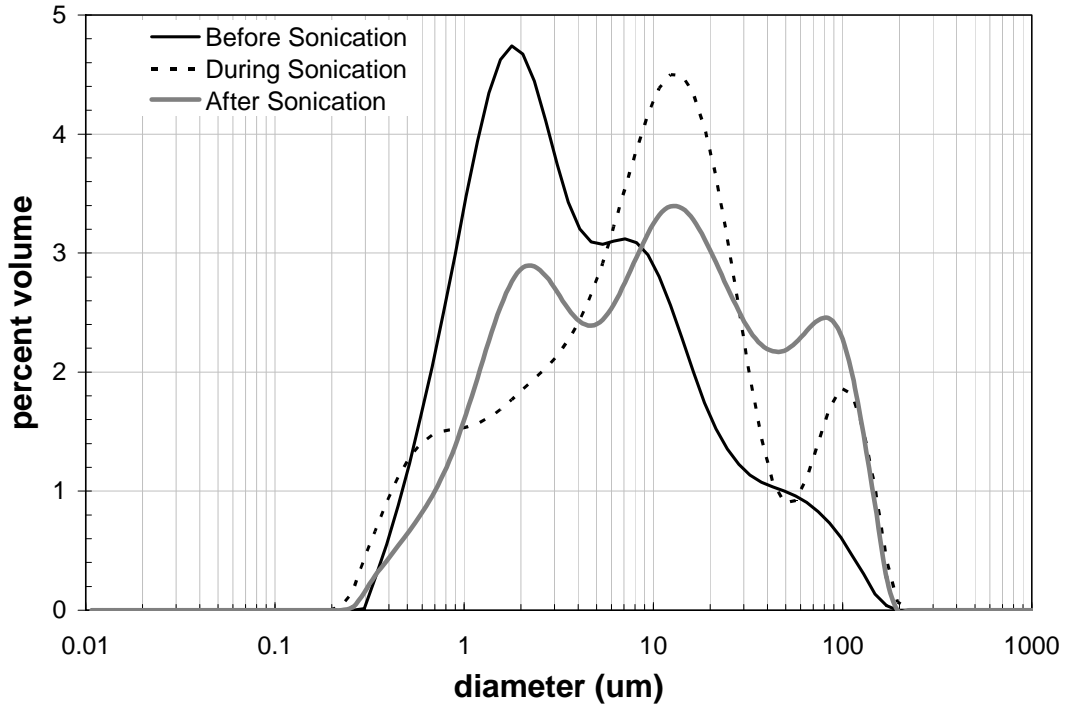


Figure 8.23. Leached Group 5 REDOX Sludge PSD (G5-W-F Measurement 2/2) as a Function of Applied Sonication

Note: The before-sonication measurement state corresponded to 3000 RPM and 0% sonic power. The during-sonication measurement state corresponded to 3000 RPM and 75% sonic power. The after-sonication measurement state corresponded to 3000 RPM and 0% sonication. Air entrainment in the flow cell was suspected for the post-sonication measurement.

The influence of caustic leaching on the PSD for Group 5 samples can be determined by comparing the results of the initial characterization samples (see Chapter 5) to those of the parametric testing sample. Figure 8.24 shows the pre-sonication PSD measured at 3000 RPM before and after caustic leaching. Pre-sonication measurements were selected as they are the most directly comparable with respect to flow history in the particle-size analyzer. Caustic leaching of Group 5 wastes increased the relative population of 1- to 3- μm particles and reduced the relative population of 4- to 20- μm particles. The increase in magnitude of the peak centered at 2 μm may result from size reduction and/or removal of larger particles or may represent the solids insoluble with respect to caustic leaching. The post caustic-leaching PSD also showed an increased fraction of 20- to 200- μm structures. These are most probably particle aggregates that formed as a result of sample instability after caustic leaching.

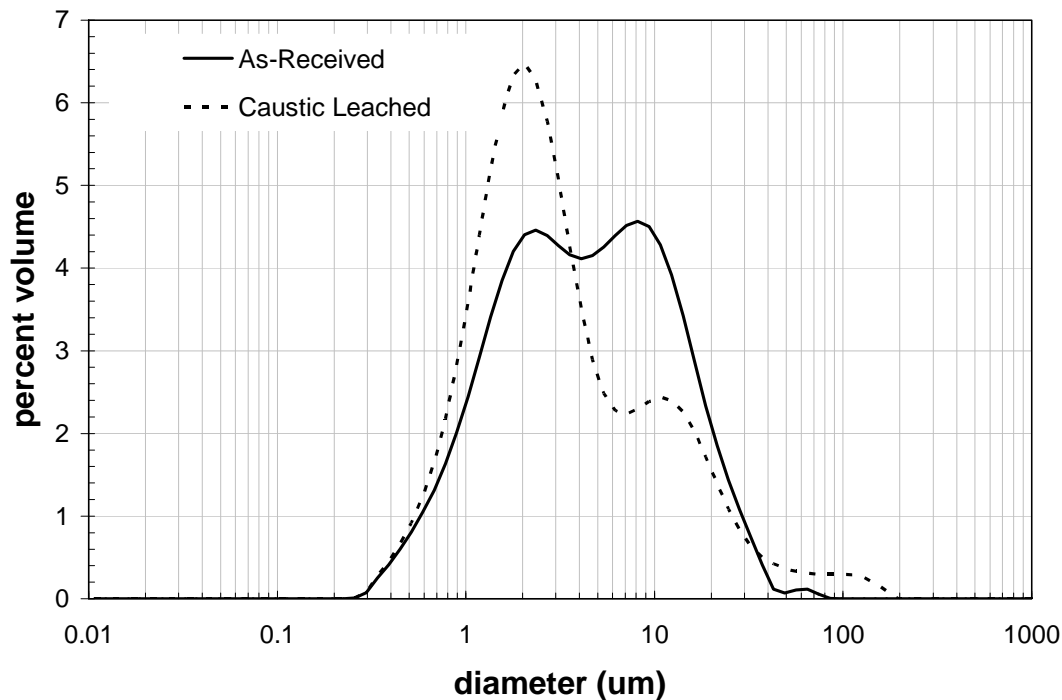


Figure 8.24. Effect of Caustic Leaching on the Measured PSD for Group 5, REDOX Sludge. The pre-leach PSD corresponds to sample TI473-G5-S-WL-PSD-1 (see Section 5); the post-leach PSD corresponds to sample G5-W-H (see Section 8). Both samples were measured before sonication at a pump speed of 3000 RPM.

8.8.4 Crystal Form and Habit

The following sections summarize the mineral-phase evaluation of the leached and washed solids.

8.8.4.1 XRD

The XRD pattern of the leached and washed solids (sample ID G5-W-E) is provided in Figure 8.25a; the background-subtracted XRD pattern with stick-figure phase identification is shown in Figure 8.25b.

The major crystalline phase identified in this sample was clarkeite, $\text{Na}[(\text{UO}_2)\text{O}(\text{OH})]$. The clarkeite XRD pattern is very similar to that of sodium uranium oxide [$\text{Na}_2\text{U}_2\text{O}_7$], but the clarkeite pattern resulted in a slightly better fit to the data. The presence of boehmite was strongly suspected but could not be confirmed. The boehmite major peak was indicated in the 15-degree peak by the non-symmetrical low-angle side of the peak. Most of the remaining boehmite peaks were either masked by other phases or at such low intensity that they could not be identified. The clarkeite phase has a much higher RIR than boehmite, so the boehmite contribution was not readily apparent. A very low intensity signal (only 2 lines observable) could be strontium manganese oxide hydrate, $\text{Sr}_2\text{Mn}_{14}\text{O}_{27}\cdot x\text{H}_2\text{O}$. Due to the very low peak intensity and the lack of sufficient confirming lines, the identification of this phase must be regarded as tentative. The presence of Fe_2O_3 was examined, but the characteristic peaks are overlapped by rutile, clarkeite, or boehmite. The pattern for this sample indicated that the material was mostly amorphous.

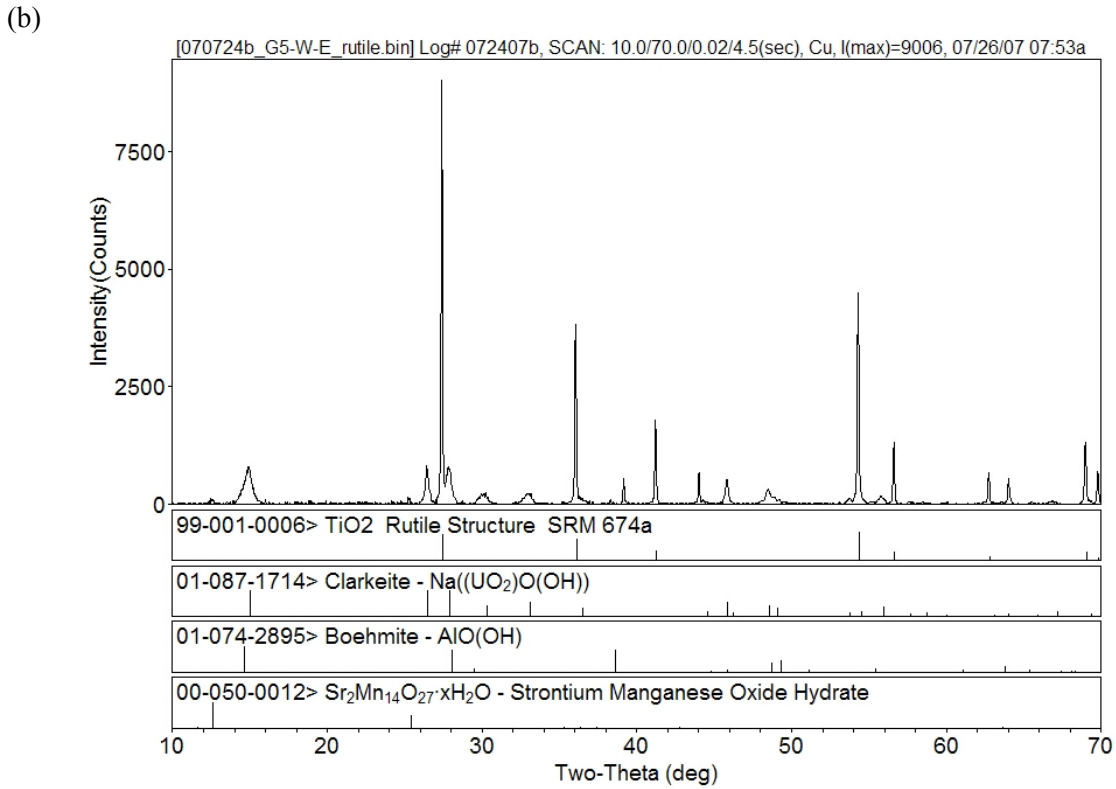
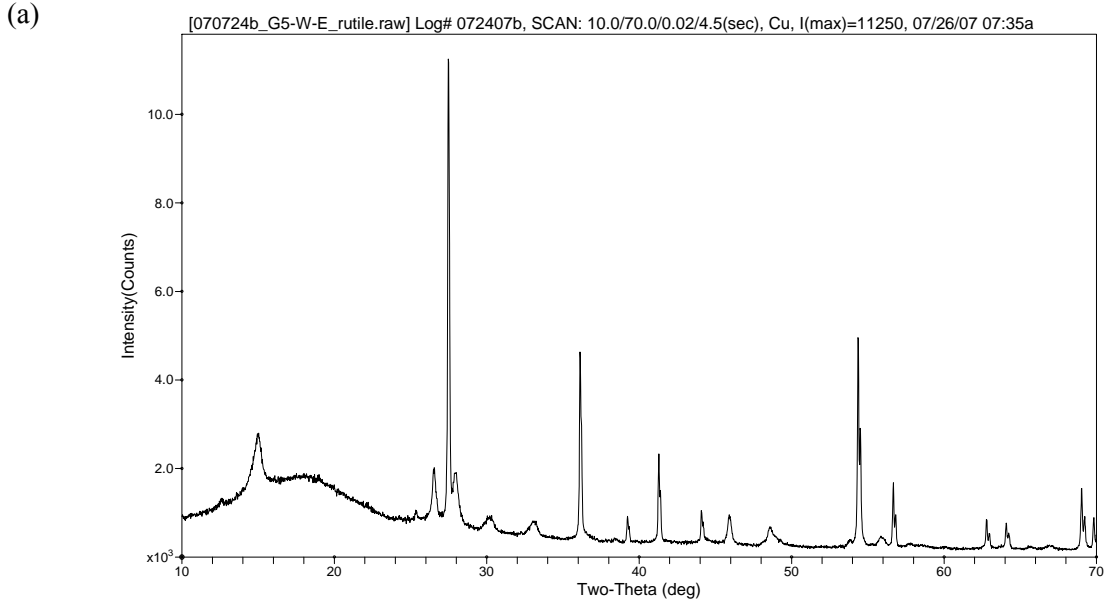


Figure 8.25. XRD Pattern of Caustic Leached Group 5 REDOX Sludge with Rutile (TiO₂) Internal Standard (a) Raw Data and (b) Background-Subtracted with Stick-Figure Peak Identification

The crystallite sizes were estimated to be 265 Å for clarkeite and 200 Å for boehmite based on the application of a simplistic crystallite size evaluation.^(a)

The best estimate of the phase identification and fractionation is summarized in Table 8.9. The mass fraction and phase identification were based on the XRD phase identification, relative intensity ratios, and chemical analysis. Clarkeite, boehmite, and strontium manganese oxide hydrate were observed; the presence of prototypic NaSiAlO₄ is proposed based on the presence of Si and tank waste chemistry.

Table 8.9. Estimated Weight Percent of Mineral Phases in the Caustic-Leached and Washed Group 5 REDOX Sludge Solids

Crystalline Phase	Chemical Structure	Weight %	Basis ^(a)
Clarkeite	Na((UO ₂)O(OH)) ^(b)	39	Observed
Boehmite	AlO(OH)	15	Observed
Strontium manganese oxide hydrate	Sr ₂ Mn ₁₄ O ₂₇ ·xH ₂ O	12	Observed
Sodium silicoaluminate (prototypic and bounding based on [Si])	NaSiAlO ₄	9	Attribution
Unknown or amorphous Fe, Cr, Ni, Ca, S	Fe, Cr, Ni, Ca, S	6.9	Chem analysis
Unidentified Na compounds	Na	3.4	Chem analysis
Assumed counter ions	oxides, hydroxides, waters of hydration, etc.	14	Balance
Sum		100	
<p>(a) <i>Observed</i> indicates that the characteristic crystal diffraction pattern of the identified crystalline phase was observed in the sample XRD pattern. <i>Attribution</i> indicates that the characteristic crystal diffraction pattern of the identified crystalline phase was not observed in the sample XRD pattern, and its listing is based on assumptions about tank waste chemistry and chemical analysis; therefore, the estimated phase assignment should be considered with caution.</p> <p>(b) The clarkeite diffraction pattern is similar to that of Na₂U₂O₇; clarkeite had the better spectral match.</p>			

For comparison, the as-received Group 5 solids XRD pattern is reproduced in Figure 8.26. Specifically, gibbsite, quartz, and iron oxide phase identifications were missing from the leached solids XRD pattern. Boehmite was significantly reduced (from ~75 wt% fraction to ~15 wt% fraction).

(a) The Jade operating software applied the Scherrer equation to estimate the crystallite size (Klug and Alexander 1974, pp. 687–690).

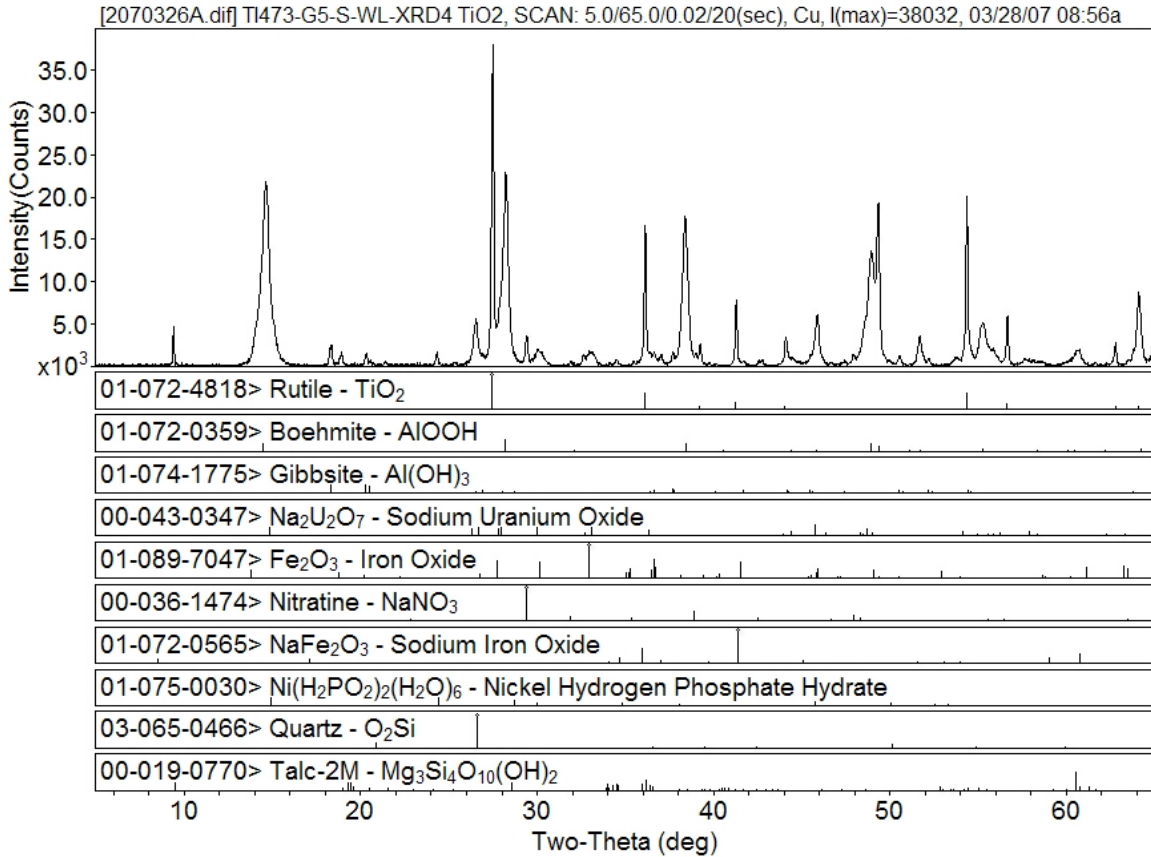


Figure 8.26. Group 5 REDOX Sludge Initial Characterization XRD Pattern

8.8.4.2 SEM and TEM

Figure 8.27 provides an SEM-EDS map of selected elements in the leached and washed solids. U dominated the composition, consistent with the chemical analysis. The Cr and Mn components did not appear to be associated with any particular phase as they appeared to be well dispersed. The Na and Si appeared to be related in structure, consistent with NaSiAlO₄. Note that Fe was dispersed with concentrates in selected areas.

Several SEM images of the washed solids are shown in Figure 8.28. The particles are generally small (< 1 micron) on a side. There appeared to be a large population of plate-like structures, consistent with boehmite.

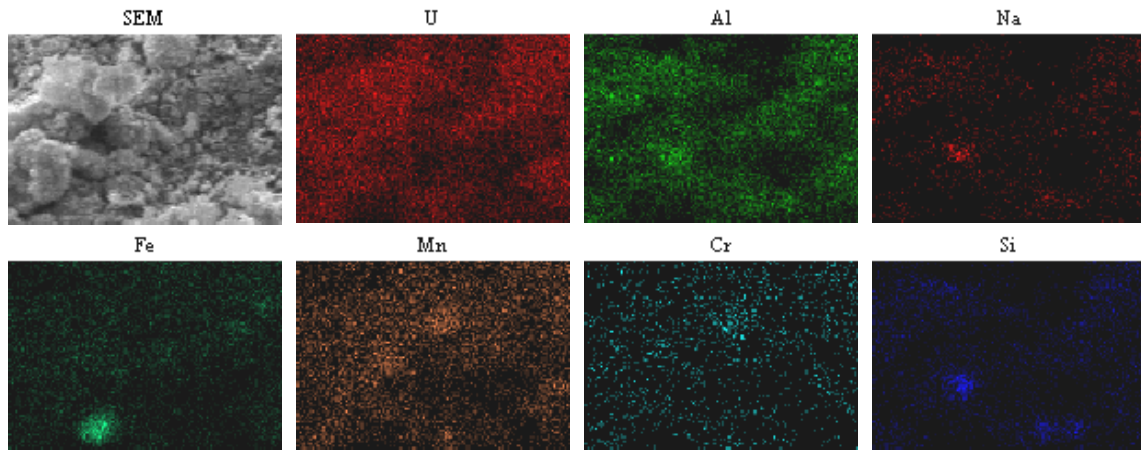


Figure 8.27. SEM-EDS Image of Group 5 REDOX Sludge Leached and Washed Solids with U, Al, Na, Fe, Mn, Cr, and Si Maps

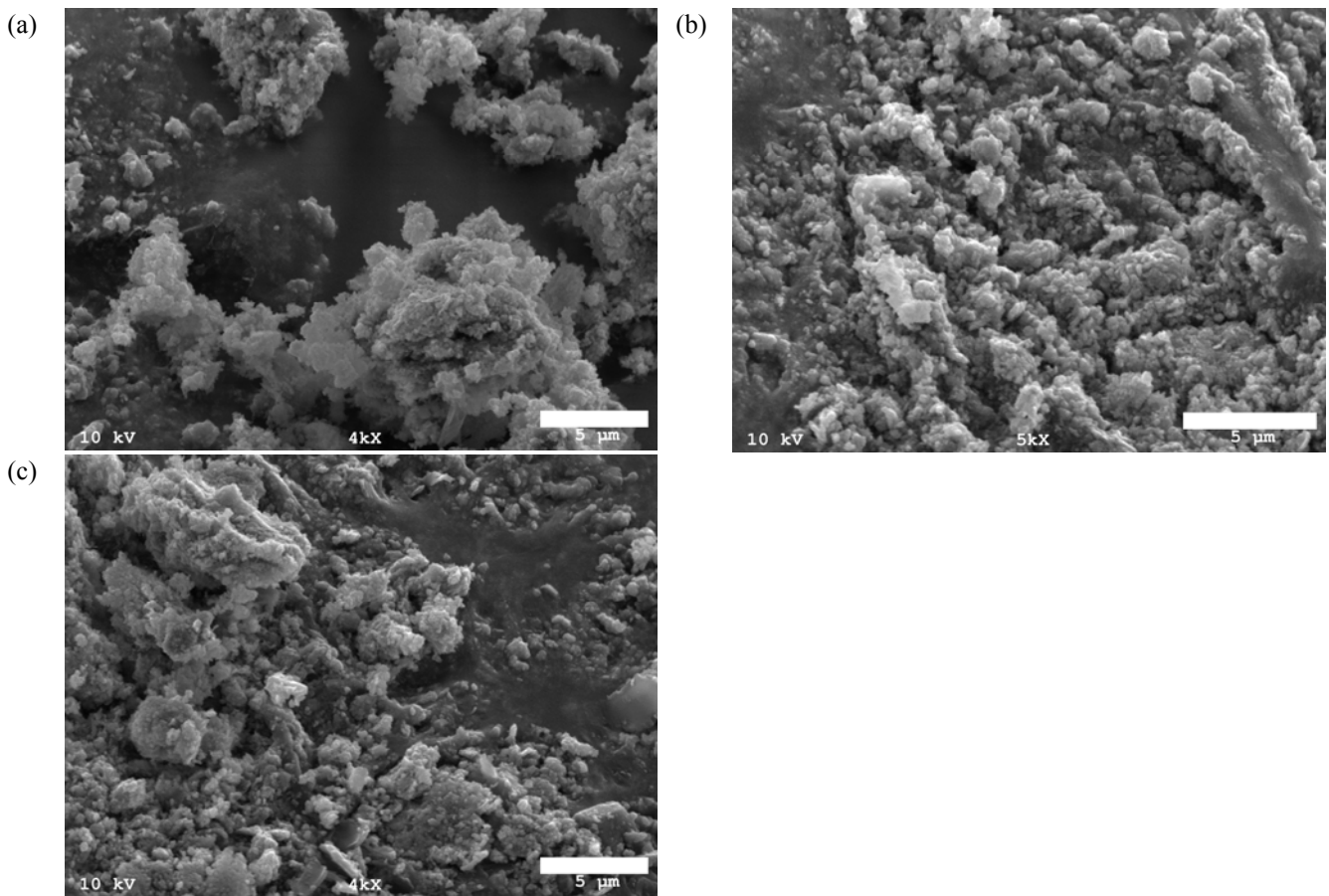


Figure 8.28. SEM Images of Group 5 REDOX Sludge Caustic Leached and Washed (a) 10 kV, 4kx; (b) 10 kV, 5kx; (c) 10 kV, 4 kx

Figure 8.29 shows TEM images of particles in the G5-IW sample (as-received following more extensive washing) that exhibit the characteristic rhombohedral shape for boehmite. The particles are lying on the lacey-carbon support grid. Other round and elongated particles are also visible. The TEM contrast demonstrates that the particles are crystalline.

The TEM images of the boehmite particles were used to estimate the size range of the particles. Using multiple images, measurements were made along the diagonals of the particles. These measurements were then listed and ordered. The data were fit to a \log_e -normal distribution. Many particle and colloid populations exhibit log-normal PSDs. Figure 8.30 is a cumulative number distribution function that describes the probability of particle sizes from the TEM images. The mathematical fit represents a log-normal distribution. The geometric mean was determined to be 82 nm. (The number distribution from the PSD measurement of the characterization sample ranged from 0.2 to 1.1 μm .)

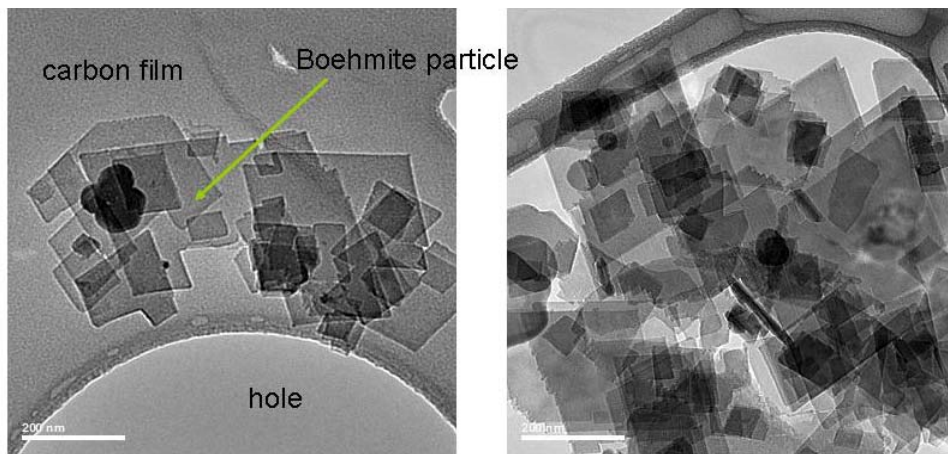


Figure 8.29. Transmission Electron Microscopy Images of Boehmite Particles in Group 5 REDOX Sludge Solids Before Caustic Leach

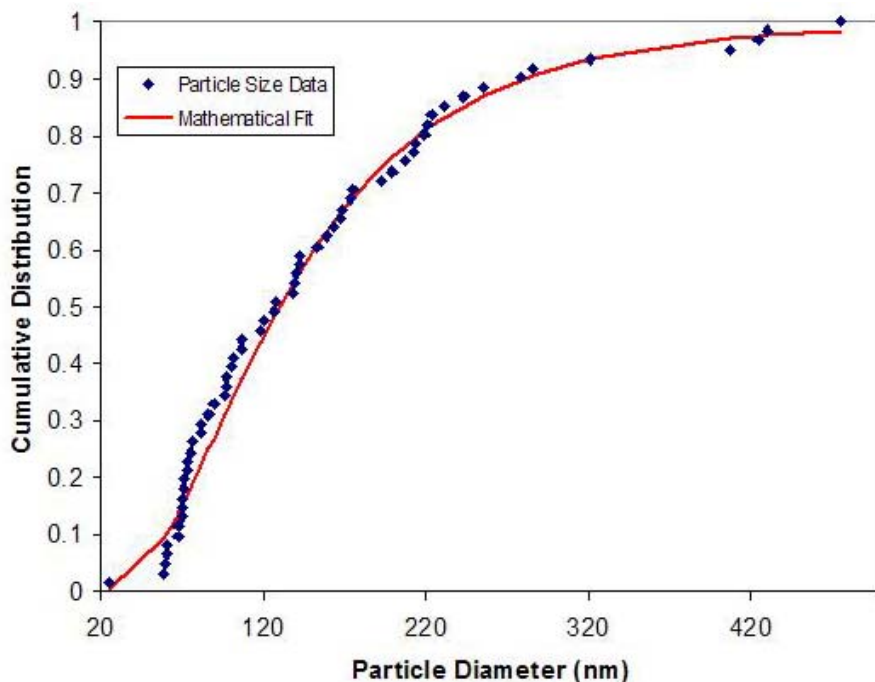


Figure 8.30. Cumulative Distribution Plot of Group 5 REDOX Sludge Boehmite Particle Sizes Before Caustic Leach and a Mathematical Fit to the Data

The acicular or needle-like uranium particles in G5-IW can be seen in Figure 8.31. The figure shows an inverted contrast STEM image (Figure 8.31a) and a normal contrast image (Figure 8.31b) where brightness reflects high Z containing solids. X-ray energy dispersive analysis of the acicular particles is shown in Figure 8.32. The large Al signal was due to the presence of the ubiquitous aluminum oxide phases in the sample.

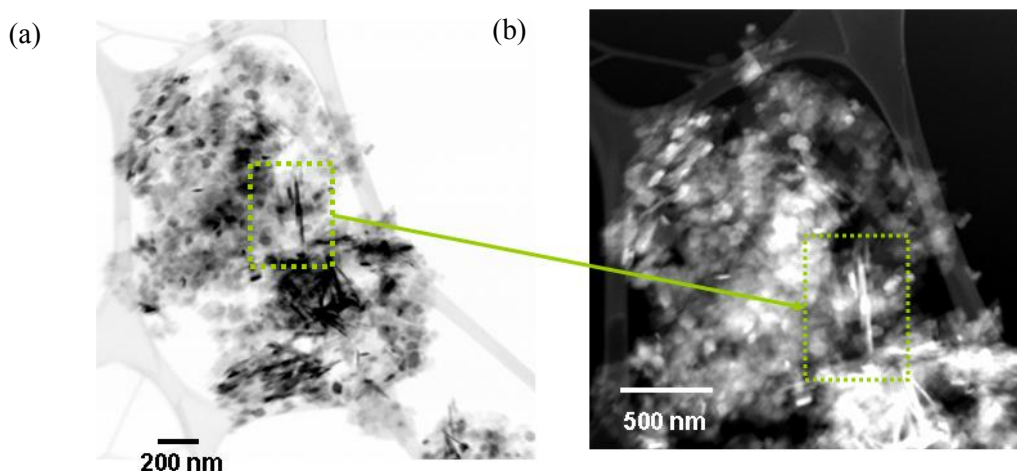


Figure 8.31. STEM Images of Particles in Group 5, REDOX Sludge Sample Before Caustic Leach (G5-IW) Showing Needle-Like Phases

(a) Inverted contrast where high atomic solids are black and (b) normal STEM-HAADF image.

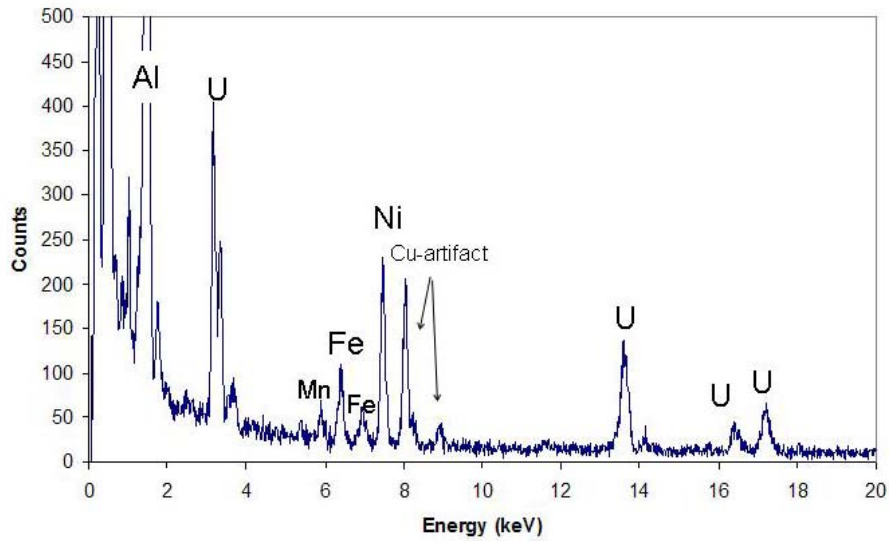


Figure 8.32. EDS Analysis of Elongated Particles in Group 5, REDOX Sludge Sample Before Caustic Leach (G5-IW)

Figure 8.33 shows TEM images of the solids remaining after caustic leach and washing (sample G5-W-B).

For the caustic-leached Group 5 solids, a higher density of uranium particles was evident based on the larger relative density of needle-like structures in Figure 8.33. Boehmite crystals were also still observable in the sample after leaching. Lower-magnification STEM images show the high surface area and fine structure of the agglomerates in sample G5-W-B (Figure 8.34).

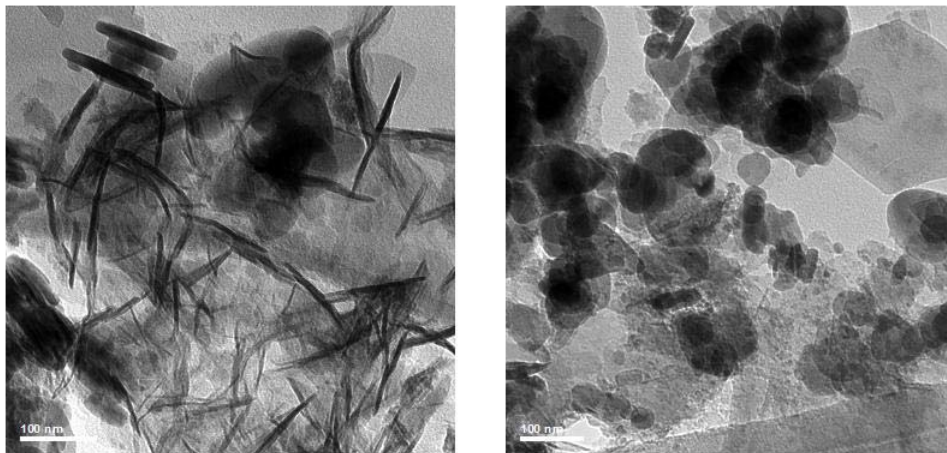


Figure 8.33. High-Magnification Images of Group 5 REDOX Sludge Solids Post-Leaching (G5-W-B) Showing Elongated Uranium Phases and Spherical Particles

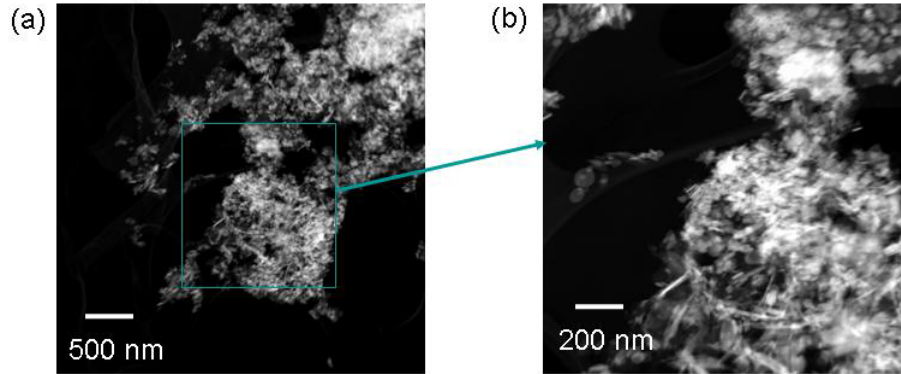


Figure 8.34. STEM Images of Group 5, REDOX Sludge Solids Post-Leaching (G5-W-B1)

Compositional analyses of high Z particles (those with high nuclear mass) in G5-W-B are shown in Figure 8.35. The EDS analysis indicated the presence of U, Mn, Cr, Ni, and a small amount of Sr. The detection of Sr in these particles is significant as it has not been observed in similar uranium crystals in tank waste previously. XRD analyses indicated the presence of a strontium manganese phase.

Determining whether the U and Mn were present in the same phases was not absolutely clear from the TEM-EDS analyses. In the bright-field TEM images, both phases exhibited high contrast (see Figure 8.36). By using energy-filtered imaging, it was possible to demonstrate that the uranium phase was discrete and separated from the Mn phases in the sample. The energy-filtered TEM images are shown in Figure 8.37.

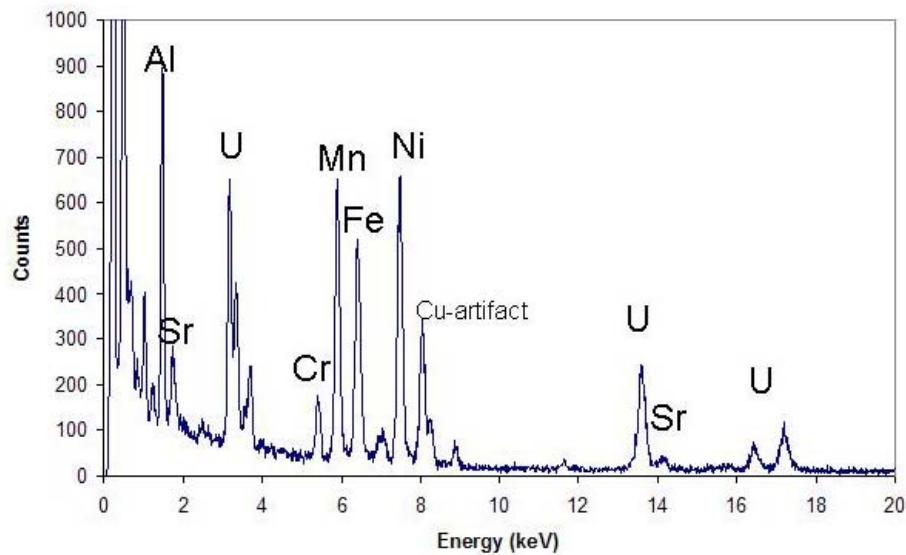


Figure 8.35. EDS Analysis of Uranium and Mn-Ni Phases in Group 5, REDOX Sludge Post-Leaching Sample G5-W-B

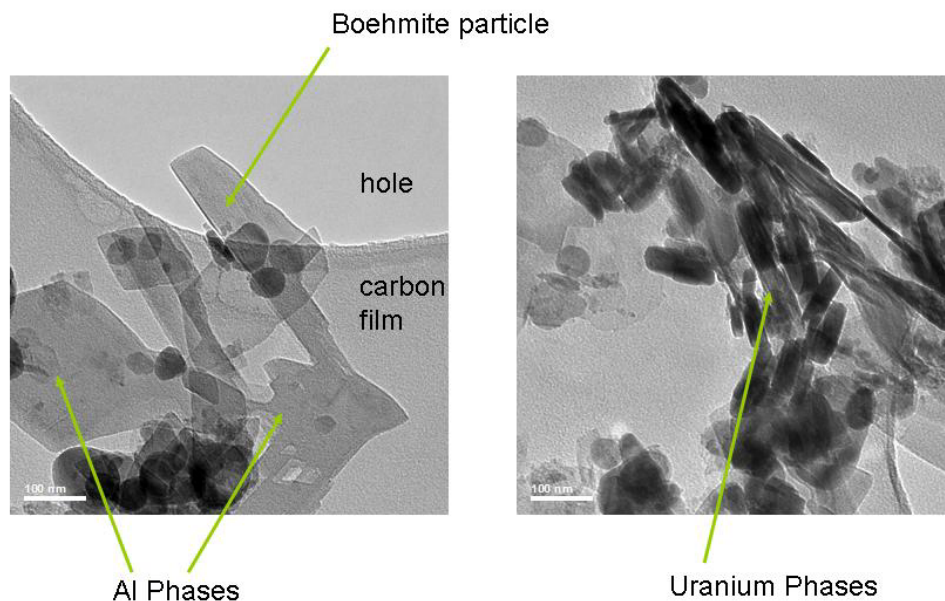


Figure 8.36. TEM images of Al and U Particles in Group 5, REDOX Sludge, Post-Leaching

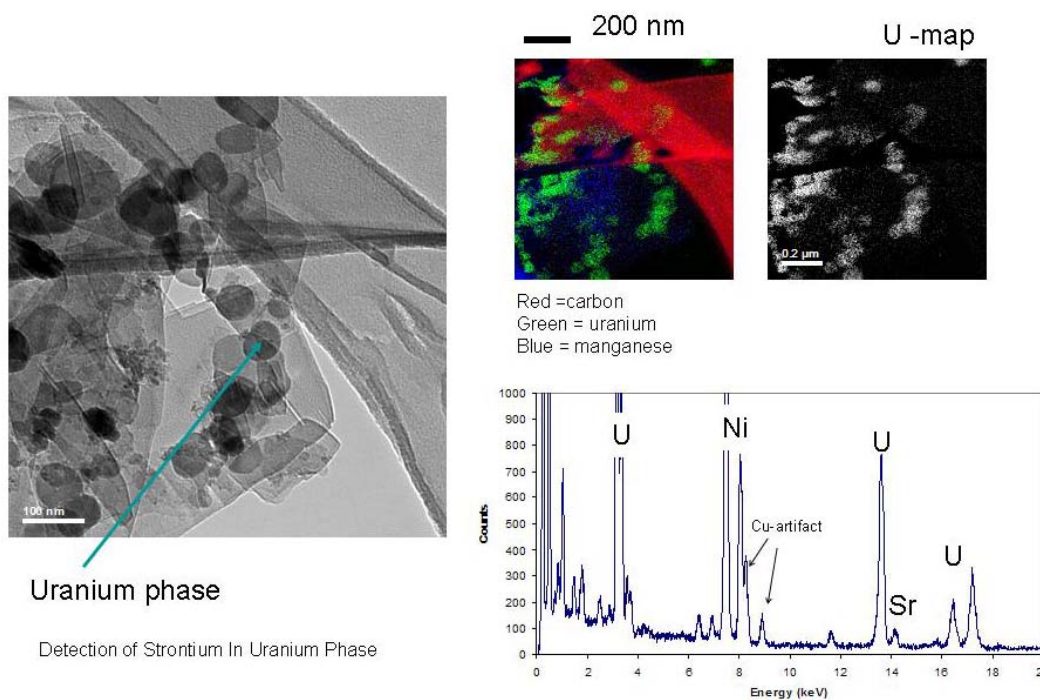


Figure 8.37. Energy-Filtered TEM Images of Group 5, REDOX Sludge Post-Leaching Sample G5-W-B1 and X-ray Analyses

The EDS analysis in Figure 8.37 shows the presence of a small strontium component in the uranium phase. The EDS analysis was repeated several times to confirm this. Although XRD indicated the presence of strontium manganese oxide, this was not confirmed during the TEM analyses. The EDS analysis in Figure 8.37 clearly showed the presence of a small quantity of Sr, but no Mn was present in

the same spectrum. However, the ratio of Sr to Mn was reasonably consistent with the predicted composition based on the XRD result, which was (1:7). The EDS result, assuming a k -factor for Mn-K and Sr-K as 1.11 and 2.44, respectively (taken from Lumpkin et al. 1994 for 200 keV) would give an approximate ratio of (1:10 to 1:7).

9.0 Group 6 S-Saltcake Water-Insoluble Solids Parametric Oxidative-Leaching Test Results

The Group 6 water-insoluble component contained a high Cr concentration (9.3 wt%). The parametric oxidative leach testing of this tank-waste sample was directed toward understanding chromium dissolution in the actual tank waste and the concurrent mobilization of Pu and thus be able to match the chromium component dissolution properties to a simulant material with minimal confounding of matrix effects. The results from the initial bulk caustic leaching, the subsequent parametric oxidative leach testing, and residual solids composition are discussed in the following sections.

9.1 Group 6 Caustic-Leached Slurry

The initial caustic leaching reduced the volume of wet centrifuged solids by 43%. The composition of the caustic leachate solution, the composite wash solution, and the suspending phase of the leached and washed solids are provided in Table 9.1. The fraction (wt%) of analyte mobilized to the solution phase during the caustic leach is also provided.

A large fraction of Al (59%) was leached from the solids with minimal mobilization of Cr, Fe, Zn, and Pu, and virtually no detected dissolution of U, Mn, and Ni. The aqueous phase was dominated by sodium, aluminate, and hydroxide. The anion/cation balance was evaluated and found to agree within 1%.

The densities of the filtered composite leach solution and the three successive wash solutions are summarized in Table 9.2. The high density of the caustic leach solution was consistent with its high ionic strength (primarily sodium, hydroxide, and aluminates). The wash-solution densities approached that of water.

The composition (major components) of the leached and washed solids, which is input to the parametric oxidative leach testing, is summarized in Table 9.3. For comparison, the washed solids composition before leaching is also provided. The solids were also sampled for PSD, SEM, TEM, XRD, and BET; these results are presented later in this section for side-by-side comparison with the post-oxidatively leached and washed solids.

9.2 Parametric Oxidative Leaching Results

The parametric leaching results for Cr mobilization to the solution phase and associated Pu mobilization are discussed in the following sub-sections. An assessment of the equilibrium solution conditions is provided as well as the residual solids composition following the oxidative leach testing.

9.2.1 Chromium Behavior During Oxidative Leaching

The Cr oxidative leach rates as functions of time, temperature, free hydroxide concentration, and Mn/Cr molar ratios were evaluated. Mobilizing 100% of the Cr would result in a Cr solution concentration of ~0.020 M. The leaching data at constant temperature and varying free hydroxide concentrations and Mn/Cr molar ratios are shown in Figure 9.1 and Figure 9.2. A measure of experimental precision is

shown by the triplicate tests conducted at 1.25 M free hydroxide at 25°C in Figure 9.1(b). The scatter was within the analytical uncertainty of ± 15%.

Table 9.1. Group 6 S-Saltcake Solids Caustic Leach Supernatant and Wash Compositions

Analyte	Caustic Leach Supernatant	Combined Washes After Caustic Leach	Fraction Mobilized from Solids Phase	Solids Suspending Medium
Cations	M	M	%	NM
Al	1.09E+0	8.60E-2	59	
B	<2.10E-4	<2.16E-4	NA	
Cr	2.88E-3	2.81E-4	0.63	
Fe	[6.46E-5]	<4.69E-5	<0.21	
Mn	<4.65E-6	<4.79E-6	<0.06	
Na	3.27	3.14E-1	NA	
Ni	<1.23E-5	<1.27E-5	<0.75	
U	<4.38E-5	<4.51E-5	<1.7	
Zn	[3.63E-5]	<1.11E-5	<1.3	
Anions,	M	M	NM	M
Nitrite	3.11E-3	2.92E-4		6.58E-5
Sulfate	6.17E-5	3.48E-5		5.47E-5
Nitrate	1.09E-2	2.31E-3		3.56E-3
Phosphate	5.03E-3	6.98E-4		8.00E-5
Free Hydroxide	M	NM	NM	M
OH ⁻	2.13			0.017
Carbon	M (as C)	NM	NM	NM
Inorganic Carbon	5.1E-3			
Organic Carbon	<2.4E-3			
Total	5.1E-3			
Radionuclides	µCi/mL	µCi/mL	%	NM
²³⁹⁺²⁴⁰ Pu	9.47E-6	2.36E-5	2.2E-2	
²³⁸ Pu	2.06E-6	2.79E-6	2.2E-2	
ASR 7979 Analyte uncertainties were typically within ±15% (2-s); results in brackets indicate that the analyte concentrations were greater than the minimum detection limit (MDL) and less than the estimated quantitation limit (EQL), and uncertainties were >15%. NM = not measured				

Under all test conditions, >50% of the Cr was successfully mobilized to the aqueous phase within the first 30 min of contact time. Equilibrium conditions had been generally achieved within a 6-hr contact time with the possible exception of the 0.25 M NaOH test condition. In the latter case, 100% Cr dissolution was observed after 6 hr with the Mn/Cr ratio of 1.25, and the dissolution percentage at 24-hr at the Mn/Cr mole ratio of 0.75 was suspected to be biased too high (the chromate result at 24 hr was equivalent to the chromate result at 6 hr).

Table 9.2. Density Measurements of Aqueous Fractions Following Caustic Leaching

Description	Density (g/mL)
Leachate from Caustic Leach	1.17
1 st wash following caustic leach	1.04
2 nd wash following caustic leach	1.01
3 rd wash following caustic leach	1.01
Combined washes	1.03
T = 21.3°C for leachate, 21.6°C for the washes	

Table 9.3. Solids Composition of Group 6 S-Saltcake (Water-Insoluble Solids) Before and After Caustic-Leaching

Analyte	Before Leach	After Leach	Analyte	Before Leach	After Leach
	µg/g	µg/g		µCi/g ^(a)	µCi/g ^(b)
Al	187,000	113,500	²³⁹⁺²⁴⁰ Pu	0.923	2.06
Bi	474	<163	²³⁸ Pu	0.122	0.290
Cd	139	259	⁹⁰ Sr	266	599.5
Cr	92,850	168,500	Total alpha	5.54	12.1
Fe	14,700	26,650	Total beta	627	1,430
Mn	4,680	8,540	Opportunistic		
Na	93,500	[65,000]	Analyte	Before Leach	After Leach
Ni	1,035	1,930		µg/g	µg/g
Si	15,500	31,500	Ca	5,365	13,500
Zn	987	1,430	P	2,230	[1,350]
U (ICP)	6,575	[9,100]	Pb	1,510	2,820
U (KPA)	4,415	12,650			
<p>(a) Reference date is May 1, 2007 (b) Reference date is May 23, 2007 ASR 7936 for ICP-OES metals. ASR 7982 for radiochemistry and U data. Analyte uncertainties were typically within ±15% (2-s); results in brackets indicate that the analyte concentrations were greater than the minimum detection limit (MDL) and less than the estimated quantitation limit (EQL), and uncertainties were >15%. Opportunistic analytes are reported for information only; QC requirements did not apply to these analytes.</p>					

Increasing the Mn/Cr mole ratio from 0.75 to 1.0 directly increased the amount of Cr in solution (initially and at equilibrium conditions). The test condition at the sub-stoichiometric Mn/Cr molar ratio of 0.75 consistently mobilized ~ 65 to 70% of the Cr. Given a presumed 1:1 mole ratio for Cr oxidation and Mn reduction, the results indicated that a high efficiency for conversion by the permanganate (~90%) was obtained. The test condition at the stoichiometric Mn/Cr molar ratio of 1.0 resulted in ~ 85 to 91% Cr dissolution, or ~90% conversion efficiency. The super-stoichiometric amount of 1.25 Mn/Cr mole ratio

resulted in ~ 93 to 106% (essentially 100%, within the experimental uncertainty) Cr dissolution, slightly higher than the 90% conversion factor.

Figure 9.3 shows the average of the 2-, 4-, and 6-hr data points taken under all conditions of temperature and NaOH concentration as a function of Mn/Cr molar ratio. The y-axis error bars define the standard deviation of all results at the given Mn/Cr mole ratios. From the 0.75 to 1 Mn/Cr mole ratio, there was no significant impact of time, temperature, or NaOH concentration on the dissolution of chromium. At the high Mn/Cr mole ratio of 1.25, there appeared to be a slight time dependence. The main factor controlling dissolution was the amount of added permanganate.

For each sample, the total chromium concentration was measured by ICP-OES, and the Cr(VI) (as chromate) concentration was measured by UV/Vis spectrophotometry. Results from the two measurement techniques for one test set are shown in Figure 9.4. Results for all tests are tabulated in Appendix C along with the percent difference between the two techniques. The agreement between the two techniques was excellent, in most cases well below 10% difference; the difference was less than the analytical uncertainty. In one case, however, the total chromium concentration (0.0166 M) showed a large deviation (+20%) from the result obtained by UV/vis (0.0133 M); see the Figure 9.1a leach condition at 25°C in 0.25 M NaOH. In this case, the total Cr concentration value was considered suspect. The Cr was shown to rapidly reach the +6 oxidation state because the total Cr and the Cr(VI) concentrations were in virtual agreement in all other cases.

Additional analytes mobilized during the oxidative leach processing included Al (~5E-3M) and Si (ranging from ~3E-4 to 3E-3 M); actual values for all samples are provided in Appendix C. These analytes were probably released from entrainment in the Cr matrix during oxidative dissolution.

9.2.2 Plutonium Behavior During Oxidative Leaching

The $^{239+240}\text{Pu}$ concentrations were measured for the highest Mn/Cr ratio (1.25) leaching condition at each sampling time. The concentrations of mobilized $^{239+240}\text{Pu}$ are shown in Figure 9.5; numeric values are provided in Appendix C. Temperature was found to have a lesser effect on the Pu dissolution. At 0.25 M NaOH concentration, the dissolved Pu concentration increased ~3× as the temperature increased from 25 to 50°C; at 3 M NaOH concentration, the dissolved Pu concentration increased ~1.2× as the temperature increased from 25 to 50°C.

The free-hydroxide concentration was found to have a large effect on the Pu dissolution. There was a large (16×) increase in the Pu concentration between 0.25 M NaOH and 1.25 M NaOH and a 20× increase as the NaOH concentration increased from 0.25 M to 3 M at 25°C. Clearly, low free-hydroxide concentrations will need to be maintained to minimize Pu mobilization during oxidative leaching of Cr.

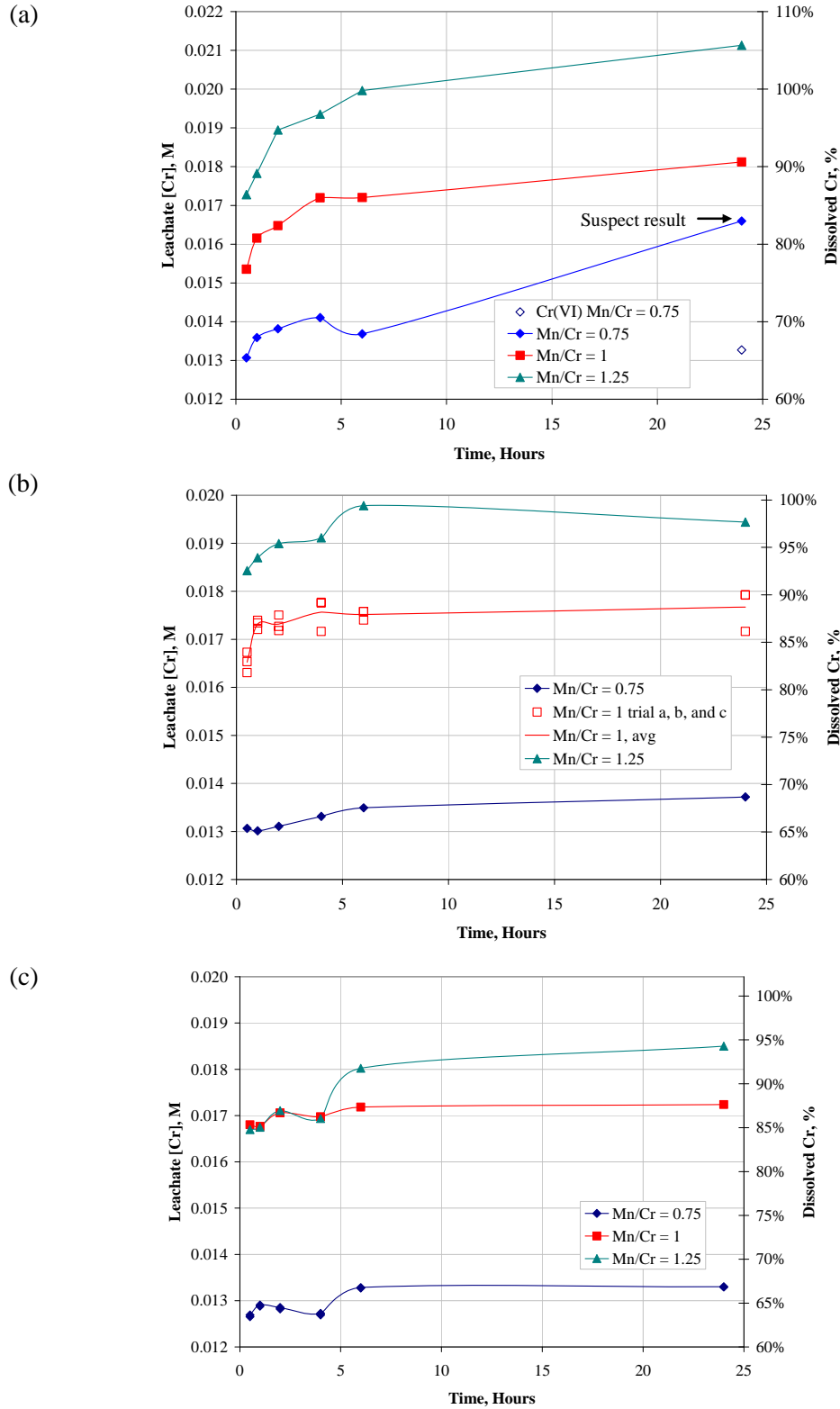


Figure 9.1. Chromium Concentration Versus Time at 25°C Leach Temperature and at Mn/Cr Mole Ratios of 0.75, 1, and 1.25 in (a) 0.25 M NaOH, (b) 1.25 M NaOH, (c) 3 M NaOH for Group 6 S-Saltcake (During Oxidative Leaching)

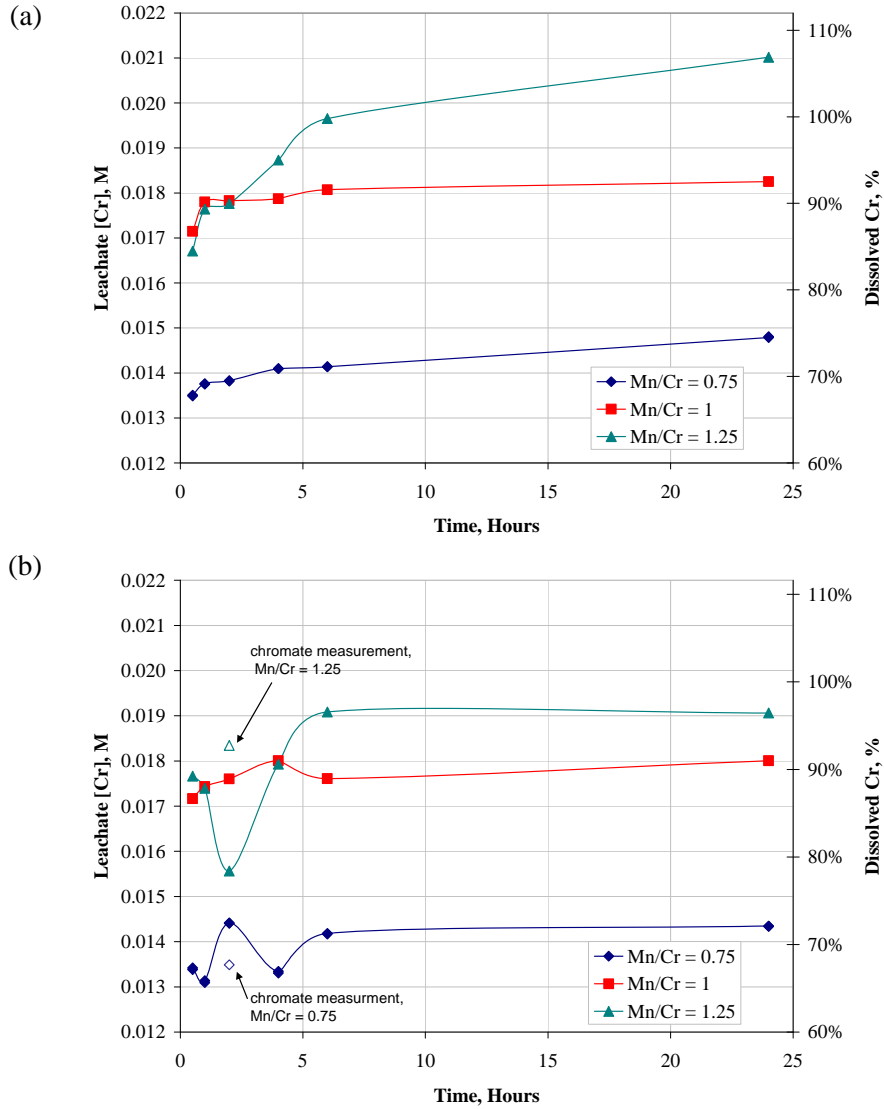


Figure 9.2. Chromium Concentration Versus Time at 50°C Leach Temperature at Mn/Cr Molar Ratios of 0.75, 1, and 1.25 in (a) 0.25 M NaOH and (b) 3 M NaOH for Group 6 S-Saltcake (During Oxidative Leaching)

Note: The two chromate values are shown for indication only, but are believed to better represent the true Cr concentration in these test samples.

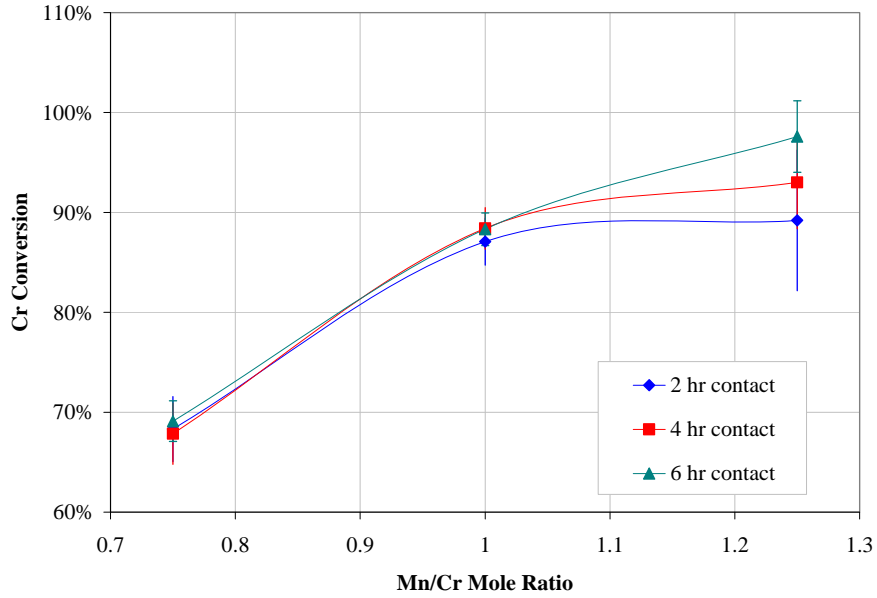


Figure 9.3. Chromium Conversion to the Aqueous Phase as a Function of Mn/Cr Mole Ratio and Time for Group 6 S-Saltcake (During Oxidative Leaching)

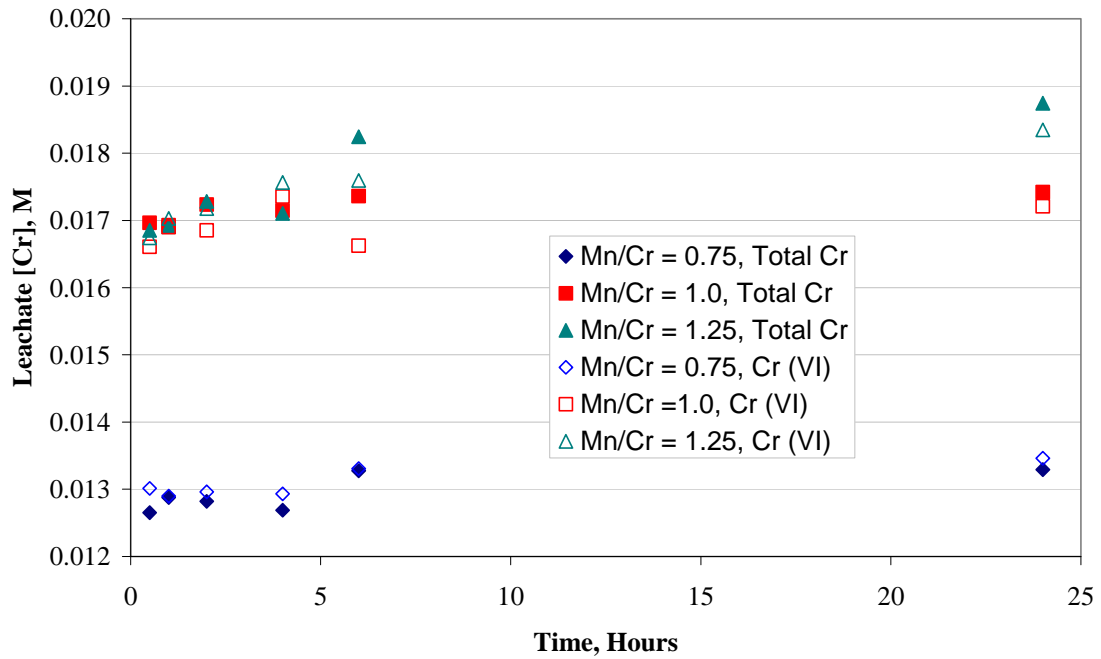


Figure 9.4. Total Chromium and Cr(VI) Concentrations Versus Time for Group 6 S-Saltcake (During Oxidative Leaching)

Conditions: 25°C leach temperature in 3 M NaOH at Mn/Cr molar ratios of 0.75, 1, and 1.25

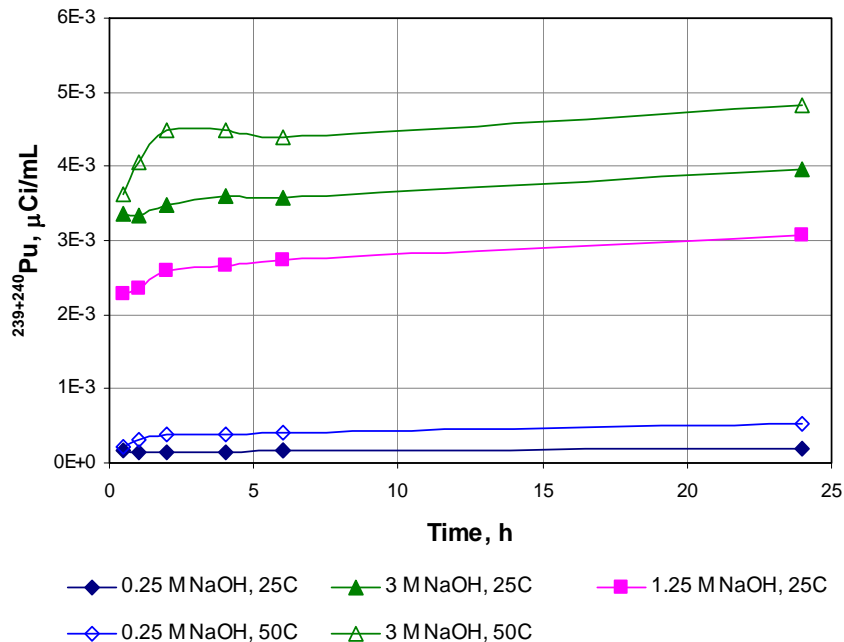


Figure 9.5. Effect of Free Hydroxide Concentration on Pu Mobilization during Oxidative Leaching for Group 6 S-Saltcake (During Oxidative Leaching)

9.2.3 Group 6 Oxidative Leaching Equilibrium Conditions

A summary of the equilibrium (24-hr) leach-solution conditions is shown in Table 9.4. The final free-hydroxide concentrations were at the targeted values, within the uncertainty of the analytical method ($\pm 15\%$). The calculated percentage of chromium that was removed at each leaching condition is also shown. One test (0.25 M free hydroxide, 25°C, Mn/Cr ratio of 1) was extended to a 48-hr contact time to ascertain equilibrium; no additional Cr dissolution occurred over the additional 24-hr leaching time. Additional selected analyte concentrations (B, Cd, Fe, Mn, Ni, Si, and U) are provided in Appendix C.

9.2.4 Composition of Group 6 Caustic and Oxidatively Leached Solids

Solids that had been oxidatively leached 24 hr at 25°C in 1.25 M NaOH at a Mn/Cr molar ratio of 1.0 were combined and washed in preparation for analysis. The chemical, radiochemical, particle size, and crystal habit of the residual solids are discussed in the following sections. The composition of the solids wash solution is also provided to close the mass balance.

9.2.4.1 Wash-Solution Composition

The densities of the individual wash solutions are shown in Table 9.5 along with the composite wash solution density, ICP-OES metals, U measured by KPA, and Pu concentration. Al and Cr were the significant materials recovered in the wash solution.

Table 9.4. Group 6 S-Saltcake Equilibrium Aqueous Phase Conditions Following Oxidative Leaching

Temp, °C	Free[OH], M	[Na], M	Mn/Cr Mole Ratio	Density, g/mL	[Cr], M	% Cr Removed
25	0.22	0.303	0.75	1.016	1.66E-2	83 ^(b)
25	0.23 ^(a)	0.283 ^(a)	1	1.023 ^(a)	1.84E-2 ^(a)	91 ^(a)
25	0.20	0.259	1.25	1.014	2.11E-2	106 ^(c)
25	1.29	1.33	0.75	1.054	1.37E-2	69
25 (trial a)	1.26	1.31	1	1.063	1.71E-2	86
25 (trial b)	1.25	1.33	1	1.065	1.79E-2	90
25 (trial c)	1.26	1.33	1	1.058	1.79E-2	90
25	1.26	1.31	1.25	1.060	1.94E-2	98
25	3.03	3.02	0.75	1.129	1.33E-2	67
25	2.98	3.06	1	1.126	1.74E-2	88
25	2.86	2.98	1.25	1.132	1.87E-2	94
50	0.23	0.277	0.75	1.014	1.48E-2	74
50	0.24	0.292	1	1.014	1.84E-2	96
50	0.21	0.268	1.25	1.015	2.12E-2	106 ^(c)
50	3.11	3.05	0.75	1.131	1.43E-2	72
50	3.09	3.12	1	1.135	1.81E-2	91
50	3.01	2.99	1.25	1.124	1.92E-2	96
<p>(a) This test was prolonged for 48 hr, and the 48-hr results are shown. The 24-hr Cr concentration was equivalent at 1.81E-2 M.</p> <p>(b) The chromate concentration was 1.33E-2 M, representing 67% Cr removal. The total Cr and Na concentrations measured by ICP-OES were suspected to be biased high by ~20%. The Na concentration measured at 6 hr was 0.252 M, 20% lower than was measured at 24 hr.</p> <p>(c) The percent Cr removal >100% was an artifact of the uncertainty of the analytical methods. Analyte uncertainties were typically within ±15% (2-s).</p>						

Table 9.5. Group 6 S-Saltcake Solids Wash Composition Following Oxidative Leaching

Analyte	M	Density ^(a)	g/mL
Al	3.23E-03	1 st wash	1.018
B	<4.3E-05	2 nd wash	1.012
Cd	<5.4E-07	3 rd wash	1.000
Cr	3.27E-03	Composite wash	1.012
Fe	<9.3E-06	Radionuclides	μCi/mL
Mn	<9.5E-07	²³⁹⁺²⁴⁰ Pu	8.99E-7
Na	0.229	²³⁸ Pu	1.22E-7
Ni	<2.5E-06		
Si	5.52E-04		
U (ICP)	<8.9E-06		
U (KPA)	3.36E-06		
(a) Temperature was 21°C. ASR 7979 Analyte uncertainties were typically within ±15% (2-s); results in brackets indicate that the analyte concentrations were greater than the minimum detection limit (MDL) and less than the estimated quantitation limit (EQL), and uncertainties were >15%.			

9.2.4.2 Solids Chemical Composition

The solids composition, after oxidative leaching for 24 hr at 25°C in 1.25 M NaOH at a Mn/Cr molar ratio of 1.0 and subsequent washing, is shown in Table 9.6. For comparison, the composition of the caustic leached and washed solids is provided. The largest mass fraction of the solids was composed of Mn followed by Al, Na, Fe, Cr, Si, Ca, and U. The fraction (percent) removed as a result of oxidative leaching is also provided. Cr and P were effectively removed from the solids. Nearly 50% of the Al, Zn, Se, and Si were also mobilized to the aqueous phase. Uranium and Fe remained in the solids phase.

Table 9.6. Leached Solids Composition and Leach Factors of Group 6 S-Saltcake (Water-Insoluble Solids)

Analyte	After Caustic Leaching, $\mu\text{g/g}^{(a)}$	After Oxidative Leaching, $\mu\text{g/g}^{(a)}$	Percent Oxidatively Leached
Al	113,500	82,500	46.0
B	<163	<114	na
Cd	259	352	0
Cr	168,500	28,425	87.5
Fe	26,650	35,125	0
Mn	8,540	214,000	na
Na	[65,000]	[76,500]	[12.6]
Ni	1,930	2,450	5.7
Si	31,500	24,200	42.9
Zn	1,430	912	52.6
U (ICP)	[9,100]	[12,000]	[0]
U (KPA)	9,735	12,700	0
Radionuclides	$\mu\text{Ci/g}^{(a)}$	$\mu\text{Ci/g}^{(a)}$	%
²³⁹⁻²⁴⁰ Pu	2.06	2.45	11.6
⁹⁰ Sr	599.5	749	7.2
Total alpha	12.1	15.9	2.4
Total beta	1430	1575	18.2
Opportunistic	$\mu\text{g/g}^{(a)}$	$\mu\text{g/g}^{(a)}$	%
Ag	[61]	[53]	[36]
As	[510]	[550]	[20]
Ba	[165]	[225]	[0]
Be	[4]	<1	[>75]
Bi	[1,030]	[1,100]	[21]
Ca	13,500	[14,750]	[19]
Ce	<374	<261	na
Co	<38	[40]	[<23]
Cu	[315]	[310]	[27]
Dy	<96	<67	na
Eu	<31	<21	na
K	<64,100	na	na
La	331	333	25.4
Li	[230]	[243]	[22]
Mg	[1,150]	[1,580]	[0]
Mo	[78]	<38	[>63]
Nd	[750]	[760]	[25]
P	[1,350]	[260]	[86]
Pb	2,820	3,460	8.8
Pd	<340	<237	na
Rh	<223	<155	na
Ru	<96	<67	na
S	[1,750]	<935	[>60]
Sb	[550]	<221	[>70]
Se	[710]	[400]	[58]

Table 9.6 (Contd)

Analyte	After Caustic Leaching, $\mu\text{g/g}^{(a)}$	After Oxidative Leaching, $\mu\text{g/g}^{(a)}$	Percent Oxidatively Leached
Sn	<505	<352	na
Sr	[145]	142	[27]
Ta	<109	<76	na
Te	<429	<299	na
Th	[500]	[730]	[0]
Ti	[81]	[123]	[0]
Tl	<389	[453]	[<13]
V	<25	<18	na
W	<170	<119	na
Y	120	[138]	[15]
Zr	[360]	[475]	[0]

(a) Dry mass basis.
ASR 7936 (after caustic leaching), radioisotope reference date: July 18, 2007
ASR 7982 (after oxidative leaching), radioisotope reference date: May 23, 2007
Analyte uncertainties were typically within $\pm 15\%$ (2-s); results in brackets indicate that the analyte concentrations were greater than the minimum detection limit (MDL) and less than the estimated quantitation limit (EQL), and uncertainties were $>15\%$.

The analysis of the leachate solutions showed that Cd, Fe, U, and Ba had not dissolved. The relative CF of these analytes averaged 1.3 in the final oxidatively leached and washed solids, based on the ratio of analyte concentration after oxidative leaching to analyte concentration after caustic leaching. This term was used to determine the leach factors of other analytes according to Equation 9.1

$$LF = \left(\frac{C_F}{C_I \times 1.3} \right) \quad (9.1)$$

where LF is the leach factor, C_F is the final analyte concentration, and C_I is the initial analyte concentration.

As shown in Figure 9.6, approximately 45 wt% of the metal solids (represented primarily by Al and Na) dissolved in the caustic leach process. The oxidative leaching resulted in additional metal solids dissolution (primarily represented by Cr with additional contributions from Al and Si) for a combined total removal of 74 wt%. However, the Mn from the oxidant contributed significant mass to the residual solids. The Mn represented an additional 20 wt% relative to the as-received solids mass and ~44 wt% of the post oxidatively leached solids.

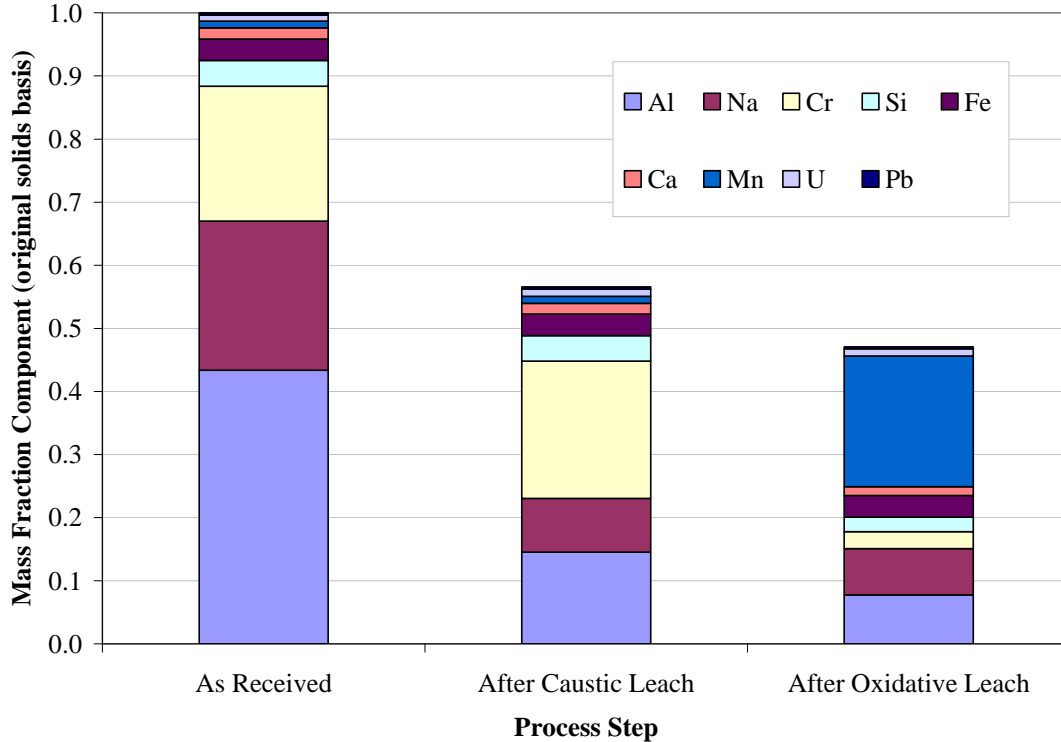


Figure 9.6. Relative Reduction in Component Mass with Caustic and Oxidative Leaching of Group 6 S-Saltcake Solids

Notes: Caustic-leaching conditions: 3 M NaOH, 100°C, 8 hr.

Oxidative-leaching conditions: 1:1 Mn:Cr mole ratio, 25°C, 1.25 M NaOH.

9.2.4.3 Particle-Size Distribution

Table 9.7 is a summary of the particle-size measurements for sample G6-IW-D (post caustic-leached solids) and G6-W-H (post oxidatively leached solids). The diameters listed correspond to the 10%, 50%, and 90% volume/weight fractiles [d(10), d(50), and d(90), respectively] and are listed as a function of test conditions.

Caustic-Leached Group 6 S-Saltcake Solids (Sample G6-IW-D)

G6-IW-D PSD measurements indicated a weakly varying d(10), d(50), and d(90) fractiles centered at 0.6, 2.1, and 9 μm , respectively. Variation of diameters was predictable. A decrease in pump RPM caused a corresponding decrease in the d(90) particle percentiles. For example, as the pump speed was reduced from 3000 to 2000 RPM before sonication, the d(90) decreased slightly from 9.8 μm to 8.9 μm . Likewise, an increase in pump speed from 2000 to 4000 RPM before sonication was accompanied by a slight increase in d(90) from 8.9 to 11 μm (~20% change). These behaviors persisted after sonication. No significant change in the d(10) and d(50) distributions was apparent as a result of changing pump speed.

Table 9.7. Summary of Results for Group 6 S-Saltcake Solids Parametric Testing Particle Size Analysis. The diameters corresponding to the 10%, 50%, and 90% volume/weight fractiles are given [d(10), d(50), and d(90), respectively].

Sample	Pump Speed	Sonication	d(10) [μm]	d(50) [μm]	d(90) [μm]
G6-IW-D Caustic-leached and washed solids	3000	pre-sonic	0.60	2.2	9.8
	2000	pre-sonic	0.59	2.2	8.9
	4000	pre-sonic	0.61	2.3	11
	3000	25%	0.60	2.2	8.4
	3000	50%	0.59	2.1	8.2
	3000	75%	0.59	2.1	8.0
	3000	post-sonic	0.59	2.2	9.7
	2000	post-sonic	0.59	2.1	8.9
	4000	post-sonic	0.60	2.2	11
G6-W-H Oxidatively leached and washed solids	3000	pre-sonic	0.84	2.4	8.9
	2000	pre-sonic	0.90	2.9	15
	4000	pre-sonic	0.94	3.3	28
	3000	25%	0.92	4.1	25
	3000	50%	0.88	5.7	33
	3000	75%	0.88	7.1	40
	3000	post-sonic	1.0	8.3	56
	2000	post-sonic	1.3	8.6	56
	4000	post-sonic	1.3	8.7	54

The application of sonic energy appeared to slightly reduce the particle diameters corresponding to the d(90) percentile. The decrease corresponding to 25%, 50%, and 75% sonic power were 8.4, 8.2, and 8.0 μm , respectively. The decrease in the d(10) and d(50) as a function of sonic power was not significant. After cessation of sonic energy, the original distribution appeared to recover to the pre-sonication behavior.

In all cases, the d(90) showed the greatest variation. This was expected, as the d(90) fraction corresponded to the largest particles and particle aggregates. These are highly susceptible to changes in size and state of aggregation and suspension as a result of mechanical action. Common causes for higher d(90) variation are as follows:

- Large particles and aggregates are sampled at lowest frequency (leading to more statistical variation).
- Large particles are more susceptible to changes in size resulting from mechanical action because their large size reduces the capability of surface forces and particle-particle interaction potentials (such as van der Waals forces) to maintain their state of aggregation.
- Large particles and/or aggregates are more difficult to suspend than smaller particles, and as such, changes in flow can alter the number and size of large particles or aggregates observed by the measurement system.

Based on the consistency of the changes in size with flow rate and sonication, it can be postulated that mechanical action (i.e., pumping and sonication) were the primary actors causing the change in distribution.

The above discussion references the size fractiles listed in Table 9.7 alone. It is often difficult to fully evaluate the effect of processing conditions on PSD based on these results alone. Graphs of the volume distribution (i.e., percent volume versus size) provide additional insight into how sonication and pump speed influence the size fraction of particles. These are discussed briefly in the following paragraphs.

Figure 9.7 shows the PSD for G6-IW-D as a function of sonication. In general, the distribution was relatively broad and showed particles ranging from 0.25 up to 200 μm . Most of the particle population fell between 0.25 μm and 20 μm under a broad single mode distribution centered around 2 μm . A small shoulder ranging from 20 to 200 μm constituted the coarse fraction of particles. Applying sonic energy eliminated this shoulder while leaving the central 2- μm distribution relatively unchanged. After sonication was removed, the 20- to 200- μm shoulder recovered. All of the observations herein were consistent with the behavior observed in the size fractiles listed in Table 9.7.

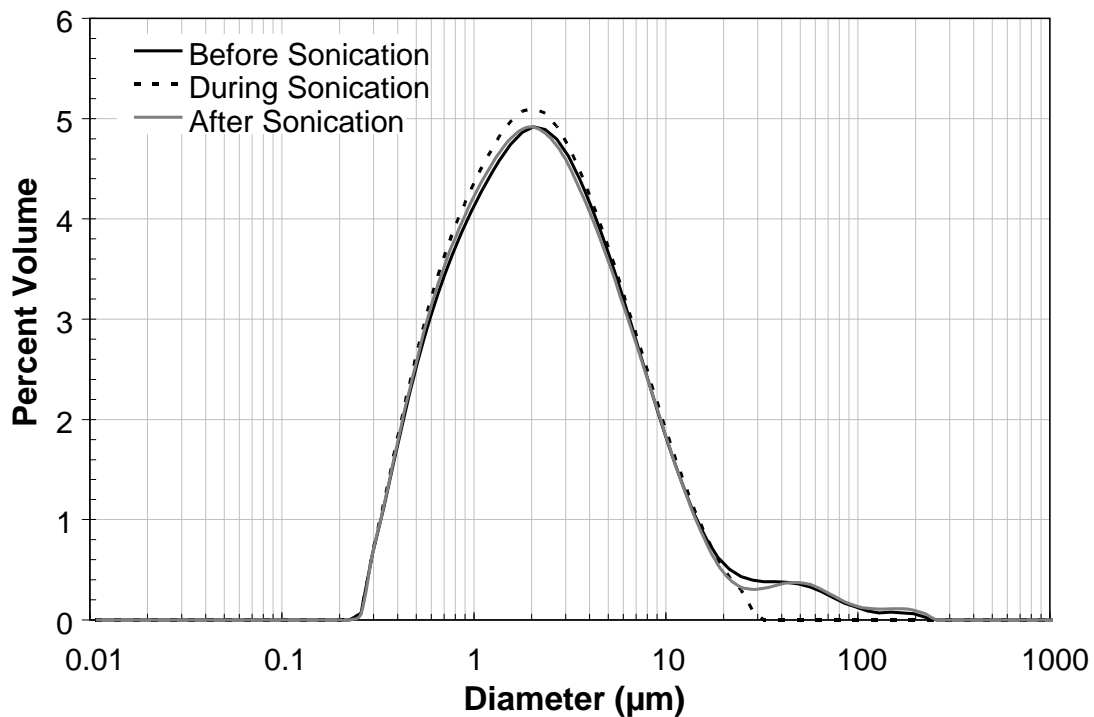


Figure 9.7. PSD for Group 6 S-Saltcake Solids Sample G6-IW-D as a Function of Sonication. G6-IW-D represented caustic-leached and washed Group 6 solids. All measurements were taken at a pump speed of 3000 RPM.

Figure 9.8 shows the PSD as a function of flow rate for pre-sonication measurements of G6-IW-D. For both low and high flow rates, the central 2- μm distribution was maintained. Indeed, as with sonication, alterations in the Malvern pump speed appeared to influence only the 20- to 200- μm shoulder. At low flow rates, the shoulder was almost completely reduced over the 30- to 100- μm range. The loss of the

large particle fraction at low flow rates was most likely a result of the inability of the flow cell to suspend this particle-size range at 2000 RPM. Particles that are not suspended will not enter into the flow cell optics and will not be sampled as a result. At 4000 RPM, the 20- to 100- μm particle fraction was increased. This increase was likely a result of improved suspension of these particles and better sampling. Figure 9.8 also appears to show a slight loss of the 100- to 200- μm particles at both higher and lower pump speeds; however, these changes are minor and may result from slight differences in particle sampling between the measurements. As before, behavior of the PSD was consistent with the trends seen in Table 9.7.

Figure 9.9 shows the PSD distribution for G6-IW-D as a function of flow rate for the post-sonication measurement state. It should be noted that the behavior was almost identical to that seen in Figure 9.8. One notable difference was the increased coarse fraction observed in the post-sonication 2000-RPM measurement relative to the pre-sonication 2000-RPM measurement. This difference was most likely a result of increased sampling of the coarse particles during this measurement and highlights the need for caution when evaluating distributions at sizes larger than 150 μm .

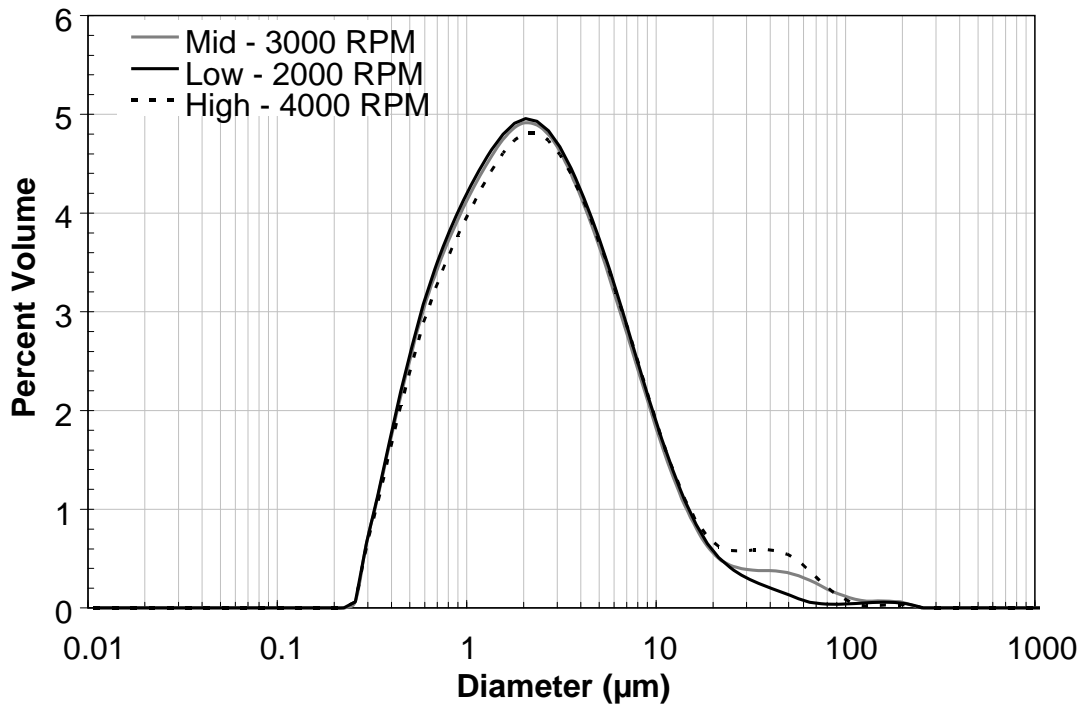


Figure 9.8. Pre-Sonication PSD for Group 6 S-Saltcake Solids Sample G6-IW-D as a Function of Flow Rate

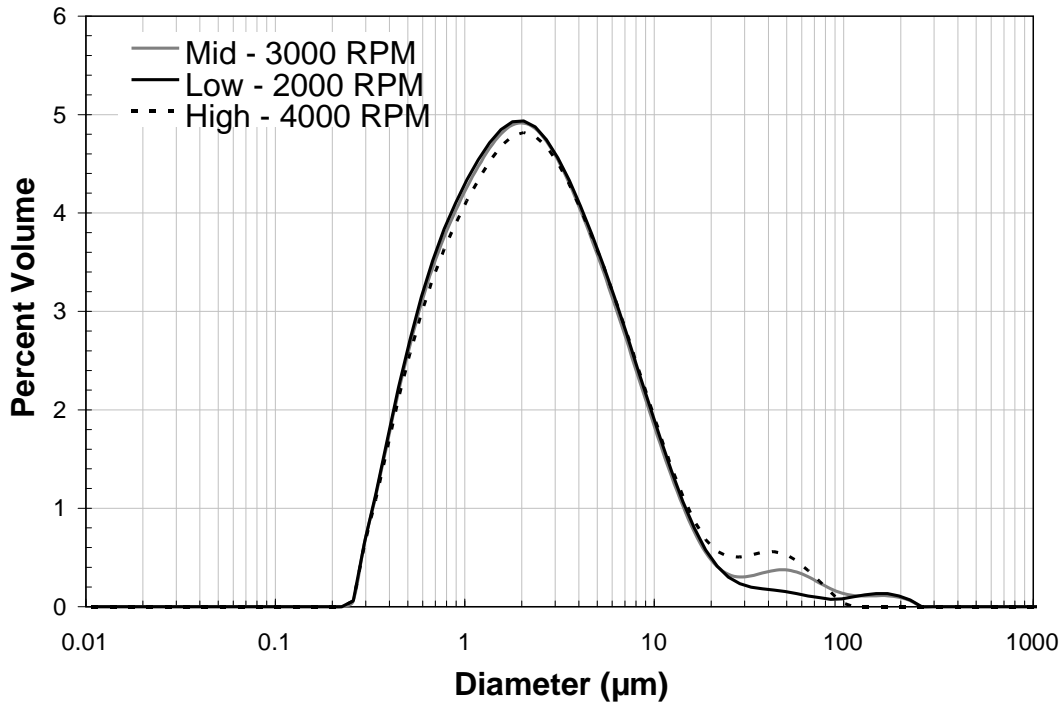


Figure 9.9. Post-Sonication PSD for Group 6 S-Saltcake Solids Sample G6-IW-D as a Function of Flow Rate

Oxidatively Leached Group 6 S-Saltcake Solids (G6-W-H)

The G6-W-H PSD results listed in Table 9.7 are suggestive of an unstable particle measuring system. In general, the d(10), d(50), and d(90) increased with increased processing time in the particle-size analyzer, regardless of measurement conditions. This was always true for measurement conditions before sonication, where all fractiles reported in Table 9.7 increased as the measurement proceeded. Pre-sonication size increases occurred even when conditions that favored lowering of the particle size (such as lower pump speeds) were active. For example, the d(50) increased from 2.4 to 2.9 μm as the pump speed was dropped from 3000 to 2000 RPM. Likewise, the d(50) continued to increase from 2.9 to 3.3 μm as the pump speed was increased from 2000 to 4000 RPM. Similar changes were observed for the other fractiles reported for pre-sonication measurement conditions.

Increased power during in-cell sonication appeared to increase the d(50) and d(90) for G6-W-H, although the effect was somewhat ambiguous for d(10) fraction diameters. Relative to the 3000 RPM pre-sonication state, all fractiles measured during the 25% sonic power test condition had increased substantially. Specifically, a 9.5%, 75%, and 180% increase was observed in the d(10), d(50), and d(90), respectively. Given that the measurement conditions appeared unstable, a significant fraction of this increase may result solely from the reaction of the PSD to the suspending phase conditions. When the 4000-RPM measurement condition immediately preceding sonication was examined, the initial application of sonic energy appeared to lower the d(10) and d(90) from 0.94 and 28 μm to 0.92 and 25 μm, respectively. However, because the application of sonic energy was preceded by a drop in the pump speed from 4000 to 3000 RPM, this decrease may have resulted from the decrease in flow rate rather than the application of ultrasonics. Continued application of sonic energy did not appear to

influence the $d(10)$ in a predictable or significant manner but yielded increases in the $d(50)$ and $d(90)$. The $d(50)$ increased from 4.1 to 7.1 μm , while the $d(90)$ increased from 25 to 40 μm .

Post-sonication $d(10)$ and $d(50)$ showed continued increases with time; the $d(90)$ appeared to increase with respect to the measurements made during sonication and then remained essentially constant at flow rates of 3000 and 2000 RPM followed by a decrease as the flow rate was increased from 2000 to 4000 RPM. While the increase of the $d(10)$ was still substantial (25%), the post-sonication $d(50)$ increased more slowly (5.3%) relative to the pre-sonication $d(50)$, which increased roughly 39% over the same range of test conditions. Both $d(50)$ and $d(90)$ trends over the post-sonication measurement conditions suggest that the suspension was approaching an equilibrium measurement state.

It should be noted that the $d(50)$ increased continuously over the duration of the test, regardless of the test conditions. Excluding data-fitting anomalies, increases in particle size are typically associated with particle aggregation or precipitation of material onto existing particles. For the current analysis, the insoluble solids had at least a week to equilibrate with respect to chemical composition. Because of this, the size changes that occurred during the course of the 23-min measurement were most likely not associated with a change in chemical state. With respect to particle aggregation, meta-stable particle configurations (termed flocculates) exist as a result of secondary minima in particle-particle interaction profiles (for additional information, please see the section on DLVO theory^(a) in Farinato and Dubin [1999]). Applying energy to the system, such as heat, mixing, or sonication, can provide sufficient energy to allow the system to enter a more stable configuration (i.e., a coagulate). As such, particle aggregation was the most likely cause of the increase seen above.

Based on the measurement data in Table 9.7, the PSD of the insoluble solids provided in G6-W-H was highly unstable in 0.01 M sodium hydroxide. Although mechanical action, such as pumping the suspension and applying sonic energy, appeared to bring the system closer to equilibrium, a stable measurement state was not reached over the 23-min measurement period observed for this sample. The cause of PSD instability for this sample is difficult to specify with any certainty; however, instability can result from large changes in processing conditions. The insoluble solids in G6-W-H had been oxidatively leached in 1.25 M NaOH with permanganate added in a 1.0 Mn/Cr mole ratio and subsequently washed in dilute hydroxide solutions. The chemical composition of the solids composite was significantly changed from the G6-IW-D sample by adding 44 wt% Mn (assumed MnO_2) and removal of much of the Cr phase. This is expected to result in significant changes in the PSD and potentially to the major particle-particle interactions. Processing conditions during the leach may not have allowed the system to reach a “stable” particle configuration. Even if a stable configuration was reached in the oxidative-leach operation, this may have been offset by dilution of the suspending phase during post-leach solids washing. Because such instability was not observed in the caustic-leached-only Group 6 solids (i.e., G6-IW-D), the instability observed in the post-oxidative-leach sample was likely a result of the oxidative leaching operation.

Figure 9.10 shows the PSD for G6-W-H as a function of sonication. The distribution showed significant changes upon the application of sonic energy. Before any sonication, the distribution was dominated by a large population peak centered from 2 to 3 μm . This primary peak was narrower than the central peak that defined the pre-oxidative-leach sample, G6-IW-D, as shown by the higher peak percent volume (i.e., 7.5 vol% versus 5 vol%). The shoulder observed in G6-IW-D was still present and spanned 10 to

(a) The DLVO theory is named after Derjaguin, Landau, Verwey, and Overbeek who developed it in the 1940s.

200 μm . Applying sonic energy appeared to shift a fraction of the particles making up the primary 2- to 3- μm peak up into 10- μm aggregates. In addition, there was an increase in the population of 80- μm particles. The origin of this increase could be particles from the 10- to 40- μm shoulder. This increase appeared to be the result of particle coagulation induced by sonication. It indicated, like the fractile results shown in Table 9.7, that the G6-W-H insoluble solids were unstable with respect to aggregation for the measurement conditions employed (i.e., room temperature, 0.01-M NaOH aqueous suspending phase, etc.). Although sonication changed the mode of the distribution, the overall size range appeared to remain unchanged.

Figure 9.11 shows the influence of pump speed on the pre-sonication measurement results for sample G6-W-H. The oxidatively leached sample PSD trends shown in Figure 9.11 were consistent with those observed for the pre-leach sample (cf. Figure 9.8). In particular, the primary (central) peak appeared to be mostly unaffected by changes in pump speed. Although this peak shifted to higher diameters as the pump speed changed from 3000 to 2000 to 4000 RPM, the shift appeared to be caused by changes in the state of particle aggregation with time rather than by changes in pump RPM. Increased pump speed was accompanied by an increased volume fraction of “coarse” particles in the 10- to 100- μm range and a decreased portion over 100 μm . This coarse-fraction behavior appeared to result from a combination of increased particle suspension in the 10- to 100- μm range and shear breakage of aggregates above 100 μm .

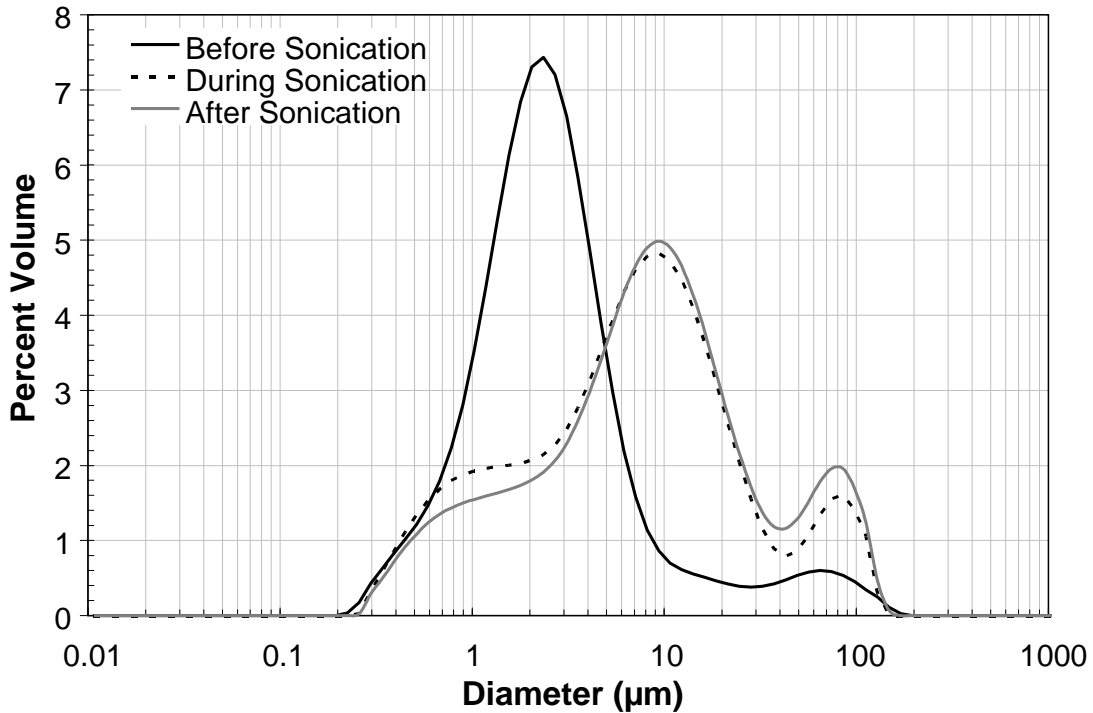


Figure 9.10. PSD for Group 6 S-Saltcake Solids Sample G6-W-H as a Function of Sonication. G6-W-H represented oxidatively leached and washed insoluble solids from Group 6. All measurements were taken at a pump speed of 3000 RPM.

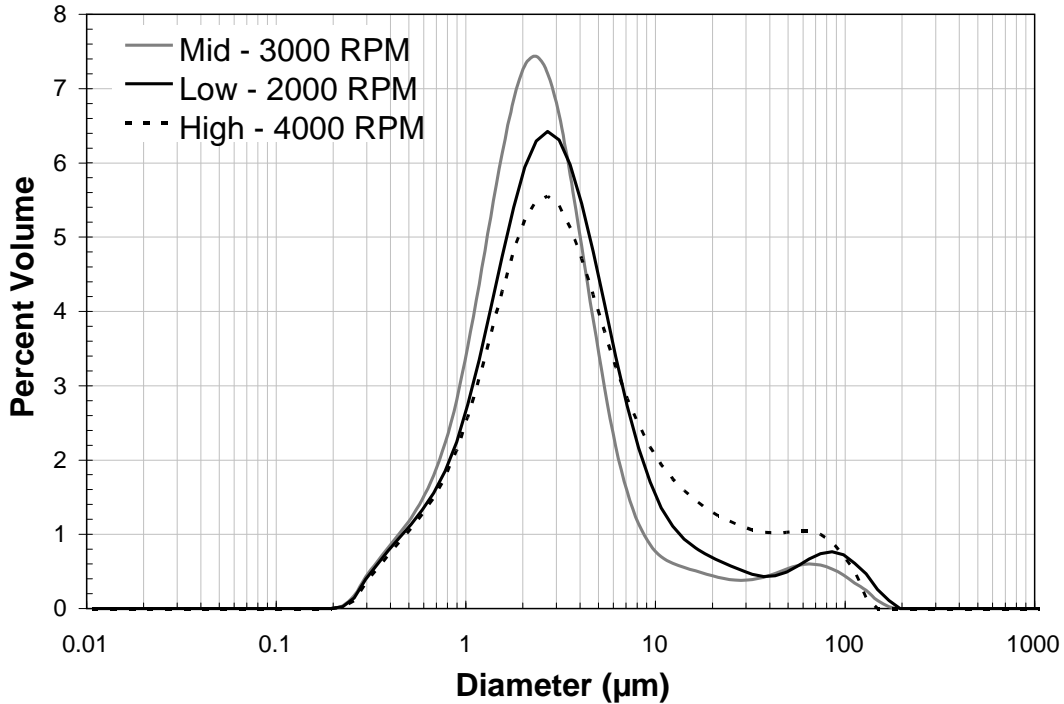


Figure 9.11. Pre-Sonication PSD for Group 6 S-Saltcake Solids Sample G6-W-H as a Function of Flow Rate

Figure 9.12 shows the influence of pump speed on the post-sonication measurement results for sample G6-W-H. Post-sonication PSDs for G6-W-H appeared to be relatively insensitive to changes in pump speed. Altering the flow rate appeared to cause a slight decrease in the population of 0.2- to 2- μm particles initially observed during the first post-sonication measurement at 3000 RPM. It is unknown if this is a time effect (i.e., a recovery of the fines fraction from sonication) or a flow-rate effect. The only change in PSD as the pump speed was increased from 2000 to 4000 RPM appeared to be a minor increase in the volume population of 20- to 50- μm particles. The post-sonication stability with respect to flow rate may have resulted from including the 10- to 100- μm particles into loose aggregates that were easily suspended.

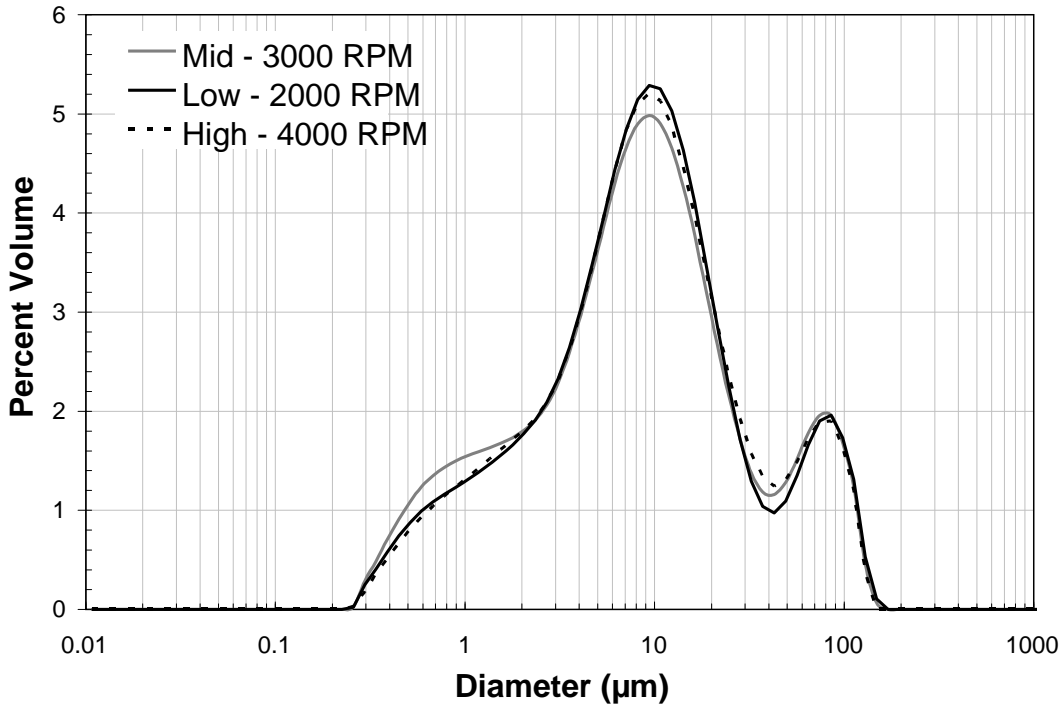


Figure 9.12. Post-Sonication PSD for Group 6 S-Saltcake Solids Sample G6-W-H as a Function of Flow Rate

Influence of Oxidative Leaching on PSD of Group 6 Solids

The influence of oxidative leaching on the PSD for Group 6 parametric testing samples can be determined by comparing G6-IW-D to G6-W-H. Figure 9.13 shows the pre-sonication PSD before and after oxidative leaching. The effect of oxidative leaching both sharpened and increased the relative population of 2- to 3- μm particles. This “central” peak may 1) result from size reduction/removal of larger particles, 2) represent the insoluble solids with respect to caustic leaching, and/or 3) represent the gross fraction of added MnO_2 particles (see TEM discussion and particle visualization). The post oxidative-leaching PSD showed an increased fraction of 40- to 200- μm “particles.” These may simply be large insoluble particles that remained after leaching (some large particles were identified in SEM mounts), particles that precipitated during leaching (like those in the central peak), or they could be particle aggregates that formed as a result of sample instability.

PSD measurements for Group 6 parametric samples not only showed changes in PSD as a result of leaching but also suggested changes in the particle-particle and particle-suspending phase interactions as a result of leaching. Pre-oxidative-leach PSDs were relatively stable and showed predictable and expected behavior with both sonication and flow rate. Post-oxidative-leach measurements showed strong time-dependent increases in particle size and appeared to be relatively insensitive to sonication and flow rate. Post-sonication behavior suggested particle coagulation and instability with respect to the suspending phase. It is suspected that these instabilities were caused by the severe changes in suspending-phase chemistry during oxidative leaching (and subsequent solids washes) and by the precipitation of new particles that, given the leaching and washing conditions, exist in a meta-stable state of aggregation.

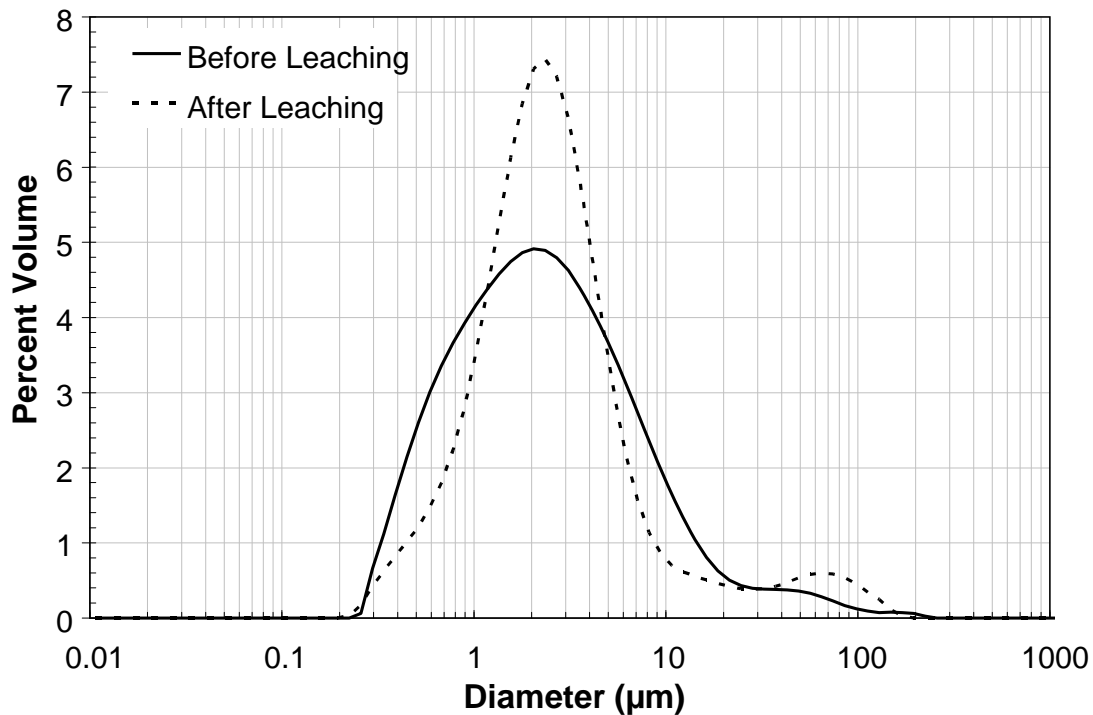


Figure 9.13. Effect of Oxidative Leaching on the Measured PSD for Group 6 S-Saltcake Solids Parametric Testing Samples. Before oxidative leaching, the PSD result was taken from G6-IW-D measurements; after oxidative leaching, the PSD result was taken from G6-W-H measurements.

9.2.4.4 Crystal Form and Habit

The XRD pattern of the caustic leached and washed solids (sample ID G6-IW-E) is provided in Figure 9.14a; the background-subtracted XRD pattern with stick-figure phase identification is shown in Figure 9.14b. Rutile (TiO_2) had been added as an internal standard. The caustic-leached sample was mostly amorphous. Boehmite was the major crystalline phase present, followed by hydroxycancrinite ($1.06\text{Na}_2\text{O}\cdot\text{Al}_2\text{O}_3\cdot 1.60\text{SiO}_2\cdot 1.6\text{H}_2\text{O}$) and gibbsite with considerably lower peak intensities. Calcium aluminum oxide (CaAl_2O_4) could be present in very low amounts; this phase was represented in the pattern by only one peak, so its presence could not be confirmed.

The XRD pattern of the oxidatively leached and washed solids (sample ID G6-W-F) is provided in Figure 9.15a; the background-subtracted XRD pattern with stick-figure phase identification is shown in Figure 9.15b. The oxidatively leached sample was also mostly amorphous. The sample peak intensity was quite low, but sufficient to identify some phases. Boehmite was present with the most intense pattern from crystalline material (although low) of the phase identified. Hydroxycancrinite and gibbsite were present with lower peak intensities. Tridymite (SiO_2) was tentatively identified, but because of chemistry phase limitations (high formation and stability temperatures), it is not a good mineralogical choice. However, in addition to matching the 19.1° $2\text{-}\theta$ line, it is a reasonably good match to the 20.3° and 21.5° $2\text{-}\theta$ lines, which otherwise are not matched. The identification as tridymite is unlikely but may be a clue to aid in identification as further data become available.

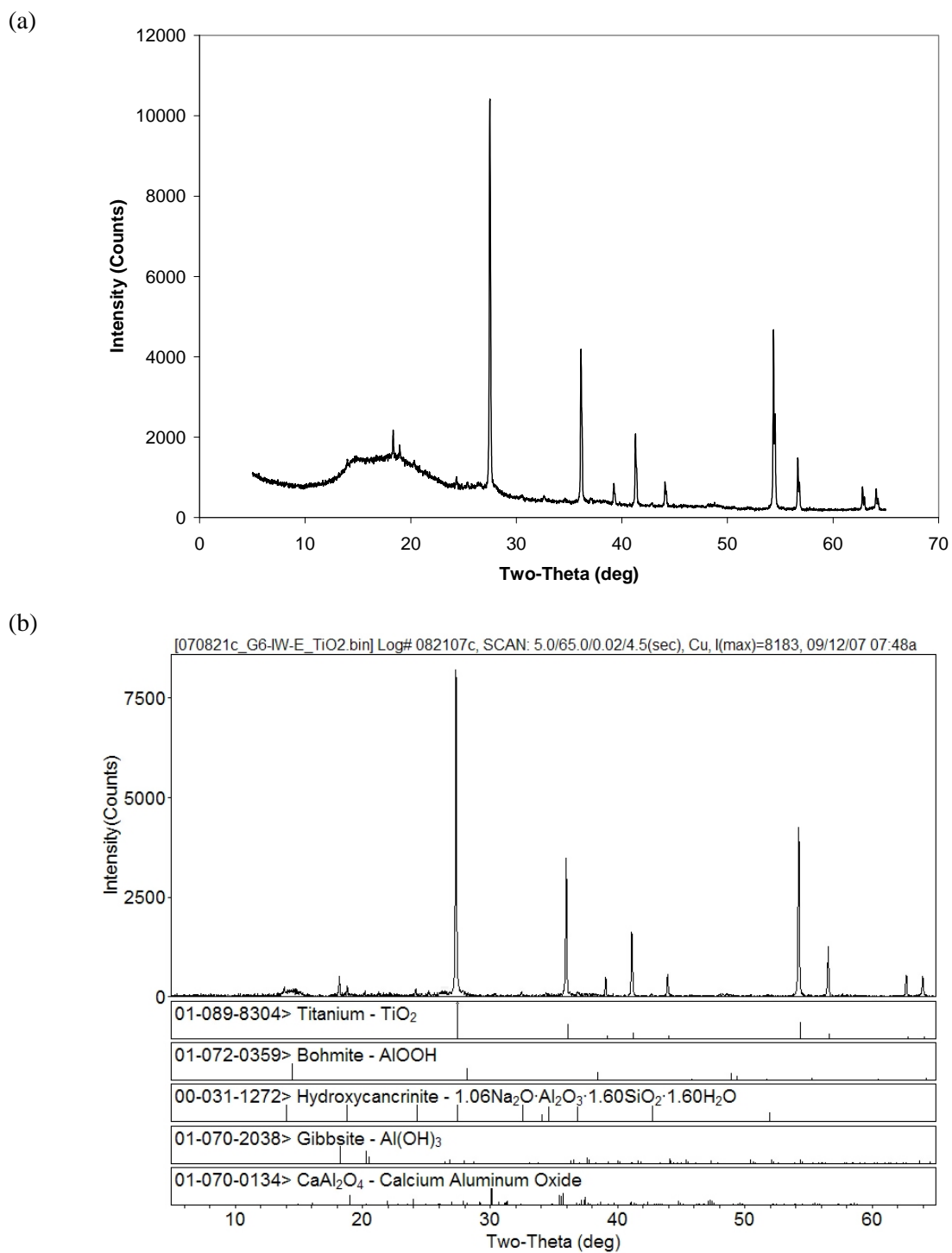


Figure 9.14. XRD Pattern of Caustic Leached Group 6 S-Saltcake Solids with Rutile (TiO_2) Internal Standard

(a) raw spectrum, (b) with background-subtracted and stick-figure peak identification

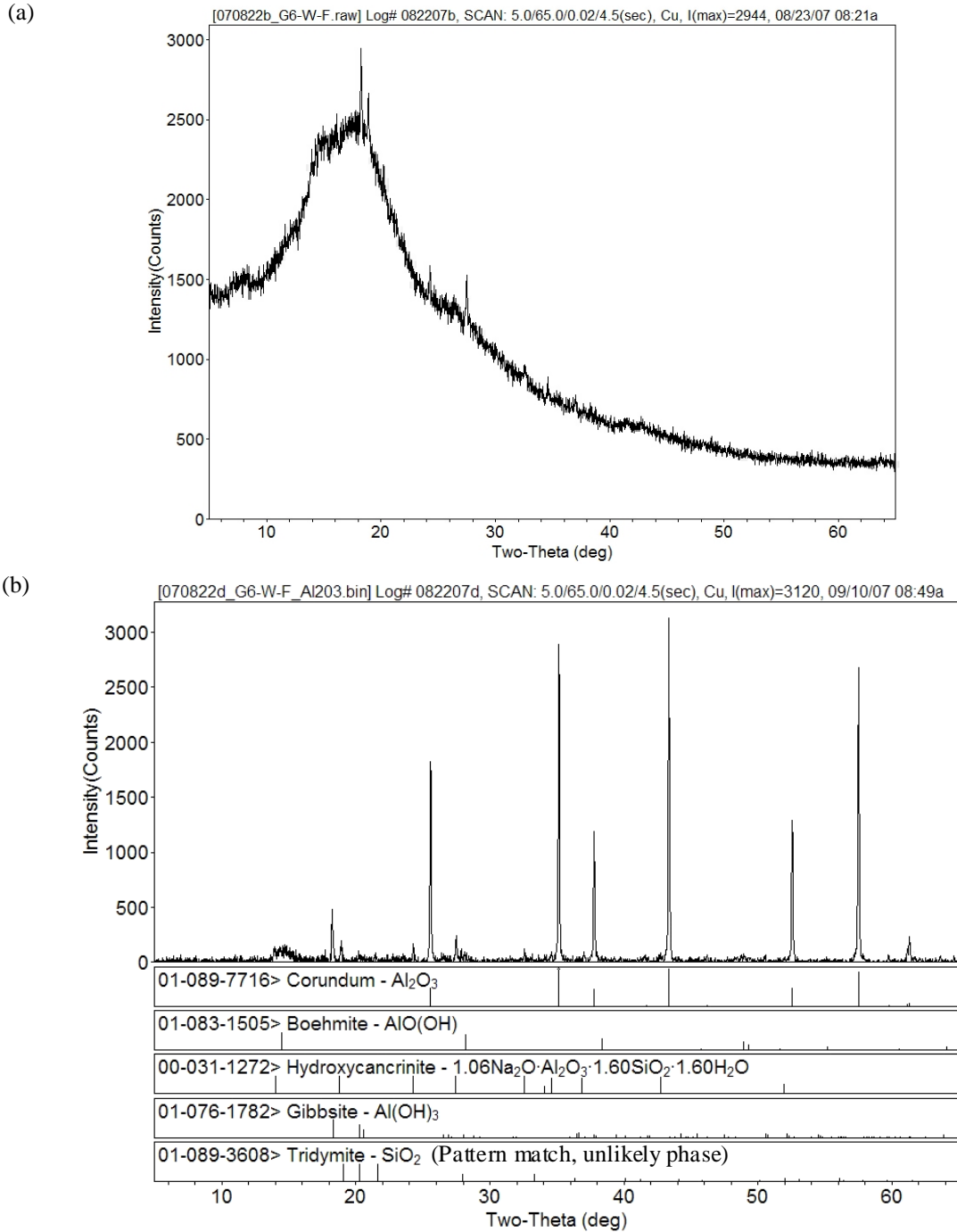


Figure 9.15. XRD Pattern of Oxidatively Leached Group 6 S-Saltcake Solids

(a) raw spectrum, no internal standard, and (b) background-subtracted spectrum with corundum (Al_2O_3) internal standard and stick-figure peak identification

Figure 9.16 provides SEM images of the residual caustic leached and washed solids. The material was dominated by small particles with a generally high surface area. Figure 9.17 and Figure 9.18 provide SEM-EDS spectra and image maps of selected elements in the caustic leached and washed solids. Al and Cr dominated the composition, consistent with the chemical analysis. The Na and Si appeared to be related in structure consistent with hydroxycancrinite. Note that Fe was dispersed with concentrates in selected areas.

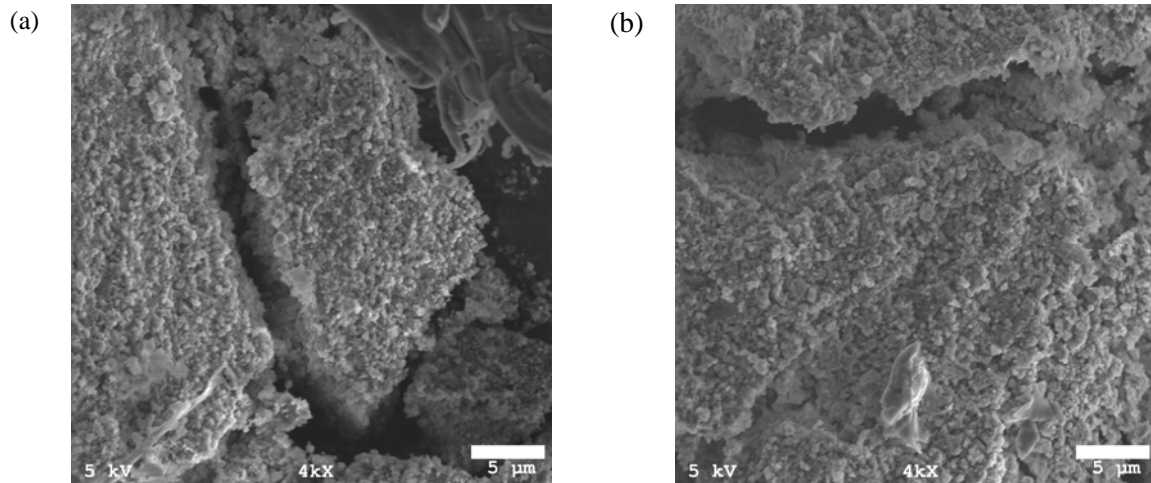


Figure 9.16. SEM Images of the Caustic-Leached and Washed Group 6 S-Saltcake Solids

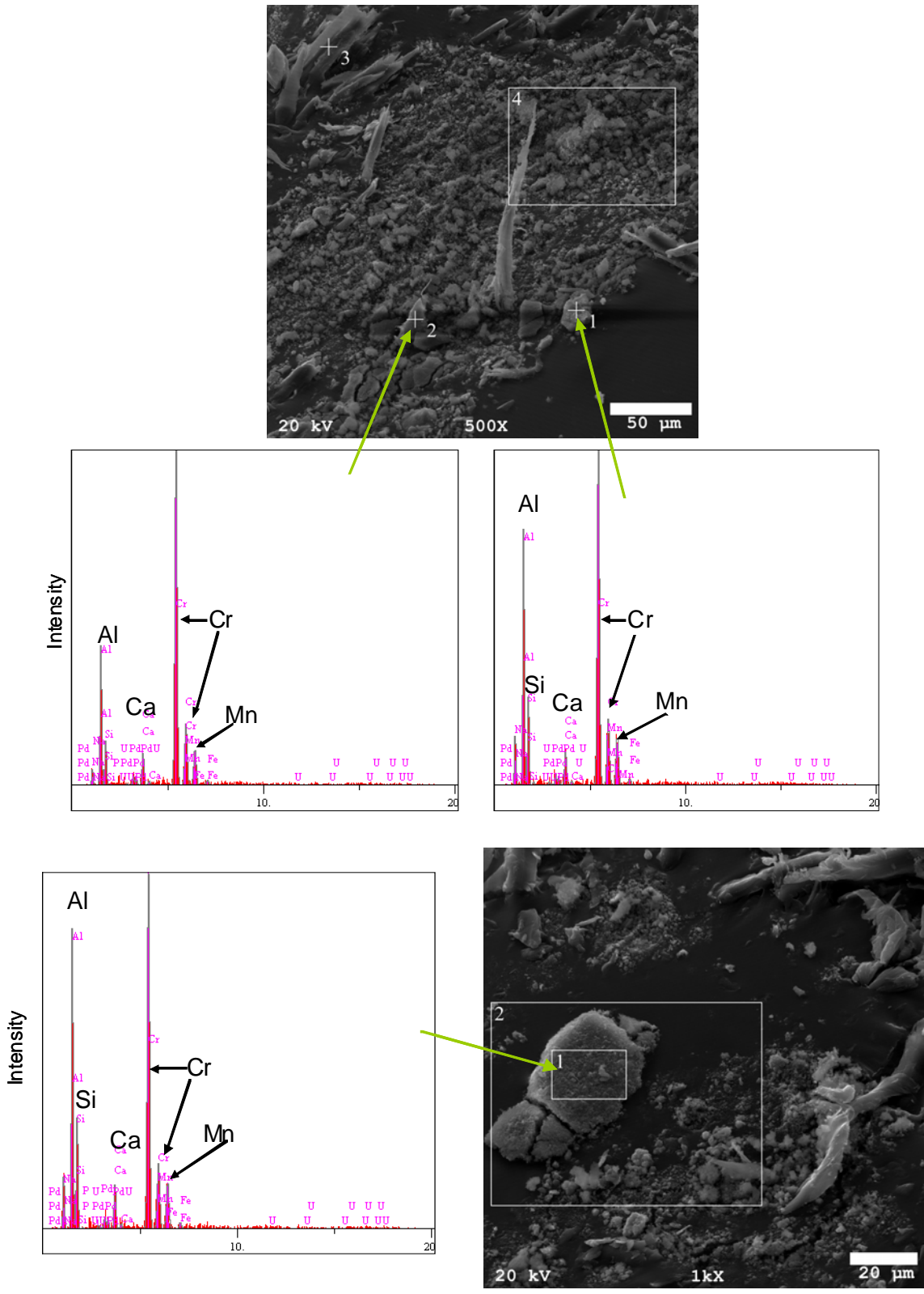


Figure 9.17. SEM-EDS Images of Group 6 S-Saltcake Caustic-Leached Solids

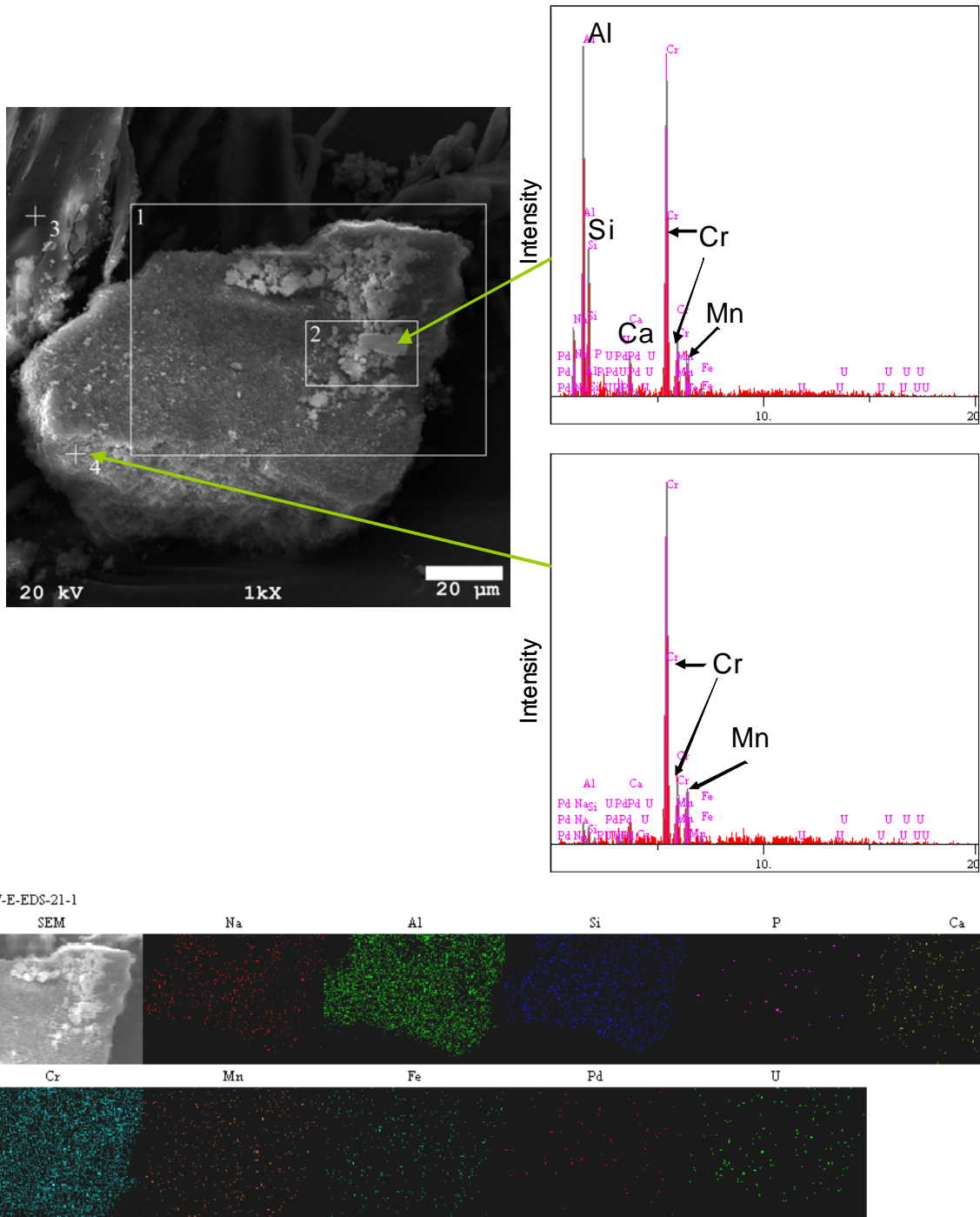


Figure 9.18. SEM Image of the Caustic Leached and Washed Group 6 S-Saltcake Solids with EDS Analysis and Map

Several SEM images of the oxidatively leached and washed solids are shown in Figure 9.19. The particles are generally small, showing a tendency toward agglomeration. An ~50-micron-long structure was found in the solids, similar to structures found in the caustic-leached solids. Figure 9.20 provides SEM-EDS analysis of the solids showing high Mn and Al phases.

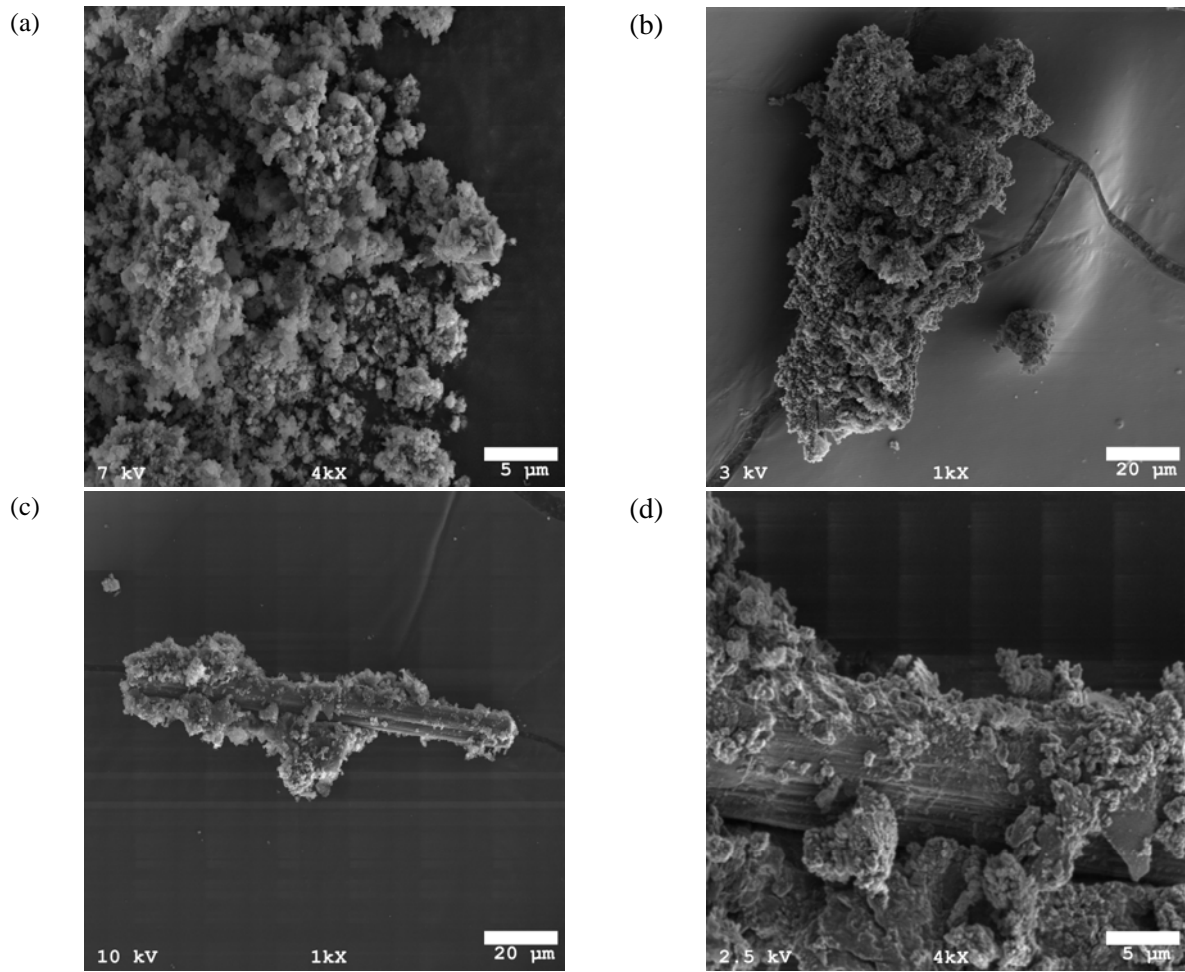


Figure 9.19. SEM Images of Group 6 S-Saltcake Solids Following Oxidative Leaching and Washing

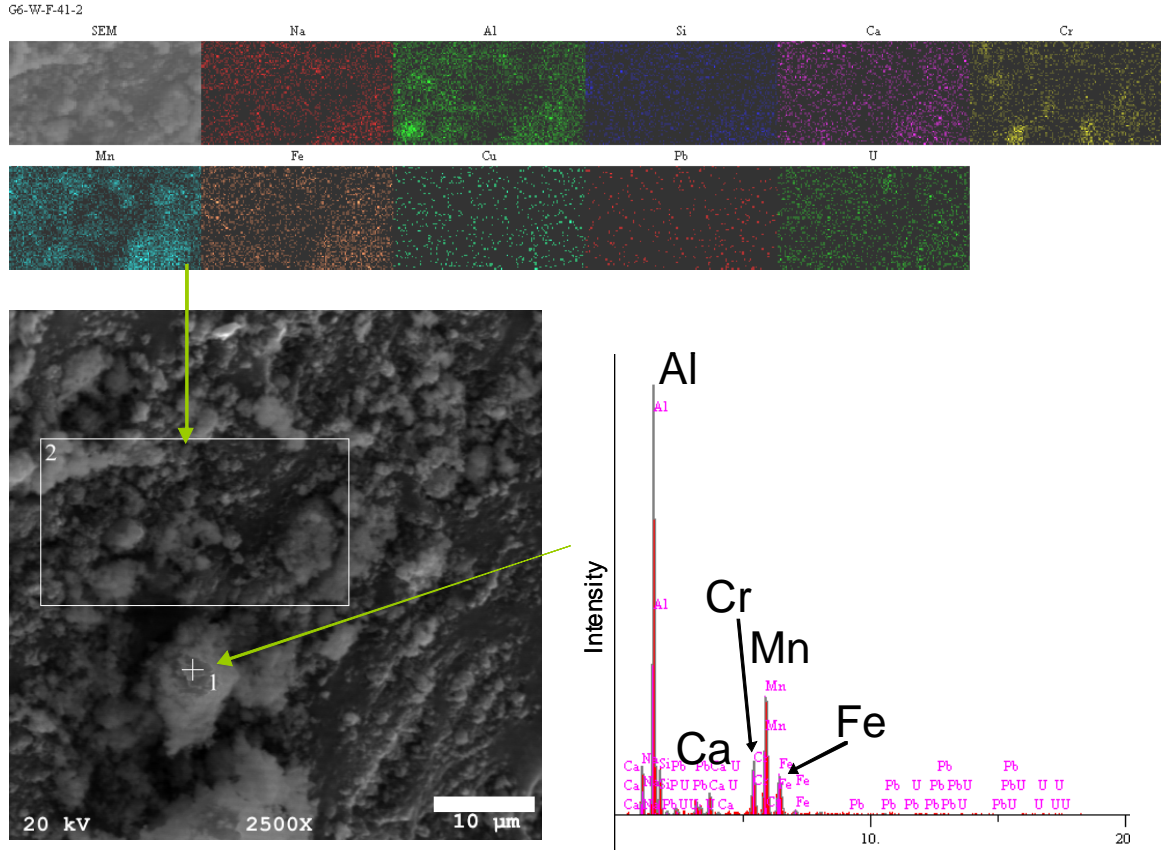


Figure 9.20. SEM-EDS Imaging and Analysis of Group 6 S-Saltcake Oxidatively Leached Solids

Figure 9.21 shows the micrograph and EDS energy-filtered map of the oxidatively leached solids. Mn, Al, Si, Fe, and Ca dominated the composition, consistent with the chemical analysis.

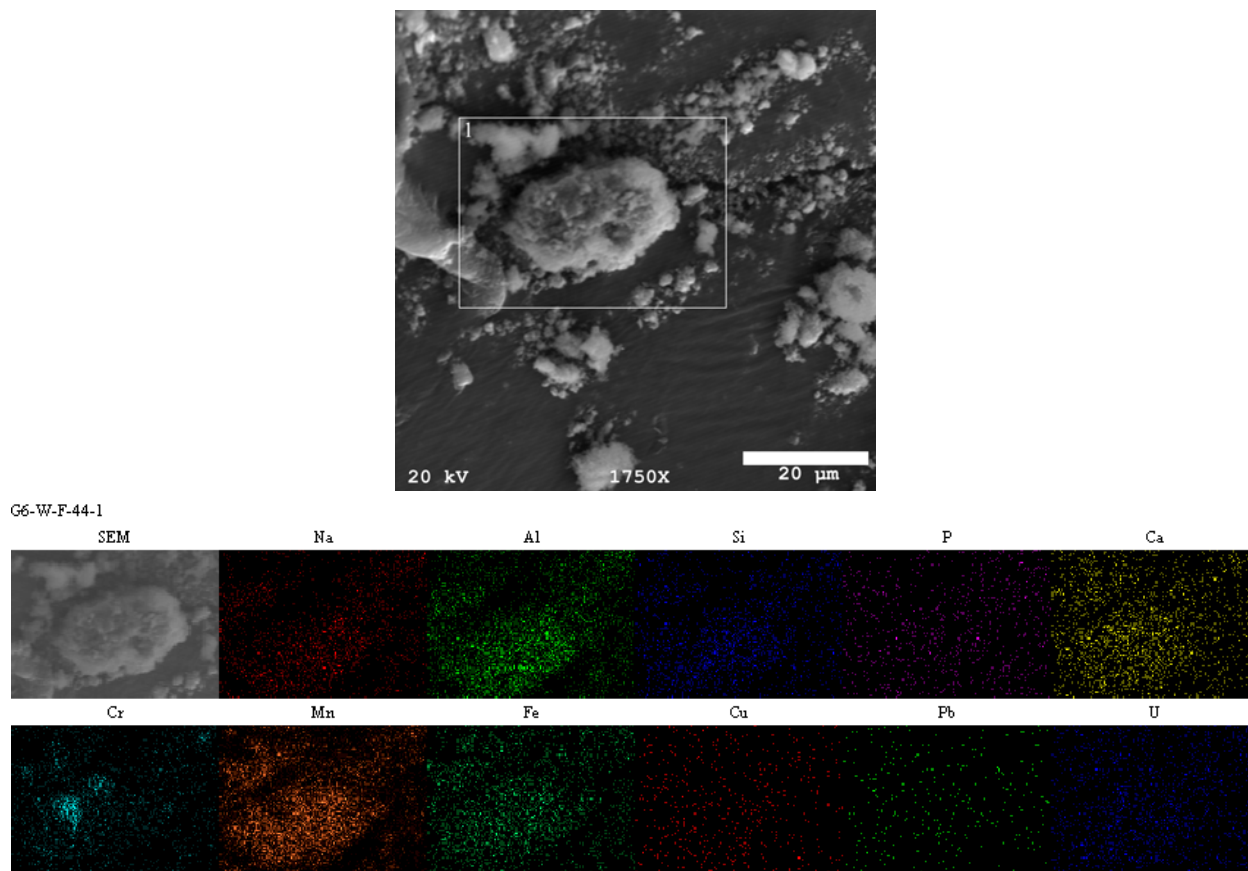


Figure 9.21. SEM-EDS Image of Group 6 S-Saltcake Oxidatively Leached Solids with Na, Al, Si, P, Ca, Cr, Mn, Fe, Cu, Pb, and U Maps

9.2.4.5 TEM

G6-IW-F

The G6-IW-F sample (caustic leached and washed solids) contained a mixed Al-Cr phase with a high surface area. The STEM image in Figure 9.22 shows the analyses of several different regions with variable amounts of chromium. The nature of the phases was examined by imaging at very high magnifications. The structure appears to be completely amorphous (see Figure 9.23). The high-magnification image in Figure 9.23b shows that the material is non-crystalline.

The energy-filtered image (Figure 9.24) revealed the presence of small uranium particles in the solid. There also appears evidence of a carbon-bearing phase in the amorphous region. A strong carbon signal is expected from the support film; however, the carbon-map indicates that carbon is also present in the phase. The carbon may be associated with a carbonate phase. Chromium and aluminum phases were ubiquitous.

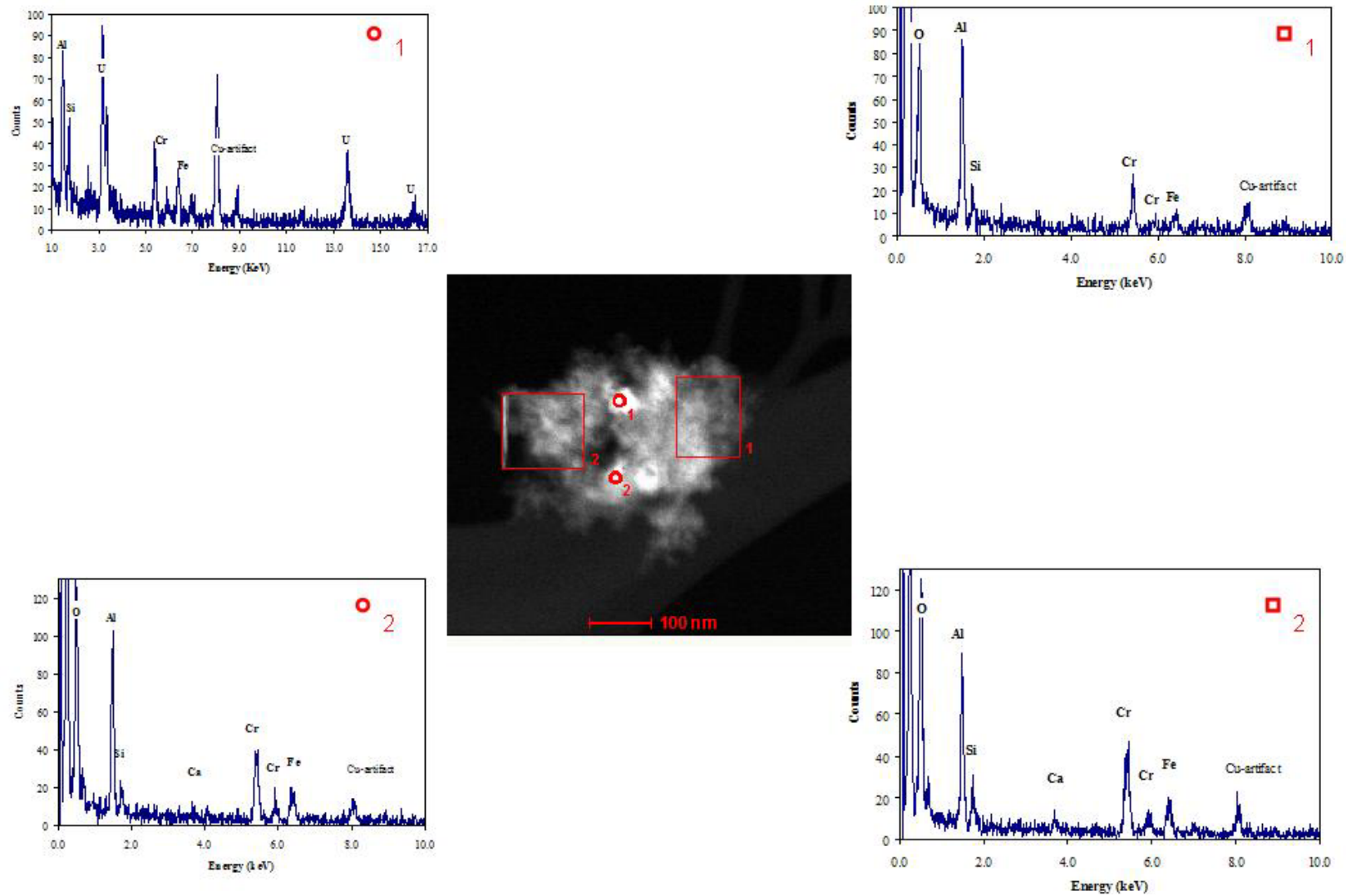


Figure 9.22. STEM and EDS Analyses of Regions in G6-IW-F (Group 6 S-saltcake sample following caustic-leaching)

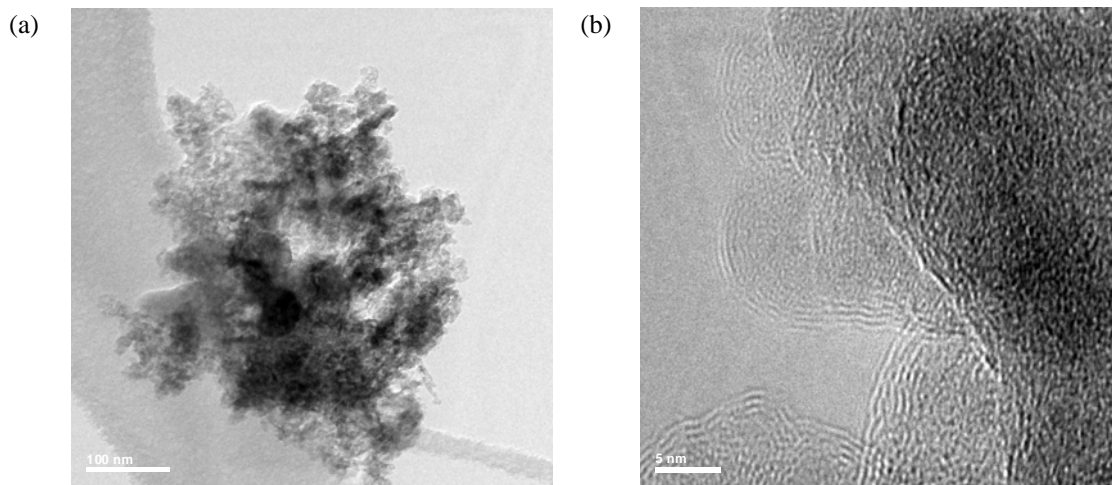


Figure 9.23. TEM Images of Amorphous Aggregates in G6-IW-F (Group 6 S-saltcake sample following caustic leaching)

(a) with 100-nm scale; (b) with 5-nm scale

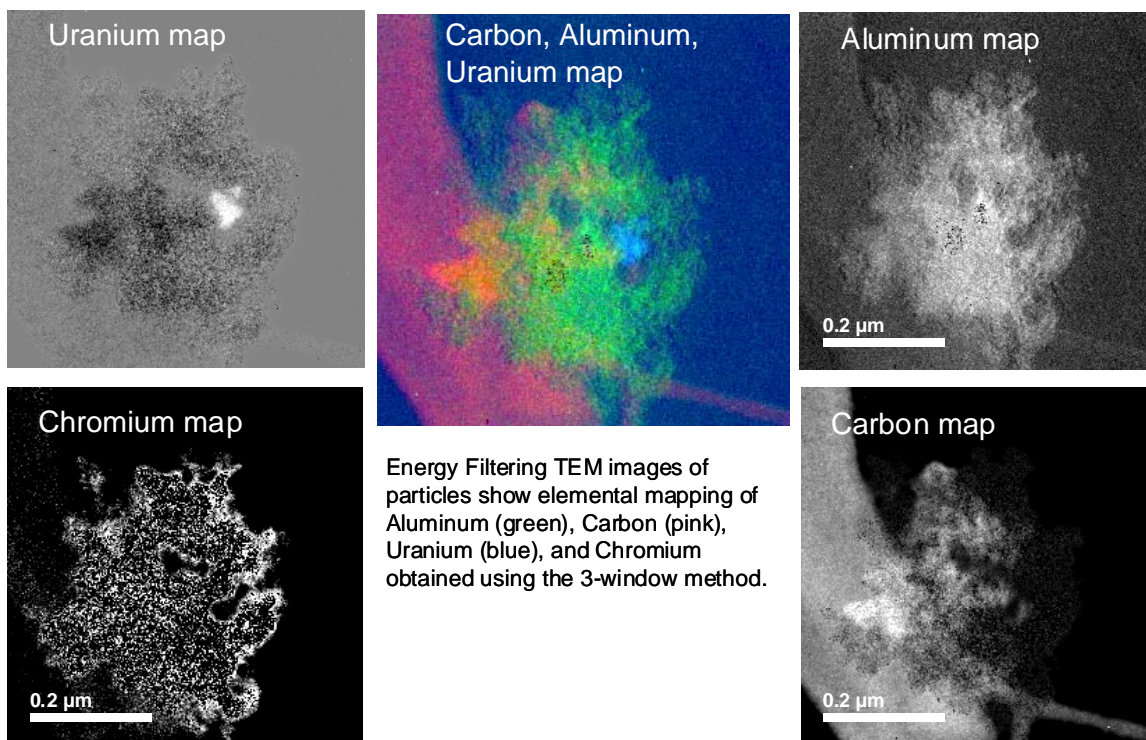


Figure 9.24. Energy-Filtered Image of G6-IW-F (Group 6 S-saltcake sample following caustic leaching)

G6-W-G

Sample G6-W-G, resulting from oxidative leaching of the caustic-leached Group 6 solids with sodium permanganate, led to the formation of MnO_2 . TEM analyses of this sample revealed a high concentration of nano-sized manganese oxide particles (Figure 9.25).

The mathematical fit (see Figure 9.26) represents a \log_e normal distribution to the data that indicates a single particle type. The fit is relatively poor; however, there are difficulties in accurately measuring the particle sizes because many of the images had overlapping particles.

In Figure 9.27, energy-filtered TEM (EFTEM) images show the occurrence of a uranium particle. The major phase in the sample was the precipitated manganese oxide from the permanganate, and therefore identifying the original or remaining tank sludge phases is difficult. By applying EFTEM, we can isolate specific phases at the nano-scale. In this case, the small uranium particle can be clearly seen and identified. In Figure 9.28, the STEM and EDS analyses show the presence of an amorphous aluminum oxide and agglomerates of the manganese-oxide particles. Higher magnification images in Figure 9.29 show the lattice fringes from the manganese phases.

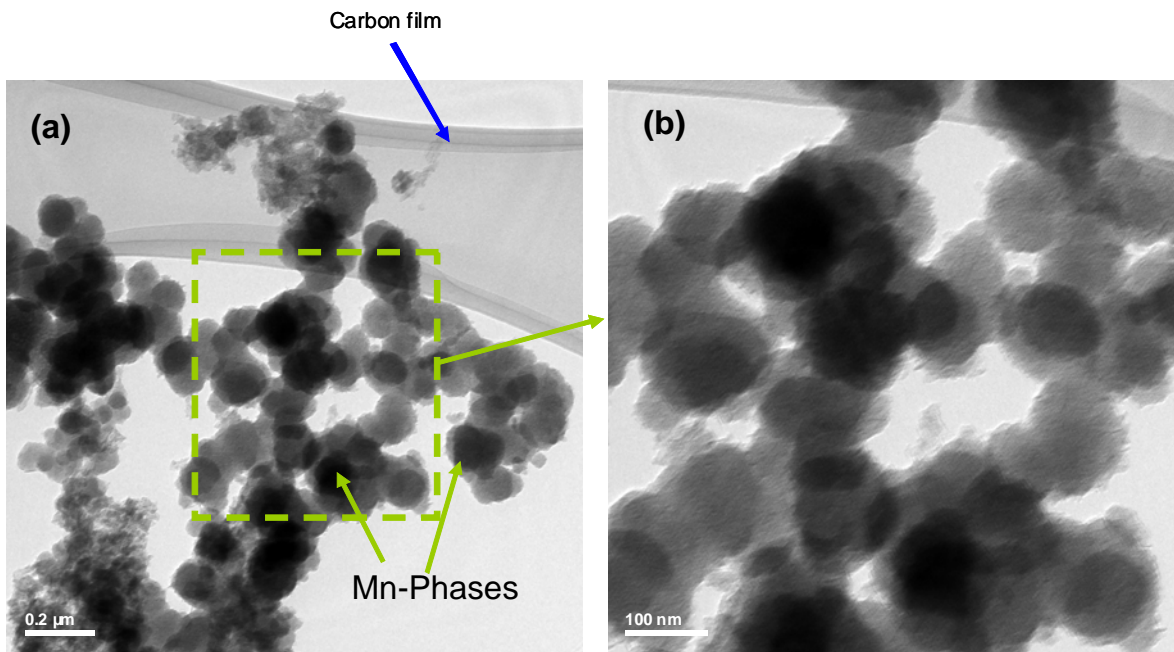


Figure 9.25. Low and High Magnification TEM Images of Manganese (Group 6 S-saltcake sample following oxidative leaching)

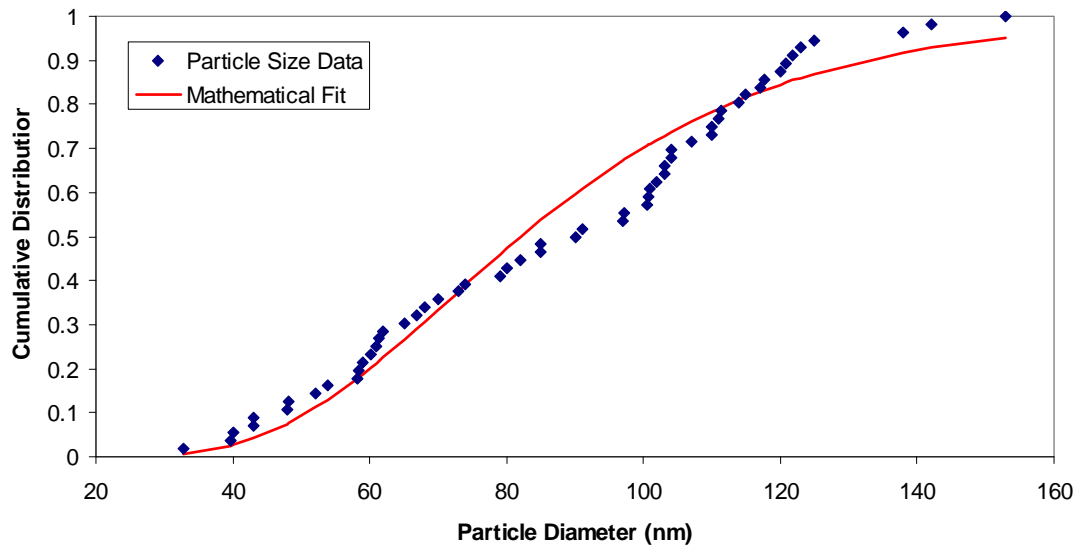


Figure 9.26. Cumulative Distribution Function that Describes the Probability of Particle Size from a Series of TEM Images of Manganese Particles (Group 6 S-saltcake following oxidative leaching)

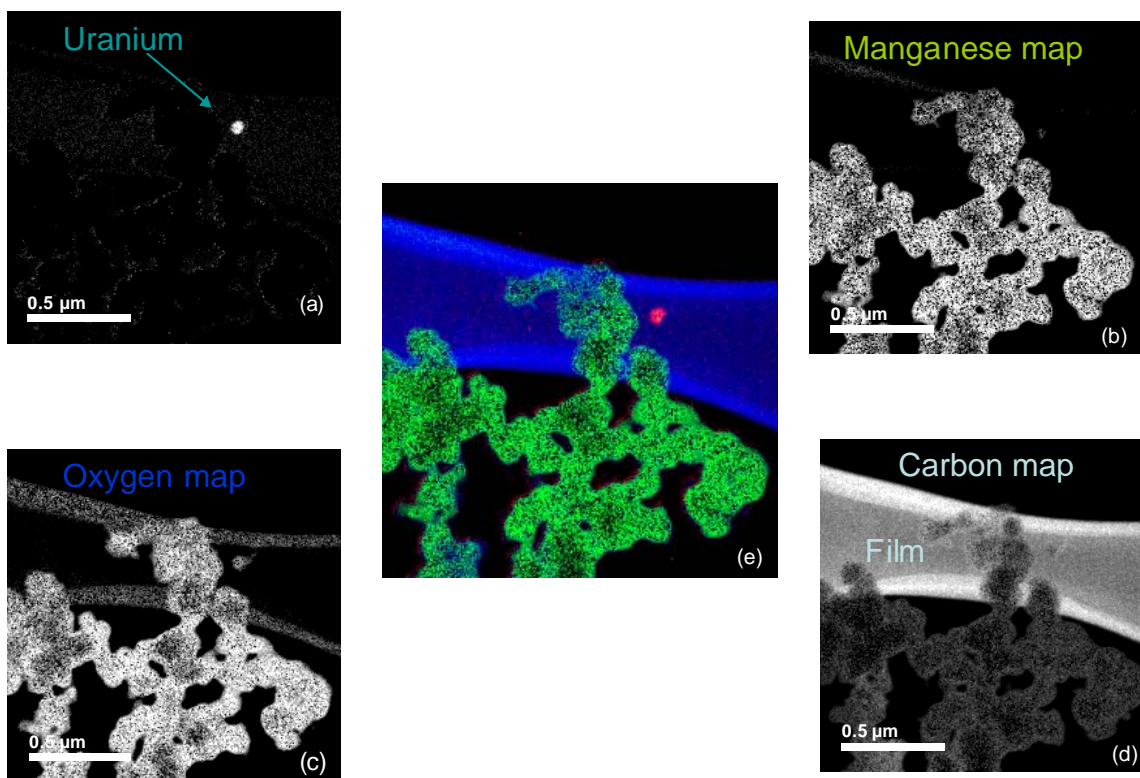


Figure 9.27. Energy-Filtered Images of G6-W-G Showing the Presence of a Nano-Particle of Uranium (Group 6 S-saltcake sample following oxidative leaching)

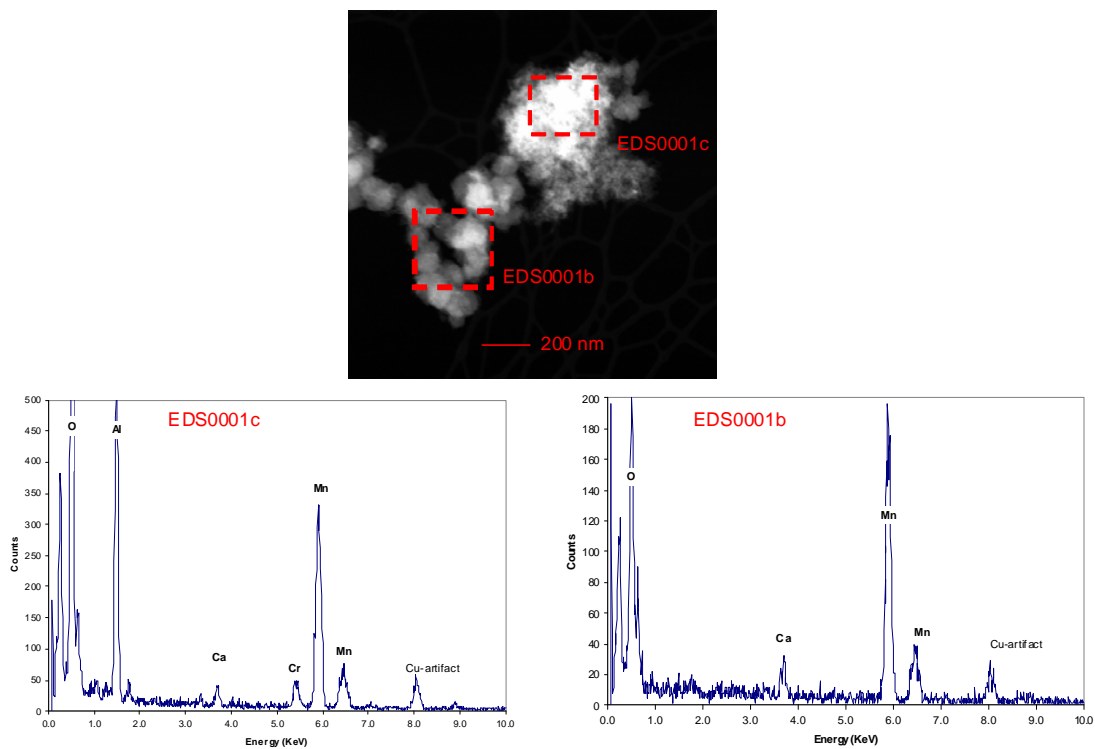


Figure 9.28. STEM and EDS Analysis of Regions in G6-W-G (Group 6 S-saltcake sample following oxidative leaching)

High magnification TEM images show lattice fringe indicating crystalline structure of particles

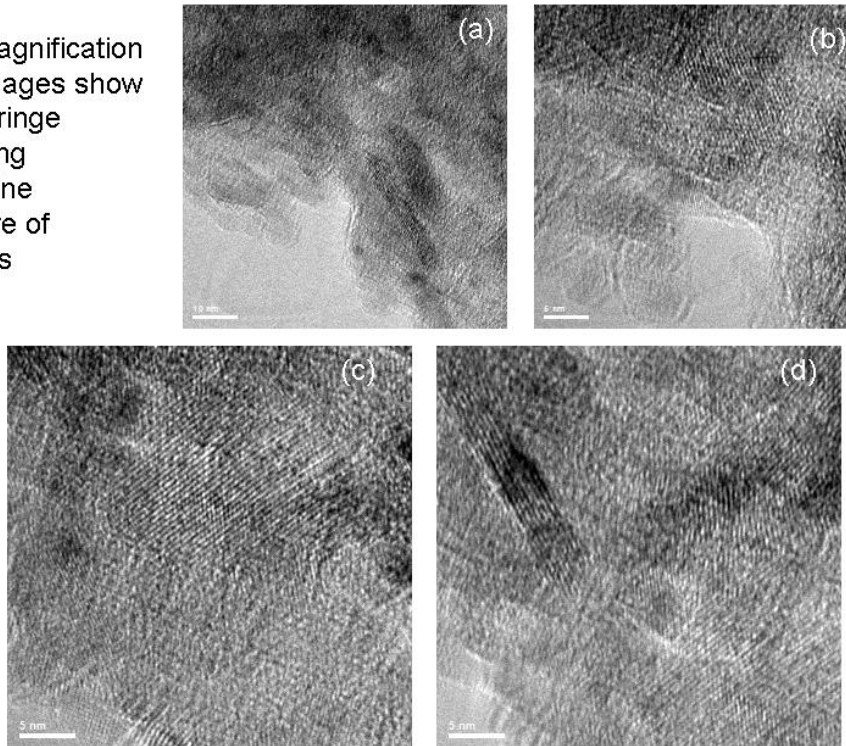


Figure 9.29. TEM Images from G6-W-G (Group 6 S-saltcake sample following oxidative leaching)

9.2.4.6 Surface Area by BET

BET measurements were conducted on the caustic-leached and washed solids and oxidatively leached and washed solids, resulting in identical surface areas of 154 and 155 m²/g, respectively. This shows an increase in relative surface area following caustic leaching from the average of 70 m²/g found in the initial, washed solids. The increased surface area of the caustic-leached material (Cr-rich fraction) further supports the small particle size attributed to the Cr species.

10.0 Summary

Tank waste sludge and saltcake at the Hanford Site have been categorized into eight general groupings representing ~75 wt% of the total high-level waste mass expected to be processed through the WTP. Two of the eight groups, Group 5 and Group 6, are the subject of this report. Group 5 represents REDOX waste containing a high fraction of boehmite; Group 6 represents S-Saltcake, which contains a large fraction of the tank waste chromium.

Multiple samples representative of these two waste groups, all of which had been stored for ~10 years, were identified in the 222S sample archive. Materials representative of Group 5 (and containing high Al) were obtained from archived samples from tanks S-101, S-110, S-107, and SX-103. Materials representative of Group 6 (and containing high Cr) were selected from archived samples from tanks SX-102, SX-105, SX-106, S-106, S-111, SY-103, U-103 and U-108. These materials were combined into their respective composite group using water to suspend solids during mixing and dissolve water-soluble species.

The tank waste composites were extensively characterized for physical properties, rheological properties, and chemical composition of the solids and liquid phases as well as the crystal habit of the insoluble solids. Table 10.1 summarizes the characterization results.

The Group 5 REDOX sludge waste was subjected to parametric caustic leach testing to understand boehmite dissolution characteristics and provide the basis for matching to a simulant boehmite material. Leaching was conducted in a 1:100 solids-mass to solution-volume ratio under varying hydroxide concentrations (1, 3, and 5 M), varying temperature (80, 90, and 100°C), and varying total sodium concentration (3, 4, and 8 M). Periodic sampling (1 to 170 hrs) and analysis was conducted to determine reaction rates at all reaction conditions. The following conclusions were obtained.

- Under the given test conditions, Al dissolution was estimated to be limited by the boehmite solubility at 1 M NaOH and temperatures of 80 and 90°C.
- Increasing Na concentration to 8 M (with NaNO₃) while maintaining constant free hydroxide concentration had no measureable effect on boehmite dissolution.
- Boehmite dissolution increased with increasing temperature and free hydroxide concentration. Initial boehmite dissolution rates were determined as shown in Table 10.2.
- An apparent activation energy of 25.2 kJ/mol was determined for the boehmite dissolution, significantly lower than the 123 kJ/mol reported by Scotford and Glastonbury (1971), suggesting that, under the current test conditions, the reaction rate is controlled primarily by mass transport (i.e., mixing) properties rather than chemical reaction at the boehmite particle surface, consistent with the small particle size and larger surface area observed in the boehmite present in the actual waste.
- Up to ~60% Cr dissolution occurred concomitantly with the boehmite dissolution during caustic leaching.
- The 8-hr Al leach factor at 3 M NaOH and 90°C (~0.32) was similar to that provided in the BBI for S-101 (0.357).

- An Al leach factor of 98% was obtained at leach conditions of 3 M free hydroxide, 90°C, 170 hrs. The leached solids were dominated by U with additional contributions from Al, Cr, Fe, Mn, Na, and Si. Selected analyte concentrations and leach factors are summarized in Table 10.3.
- The PSD of the leached solids resulted in a tri-modal pattern with maxima decreasing with increasing shear and increased aggregate formation with sonication.
- Approximately 95% of the Al will need to be removed from the Group 5 waste form to eliminate Al as the waste-loading limiting factor into product glass. This condition was met after a ~28-hr contact time with 5 M NaOH at 100°C. All other leaching conditions required significantly longer leaching duration.
- The PSD of the leached solids resulted in a tri-modal pattern with maxima decreasing with increasing shear and increased aggregate formation with sonication.
- Approximately 95% of the Al will need to be removed from the Group 5 waste form to eliminate Al as the waste-loading limiting factor into product glass. This condition was met after a ~28-hr contact time with 5 M NaOH at 100°C. All other leaching conditions required significantly longer leaching duration.

Table 10.1. Summary of Major Properties and Analytes of Group 5 REDOX Sludge and Group 6 S-Saltcake

Physical Properties	Group 5 REDOX Sludge	Group 6 S-Saltcake	
	Slurry	Concentrated Slurry Solids	Supernatant
Total slurry volume	3,450 mL	841 mL	2,240 mL
Total UDS	18.5 wt%	14.7 wt%	na
Bulk density	1.24 g/mL	1.38 g/mL	1.23 g/mL
Centrifuged solids	52 vol%	28.2 vol%	na
Shear strength ^(a)	72 Pa	20 Pa	na
Apparent viscosity ^(b)	>1,000 cP	8 cP	1.5 cP
Behavior	non-Newtonian	Newtonian	Newtonian
Bingham Yield Stress ^(c)	57 Pa	na	na
Bingham Consistency/ Newtonian Viscosity ^(c)	13 cP	8 cP	1.5 cP
Dominant Mineral Forms^(d)			
Boehmite	75 wt% small rhombohedral platelets	11 wt% small rhombohedral platelets	na
Gibbsite	5.8 wt%	47 wt%	na
Sodium uranium oxide	3 wt%	0.7 wt%	na
Chromium oxide	--	16 wt% small particles, high surface area, amorphous	na
Cancrinite	1.9 wt%	8.1 wt%	na
Other	14 wt%	17 wt%	na
PSD	2 maxima: 2 μm and 7 μm , range: 0.3–100 μm .	2 maxima 1–10 and 30–100 μm	na
Surface Area	26 m ² /g	70 m ² /g	na
(a) Strength of settled solids 48-72 hours after mixing.			
(b) Apparent viscosity taken at a shear rate of 33 s ⁻¹ .			
(c) At 25°C. Bingham-Plastic and Newtonian viscosity model parameters provide a conservative upper bound of the slurry/supernatant rheology. Please see Section 5 and 6 for more detail.			
(d) Mineral concentrations (wt%) were based on the washed dry solids.			

Major Analytes	Group 5 REDOX Sludge		Group 6 S-Saltcake	
	Solids, $\mu\text{g/g}^{(a)}$	Aqueous, $\mu\text{g/mL}$	Solids, $\mu\text{g/g}^{(a)}$	Aqueous, $\mu\text{g/mL}$
Al	326,500	2,595	187,000	7,590
Na	55,200	73,700	93,500	117,500
Cr	2,110	1,225	92,850	535
Fe	7,265	<2	14,700	<2
Mn	4,500	<0.2	4680	<0.2
Si	8,760	54	15,500	90
U	19,700	<9	6,575	<9
(a) Dry mass basis of washed solids.				

Table 10.2. Initial Al (Boehmite) Dissolution Rates

[NaOH], M	d[Al]/dt, mole L ⁻¹ h ⁻¹		
	80°C	90°C	100°C
1	5.26E-3	5.90E-3	8.16E-3
3	6.21E-3	6.59E-3	1.05E-2
5	7.02E-3	7.82E-3	1.30E-2

Table 10.3. Composition of Caustic-Leached Solids from Group 5 REDOX Sludge with Leach Factors of Selected Analytes (3 M NaOH, 90°C, 170 hrs)

Analyte	Leached Solids, µg/g ^(a)	Percent Leached	Analyte	Leached Solids, µCi/g ^(a)	Percent Leached
Al	83,675	98%	⁶⁰ Co	0.177	38%
B	<443	--	⁹⁰ Sr	8,900	0%
Bi	[1,125]	--	¹³⁷ Cs	7.63	98%
Ca ^(b)	22,975	80%	²³⁹⁺²⁴⁰ Pu	11.3	-2%
Cd	<39	--	²⁴¹ Am	3.99	26% ^(c)
Cr	9,770	54%	No data		
Fe	73,825	29%			
Mn	62,650	6%			
Na	[76,500]	--			
Ni	5,185	38%			
P	<664	--			
S	[3,921]	--			
Si	[17,875]	90%			
Sr	15,125	1%			
Zn	[268]	--			
U (KPA)	318,000	3%			

(a) Dry mass basis of washed solids.
(b) Measured opportunistically.
(c) Probable high bias; ²⁴¹Am was not detected in the aqueous phase.
Analyte uncertainties were typically within ±15% (2-σ); results in brackets indicate that the analyte concentrations were less than the minimum detection limit (MDL) and greater than the estimated quantitation limit (EQL), and uncertainties were >15%.
Radionuclide reference date: June 7, 2007.
"--" calculation could not be made from one or more "less-than" values.

The Group 6 S-Saltcake solids contained a high Cr concentration, which limits the waste glass loading. The Cr component was amorphous to XRD examination and was found to be very small in particle size as determined by TEM. The Cr mineralogical composition was assigned to be > 90 wt% Cr₂O₃ based on examination by TGA.

The Group 6 waste was subjected to caustic leaching and then parametric oxidative leach testing to determine the Cr and Pu dissolution characteristics and provide the basis for matching to a simulant insoluble chromium material. The parametric oxidative leach testing was in a 1:100 solids-mass to solution-volume ratio under varying MnO₄⁻/Cr mole ratios (0.75, 1.0, and 1.25), varying NaOH matrices (0.25, 1.25, and 3 M), and at two process temperatures (25 and 50°C). Periodic sampling (0.5 to 24 hrs)

and analysis were conducted to determine reaction rates at all reaction conditions. The following conclusions were obtained.

- Under all test conditions, >50% of the Cr was successfully mobilized to the aqueous phase within the first 30 min of contact time. Equilibrium conditions had been generally achieved within a 6-hr contact time.
- Cr dissolution was directly related to the MnO_4^-/Cr mole ratio; a 1:1 MnO_4^-/Cr mole ratio resulted in 90% Cr mobilization to the aqueous phase.
- Variation of NaOH concentration from 0.25 to 3 M and temperature from 25°C to 50°C did not significantly affect the Cr dissolution.
- Free hydroxide concentration was found to have a large effect on the Pu dissolution. There was a large (16×) increase in dissolution of Pu between 0.25 M NaOH and 1.25 M NaOH and a 20× increase as NaOH concentration increased from 0.25 M to 3 M at 25°C.
- The 1:1 MnO_4^-/Cr mole ratio resulted in a leached solid containing 21 wt% Mn (Table 10.4). Thus, although Cr is successfully removed through oxidative leaching, insoluble Mn solids are left behind in a stoichiometric ratio. The impact of these additional Mn-containing solids on downstream processing must be assessed.
- Removing 85% of the Cr (per the WTP baseline assumption) was calculated to result in ~6× decrease in waste glass production; however, the waste would still be Cr-limited with respect to glass loading. Blending of the Cr-leached Group 6 material with a low-Cr HLW feed should be considered to eliminate the Cr-constraint on glass loading.
- Note that a Cr leach factor of 88% was obtained at leach conditions of 1.25 M free hydroxide, 25°C, 24 hrs. The leached solids were dominated by Mn with additional contributions from Al, Cr, Fe, Mn, Na, and Si. Selected analyte concentrations and leach factors are summarized in Table 10.4.

Table 10.4. Composition of Leached Solids from Group 6 S-Saltcake with Leach Factors of Selected Analytes (caustic leach at 3 M NaOH and 100°C; oxidative leach at 1.25 M NaOH, 25°C, 24 hrs, Mn/Cr mole ratio of 1)

Analyte	Leached Solids, µg/g	Percent Leached	Analyte	Leached Solids, µg/g	Percent Leached
Al	82,500	83%	Sr	142	0%
B	<114	--	Zn	912	65%
Bi	[1,100]	12%	Zr	[475]	54%
Cd	352	4%	U (KPA)	12,700	-9%
Cr	28,425	88%	Analyte	Leached Solids, µCi/g	Percent Leached
Fe	35,125	9%			
Mn	214,000	na	²³⁸ Pu	0.38	-18%
Na	[76,500]	69%	²³⁹⁺²⁴⁰ Pu	2.45	-1%
Ni	2,450	10%	⁹⁰ Sr	749	-7%
Si	24,200	41%	²⁴¹ Am	13.1	-9%
Analyte uncertainties were typically within ±15% (2-σ); results in brackets indicate that the analyte concentration were less than the minimum detection limit (MDL) and greater than the estimated quantitation limit (EQL), and uncertainties were >15%. Radionuclide reference date: June 7, 2007. "--" calculation could not be made from one or more "less-than" values.					

Appendix A

Group 5 Parametric-Leach-Temperature Variation

Appendix A: Group 5 Parametric-Leach-Temperature Variation

On Thursday, April 12, 2007, during the 72-hr sampling of the 80°C Group 5 caustic leach testing, it was discovered that the temperature controller was not operating (the temperature controller was operating properly at the beginning of the 72-hr sampling operation). Upon investigation, it was determined that the thermocouple interfaced to the temperature controller had failed. A suitable calibrated thermocouple was not immediately available. In order to maintain temperature, the temperature controller and thermocouple were temporarily replaced with uncalibrated equipment. A thermocouple was taken to the PNNL Instrument Calibration Facility for urgent calibration. The latter thermocouple was calibrated and returned on the afternoon of April 12, 2007. However, when this thermocouple was connected to the calibrated temperature controller, the equipment still was not functioning properly. Because the normal daily work shift had ended by this time, the temperature was maintained with the uncalibrated equipment overnight.

On Friday, April 13, 2007, the problem with operating the new calibrated thermocouple was traced to a faulty connecting wire. The connecting wire was replaced, and control of the heating block was transferred back to the calibrated equipment (this was completed at ~8:15 am). Throughout the day on April 13, the temperatures were recorded for both the non-calibrated and the newly calibrated thermocouples and temperature controllers. Within the calibration uncertainty, the temperature values were the same. The results are shown in Table A.1.

Table A.1. Temperature Assessment for Group 5 80°C Caustic Leach Test After Initial Thermocouple Failure

Time ^(a)	Temperature, °C		
	Calibrated Thermocouple	Non-Calibrated Thermocouple	Difference
8:45	77.5	76.6	0.9
9:15	80.9	79.6	1.3
9:45	80.6	79.2	1.4
10:55	79.9	78.5	1.4
11:50	80.1	78.7	1.4
14:20	80.1	78.6	1.5
15:30	80.0	78.5	1.5
15:50	80.5	78.9	1.6

(a) Time represented leach interval of 96 hr through 103 hr.

On the final day of the 80°C caustic-leach test (Monday, April 16), it was discovered at 7:55 am that the temperature controller was not operating. The temperature in the heating block had fallen to 22°C. The last time the temperature had been checked was at 6:30 pm on the preceding Friday, April 13. The

controller was re-set and returned back to temperature. As a result, the data taken at 170 hours for the 80°C test are to be used for indication only.

A Corrective Action Report (CAR) was submitted to WTP describing the loss of temperature control (CAR # 21094.4).

Appendix B

Group 5 Parametric Analytical Results from Parametric Leaching

Appendix B: Group 5 Parametric Analytical Results from Parametric Leaching

Table B.1. Analyte Concentrations as a Function of Time for Leaching at 80°C

Analyte	Analyte Concentration and Density at Given Time and Ambient (~21°C) Temperature; g/mL for Density; µg/mL for Metals and Anions; µCi/mL for Radionuclides					
	1 hr	4 hr	8 hr	24 hr	72 hr	170 hr
1 M NaOH						
Density	1.060	1.065	1.071	1.075	1.081	1.083
Al	188	777	1,197	2,070	3,336	4,205
Cr	[1.68]	[3.39]	4.86	6.51	8.46	9.76
Fe	<2.6	<2.6	<2.6	[4.65]	[3.4]	[2.6]
Na	22,811	23,759	24,245	24,137	25,480	26,490
P	[10.0]	<6.9	[10.8]	[10.8]	[14.2]	[11.4]
Si	31.3	73.7	73.5	66.3	68.0	70.6
Fluoride	0.96	0.97	0.97	0.96	0.96	0.96
Nitrite	1.82	2.02	2.12	2.19	2.42	2.69
Nitrate	27.5	41.1	40.2	39.9	39.0	43.0
Phosphate	8.35	6.85	7.16	7.11	7.12	7.43
Sulfate	2.32	2.34	2.34	2.32	2.32	2.32
⁶⁰ Co						<3E-6
¹³⁷ Cs						0.456
²⁴¹ Am						<3E-4
3 M NaOH						
Density	1.134	1.166	1.142	1.151	1.159	1.152
Al	243	993	1,437	2,792	4,443	5,501
Cr	[2.50]	5.45	6.18	8.50	10.2	11.6
Fe	<2.6	[3.73]	[4.64]	[12.4]	[20.7]	[14.6]
Na	70,370	72,502	72,643	75,084	76,517	80,836
P	10.2	10.6	9.89	<7.0	8.64	11.6
Si	49.1	109	111	117	122	129
Fluoride	0.96	1.02	0.99	0.96	0.96	0.97
Nitrite	1.55	1.54	1.55	1.55	1.55	1.56
Nitrate	40.6	65.8	64.9	67.9	69.7	73.9
Phosphate	9.29	9.89	10.2	13.0	12.7	15.3
Sulfate	2.32	2.32	2.33	2.32	2.32	2.34
⁶⁰ Co						<3E-6
¹³⁷ Cs						0.545
²⁴¹ Am						<3E-4
5 M NaOH						
Density	1.219	1.249	1.215	1.218	1.148	1.238
Al	214	1,099	1,567	2,894	4,877	5,219
Cr	[2.46]	5.65	6.50	8.42	11.2	10.9
Fe	<2.6	[5.59]	[8.36]	[18.8]	35.1	28.6
Na	118,898	122,302	118,935	120,620	134,293	122,502

Table B.1 (Contd)

Analyte	Analyte Concentration and Density at Given Time and Ambient (~21°C) Temperature g/mL for Density; µg/mL for Metals and Anions; µCi/mL for Radionuclides					
	1 hr	4 hr	8 hr	24 hr	72 hr	170 hr
P	[8.01]	[8.38]	[8.36]	[11.4]	[13.4]	[9.21]
Si	53.3	113.3	114.6	118.5	137.6	130.5
Fluoride	0.96	0.96	0.96	0.96	0.89	0.96
Nitrite	1.55	1.55	1.55	1.56	1.44	1.55
Nitrate	50.0	73.1	74.1	76.2	66.5	73.3
Phosphate	3.42	9.30	2.63	4.04	3.45	11.4
Sulfate	2.33	2.32	2.32	2.33	2.16	2.32
⁶⁰ Co						<3E-6
¹³⁷ Cs						0.496
²⁴¹ Am						<3E-4

Table B.2. Analyte Concentrations as a Function of Time for Leaching at 90°C

Analyte	Analyte Concentration and Density at Given Time and Ambient (~21°C) Temperature; g/mL for Density; µg/mL for Metals and Anions; µCi/mL for Radionuclides					
	1 hr	4 hr	8 hr	24 hr	72 hr	170 hr
1 M NaOH						
Density	1.063	1.070	1.076	1.071	1.070	1.108
Al	393	1,065	1,524	2,521	3,822	4,871
Cr	[2.37]	[4.27]	5.39	7.26	8.13	10.4
Fe	<2.6	<2.6	[2.91]	[6.43]	[3.01]	[3.06]
Na	24,444	24,557	25,344	25,153	26,185	27,203
P	<4.7	<6.9	[8.57]	<6.9	<6.8	<6.9
Si	83.2	87.2	85.7	83.6	80.4	77.8
Fluoride	[0.96]	[0.96]	[0.96]	[0.96]	[0.97]	[0.95]
Nitrite	2.20	2.26	2.29	2.34	2.52	2.71
Nitrate	49.9	49.9	49.5	48.4	50.1	49.0
Phosphate	22.9	7.74	8.35	8.33	7.79	6.77
Sulfate	2.32	2.32	2.32	2.31	2.34	2.31
⁶⁰ Co						<3E-6
¹³⁷ Cs						0.477
²⁴¹ Am						<3E-4
3 M NaOH, Trial a						
Density	1.142	1.155	1.155	1.155	1.135	1.182
Al	541	1,256	1,910	3,385	4,926	5,343
Cr	[3.38]	5.48	7.25	8.66	10.1	10.5
Fe	<2.6	[4.62]	[7.96]	[18.6]	[18.3]	[11.1]
Na	72,170	73,550	74,070	73,800	74,810	74,010
P	<7.0	<7.0	[7.65]	[8.54]	[7.30]	[8.91]
Si	92.5	106	111	112	112	107
Fluoride	[0.96]	[0.96]	[0.96]	[0.96]	[0.96]	[0.95]
Nitrite	[1.55]	[1.54]	[1.54]	[1.55]	[1.54]	[1.53]
Nitrate	59.0	67.2	65.2	66.1	62.9	61.3
Phosphate	9.27	9.86	12.67	11.2	11.7	13.2

Table B.2 (Contd)

Analyte	Analyte Concentration and Density at Given Time and Ambient (~21°C) Temperature g/mL for Density; µg/mL for Metals and Anions; µCi/mL for Radionuclides					
	1 hr	4 hr	8 hr	24 hr	72 hr	170 hr
Sulfate	[2.32]	[2.31]	[2.32]	[2.33]	[2.31]	[2.30]
⁶⁰ Co						<3E-6
¹³⁷ Cs						0.453
²⁴¹ Am						<4E-4
3 M NaOH, Trial b						
Density	1.144	1.149	1.154	1.158	1.137	1.162
Al	477	1,114	1,651	3,095	4,446	5,366
Cr	[3.07]	5.75	6.64	8.58	10.0	11.0
Fe	<2.6	[3.98]	[6.15]	[15.3]	[18.7]	[11.6]
Na	66,720	73,150	72,560	72,920	72,050	73,900
P	[8.30]	[8.57]	[7.99]	<7.1	<7.1	[9.51]
Si	89.2	114	116	118	122	130
Fluoride	1.05	0.99	0.96	[0.96]	[0.95]	[0.95]
Nitrite	[1.54]	[1.54]	[1.54]	[1.54]	[1.53]	[1.53]
Nitrate	61.4	67.1	66.9	66.9	64.8	65.2
Phosphate	9.56	17.6	10.5	11.4	11.6	11.6
Sulfate	[2.31]	[2.32]	[2.31]	[2.31]	[2.29]	[2.30]
⁶⁰ Co						<3E-6
¹³⁷ Cs						0.499
²⁴¹ Am						<2E-4
3 M NaOH, Trial c						
Density	1.145	1.137	1.153	1.162	1.146	1.164
Al	473	1,077	1,691	3,155	4,608	5,328
Cr	3.38	5.38	6.35	8.69	9.49	10.4
Fe	[2.67]	[3.98]	[6.45]	[16.4]	[18.0]	[10.9]
Na	72,182	70,976	72,742	72,689	73,247	74,768
P	<7.0	<7.0	<7.0	<7.0	7.94	<6.9
Si	97.4	104	108	110	108	108
Fluoride	[0.96]	1.05	1.94	1.28	[0.95]	[0.96]
Nitrite	[1.54]	[1.55]	[1.54]	[1.53]	[1.53]	[1.56]
Nitrate	64.8	66.5	67.4	70.9	68.6	74.0
Phosphate	11.4	12.1	8.00	11.3	11.6	13.1
Sulfate	[2.31]	[2.32]	[2.31]	[2.29]	[2.30]	[2.33]
⁶⁰ Co						<3E-6
¹³⁷ Cs						0.480
²⁴¹ Am						<2E-4
3 M NaOH, 1 M NaNO₃						
Density	1.211	1.194	1.184	1.181	1.201	1.190
Al	561	1,281	2,040	3,477	5,016	5,105
Cr	3.01	5.98	7.15	8.62	10.2	10.1
Fe	[1.99]	[5.49]	[10.0]	[18.1]	[9.55]	[6.40]
Na	97,209	95,760	96,702	96,409	97,934	97,106
P	<7.0	<6.9	<6.9	<6.6	<6.7	<7.1

Table B.2 (Contd)

Analyte	Analyte Concentration and Density at Given Time and Ambient (~21°C) Temperature g/mL for Density; µg/mL for Metals and Anions; µCi/mL for Radionuclides					
	1 hr	4 hr	8 hr	24 hr	72 hr	170 hr
Si	51.8	53.4	48.3	37.1	29.0	23.9
Fluoride	[9.45]	[9.48]	[9.53]	[9.81]	[9.68]	[9.22]
Nitrite	[15.2]	[15.3]	[15.4]	[15.8]	[15.6]	[14.9]
Nitrate	68,565	67,277	67,608	67,401	68,680	69,038
Phosphate	23.8	18.3	18.4	19.0	18.7	17.8
Sulfate	[22.9]	[22.9]	[23.0]	[23.7]	[23.4]	[22.3]
⁶⁰ Co						<3E-6
¹³⁷ Cs						0.328
²⁴¹ Am						<4E-4
3 M NaOH, 5 M NaNO₃						
Density	1.355	1.402	1.378	1.370	1.395	1.420
Al	379	1,107	1,837	3,319	4,494	4,959
Cr	[3.44]	[5.79]	[6.74]	[8.83]	9.54	10.4
Fe	<5.3	[5.18]	[10.1]	[22.8]	[11.0]	[7.56]
Na	179,041	190,874	188,342	186,062	183,143	194,413
P	<14	<14	<14	<14	<14	<14
Si	39.75	39.94	33.99	[23.5]	[15.3]	[14.2]
Fluoride	[48.0]	[49.1]	[48.8]	[48.4]	[48.8]	[49.1]
Nitrite	74.9	76.7	76.2	75.7	76.3	76.7
Nitrate	317,781	337,519	332,277	330,052	326,541	346,834
Phosphate	[89.9]	[92.1]	[91.5]	[90.8]	[91.6]	[92.1]
Sulfate	[111]	[114]	[76.2]	[112]	[113]	[114]
⁶⁰ Co						<3E-6
¹³⁷ Cs						0.283
²⁴¹ Am						<4E-4
5 NaOH						
Density	1.220	1.218	1.197	1.192	1.107	1.227
Al	658	1,408	2,146	3,752	4,631	5,145
Cr	[4.31]	6.54	7.60	9.62	9.92	11.1
Fe	[3.69]	[8.25]	[13.2]	27.6	30.9	[23.9]
Na	116,870	117,576	114,672	117,465	110,337	118,629
P	[8.30]	<7.0	[8.28]	[8.30]	[7.43]	[7.26]
Si	96.0	110	113	119	116	128
Fluoride	[0.94]	[0.95]	[0.94]	[0.93]	[1.02]	[0.95]
Nitrite	[1.52]	[1.53]	[1.52]	[1.50]	[1.64]	[1.53]
Nitrate	56.4	61.3	61.9	61.3	55.1	61.1
Phosphate	12.5	5.83	3.96	4.81	3.61	3.99
Sulfate	[2.29]	[2.30]	[2.29]	[2.26]	[2.46]	[2.30]
⁶⁰ Co						<3E-6
¹³⁷ Cs						0.464
²⁴¹ Am						<4E-4

Table B.3. Analyte Concentrations as a Function of Time for Leaching at 100°C

Analyte	Analyte Concentration and Density at Given Time and Ambient (~21°C) Temperature; g/mL for Density; µg/mL for Metals and Anions; µCi/mL for Radionuclides					
	1 hr	4 hr	8 hr	24 hr	72 hr	170 hr
1 M NaOH						
Density	1.070	1.112	1.100	1.085	1.081	1.089
Al	559	1,654	2,358	3,681	4,837	5,344
Cr	[2.83]	5.35	6.96	8.65	10.3	11.6
Fe	<2.6	[3.44]	[6.81]	[5.22]	[3.39]	[3.06]
Na	24,446	25,457	24,761	24,911	24,830	25,485
P	<4.8	[8.44]	<7.0	<7.0	[10.5]	[7.10]
Si	88.6	91.9	88.2	89.9	83.8	72.9
Fluoride	[1.13]	[1.13]	[1.12]	[1.12]	[1.12]	[1.13]
Nitrite	2.68	2.74	2.60	2.59	2.66	2.78
Nitrate	54.4	55.3	53.5	48.5	46.8	50.8
Phosphate	10.7	8.34	8.27	7.07	5.90	4.74
Sulfate	[2.68]	[2.68]	[2.66]	[2.65]	[2.66]	[2.67]
⁶⁰ Co						<3E-6
¹³⁷ Cs						0.437
²⁴¹ Am						<4E-4
3 M NaOH						
Density	1.104	1.197	1.178	1.176	1.178	1.162
Al	519	1,767	2,842	4,515	5,350	5,421
Cr	[3.42]	6.94	8.58	9.83	10.7	11.5
Fe	<2.6	[7.57]	[14.7]	[24.7]	[15.1]	[11.2]
Na	69,259	74,158	73,559	73,602	73,796	74,031
P	<7.1	<7.1	<7.1	[7.73]	<7.0	<7.0
Si	106	122	122	123	122	122
Fluoride	[1.14]	[1.14]	[1.12]	[1.12]	1.19	1.48
Nitrite	2.16	1.98	2.06	2.00	2.08	2.31
Nitrate	70.9	74.9	68.9	69.5	65.5	64.7
Phosphate	9.61	13.2	12.4	12.4	14.3	12.5
Sulfate	[2.70]	[2.70]	[2.65]	[2.65]	[2.68]	[2.67]
⁶⁰ Co						<3E-6
¹³⁷ Cs						0.483
²⁴¹ Am						<2E-4
5 M NaOH						
Density	1.232	1.267	1.263	1.223	1.259	1.250
Al	734	2,478	3,605	5,022	5,452	5,595
Cr	[4.34]	7.90	9.48	10.8	11.2	12.3
Fe	[3.72]	[16.8]	27.0	40.0	36.6	26.8
Na	119,890	126,724	123,684	121,838	124,226	128,275
P	<7.0	<7.2	<7.0	<7.0	<7.0	[9.27]
Si	93.9	123	124	126	130	134
Fluoride	[1.14]	[1.14]	[1.13]	[1.12]	[1.12]	[1.13]
Nitrite	[1.80]	[1.80]	[1.78]	[1.77]	[1.77]	1.78]
Nitrate	64.8	76.1	74.7	68.2	73.2	80.3
Phosphate	3.54	2.94	3.08	3.94	3.72	4.22

Table B.3 (Contd)

Analyte	Analyte Concentration and Density at Given Time and Ambient (~21°C) Temperature g/mL for Density; µg/mL for Metals and Anions; µCi/mL for Radionuclides					
	1 hr	4 hr	8 hr	24 hr	72 hr	170 hr
Sulfate	[2.70]	[2.70]	[2.67]	[2.65]	[2.65]	[2.68]
⁶⁰ Co						<3E-6
¹³⁷ Cs						0.487
²⁴¹ Am						<5E-4

Appendix C

Group 6 Parametric Leach Data

Appendix C: Group 6 Parametric Leach Data

Table C.1 and Table C.2 show the total Cr, Cr(VI), Al, B, Cd, Fe, Mn, Ni, Si, U and Pu concentrations during oxidative leaching.

Table C.1. Tabulated Conditions and Results at 25°C with Comparison of Cr(VI) and Total Cr Concentrations and Metals and Pu (3 pages)

Process Conditions			Concentration, M			Concentration, M									²³⁹⁺²⁴⁰ Pu, $\mu\text{Ci/mL}$
[NaOH], M	Mn/Cr, Mole Ratio	Time, h	Total Cr	Cr (VI) ^(a)	% Diff.	Al	B	Cd	Fe	Mn	Ni	Si	U		
0.25	0.75	0.5	1.31E-2	1.26E-2	3.8	3.85E-3	[4.59E-5]	<5.5E-7	<9.4E-6	[1.44E-6]	<2.5E-6	3.07E-4	<9.0E-6	na	
		1	1.36E-2	1.26E-2	7.4	4.11E-3	[5.50E-5]	<5.6E-7	<9.5E-6	[1.48E-6]	<2.6E-6	3.09E-4	<9.1E-6		
		2	1.38E-2	1.26E-2	8.7	4.29E-3	[7.16E-5]	<5.5E-7	<9.4E-6	[9.58E-7]	<2.5E-6	3.26E-4	[1.24E-5]		
		4	1.41E-2	1.30E-2	7.8	4.52E-3	[6.11E-5]	<5.6E-7	<9.5E-6	<9.7E-7	<2.6E-6	3.61E-4	<9.2E-6		
		6	1.37E-2	1.31E-2	4.4	4.53E-3	[6.24E-5]	<5.5E-7	<9.3E-6	<9.5E-7	<2.5E-6	4.05E-4	<8.9E-6		
		24	1.66E-2	1.33E-2	19.9	6.26E-3	[7.38E-5]	<6.5E-7	<1.1E-5	<1.1E-6	<3.0E-6	7.69E-4	<1.1E-5		
0.25	1.0	0.5	1.54E-2	1.44E-2	6.5	4.54E-3	[7.47E-5]	<5.5E-7	<9.4E-6	3.01E-3	<2.5E-6	3.53E-4	<9.1E-6	na	
		1	1.62E-2	1.49E-2	8.0	4.87E-3	[7.35E-5]	[5.43E-7]	<9.2E-6	2.52E-3	<2.5E-6	3.73E-4	<8.9E-6		
		2	1.65E-2	1.51E-2	8.5	4.99E-3	[7.21E-5]	<5.5E-7	<9.4E-6	2.57E-3	<2.6E-6	3.75E-4	<9.1E-6		
		4	1.72E-2	1.57E-2	8.7	5.66E-3	[7.52E-5]	<5.6E-7	<9.5E-6	1.12E-3	<2.6E-6	4.26E-4	<9.1E-6		
		6	1.72E-2	1.58E-2	8.1	5.91E-3	[7.73E-5]	<5.5E-7	<9.4E-6	5.97E-4	<2.5E-6	4.52E-4	<9.0E-6		
		24	1.81E-2	1.71E-2	5.5	7.32E-3	[7.41E-5]	[5.48E-7]	<9.3E-6	[4.15E-6]	<2.5E-6	5.83E-4	<9.0E-6		
		48	1.84E-2	1.78E-2	3.3	8.14E-3	[8.02E-5]	<5.51E-7	<9.4E-6	<9.6E-7	<2.5E-6	6.05E-4	<9.0E-6		
0.25	1.25	0.5	1.73E-2	1.60E-2	7.5	4.93E-3	[7.24E-5]	<5.6E-7	<9.5E-6	1.84E-3	<2.6E-6	3.54E-4	<9.1E-6	1.60E-4	
		1	1.78E-2	1.61E-2	9.6	5.22E-3	[9.69E-5]	[6.85E-7]	<9.3E-6	6.50E-4	<2.5E-6	3.89E-4	<9.0E-6	1.53E-4	
		2	1.89E-2	1.67E-2	11.6	5.68E-3	[1.01E-4]	[6.08E-7]	<9.4E-6	4.71E-3	<2.5E-6	3.93E-4	<9.1E-6	1.50E-4	
		4	1.94E-2	1.74E-2	10.3	6.07E-3	[9.86E-5]	<5.6E-7	<9.5E-6	4.03E-4	<2.6E-6	4.15E-4	<9.1E-6	1.51E-4	
		6	2.00E-2	1.81E-2	9.5	6.51E-3	[9.23E-5]	<5.6E-7	<9.4E-6	2.08E-3	<2.6E-6	4.23E-4	<9.1E-6	1.74E-4	
		24	2.11E-2	1.93E-2	8.5	8.04E-3	[9.76E-5]	<5.5E-7	<9.4E-6	2.11E-3	<2.5E-6	4.96E-4	<9.0E-6	1.89E-4	
1.25	0.75	0.5	1.30E-2	1.31E-2	0.8	4.94E-3	[2.76E-4]	<2.7E-6	<4.6E-5	<4.7E-6	<1.3E-5	1.33E-3	<4.5E-5	na	
		1	1.29E-2	1.33E-2	3.1	5.26E-3	[2.26E-4]	<2.7E-6	[2.25E-4]	<4.7E-6	<1.3E-5	1.57E-3	<4.5E-5		
		2	1.30E-2	1.35E-2	3.8	5.71E-3	[2.16E-4]	<2.7E-6	<4.6E-5	<4.8E-6	<1.3E-5	1.98E-3	<4.5E-5		
		4	1.32E-2	1.35E-2	2.3	6.59E-3	<2.2E-4	<2.7E-6	<4.7E-5	<4.8E-6	<1.3E-5	2.60E-3	<4.5E-5		

C.1

Table C.1. Tabulated Conditions and Results at 25°C with Comparison of Cr(VI) and Total Cr Concentrations and Metals and Pu (3 pages)

Process Conditions			Concentration, M			Concentration, M								²³⁹⁺²⁴⁰ Pu, $\mu\text{Ci/mL}$
[NaOH], M	Mn/Cr, Mole Ratio	Time, h	Total Cr	Cr (VI) ^(a)	% Diff.	Al	B	Cd	Fe	Mn	Ni	Si	U	
		6	1.34E-2	1.32E-2	1.5	7.21E-3	<2.2E-4	<2.8E-6	<4.7E-5	<4.8E-6	<1.3E-5	2.86E-3	<4.5E-5	
		24	1.37E-2	1.40E-2	2.2	8.91E-3	<2.2E-4	<2.8E-6	<4.7E-5	<4.8E-6	<1.3E-5	3.72E-3	<4.5E-5	
1.25	1.0 Trial a	0.5	1.67E-2	1.66E-2	0.6	5.98E-3	<2.2E-4	<2.7E-6	<4.6E-5	[4.47E-5]	<1.2E-5	1.58E-3	<4.4E-5	na
		1	1.74E-2	1.70E-2	2.3	6.40E-3	<2.2E-4	<2.8E-6	<4.7E-5	<4.8E-6	[1.80E-5]	1.86E-3	<4.5E-5	
		2	1.75E-2	1.70E-2	2.9	6.85E-3	<2.2E-4	<2.8E-6	<4.7E-5	<4.9E-6	<1.3E-5	2.32E-3	<4.6E-5	
		4	1.77E-2	1.72E-2	2.8	7.51E-3	<2.1E-4	[3.79E-6]	<4.6E-5	<4.7E-6	[1.30E-5]	2.56E-3	<4.4E-5	
		6	1.74E-2	1.75E-2	0.6	7.88E-3	<2.2E-4	<2.7E-6	<4.7E-5	<4.8E-6	<1.3E-5	3.43E-3	<4.5E-5	
		24	1.71E-2	1.70E-2	0.6	9.41E-3	<2.1E-4	<2.7E-6	<4.6E-5	<4.7E-6	<1.2E-5	3.46E-3	<4.4E-5	
1.25	1.0 Trial b	0.5	1.63E-2	1.59E-2	2.5	5.82E-3	<2.1E-4	<2.7E-6	<4.5E-5	7.97E-4	<1.2E-5	1.31E-3	<4.4E-5	na
		1	1.72E-2	1.68E-2	2.3	6.37E-3	<2.1E-4	<2.7E-6	<4.6E-5	<4.7E-6	<1.2E-5	1.49E-3	<4.4E-5	
		2	1.71E-2	1.70E-2	0.6	6.73E-3	<2.1E-4	<2.7E-6	<4.6E-5	<4.7E-6	[1.60E-5]	1.78E-3	<4.4E-5	
		4	1.77E-2	1.69E-2	4.5	7.51E-3	<2.1E-4	[4.10E-6]	<4.7E-5	<4.8E-6	<1.3E-5	2.21E-3	<4.5E-5	
		6	1.75E-2	1.68E-2	4.0	7.96E-3	[2.56E-4]	<2.6E-6	<4.5E-5	<4.6E-6	[1.35E-5]	2.60E-3	<4.3E-5	
		24	1.79E-2	1.69E-2	5.6	9.94E-3	[2.43E-4]	2.78E-06	<4.7E-5	<4.8E-6	[1.28E-5]	3.60E-3	<4.5E-5	
1.25	1.0 Trial c	0.5	1.65E-2	1.62E-2	1.8	5.83E-3	<2.2E-4	<2.7E-6	<4.7E-5	1.17E-3	[1.52E-5]	1.29E-3	<4.5E-5	na
		1	1.73E-2	1.62E-2	6.4	6.37E-3	<2.1E-4	<2.7E-6	<4.7E-5	8.27E-4	[1.78E-5]	1.47E-3	<4.5E-5	
		2	1.72E-2	1.60E-2	7.0	6.82E-3	[2.19E-4]	[3.29E-6]	<4.7E-5	4.85E-4	[1.99E-5]	1.71E-3	<4.5E-5	
		4	1.71E-2	1.62E-2	5.3	7.64E-3	<2.1E-4	<2.7E-6	<4.6E-5	2.14E-4	[1.76E-5]	2.16E-3	<4.4E-5	
		6	1.75E-2	1.63E-2	6.9	8.35E-3	<2.1E-4	[3.77E-6]	<4.6E-5	[4.58E-5]	[1.91E-5]	2.57E-3	<4.4E-5	
		24	1.79E-2	1.68E-2	6.1	1.04E-2	<2.1E-4	[2.71E-6]	<4.6E-5	<4.7E-6	[1.56E-5]	3.37E-3	<4.4E-5	
1.25	1.25	0.5	1.84E-2	1.81E-2	1.6	6.53E-3	<2.2E-4	<2.7E-6	<4.7E-5	2.96E-3	<1.3E-5	1.38E-3	<4.5E-5	2.28E-3
		1	1.87E-2	1.86E-2	0.5	6.93E-3	<2.1E-4	<2.7E-6	<4.6E-5	3.10E-3	<1.3E-5	1.52E-3	<4.5E-5	2.35E-3
		2	1.90E-2	1.91E-2	0.5	7.57E-3	<2.2E-4	<2.8E-6	<4.7E-5	3.50E-3	<1.3E-5	1.76E-3	<4.5E-5	2.60E-3
		4	1.91E-2	1.88E-2	1.6	8.64E-3	<2.2E-4	<2.8E-6	<4.7E-5	3.26E-3	<1.3E-5	2.19E-3	<4.5E-5	2.66E-3
		6	1.98E-2	1.86E-2	6.1	9.48E-3	<2.2E-4	<2.8E-6	<4.7E-5	2.27E-3	<1.3E-5	1.41E-3	<4.5E-5	2.74E-3
		24	1.94E-2	1.87E-2	3.6	1.17E-2	<2.1E-4	<2.7E-6	<4.6E-5	3.13E-3	<1.3E-5	3.09E-3	<4.5E-5	3.07E-3

Table C.1. Tabulated Conditions and Results at 25°C with Comparison of Cr(VI) and Total Cr Concentrations and Metals and Pu (3 pages)

Process Conditions			Concentration, M			Concentration, M								²³⁹⁺²⁴⁰ Pu, $\mu\text{Ci/mL}$
[NaOH], M	Mn/Cr, Mole Ratio	Time, h	Total Cr	Cr (VI) ^(a)	% Diff.	Al	B	Cd	Fe	Mn	Ni	Si	U	
3.0	0.75	0.5	1.27E-2	1.30E-2	2.4	6.81E-3	[2.59E-4]	<2.7E-6	<4.6E-5	<4.7E-6	[1.92E-5]	2.95E-3	<4.4E-5	na
		1	1.29E-2	1.29E-2	0	7.24E-3	[2.84E-4]	<2.7E-6	<4.7E-5	<4.8E-6	[1.47E-5]	3.26E-3	<4.5E-5	
		2	1.28E-2	1.30E-2	1.6	7.64E-3	[2.14E-4]	<2.7E-6	<4.5E-5	<4.7E-6	<1.3E-5	3.59E-3	<4.4E-5	
		4	1.27E-2	1.29E-2	1.6	8.29E-3	<2.1E-4	<2.6E-6	<4.5E-5	<4.6E-6	<1.2E-5	4.15E-3	<4.3E-5	
		6	1.33E-2	1.33E-2	0	9.31E-3	<2.6E-4	<2.7E-6	<4.6E-5	<4.7E-6	<1.2E-5	4.76E-3	<4.4E-5	
		24	1.33E-2	1.35E-2	1.5	1.07E-2	<2.1E-4	<2.7E-6	<4.6E-5	<4.7E-6	[1.60E-5]	5.83E-3	<4.4E-5	
3.0	1.0	0.5	1.70E-2	1.66E-2	2.4	8.08E-3	<2.1E-4	<2.7E-6	<4.6E-5	<4.7E-6	<1.2E-5	3.17E-3	<4.4E-5	na
		1	1.69E-2	1.69E-2	0	8.38E-3	<2.4E-4	<2.7E-6	<4.5E-5	<4.6E-6	<1.2E-5	3.44E-3	<4.4E-5	
		2	1.72E-2	1.69E-2	1.7	9.03E-3	<2.1E-4	<2.7E-6	<4.5E-5	<4.7E-6	<1.2E-5	3.78E-3	<4.4E-5	
		4	1.71E-2	1.74E-2	1.8	9.68E-3	<2.1E-4	<2.6E-6	<4.5E-5	<4.6E-6	<1.2E-5	4.32E-3	<4.3E-5	
		6	1.74E-2	1.66E-2	4.6	1.04E-2	<2.1E-4	<2.7E-6	<4.5E-5	<4.6E-6	<1.3E-5	4.83E-3	<4.4E-5	
		24	1.74E-2	1.72E-2	1.1	1.19E-2	<2.1E-4	<2.7E-6	<4.5E-5	<4.6E-6	<1.2E-5	5.81E-3	<4.4E-5	
3.0	1.25	0.5	1.69E-2	1.67E-2	1.2	7.87E-3	<2.6E-4	<2.7E-6	<4.6E-5	1.12E-3	[1.49E-5]	3.00E-3	<4.4E-5	3.36E-3
		1	1.69E-2	1.70E-2	0.6	8.21E-3	[2.41E-4]	<2.7E-6	<4.6E-5	5.49E-4	[1.51E-5]	3.15E-3	<4.5E-5	3.34E-3
		2	1.73E-2	1.72E-2	0.6	8.90E-3	[2.32E-4]	<2.7E-6	<4.6E-5	9.66E-4	[1.28E-5]	3.56E-3	<4.4E-5	3.48E-3
		4	1.71E-2	1.76E-2	2.9	9.55E-3	<2.1E-4	<2.7E-6	<4.5E-5	2.06E-3	[1.28E-5]	4.01E-3	<4.4E-5	3.60E-3
		6	1.82E-2	1.76E-2	3.3	1.10E-2	<2.1E-4	<2.7E-6	<4.5E-5	3.44E-3	<1.2E-5	4.55E-3	<4.3E-5	3.58E-3
		24	1.87E-2	1.83E-2	2.1	1.31E-2	<2.1E-4	<2.7E-6	<4.6E-5	5.91E-4	<1.2E-5	5.56E-3	<4.4E-5	3.97E-3

(a) Chromate was measured for indication only.
na = not analyzed.

Table C.2. Tabulated Process Conditions and Results—50°C with Comparison of Cr(VI) and Total Cr Concentrations (2 pages)

Process Conditions			Concentration, M			% Diff.	Concentration, M							²³⁹⁺²⁴⁰ Pu,
[NaOH], M	Mn/Cr, Mole Ratio	Time, h	Cr (VI)	Total Cr	Al		B	Cd	Fe	Mn	Ni	Si	U	μCi/mL
0.25	0.75	0.5	1.35E-2	1.27E-2	5.9	4.20E-3	[7.35E-5]	<9.6E-7	<9.4E-6	<9.6E-7	<2.6E-6	3.63E-4	<9.1E-6	na
		1	1.38E-2	1.34E-2	2.9	4.73E-3	[7.98E-5]	<5.5E-7	<9.3E-6	<9.5E-7	<2.5E-6	4.45E-4	<9.0E-6	
		2	1.38E-2	1.35E-2	2.2	5.34E-3	[6.51E-5]	<5.4E-7	<9.3E-6	<9.5E-7	<2.5E-6	6.27E-4	<8.9E-6	
		4	1.41E-2	1.36E-2	3.5	6.28E-3	[7.03E-5]	<5.4E-7	<9.2E-6	<9.4E-7	<2.5E-6	8.56E-4	<8.9E-6	
		6	1.41E-2	1.38E-2	2.1	6.89E-3	[7.37E-5]	<5.5E-7	<9.3E-6	<9.5E-7	<2.5E-6	9.79E-4	<8.9E-6	
		24	1.48E-2	1.43E-2	3.4	8.69E-3	[8.22E-5]	<5.5E-7	<9.3E-6	<9.4E-7	<2.5E-6	1.19E-3	<8.9E-6	
0.25	1.0	0.5	1.72E-2	1.58E-2	8.1	5.27E-3	[8.18E-5]	<5.4E-7	<9.2E-6	1.24E-3	<2.5E-6	4.32E-4	<8.9E-6	na
		1	1.79E-2	1.68E-2	6.1	6.15E-3	[8.12E-5]	<5.4E-7	<9.2E-6	<9.4E-7	<2.5E-6	5.24E-4	<8.8E-6	
		2	1.80E-2	1.69E-2	6.1	6.93E-3	[7.98E-5]	<5.3E-7	<9.0E-6	<9.2E-7	<2.4E-6	6.22E-4	<8.7E-6	
		4	1.80E-2	1.74E-2	3.3	7.81E-3	[8.69E-5]	<5.4E-7	<9.2E-6	<9.4E-7	<2.5E-6	7.81E-4	<8.8E-6	
		6	1.82E-2	1.71E-2	6.0	8.43E-3	[8.30E-5]	<5.5E-7	<9.4E-6	<9.6E-7	<2.5E-6	8.75E-4	<9.0E-6	
		24	1.84E-2	1.69E-2	8.2	1.04E-2	[8.71E-5]	<5.4E-7	<9.2E-6	<9.4E-7	<2.5E-6	1.01E-3	<8.8E-6	
0.25	1.25	0.5	1.68E-2	1.54E-2	8.3	5.12E-3	[7.52E-5]	<5.4E-7	<9.1E-6	2.66E-3	<2.5E-6	4.03E-4	<8.8E-6	2.17E-4
		1	1.78E-2	1.62E-2	9.0	6.36E-3	[7.95E-5]	<5.5E-7	<9.3E-6	2.26E-3	<2.5E-6	4.52E-4	<8.9E-6	3.06E-4
		2	1.79E-2	1.67E-2	6.7	7.60E-3	[9.90E-5]	<5.4E-7	<9.3E-6	1.58E-3	<2.5E-6	5.33E-4	<8.9E-6	3.82E-4
		4	1.89E-2	1.74E-2	7.9	9.65E-3	[9.77E-5]	<5.5E-7	<9.4E-6	8.48E-4	[2.59E-6]	6.48E-4	<9.1E-6	3.79E-4
		6	1.98E-2	1.86E-2	6.1	1.09E-2	[9.51E-5]	<5.5E-7	<9.4E-6	1.41E-3	<2.6E-6	6.91E-4	<9.1E-6	4.10E-4
		24	2.12E-2	1.95E-2	8.0	1.51E-2	[8.83E-5]	<5.5E-7	<9.3E-6	1.00E-3	<2.5E-6	7.39E-4	<9.0E-6	5.26E-4
3.0	0.75	0.5	1.34E-2	1.32E-2	1.5	8.79E-3	<2.1E-4	<2.7E-6	<4.6E-5	<4.7E-6	[1.35E-9]	4.36E-3	<4.4E-5	na
		1	1.31E-2	1.37E-2	4.6	9.94E-3	<2.1E-4	<2.7E-6	<4.6E-5	<4.7E-6	[1.69E-5]	5.15E-3	<4.4E-5	
		2	1.44E-2	1.35E-2	6.3	1.20E-2	<2.3E-4	<2.9E-6	<4.9E-5	<5.0E-6	[2.28E-5]	6.16E-3	<4.7E-5	
		4	1.33E-2	1.41E-2	6.0	1.18E-2	<2.1E-4	<2.6E-6	<4.5E-5	<4.6E-6	<1.2E-5	6.00E-3	<4.3E-5	
		6	1.42E-2	1.40E-2	1.4	1.33E-2	<2.1E-4	<2.7E-6	<4.5E-5	<4.6E-6	<1.2E-5	6.12E-3	<4.3E-5	
		24	1.43E-2	1.50E-2	4.9	1.50E-2	<2.1E-4	<2.7E-6	<4.5E-5	<4.6E-6	[1.27E-5]	6.22E-3	<4.3E-5	
3.0	1.0	0.5	1.72E-2	1.68E-2	2.3	9.89E-3	<2.1E-4	<2.7E-6	<4.5E-5	<4.6E-6	<1.2E-5	4.26E-3	<4.4E-5	na
		1	1.75E-2	1.70E-2	2.9	1.14E-2	<2.1E-4	<2.7E-6	<4.6E-5	<4.7E-6	<1.2E-5	5.09E-3	<4.4E-5	
		2	1.77E-2	1.73E-2	2.3	1.25E-2	[2.48E-4]	<2.7E-6	<4.6E-5	<4.7E-6	<1.2E-5	5.71E-3	<4.4E-5	

C.4

Table C.2. Tabulated Process Conditions and Results—50°C with Comparison of Cr(VI) and Total Cr Concentrations (2 pages)

Process Conditions			Concentration, M			% Diff.	Concentration, M							²³⁹⁺²⁴⁰ Pu, μCi/mL
[NaOH], M	Mn/Cr, Mole Ratio	Time, h	Cr (VI)	Total Cr	Al		B	Cd	Fe	Mn	Ni	Si	U	
		4	1.81E-2	1.76E-2	2.8	1.39E-2	<2.2E-4	<2.7E-6	<4.7E-5	<4.8E-6	<1.3E-5	6.19E-3	<4.5E-5	
		6	1.77E-2	1.70E-2	4.0	1.43E-2	<2.2E-4	<2.8E-6	<4.7E-5	<4.8E-6	<1.3E-5	6.22E-3	<4.5E-5	
		24	1.81E-2	1.74E-2	3.9	1.70E-2	<2.1E-4	<2.7E-6	<4.6E-5	<4.7E-6	<1.2E-5	6.36E-3	<4.4E-5	
3.0	1.25	0.5	1.77E-2	1.65E-2	6.8	1.05E-2	<2.1E-04	<2.7E-6	<4.6E-5	1.50E-3	[1.55E-5]	4.21E-3	<4.4E-5	3.62E-3
		1	1.75E-2	1.81E-2	3.4	1.20E-2	<2.1E-4	<2.6E-6	<4.4E-5	1.50E-3	[1.40E-5]	4.81E-3	<4.3E-5	4.06E-3
		2	1.56E-2	1.83E-2	17.3	1.22E-2	<2.1E-4	<2.6E-6	<4.5E-5	9.96E-4	[1.96E-5]	4.55E-3	<4.3E-5	4.49E-3
		4	1.80E-2	1.90E-2	5.6	1.56E-2	<2.1E-4	<2.7E-6	<4.5E-5	8.74E-4	[2.34E-5]	5.55E-3	<4.3E-5	4.49E-3
		6	1.92E-2	1.90E-2	1.0	1.75E-2	<2.2E-4	<2.8E-6	<4.7E-5	2.74E-3	<1.3E-5	5.70E-3	<4.5E-5	4.40E-3
		24	1.92E-2	1.97E-2	2.6	2.02E-2	[2.21E-4]	<2.7E-6	<4.6E-5	1.56E-4	[2.30E-5]	5.78E-3	<4.5E-5	4.82E-3
(a) Chromate was measured for indication only. na = not analyzed.														

Tables C.3 and C.4 show the oxidative leaching solution densities. All densities were determined at ambient conditions (nominally 20°C).

Table C.3. Tabulated Densities at 25°C Process Conditions

[NaOH], M	Time, h	Mn/Cr, Mole Ratio	Density, g/mL	Mn/Cr, Mole Ratio	Density, g/mL	Mn/Cr, Mole Ratio	Density, g/mL
0.25	0.5	0.75	1.015	1.0	1.016	1.25	1.015
	1		1.020		1.015		1.014
	2		1.013		1.014		1.020
	4		1.018		1.021		1.015
	6		1.015		1.022		1.029
	24		1.016		1.022		1.014
	1.25		0.5		0.75		1.063
1		1.059	1.054				
2		1.061	1.067				
4		1.059	1.062				
6		1.057	1.063				
24		1.054	1.060				
1.25		0.5	1.0, Trial a	1.061		1.0, Trial b	1.059
	1	1.061		1.061	1.065		
	2	1.056		1.056	1.060		
	4	1.064		1.060	1.065		
	6	1.060		1.055	1.068		
	24	1.063		1.065	1.058		
	3.0	0.5		0.75	1.123		1.0
1		1.129	1.122		1.114		
2		1.128	1.123		1.120		
4		1.127	1.126		1.120		
6		1.133	1.129		1.126		
24		1.129	1.126		1.132		

Table C.4. Tabulated Densities at 50°C Process Conditions

[NaOH], M	Time, h	Mn/Cr, Mole Ratio	Density, g/mL	Mn/Cr, Mole Ratio	Density, g/mL	Mn/Cr, Mole Ratio	Density, g/mL
0.25	0.5	0.75	1.023	1.0	1.027	1.25	1.022
	1		1.022		1.024		1.029
	2		1.024		1.018		1.017
	4		1.021		1.021		1.027
	6		1.011		1.021		1.021
	24		1.014		1.014		1.015
3.0	0.5	0.75	1.136	1.0	1.125	1.25	1.135
	1		1.135		1.127		1.123
	2		1.129		1.141		1.125
	4		1.146		1.143		1.131
	6		1.132		1.143		1.125
	24		1.131		1.135		1.124

Appendix D

Thermogravimetric Analysis for Chromium Phase Characterization

Contents

D.1	Experimental.....	D.1
D.1.1	Experiments With Candidate Materials.....	D.2
D.1.2	Mixtures Testing.....	D.3
D.1.3	Chromium Dilution Experiments.....	D.3
D.1.4	Tank Waste Sample G6-Cr-TGA	D.3
D.1.5	Moisture Adsorption Test on Tank Waste Sample G6-Cr-TGA	D.6
D.2	Results and Discussion	D.6
D.2.1	Chromium, Iron, and Aluminum Candidate Compounds.....	D.6
D.2.2	Mixtures.....	D.8
D.2.3	Chromium Dilution Experiments.....	D.10
D.2.4	Tank Waste Samples G6-Cr-TGA.....	D.10
D.2.5	Mass Loss in the Temperature Interval 20 to 150°C	D.13
D.2.6	Mass Loss in the Temperature Interval 180 to 500°C	D.14
D.2.7	Mass Loss Above 500°C	D.14
D.2.8	Speciation of Tank Waste Sample G6-Cr-TGA	D.17
D.2.9	Mass Loss Estimates and Discussion.....	D.17
D.3	Summary.....	D.18

Figures

D.1. Digital Picture of the Caustic-Leached, Water-Washed G6-Cr-TGA Sample Before TG Experiments	D.5
D.2. XRD Pattern of G6-Cr-TGA Following Alkali Leaching and Water-Washing	D.6
D.3. Differential Thermal Analysis (DTA) and % Mass Loss for pure a) $\text{Cr}(\text{OH})_3 \cdot 2\text{H}_2\text{O}$ and b) $\text{CrO}(\text{OH}) \cdot \text{H}_2\text{O}$	D.7
D.4. DTA and % Mass Loss for Pure Chromium Oxide, Cr_2O_3	D.7
D.5. DTA and % Mass Loss for Pure a) $\text{Fe}(\text{OH})_3 \cdot \text{H}_2\text{O}$ and b) Magnetite, Fe_3O_4	D.8
D.6. TG Scan of Gibbsite, Boehmite, and Chromium Hydroxide Mixture	D.9
D.7. TG Scan Display the Effect of Diminishing Chromium Concentration in 20 to 30 mg Samples	D.10
D.8. Scoping Test TG Scan of a Small G6-Cr-TGA Sample	D.11
D.9. TG Scan of a Dried G6-Cr-TGA Sample Run in Argon	D.11
D.10. TG Scan of a Dried G6-Cr-TGA Sample Run in Dry Air	D.12

Tables

D.1. Candidate Chromium, Aluminum, and Iron Compounds and Associated Characterization Data	D.2
D.2. Chromium Dilution in Iron Oxides and Oxy-Hydroxide	D.3
D.3. Metal Composition of G6-Cr-Fusion	D.4
D.4. A Representative Mixture Experiment Wherein Mixtures of the Standard Compounds Were Prepared and the Thermal Scans Acquired	D.9
D.5. Observed Mass Loss from G6-Cr-TGA over TG Temperature Gradient	D.13
D.6. Expected Mass Loss Calculation for a 12-mg Tank Waste Sample Based on ICP Data and the Thermal Analysis of the G6-Cr-TGA Sample	D.15
D.7. Expected Mass-Loss Calculation for a 12-mg Tank Waste Sample Based on ICP Data and the Thermal Analysis of the G6-Cr-TGA Sample	D.16

Appendix D: Thermogravimetric Analysis for Chromium Phase Characterization

After caustic leaching and washing pretreatments were completed on the Group 6 tank waste solids, the residual composite was found to have 24 wt% insoluble chromium. At these levels, the trivalent hydroxide, oxy-hydroxide, and chromium oxide are the most likely candidates for insoluble chromium in the tank wastes. The chromium-phase identification was not discerned by XRD, STEM, EELS, or X-ray photoelectron spectroscopy (XPS). The thermogravimetric characterization method was evaluated for efficacy in phase characterization. The chromium speciation is important as it will impact the oxidative leaching pretreatments, in particular, the oxidative leaching time increases in the order: hydroxide<oxy-hydroxide<chromium oxide, when the particle sizes are nominally the same (Rapko 2007).

Thermal gravimetric analysis (TGA) is an effective method to characterize both amorphous and crystalline materials. Thermolysis of pure candidate chromium, aluminum, and iron compounds leads to unique thermal signatures. There are three relevant types of signatures used herein. The first is quantifiable mass loss as the sample is heated, the second is related to the thermodynamics of a thermal event, and the third is related to kinetics of the thermal event. The latter is important because the position of the thermal event on the temperature axis is often a direct reflection of the activation energy of the thermal event. Thermal signatures in general are commonly due to chemical changes and physical changes in state:

1. loss of water, carbonate, nitrate, or other ligands (endothermic mass loss)
2. melting (endothermic—no mass loss)
3. sublimation (endothermic—mass loss)
4. red-ox behavior (exo- or endothermic—mass loss or gain)
5. primary phase alteration (generally endothermic—mass loss)
6. secondary phase changes (generally endothermic—commonly no mass loss).

The characteristic of a given thermal signature is a function of several variables, including material

1. purity
2. process history
3. crystallinity
4. particle size.

D.1 Experimental

A Seiko model 350 TGA was used to collect thermal gravimetric (TG) data. Three types of TG screening experiments were run to evaluate the chemical identity of the chromium G6 tank sludge. These included acquisition of TG scans of

1. candidate compounds
2. mixtures of the candidate compounds
3. dilution of the candidate chromium compounds in iron (to establish a chromium detection limit capability).

The TG scans for the candidate compounds were analyzed and compared to the TG scans of actual tank waste samples.

A set of candidate chromium and iron compounds were either purchased or prepared by the project. All materials had been previously characterized by one or more techniques, including PSD, SEM, XRD, infrared (IR) spectroscopy, and/or TGA. Table D.1 lists the candidate materials and their available characterization. The trivalent chromium compounds, in particular, were amorphous in nature. The smallest particle sizes were prepared by passing the chromium hydroxide, oxy-hydroxide, and oxide through a 450-mesh screen, resulting in particles ≤ 32 microns in preparation for TGA.

Table D.1. Candidate Chromium, Aluminum, and Iron Compounds and Associated Characterization Data

Mineral Name	Formula	Metal Oxidation State	Origin	Characterization	Condition
Eskolaite	Cr_2O_3	3	Baker and Adamson, (Easton, Pa)	XRD, TGA, SEM	crystalline
Chromium hydroxide	$\text{Cr}(\text{OH})_3 \cdot 2\text{H}_2\text{O}$	3	G. Lumetta ^(a)	TGA, FTIR,	amorphous
Chromium oxy hydroxide	$\text{CrO}(\text{OH}) \cdot 2\text{H}_2\text{O}$	3	B. Rapko ^(a)	XRD, TGA, FTIR, ^(b) BET	amorphous
Chromium trioxide	CrO_3	6	Baker and Adamson, (Easton, Pa)	TGA	crystalline
Chromium dioxide	CrO_2 Cr_8O_{21} Cr_5O_9	4 (5,6) (3,4)	B. McNamara ^(a)	TGA, XRD	amorphous
Iron hydroxide	$\text{Fe}(\text{OH})_3$	3	G. Lumetta ^(a)	TGA	amorphous
Magnetite	Fe_3O_4	2,3	Strem Chemicals, Inc. (Newburyport, MA)	TGA, XRD	crystalline
Goethite	$\text{FeO}(\text{OH})$	3	Alfa Aesar (Ward Hill, MA)	TGA, XRD	crystalline fine powder
Hematite	Fe_2O_3	3	Strem Chemicals, Inc. (Newburyport, MA)	TGA, XRD	crystalline fine powder
Gibbsite	$\text{Al}(\text{OH})_3$	3	Almatis, Inc. (Bauxite, AR)	XRD, TGA, SEM, BET, PSD	crystalline fine powder
Boehmite	AlOOH	3	Nabaltec GmbH, (Schwandorf, Germany)	XRD, TGA, SEM, BET, PSD	crystalline fine powder
(a) In-house preparation					
(b) FTIR = Fourier transform infrared					

D.1.1 Experiments With Candidate Materials

Nominally 20 to 40 mg of the materials in Table D.1 were used in the TG experiments. In these experiments, the sample was heated under an argon purge or in air to 850°C at a ramp rate of 5°C/min.

D.1.2 Mixtures Testing

Several mixtures containing chromium hydroxide, chromium oxy-hydroxide, magnetite, hematite, gibbsite, boehmite, and silica were tested to evaluate if such mixtures produced an array of thermal events too complex to be of analytical use. The TG sample mass varied from 20 to 35 mg in the mixture experiments. The samples were prepared by mixing the desired components in water followed by drying in a vacuum oven at 60°C overnight to eliminate water. The mixtures were heated in Pt or quartz crucibles at a ramp rate of 5°C/min to 850°C under argon or in a dry air purge.

D.1.3 Chromium Dilution Experiments

Chromium dilution experiments were evaluated to estimate a detection limit for chromium hydroxide and oxy-hydroxide. Table D.2 lists the composition of a set of samples that were prepared in which $\text{Cr}(\text{OH})_3 \cdot x\text{H}_2\text{O}$ was diluted with various iron compounds. The TG sample mass varied from 12 to 35 mg in the chromium dilution experiments. TG experiments were run in Pt or quartz crucibles at a ramp rate of 5°C/min to 850°C under argon or in a dry air purge.

Table D.2. Chromium Dilution in Iron Oxides and Oxy-Hydroxide

Mixture	% Chromium	Purge	Observable Signal
50%Cr(OH) ₃ /50% Fe ₂ O ₃	50.1	Ar	yes
50%Cr(OH) ₃ /50% Fe(OH) ₃	49.8	Ar	yes
30%Cr(OH) ₃ /70% Fe ₃ O ₄	29.6	Ar	yes
20%Cr(OH) ₃ /80% Fe ₃ O ₄	19.4	Ar	yes
10%Cr(OH) ₃ /90% Fe ₃ O ₄	11.4	Ar	yes
5%Cr(OH) ₃ /95% Fe ₃ O ₄	5.24	Ar	yes
1%Cr(OH) ₃ /99% Fe ₃ O ₄	0.99	Ar	no
1%Cr(OH) ₃ /99% Fe ₃ O ₄	0.99	Air	yes

D.1.4 Tank Waste Sample G6-Cr-TGA

A separate aliquot of the Group 6 composite equivalent to 1.5 g of saltcake solids was washed and then rigorously leached with 100 mL 3 M NaOH for 8 hrs at 100°C.^(a) The leached material was washed with 0.01 M NaOH and centrifuged three sequential times to remove residual water-soluble materials such as sodium salts of aluminate, nitrate, nitrite, and oxalate. A sub-sample (G6-Cr-Fusion) was prepared by KOH fusion for the ICP-OES analysis. The constituent metal composition is shown in Table D.3; Cr represented 24 wt% of the solids.

A second subsample, referred to here as G6-Cr-TGA, was further washed using three sequential rinses with water to remove any residual soluble sodium salts. The wet solids in the final sample (G6-Cr-TGA) were dark brown; the suspending solution was essentially water. The ICP data shown in Table D.3

(a) Sample preparation was conducted according to TI-RPP-WTP-512, *Caustic Leach of Group 6 Hanford Saltcake Waste Sample*, L. Snow, June 2007.

indicate that the presence of chromium, iron, aluminum, calcium, silicon, and uranium were the major constituents. Because the sequential water wash removed potentially soluble sodium salts, the value for sodium should have dropped and consequently perturbed the chromium, iron, some aluminum, calcium, silicon, and uranium to slightly higher values.

Table D.3. Metal Composition of G6-Cr-Fusion

Analyte	Metal Concentration, $\mu\text{g/g}^{(a, b)}$	Metal Concentration, wt %
Al	73,600	7.36
B	345	0.035
Bi	1,400	0.14
Cd	422	0.042
Cr	240,500	24.05 ^(c)
Fe	42,700	4.27
Mn	13,600	1.36
Na	41,000	4.10
Si	21,550	2.16
U	11,500	1.15
Zn	1,445	0.14
Zr	955	0.096
Ba	290	0.029
Ca	13,500	1.35
Cu	325	0.033
Mg	1,950	0.195
La	331	0.033
Pb	2,820	0.28
Ti	105	0.011
Y	120	0.012

(a) Analyte uncertainties were typically within $\pm 15\%$ ($2\text{-}\sigma$); results in brackets indicate that the analyte concentrations were less than the minimum detection limit (MDL) and greater than the estimated quantitation limit (EQL), and uncertainties were $>15\%$.

(b) Dry mass basis.

(c) 24 wt% Cr concentration corresponds to 35 wt% Cr_2O_3 , 48 wt% $\text{CrO}(\text{OH})$, or 65 wt% $\text{Cr}(\text{OH})_3 \cdot 2\text{H}_2\text{O}$.

Tank waste samples that were washed, leached, and then water washed three times and dried appeared dark brown, but on closer inspection with a digital camera were in fact dark green with distinct red brown spots. The color is important because with the exception of iron and chromium, the higher concentration constituents (U, Al) exist as oxides or oxy-hydroxides in the tank waste and should appear black, white, or light yellow. The dark green color is characteristic of the chromium in the sample as shown in Figure D.1. The red spots suggest the presence of iron as $\text{Fe}(\text{OH})_3$, $\text{FeO}(\text{OH})$, or Fe_2O_3 .



Figure D.1. Digital Picture of the Caustic-Leached, Water-Washed G6-Cr-TGA Sample Before TG Experiments

An X-ray diffraction pattern of the tank waste sample G6-Cr-TGA was obtained. Seven patterns were summed to obtain the diffraction pattern shown in Figure D.2. Only 3 wt% Rutile (TiO_2) was used as the internal standard, yet it still had the largest intensity in the spectrum, despite the fact that the slide was quite dark with sample. Comparing this spectrum to the one in Figure 6.8 indicated that the caustic leaching and sequential water washing was effective at removing gibbsite and SiO_2 , and water soluble species, respectively. Cancrinite was identified to be present in this sample by XRD. Because the well identified spectrum of water-insoluble cancrinite in Figure 6.8 was absent in Figure D.2, it was assumed that the boehmite spectrum overlapped with that of this alumino-silicate or that a substantial amount of it (≈ 10 micron particle size) was removed through the filtration steps between water washes. The broad peak centered near 12° (2θ) was identified in both powder patterns as a convolution of the signals of the mostly amorphous clarkeite [$\text{Na}(\text{UO}_2)\text{O}(\text{OH})$] and boehmite [$\text{AlO}(\text{OH})$]. The ICP data suggest that the uranium concentration in these solids was about 1.2%, and the low intensity of uranium in the XRD spectrum is qualitatively consistent with this concentration of uranium. Most significant is the absence of any XRD signal for the 24 wt% Cr or 4.3 wt% iron in the sample.

Three small-mass slurry samples of G6-Cr-TGA were added to platinum TGA pans. These were run directly on the TGA as wetted slurries at a ramp rate of $5^\circ\text{C}/\text{min}$ to 600 or 850°C under an argon purge. There was no apparent attack of hydroxide on the crucibles, which indicated that the samples had been washed well enough to reduce the corrosive hydroxide constituents, e.g., NaOH.

To obtain larger sample masses than used in the scoping tests, concentrated slurry aliquots of G6-Cr-TGA were added to each of four quartz sample pans followed by air drying overnight. The sample loading procedure was repeated until the average dried sample masses in the quartz pans were ~ 12 mg. Two samples were run under an argon purge and two under a purge of dry air, each at a ramp rate of $5^\circ\text{C}/\text{min}$ to 850°C .

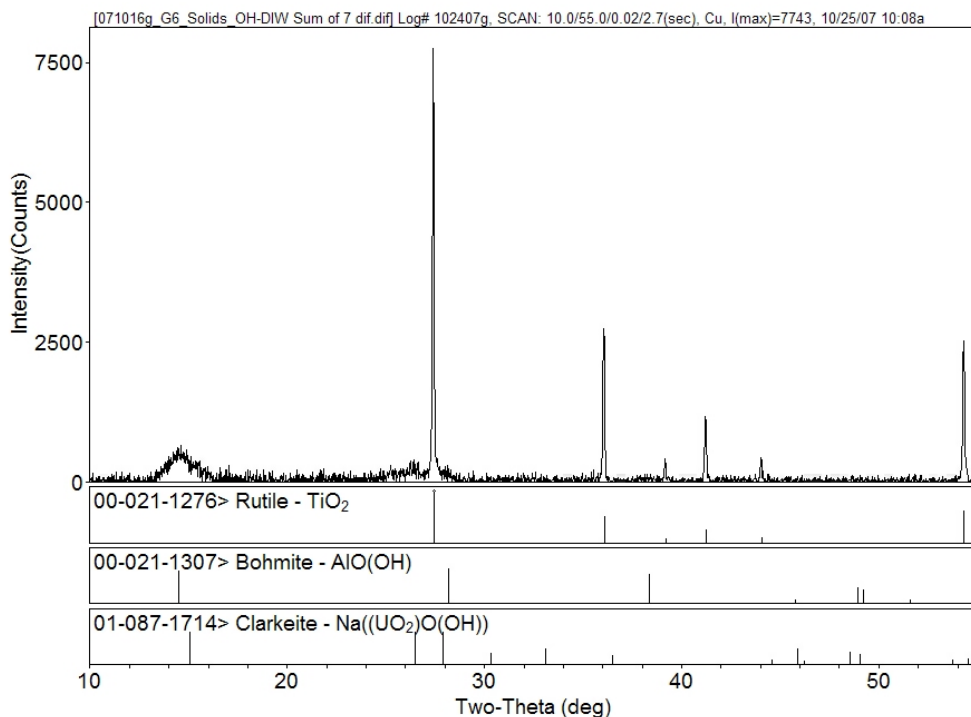


Figure D.2. XRD Pattern of G6-Cr-TGA Following Alkali Leaching and Water-Washing
 Note: This sample contains 24 wt% Cr (see Table D.3).

D.1.5 Moisture Adsorption Test on Tank Waste Sample G6-Cr-TGA

Two of the samples that were run in air were archived in a closed sample vial. After 1 month, the samples were heated to 200°C to examine the amount of moisture that had been picked up. The samples were then hydrated for 1 and 2 days at 100% relative humidity and then were heated to 200°C to examine if the forced hydration increased the water adsorption. The samples were then re-hydrated for 2 days at 100% relative humidity and then were equilibrated for 2 days, open to the air in a fume hood. The conditions were meant to emulate those used originally to prepare the dried TGA samples. The samples were then heated to 180°C.

D.2 Results and Discussion

D.2.1 Chromium, Iron, and Aluminum Candidate Compounds

The notion of attempting to use TGA to determine chemical species present in tank waste solids is predicated on the uniqueness of the thermal signature and its response to parametric variation. Using thermal gravimetric analysis, one can alter the sample heating rate or mode and can change the purge gas, i.e., inert or reactive. These variations result in changes in sample mass as well as changes in the kinetic information associated with a given thermal event. Because the large majority of signatures associated with phase changes and chemical decomposition of minerals are endothermic, exothermic signatures are particularly unique. We found after some screening studies that thermal decomposition of the trivalent chromium compounds of interest involved such exothermic events. It was also of interest that the decomposition of the amorphous hydroxide $\text{Cr}(\text{OH})_3 \cdot x\text{H}_2\text{O}$ resulted in two exothermic signatures, and

decomposition of the amorphous oxy-hydroxide $\text{CrO}(\text{OH})\cdot x\text{H}_2\text{O}$ resulted in a single exothermic response. The later response was observed to be common to both compounds, each of which transform to Cr_2O_3 above 400°C . The overall transformation involves the chemical reduction of higher valence chromium compounds. These thermal events are oxidative in nature and are shown for the hydroxide in Figure D.3a and for the oxy-hydroxide in Figure D.3b. The TG scan of chromium oxide, Cr_2O_3 (Figure D.4) was devoid of any thermal event, including any water loss below 200°C . The total mass loss for the crystalline Cr_2O_3 sample was about 1.5 wt% at 850°C compared to $> 40\%$ loss experienced by the chromium hydroxides. A final relevant point concerning $\text{Cr}(\text{OH})_3\cdot x\text{H}_2\text{O}$ and $\text{CrO}(\text{OH})\cdot x\text{H}_2\text{O}$ is that the value of x is highly dependent on the preparation but can likely reach values of 9. This results in large mass losses below 180°C during heating that are not observed for gibbsite and boehmite or most of the iron species and so again confers a uniqueness to the chromium thermal signature set.

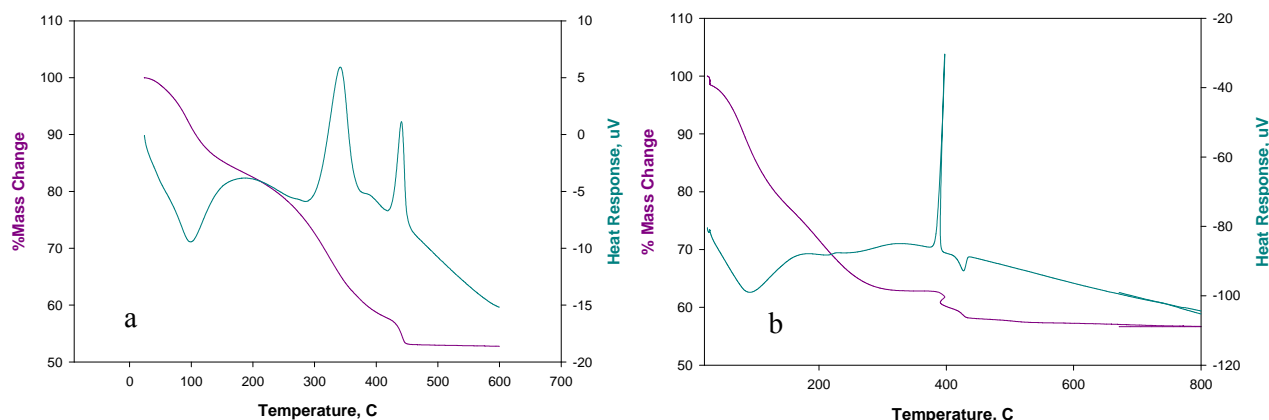


Figure D.3. Differential Thermal Analysis (DTA) and % Mass Loss for pure a) $\text{Cr}(\text{OH})_3\cdot 2\text{H}_2\text{O}$ and b) $\text{CrO}(\text{OH})\cdot \text{H}_2\text{O}$

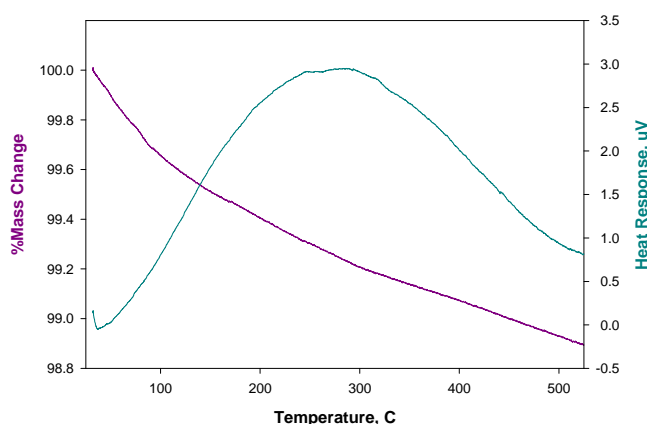


Figure D.4. DTA and % Mass Loss for Pure Chromium Oxide, Cr_2O_3

Analogous to the chromium compounds, iron hydroxide, goethite [$\text{FeO}(\text{OH})$], and magnetite (Fe_3O_4) each transform to Fe_2O_3 when heated above 400°C . Figure D.5a shows the water loss for iron hydroxide. The water is loosely bound in both iron hydroxide and goethite as it is released nearly completely below 60°C . The thermal scan of goethite (not shown) displays a large endotherm near 300°C as it converts to Fe_2O_3 . A broad mass gain was observed when magnetite was heated (Figure D.5b). Magnetite is a mixed

oxidation state compound Fe(II, III). The mass increase occurs because of oxidation to pure Fe₂O₃ (Fe III).

D.2.2 Mixtures

The mixture testing was carried out to evaluate whether a multitude of potential thermal events would “wash out” thermal signatures of interest. In no case were the signatures for chromium, aluminum, or iron made undetectable, even using loadings of the standards that exceeded known values (Table D.4). For the test shown, the standards were mixed in water, dried in a vacuum oven at 60°C overnight to eliminate water and loosely bound hydroxide, and run on the TGA immediately. The composition of a representative mixture experiment is shown in Table D.4. The sample mass was 26.11 mg. The TGA scan of the mixture is shown in Figure D.6. The majority of water on the iron and the chromium was removed by the vacuum drying as observed by the lack of any distinctive endotherm near 100°C. Consequently, the chromium and aluminum hydroxide forms had been converted to the oxy-hydroxides by the vacuum drying. The total mass lost was about 16 wt%. One can clearly see one of the exotherms for chromium and the endotherms for boehmite and gibbsite at 15 and 5 wt%, respectively. The low-temperature exotherm for the chromium was washed out by the presence of a large endotherm for the gibbsite to boehmite transition near 275°C. From the mixture testing, it could be estimated that Al as boehmite and gibbsite would be detectable to below 5 wt% in a nominal 30-mg sample.

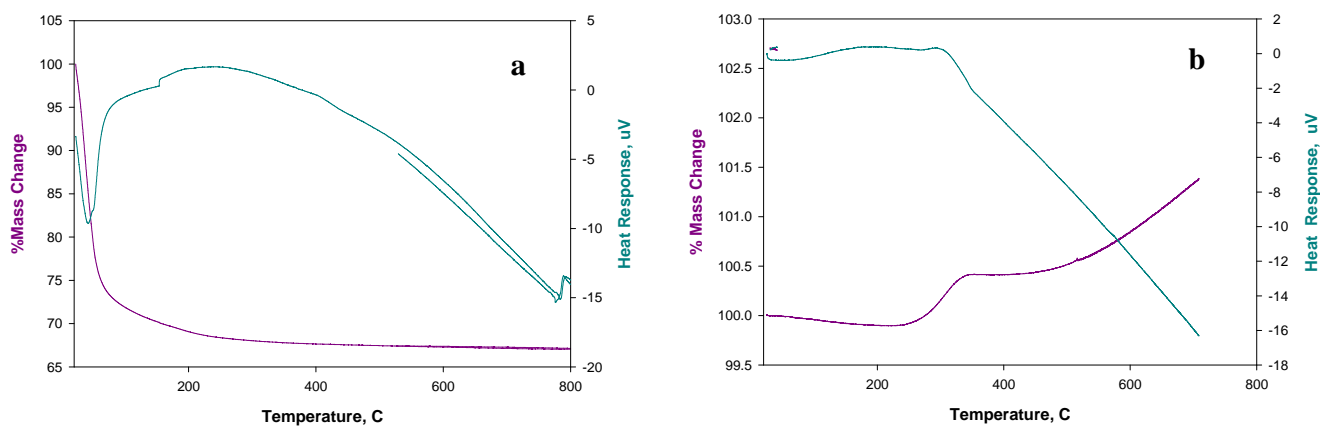


Figure D.5. DTA and % Mass Loss for Pure a) Fe(OH)₃·H₂O and b) Magnetite, Fe₃O₄

Table D.4 additionally provides a mass balance calculation for the expected mass loss, assuming all mass lost between 200 and 600°C could be attributable to hydroxide as water lost. The estimate of 15.9 wt% loss is a bit lower than observed (17 wt%) because waters of hydration were not accounted for in the calculation.

Table D.4. A Representative Mixture Experiment Wherein Mixtures of the Standard Compounds Were Prepared and the Thermal Scans Acquired

Start Compound	$M_i^{(a)}$ mg	MWT Start, g/mol	Thermal Endpoint	MWT Finish, g/mol	$M_f^{(b)}$ mg	$\Delta^{(c)}$ mg	% Change
Boehmite	4.1	60.0	Al ₂ O ₃	102.0	3.48	0.616	2.3
Gibbsite	1.1	78.0	Al ₂ O ₃	102.0	0.72	0.381	1.5
Cr(OH) ₃	10.0	103.0	Cr ₂ O ₃	152.0	7.38	2.622	10.1
Goethite	6.0	88.9	Fe ₂ O ₃	159.7	5.39	0.608	2.3
Magnetite	3.0	231.5	Fe ₂ O ₃	159.7	3.10	-0.104	-0.4
Silica	2.0	60.1	SiO ₂	60.1	2.1	0	0
Total	26.2						15.7% ^(d)

(a) M_i = Initial mass of constituent i
 (b) M_f = Final mass of constituent i
 (c) Δ = change in mass
 (d) Total mass change

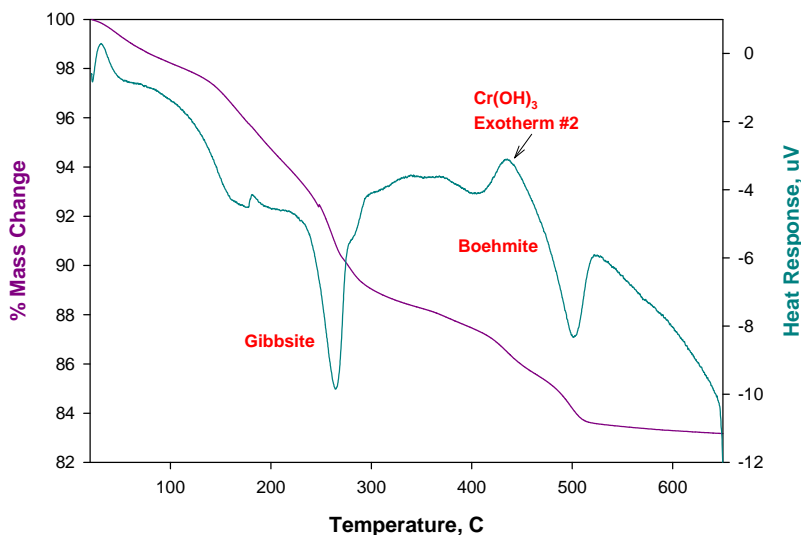


Figure D.6. TG Scan of Gibbsite, Boehmite, and Chromium Hydroxide Mixture
 (Note: This figure demonstrates that chromium hydroxide or oxy hydroxide could be observed in a mixture of relevant compounds. Actual sample composition is shown in Table D.3.)

The TG experiment as based on mass percent loss is accurate to changes in the tenths of micrograms. The visual identification of endothermic/exothermic events can be misleading in that the detectable heat released or gained from a given event is proportional to the sample mass. Lower sample mass leads to lower intensity in the thermal signature. The magnitude of the endothermic/exothermic event is of course variable from compound to compound.

D.2.3 Chromium Dilution Experiments

To place a limit of detection for chromium hydroxide in the TG experiment, chromium dilution preparations listed in Table D.2 were tested. The chromium dilution at the 50% level approximated the Cr oxide or hydroxide concentration expected to be in tank waste sample G6-Cr-TGA. Because it was possible that the chromium, aluminum, and/or iron could exist as mixtures of structures, lower chromium percentages were investigated.

Figure D.7 shows the scans of the thermal decomposition of several of the mixtures to 600°C under an argon purge. The curves at first look are misleading in that it appears that the first exotherm can be seen down to 1% chromium hydroxide. This in fact is not the chromium oxidation signature but a “wash out” of that signal caused by the oxidation of magnetite ($\text{Fe}_3^{\text{II,III}}\text{O}_4$). The second exotherm, as shown in Figure D.3a and Figure D.3b, then becomes a better marker for the chromium as it was visible to about 5% under the argon purge. At the 1 to 5% level, it was easier to detect the chromium hydroxide exotherm between 400 and 450°C using a purge of air. It is for this reason that the dried tank waste samples were tested under both argon and dry air purges.

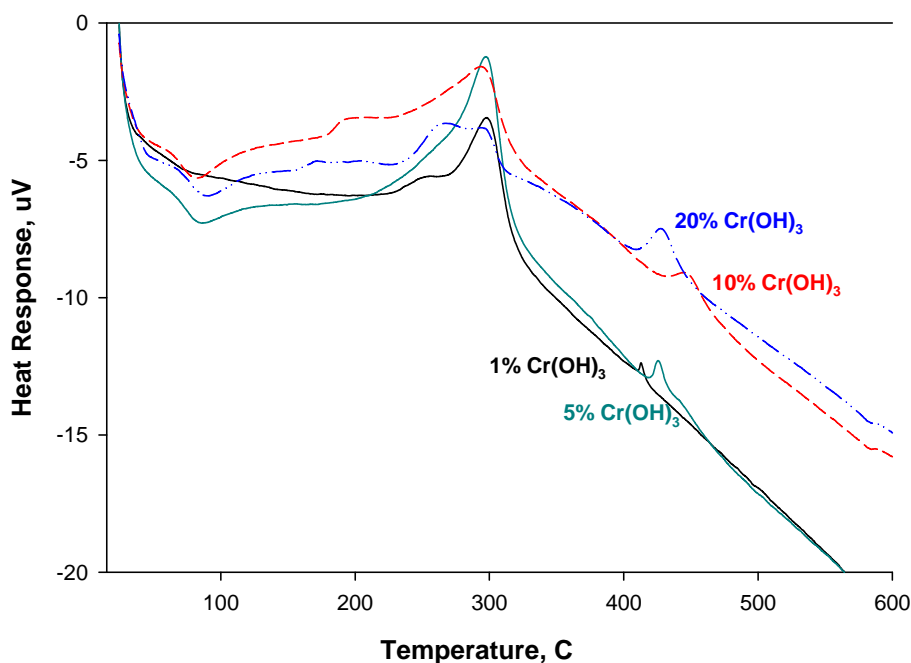


Figure D.7. TG Scans Display the Effect of Diminishing Chromium Concentration in 20 to 30 mg Samples

D.2.4 Tank Waste Samples G6-Cr-TGA

The TGA scans of the wet slurry samples at first appeared to be not informative as no obvious exotherm or endothermic signatures were observed (see Figure D.8). As expected, most of the sample mass loss was from water. About 10 ± 2 wt% of the sample mass loss occurred after 100°C. In the example shown, a very small exotherm (blue arrow) could be observed between 300 and 400°C. Furthermore, above

500°C (red arrow), a weak signature that occurred with no mass loss was common to two of the samples. The small thermal features (arrows) occurred in each scan but were too small to designate as endothermic or exothermic. These were presumably low wt% signatures of specific tank waste constituents, presumably Cr, Fe, or Al. The slurry samples continued to lose mass after 500°C.

Similar to the scans obtained from the slurry samples (as shown in Figure D.8) the scans obtained with the larger-mass, dried samples (shown in Figure D.9 and Figure D.10) indicated an overall lack of thermal activity above 180°C.

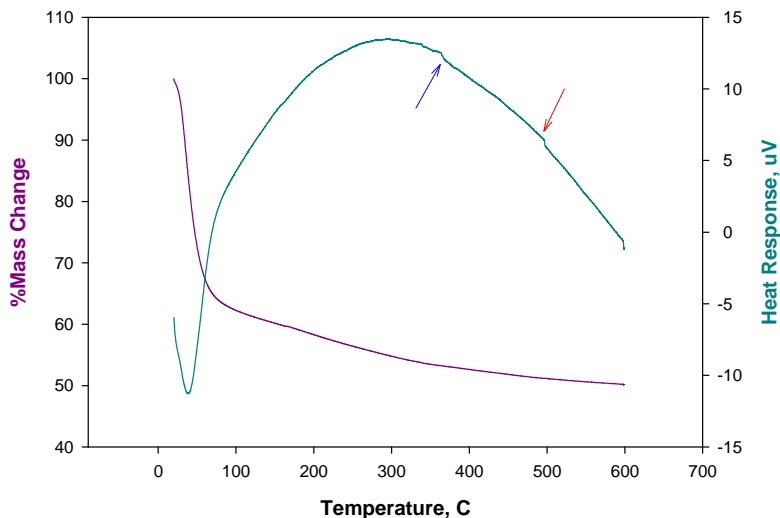


Figure D.8. Scoping Test TG Scan of a Small G6-Cr-TGA Sample
(Note: Arrows indicate small thermal signatures.)

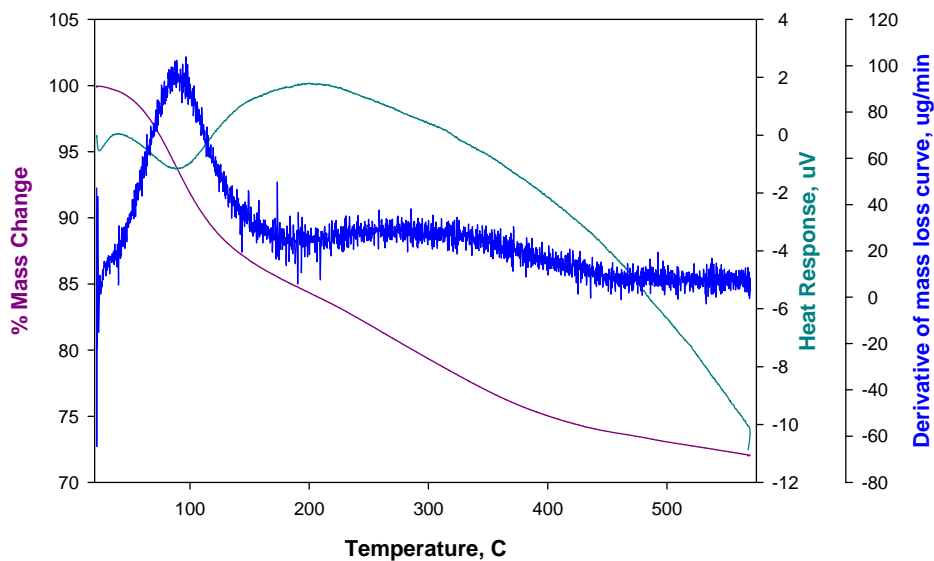


Figure D.9. TG Scan of a Dried G6-Cr-TGA Sample Run in Argon

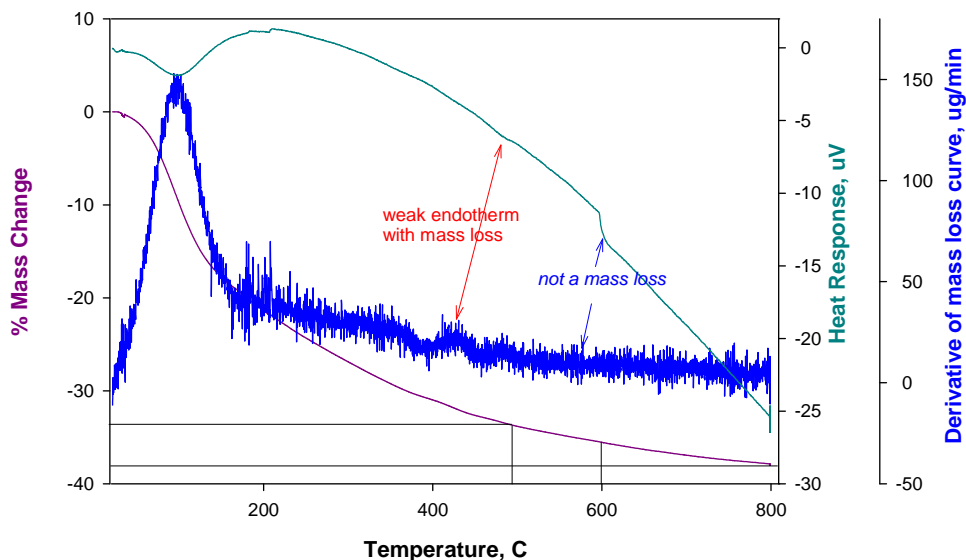


Figure D.10. TG Scan of a Dried G6-Cr-TGA Sample Run in Dry Air

Duplicate TG dried tank waste samples that were run in argon experienced a mass loss total of 27 ± 0.1 wt% during heating to 500°C . Physisorbed water and waters of hydration below 200°C presumably accounted for 15 ± 0.1 wt% of that total. The derivative curve (blue) shown in Figure D.9 shows that this type of mass loss actually ceased at about 180°C and then an additional 12.7 wt% mass loss occurred when heated from 180 to 500°C . Heating to 800°C caused a further 3% mass loss. Duplicate TG experiments^(a) were then conducted with an air purge to observe thermal events that might be aided by oxygen. The sample (shown in Figure D.10) lost a total of 37 wt%; a 20 wt% loss occurred below 180°C , a 13.5 wt% loss occurred between 180 and 500°C , and a 4 wt% loss occurred from 500 to 800°C . Between 180 and 500°C , the mass loss agreement for the three (2 in argon and 1 in air) samples was 12.9 ± 0.6 wt% (see Table D.5). The combined mass loss between 180 and 800°C was about 16 ± 1 wt%.

(a) Duplicate samples were prepared. One of the samples was lost to a large vibration that rocked the sample off the analytical balance inside the TG unit.

Table D.5. Observed Mass Loss from G6-Cr-TGA over TG Temperature Gradient

G6-Cr-TGA	Wt% Mass Loss, 20-180°C	Wt% Mass Loss, 180-500°C	Wt% Mass Loss, 500-800°C
#1 Argon	15.7	12.4	3
#2 Argon	14.8	13.0	3
#3 Air	20.2	13.5	4
Average and Standard Deviation	16.9±2.9	12.9±0.6	3±0.6
Major Mass Loss Constituent	Adsorbed H ₂ O Chemically bound H ₂ O	OH ⁻ as H ₂ O CO ₃ ²⁻ , C ₂ O ₄ ²⁻	CO ₃ ²⁻ , C ₂ O ₄ ²⁻
Minor Mass Loss Constituent	NH ₃ , CO ₂ , NO _x	F ⁻ , organic C, NO ₃ ⁻ , NO ₂ ⁻	PO ₄ ³⁻

D.2.5 Mass Loss in the Temperature Interval 20 to 150°C

Quantification of the extent of moisture absorption/adsorption affords insight to the factors that caused low-temperature (<180°C) mass loss. The washed and leached G6 tank waste solids have a very high surface area as was evidenced by the TEM images of the solids in Figure 6.16 e-f. The TEM micrographs coupled with the particle-size data are consistent with >0.1-micron-aggregates, the particles of which were <10 nm (100 Å) in size. The apparent high surface area would result in moisture absorption/adsorption to the sample as opposed to a chemical affinity necessarily being responsible for the activity. It should be noted that below 200°C, low wt% desorption of CO₂, NO_x, and NH₃, in addition to water desorption, might be expected from the native tank waste solids.

Dried tank waste samples that had been heated to 800°C provided duplicate samples that were nearly devoid of chemical functionality, i.e., -H, -O, -CO₃²⁻. Except for the presence of very low wt% free alkali hydroxide residuals at room temperature, adding water to these samples would result in little chemically bound water. Of interest was to what extent could such a sample absorb (or adsorb) moisture. It was found from moisture uptake experiments that the heat-treated samples could adsorb greater than 80 wt% water. Two types of water were present. The absorbed water was quickly lost when the hydrated samples were heated to 60°C or equilibrated in the open air at room temperature for 2 days. The samples retained between 3 and 5 wt% adsorbed water under these conditions, but when heated between 60 and 100°C lost the adsorbed water. This latter type of water is considered here as a reversible adsorbate. Before heating to 800°C, the sample metal constituents were assumed to be mostly hydroxide as listed in Table D.6 and Table D.7. These would encourage additional retention of water considered to be chemically bound water. Chemically bound water can be loosely or tightly bound so that temperatures between 30 and 150°C are typical for its removal.

The sample's combined affinity for water can now be estimated by using the average value for water loss of 17 wt%, as observed in the G6-Cr-TGA experiments. Of this amount, the adsorption experiment suggests that about 3 to 5 wt% was adsorbed water. A conservative estimate of the amount of adsorbate water fixed to the fully functionalized surface (before heating) might be 5 wt% or greater, and consequently, the mass of chemically bound waters was also about 5% wt%. The latter estimate of 5 wt%

chemically bound water severely limits the amount of hydration that could have been present from chromium compounds such as $\text{Cr}(\text{OH})_3 \cdot x\text{H}_2\text{O}$ or $\text{CrO}(\text{OH}) \cdot x\text{H}_2\text{O}$.

D.2.6 Mass Loss in the Temperature Interval 180 to 500°C

It is expected that the mass loss between 180 and 500°C was predominantly hydroxide, removed as water. Lesser mass-loss contributors include metal oxy-nitrates and nitrites and organic carbon that can form residual tars, which typically decompose fully near 500°C in air. All of the tank waste samples continued to decompose past 500°C and lost about 3 wt% additional mass to 800°C as marked in Figure D.9. This mass loss cannot be attributed to hydroxide (as water), or organic carbon loss.

D.2.7 Mass Loss Above 500°C

Inorganic compounds of those listed in the ICP data in Table D.4 that would lose mass above 500°C include the metal oxy-fluorides, phosphates, oxalates, and carbonates. Of the listed anions, carbonate and oxalate are likely of higher concentration in the Group 6 solids. The sequential water wash would have substantially removed sodium phosphate, the alkali carbonates, and oxalates. Fe, Mn, Ca, and the lanthanides form oxalates and carbonates that have both low solubility in basic media or water solution and the requisite thermal stability. As examples relevant to the ICP data in Table D.6, natural siderite (FeCO_3), the dolomite group, e.g., ankerite and kutnohorite ($\text{Ca}(\text{Mg,Fe,Mn})(\text{CO}_3)_2$), CaCO_3 , and MnCO_3 all thermally decompose to the respective oxides with gradual decomposition of CO_2 at temperatures greater than 500 to 800°C. Table D.5 above summarizes the known mass loss ranges and expected speciation lost for each trial of tank waste sample G6-Cr-TGA.

Table D.6. Expected Mass Loss Calculation for a 12-mg Tank Waste Sample Based on ICP Data and the Thermal Analysis of the G6-Cr- TGA Sample. The calculation includes mass loss from metal oxy-hydroxides and hydroxides only.

ICP-OES Analyte	Average, ^(e) µg/g	FW analyte, g/mol	Start Species ^(f)	FW, g/mol	M _I , ^(g) mg	Final Species ^(h)	FW, g/mol	M _F , ⁽ⁱ⁾ mg	Δ, ^(j) mg
Al ^(a)	73600	26.98	AlO(OH)	59.988	0.1555	Al ₂ O ₃	101.96	0.132	2.33E-02
Al ^(a)	26.98	Al ₂ O ₃	102	2.3790	Al ₂ O ₃	102.00	2.379	0.00E+00
Bi	1400	208.98	Bi(OH) ₃	259.9	0.0145	Bi ₂ O ₃	466.0	0.015	1.71E-03
Cd	421.5	112.41	Cd(OH) ₂	130	0.0046	CdO	128.40	0.005	5.70E-05
Cr ^(b)	240500	52.00	Cr(OH) ₃	103	0.6108	Cr ₂ O ₃	151.99	0.334	2.77E-01
Cr ^(b)	52.00	Cr ₂ O ₃	151.99	6.0107	Cr ₂ O ₃	151.99	6.011	0.00E+00
Fe	42700	55.80	Fe(OH) ₃	106.8	0.7764	Fe ₂ O ₃	159.69	0.580	1.96E-01
Mn	13600	54.94	MnO ₂	86.9	0.2044	MnO ₂	86.90	0.204	0.00E+00
Na ^(c)	41000	23.00	NaOH	40	0.6774	Na ₂ O	61.97	0.525	1.53E-01
Si	21550	28.09	SiO ₂	60.1	0.4381	SiO ₂	60.10	0.438	0.00E+00
U ^(d)	11500	238.0	Na(UO ₂)O(OH)	326.02	0.1497	Na ₂ U ₂ O ₇	634.0	0.146	4.14E-03
Zn	1445	65.39	Zn(OH) ₂	83.41	0.0175	ZnO	81.39	0.017	4.24E-04
Zr	955	91.22	Zr(OH) ₄	83.41	0.0083	ZrO ₂	123.22	0.012	-3.96E-03
Ag	79	107.87	AgOH	124	0.0016	Ag ₂ O	231.7	0.002	1.06E-04
Ba	290	137.33	Ba(OH) ₂	155.34	0.0011	BaO	153.33	0.001	1.40E-05
Ca	13500	40.07	Ca(OH) ₂	58.09	0.0012	CaO	56.08	0.001	4.03E-05
Cu	325	63.55	Cu(OH) ₂	82.57	0.3622	CuO	79.55	0.255	1.32E-02
La	331	138.91	La(OH) ₃	157.93	0.0077	La ₂ O ₃	325.81	0.008	-2.42E-04
Mg	1950	24.31	Mg(OH) ₂	42.32	0.0010	MgO	40.30	0.001	4.81E-05
Pb	2820	207.0	Pb(OH) ₄	227.23	0.1732	PbO ₂	239.20	0.182	-9.12E-03
Ti	105	47.88	TiO ₂	31.9	0.0048	TiO ₂	31.90	0.004	0.00E+00
Y	120	88.91	Y(OH) ₃	107.93	0.0022	Y ₂ O ₃	225.81	0.002	-1.04E-04
total	468,192	--	--	--	11.905	--	--	11.254	0.652
									5.47% ^(k)
<p>(a) Aluminum 10% as AlO(OH), aluminum 90% as Al₂O₃ (b) Chromium 10% as CrO(OH), chromium 90% as Cr₂O₃ (c) 2.4% Na was used for the clarkeite, 6.23% used as NaOH (d) 2.4% U used as clarkeite per the XRD spectrum in Figure D.2 (e) Reported ICP average of element (f) Assumed starting species (g) M_i = Initial mass of constituent I, total initial mass was 12.0 mg (h) M_f = Final mass of constituent i (i) Assumed thermal end point (j) Δ = change in mass (k) Total mass change</p>									

Table D.7. Expected Mass-Loss Calculation for a 12-mg Tank Waste Sample Based on ICP Data and the Thermal Analysis of the G6-Cr- TGA Sample. The calculation includes mass loss from metal carbonates and hydroxyl metal carbonates.

ICP-OES Analyte	Average, ^(f) $\mu\text{g/g}$	FW Analyte, g/mol	Start Species ^(g)	FW, g/mol	M_i , ^(h) mg	Final Species ⁽ⁱ⁾	FW, g/mol	M_f , ^(j) mg	Δ , ^(k) mg
Al ^(a)	73600	26.981	AlO(OH)	60.0	0.0900	Al ₂ O ₃	101.96	0.076	1.35E-02
Al ^(a)	26.981	NaAl(OH) ₂ CO ₃	143.99	3.4565	NaAlO ₂	81.97	1.968	1.49E+00
Al ^(a)	26.981	Al ₂ O ₃	102.0	0.4589	Al ₂ O ₃	101.96	0.459	0.00E+00
Bi	1400	208.98	Bi(OH) ₃	259.9	0.0168	Bi ₂ O ₃	466	0.017	1.92E-03
Cd	421.5	112.41	Cd(OH) ₂	130.0	0.0054	CdO	128.4	0.005	6.60E-05
Cr ^(b)	240500	51.996	Cr(OH) ₃	103.0	0.3536	Cr ₂ O ₃	151.99	0.193	1.60E-01
Cr ^(b)		51.996	Cr ₂ O ₃	152.0	3.6732	Cr ₂ O ₃	151.99	3.673	0.00E+00
Fe ^(c)	42700	55.8	Fe ₂ (OH) ₂ CO ₃	205.7	0.8658	Fe ₂ O ₃	159.7	0.336	5.30E-01
Fe ^(c)			Fe(OH) ₃	106.9	0.4498	Fe ₂ O ₃	159.7	0.336	1.14E-01
Mn	13600	54.938	Mn(CO ₃) ₂	174.9	0.4764	MnO ₂	86.9	0.237	2.40E-01
Na ^(d)	41000	23	NaOH	40.0	0.7843	Na ₂ O	61.97	1.215	-4.31E-01
Si	21550	28.086	SiO ₂	60.1	0.5073	SiO ₂	60.1	0.507	0.00E+00
U ^(e)	11500	238	Na(UO ₂)O(OH)	326.0	0.1733	Na ₂ U ₂ O ₇	634	0.168	4.80E-03
Zn	1445	65.39	Zn(OH) ₂	83.4	0.0203	ZnO	81.39	0.020	4.91E-04
Zr	955	91.224	Zr(OH) ₄	83.4	0.0096	ZrO ₂	123.22	0.014	-4.58E-03
Ag	79	107.868	AgOH	124	0.0010	Ag ₂ O	231.7	0.002	-8.68E-04
Ba	290	137.33	BaCO ₃	197.3	0.0016	BaO	153.33	0.001	3.54E-04
Ca	13500	40.07	CaAl ₂ (CO ₃) ₂ (OH) ₄ ·3(H ₂ O)	336.1	0.0078	CaO	56.08	0.001	6.51E-03
Cu	325	63.546	Cu(OH) ₂	82.6	0.4193	CuO	79.55	0.295	1.53E-02
La	331	138.905	La(OH) ₃	157.9	0.0089	La ₂ O ₃	325.81	0.009	-2.80E-04
Mg	1950	24.305	MgCO ₃	83.3	0.0023	MgO	40.3	0.001	1.19E-03
Pb	2820	207	Pb(CO ₃) ₂	327.2	0.2888	PbO ₂	239.2	0.211	7.77E-02
Ti	105	47.88	TiO ₂	31.9	0.0056	TiO ₂	31.9	0.005	0.00E+00
Y	120	88.906	Y(OH) ₃	107.9	0.0026	Y ₂ O ₃	225.81	0.003	-1.20E-04
Total	468,192	--	--	--	11.967	--	--	9.754	2.213
									18.50% ^(l)

(a) Aluminum 5 % as AlO(OH), Aluminum 15 % as Al₂O₃, 80% as NaAl(OH)₂CO₃

(b) Chromium 5 % as Cr (OH)₃, Chromium 95 % as Cr₂O₃

(c) Iron 50% as Fe₂(OH)₂CO₃, 50% as Fe(OH)₃

(d) 2.4% Na was used for the Clarkeite, 6.23% used as NaOH

(e) 2.4% U used as Clarkeite per the XRD spectrum in Figure D.2

(f) Reported ICP average of element

(g) Assumed starting species.

(h) Initial mass of constituent I, total initial mass was 12.7 mg

(i) Assumed thermal end point

(j) M_f = Final mass of constituent i

(k) Δ = change in mass

(l) Total mass change

D.2.8 Speciation of Tank Waste Sample G6-Cr-TGA

The DTA curve (cyan) in Figure D.7 through Figure D.9 of the slurried and the dry tank waste samples were thermally uneventful except for the endothermic removal of waters of hydration. It is this lack of signature that lowers the probability of the chromium speciation being $\text{Cr}(\text{OH})_3 \cdot x\text{H}_2\text{O}$ or $\text{CrO}(\text{OH}) \cdot x\text{H}_2\text{O}$, or of the aluminum speciation as being purely boehmite. As seen in Figure D.3a and Figure D.3b, and 6.23, the former compounds decompose with thermal signatures not observed in the tank waste scans. From the chromium dilution and the standard mixture experiments discussed above, it can be conservatively estimated that these compounds were not present in tank waste sample G6-Cr-TGA in excess of 10 wt% as the hydroxide or oxy-hydroxide.

Additionally, the analysis of mass data between 20 and 180°C suggests that the chromium could not exist as $\text{Cr}(\text{OH})_3 \cdot x\text{H}_2\text{O}$ or $\text{CrO}(\text{OH}) \cdot x\text{H}_2\text{O}$ in tank waste sample G6-Cr-TGA because the expected mass loss experienced from water loss alone from these compounds should be greater than 20% as seen in the standards experiments (see Figure D.3a and Figure D.3b). For example, a typical preparation of $\text{Cr}(\text{OH})_3$ would yield $\text{Cr}(\text{OH})_3 \cdot 4\text{H}_2\text{O}$. A high-surface-area sample might further adsorb two molecules of water to give $\text{Cr}(\text{OH})_3 \cdot 6\text{H}_2\text{O}$. Dehydration of a 12-mg sample containing 50% $\text{Cr}(\text{OH})_3 \cdot 2\text{H}_2\text{O}$ to anhydrous $\text{Cr}(\text{OH})_3$ would represent a 26 wt% mass change. The tank waste samples lost only 17 wt% below 180°C. Accordingly, either a lower % chromium as hydroxide or an alternative chromium speciation is required for the G6-Cr-TGA tank waste sample.

The crystalline sample of boehmite used for our TG standards characterization exhibited no water loss. The boehmite crystallites (0.2 micron) displayed in the TEM images of the G6 solids (Figure 6.16g) would likely resist adsorption of water. The iron hydroxide TG standard, on the other hand, lost 30 wt% water below 60°C, consistent with the formula $\text{Fe}(\text{OH})_3 \cdot 1\text{H}_2\text{O}$. This indicates that iron loses its water(s) of hydration and the majority of its hydroxide below this temperature. Dehydration of a 12-mg sample containing 9 wt% Fe to anhydrous Fe_2O_3 would represent a 3 wt% change. Based on mass analysis, aluminum existed as < 15 wt% boehmite (of the ICP amount) and the iron as > 90% (of the ICP amount) in some hydroxide form in the leached and washed tank waste sample G6-Cr-TGA.

We have tentatively assigned the predominant chromium as > 90 wt% Cr_2O_3 (of the ICP amount) based on the lack of the known signatures in the TG scans and on the low mass loss below 180°C. The absence of a chromium signature in the XRD spectrum and the TEM images of the leached and water-washed Group 6 tank waste solids are consistent with an amorphous aggregate of Cr_2O_3 .

The lack of any endotherm for iron above 100°C suggests the iron was iron hydroxide, Fe_3O_4 or Fe_2O_3 . Similarly, the lack of an endotherm for the aluminum content above 180°C is consistent with an aluminum speciation that is less than 5 to 10% boehmite. Again, the TEM images, composition maps, and XRD spectra are consistent with amorphous iron and aluminum.

D.2.9 Mass Loss Estimates and Discussion

The reproducibility of the TG data from the dried tank waste samples suggests that mass-balance calculations might be used to understand the mass loss in greater detail. The mass-balance calculation should account for the following regions in the TG data:

- Adsorbed water and chemically bound water, 20 to 180°C
- Water loss as hydroxide or oxide, 180 to 600°C
- Other sources of mass loss, 600 to 800°C.

The elements that were detectable in the leached G6 tank waste sample by ICP-OES are listed in the first column of Table D.6. These data were used to estimate several expected mass-loss results for the thermal loss of water or hydroxide between an initial assumed speciation of the ICP analyte and the known thermal endpoints that would exist between 600 and 800°C. The highest concentration elements in the tank waste sample were Cr, Fe, and Al, so that adjustment of these contributes the greatest change in the calculation. The estimated mass change for the combined remainder species in Table D.6 was only about 2 wt%. The result is conservatively based on the assumption of water loss alone from the dehydrated or anhydrous metal hydroxides. That is, waters of hydration and adsorbed water were considered removed in the calculation. This (calculated) water removal should be complete below 180°C so that the calculation of weight loss should be compared to the experimental data above 180°C. If indeed, the chromium and aluminum existed in the tank waste to about 90% as the sesquioxides and the iron existed as 100% iron hydroxide, then the total expected mass loss could be calculated, as shown in Table D.6, as about 5.4% mass loss. The calculated value is lower than the observed mass loss (≈ 13 wt%) between 180 and 600°C and does not account for the further 3% mass loss observed in the TG experiments to 800°C. Adjustment of total chromium to 50% chromium hydroxide (the remainder being Cr_2O_3) and total aluminum to 50% boehmite (the remainder being Al_2O_3) increased the calculated mass loss to 16.2 wt%. While the value is in line with the observed mass loss between 180 and 600°C, the thermal signature for the chromium hydroxide and boehmite decompositions would be quite distinctive at the 50 wt% ($\text{Cr}(\text{OH})_3 \cdot 2\text{H}_2\text{O}$) level, and these were not observed.

The apparent disparity between the mass-balance calculation and the lack of clear thermal signatures directs attention to the mass loss that occurred above 500°C in the TG experiments. As discussed above, the most plausible explanation for this mass loss is the presence of metal carbonate species. While it is not possible to assign specific chemical identities for these, the alkaline Hanford tank wastes are known to absorb CO_2 such that pure metal carbonates or hydroxy carbonates could form.

Accordingly, alternate calculations that were based on an initial speciation that would reproduce the observed lack of $\text{Cr}(\text{OH})_3$, $\text{CrO}(\text{OH})$, and $\text{AlO}(\text{OH})$ thermal signatures and allow for carbonate interaction with the tank waste were attempted. Such interactions would lead to the formation of known aluminos carbonates for instance. The calculation in Table D.7 uses a mixture of 5% boehmite, 85% dawsonite, and 15% alumina. Decomposition of the dawsonite or of the carbonates in general would display a very broad endothermic signature because loss of CO_2 would be gradual between 350 and 650°C. Some other metal carbonates are added in the calculation but do not cumulatively affect the mass change by more than 2 wt%. Of course, the choice and quantity of the carbonate species is arbitrary. The calculation is displayed here to demonstrate that such mass changes are possible with realistic materials that furthermore would produce the observed thermal features.

D.3 Summary

We have assigned the predominant chromium as > 90 wt% Cr_2O_3 and the aluminum as less than 10 wt% boehmite in tank waste sample G6-Cr-TGA (caustic-leached and water-washed Group 6 solids). The

assignments are based on the following experiments and observations concerning tank waste samples G6-Cr-TGA:

- Acquisition of thermal scans of realistic candidate materials used for control standards
- Lack of TG signatures from tank waste sample G6-Cr-TGA that would identify $\text{Cr}(\text{OH})_3$ or $\text{CrO}(\text{OH})$ to below 10 wt%
- Lack of TG signatures from tank waste sample G6-Cr-TGA that would identify $\text{Al}(\text{OH})_3$, $\text{AlO}(\text{OH})$ to below 10 wt%
- Thermal mass loss because adsorbed and chemically bound water below 180°C was too low for 50.7% $\text{Cr}(\text{OH})_3 \cdot x\text{H}_2\text{O}$ speciation.
- Mass-balance calculations, based on hydroxide to oxide conversion only, suggest that nearly 50% $\text{Cr}(\text{OH})_3$ or $\text{CrO}(\text{OH})$ would be required to obtain the observed mass loss. Several control experiments with these materials indicate that at these levels, the thermal signatures should be obvious for both Cr and Al.
- It was postulated that Al and Fe might exist as a mixture of metal hydroxy carbonates. This in turn suggests that mixed hydroxy carbonate species are responsible for some of the mass lost from 200 to 800°C. The latter have the requisite thermal stability, thermal-decomposition scans, and likelihood of existence in the saltcake tank waste type.

The assignment of the Cr speciation as the more intractable Cr_2O_3 may have some impact on the oxidative leaching times of the insoluble chromium. The impact may be minimal because the Cr particle size is approximately 1000 times smaller in the Group 6 solids than those used in the oxidative leaching studies previously reported (Rapko 2007).

Distribution

**No. of
Copies**

ONSITE

4	Bechtel National, Inc.	
	V. Guynes (2)	H4-02
	P. S. Sundar	H4-02
	S. Barnes	H4-02
22	Pacific Northwest National Laboratory	
	S. K. Fiskum (2)	P7-25
	E. C. Buck	P7-27
	R. C. Daniel	P7-22
	K. E. Draper	K6-75
	M. K. Edwards	P7-25
	T. L. Hubler	K8-93
	L. K. Jagoda	K6-24
	E. D. Jenson	P7-22
	D. E. Kurath	K3-52
	G. J. Lumetta	P7-25
	B. K. McNamara	P7-25
	L. M. Perrung	K9-09
	R. A. Peterson	P7-22
	B. M. Rapko	P7-25
	R. L. Russell	K6-24
	R. W. Shimskey	P7-27
	S. I. Sinkov	P7-25
	G. L. Smith	K6-24
	L. A. Snow	P7-25
	Project File (2)	P7-28